UNIVERSIDADE DE SÃO PAULO

ESCOLA POLITÉCNICA

ALEXIS ZAKARTCHOUK JUNIOR

COOPERATIVE PATH FOLLOWING CONTROL OF OCEAN VEHICLES USING LYAPUNOV - BASED MODEL PREDICTIVE CONTROL / MOVING HORIZON ESTIMATION AND CONSENSUS THEORY

São Paulo

2023

ALEXIS ZAKARTCHOUK JUNIOR

COOPERATIVE PATH FOLLOWING CONTROL OF OCEAN VEHICLES

USING LYAPUNOV - BASED MODEL PREDICTIVE CONTROL /

MOVING HORIZON ESTIMATION AND CONSENSUS THEORY

Doctoral Thesis submitted to the Escola Politécnica da Universidade de São Paulo, in partial fulfillment of the requirements for the Doctor of Science Degree (D.Sc)

São Paulo
2023

ALEXIS ZAKARTCHOUK JUNIOR

COOPERATIVE PATH FOLLOWING CONTROL OF OCEAN VEHICLES

USING LYAPUNOV - BASED MODEL PREDICTIVE CONTROL /

MOVING HORIZON ESTIMATION AND CONSENSUS THEORY

Revised Version

Doctoral Thesis submitted to the Escola Politécnica da Universidade de São Paulo, in partial fulfillment of the requirements for the Doctor of Science Degree (D.Sc)

Research Area:
Naval Architecture and Ocean Engineering

Supervisor:
Professor Helio Mitio Morishita (D.Sc)

São Paulo
2023

Autorizo a reprodução e divulgação total ou parcial deste trabalho, por qualquer meio convencional ou eletrônico, para fins de estudo e pesquisa, desde que citada a fonte.

Este exemplar foi revisado e corrigido em relação à versão original, sob responsabilidade única do autor e com a anuência de seu orientador.

São Paulo, 20 de maio de 2023.

Assinatura do autor:_____

Assinatura do orientador:_____

FICHA CATALOGRÁFICA

To my wife Natalia

To my children Vladimir, Aleksandr and Darina

ACKNOWLEDGMENTS

A principle for managing a successful program is to resist the natural human inclination to hope things will work out, despite evidence or doubt to the contrary.

Complex jobs cannot be accomplished effectively with transients.

(Admiral Hyman G. Rickover)

Product of optimism and knowledge is a constant.

(Lev Davidovich Landau)

E quindi uscimmo a riveder le stelle.

(Dante Alighieri, il personaggio)

ABSTRACT

Boosted by recent developments in control techniques, computing power, communication capabilities and miniaturization technologies, the cooperative deployment of multi-agent systems has been drawing the attention of the scientific community and industry, for applications in distinct areas such as military battle systems, mobile sensor networks, survey & inspection, transport systems and others. Inspired by natural biological systems, the use of a cluster of cooperative distributed agents has proved to be advantageous in terms of cost, efficiency, flexibility and reliability, when compared to conventional monolithic structures relying on a single agent. These advantages become even more preeminent for marine applications, since autonomous marine vehicles are much cheaper than conventional vessels in terms of capital and operational costs, can safely explore previously impenetrable environments of the sea, are less subjected to be hampered by rough weather, and are more discrete in terms of magnetic and acoustic signatures. To solve the associated control problem, this thesis envisages a control strategy relying on two layers of implementation. The lower-level layer, based on the receding horizon concept (model predictive control and moving horizon estimation), controls the vehicles' individual motion. The higher-level layer, based on consensus theory, controls the motion of the entire formation. The receding horizon concept is particularly interesting for motion control of marine vehicles due to its capability to deal with nonlinear dynamics, parametric uncertainties and external disturbances, besides its inherent ability to systematically handle practical constraints on control signals and states. Consensus theory is interesting for formation control due to the simplicity of the associated control law. The performance of the designed control system is assessed through numerical simulations.

Keywords: nonlinear control. cooperative control. path following. model predictive control. moving horizon estimation.

RESUMO

Impulsionado pelos desenvolvimentos recentes nas áreas de controle, capacidade computacional, comunicações e miniaturização, o emprego de controle cooperativo de sistemas com vários agentes tem atraído a atenção da comunidade científica e da indústria, para aplicações em diversas áreas como sistemas militares de combate, redes de sensores móveis, pesquisa & inspeção, sistemas de transportes, dentre outras. Inspirado pelos sistemas biológicos da natureza, o uso de um grupo de agentes distribuídos, operando em modo cooperativo, prova ser vantajoso em termos de custo, eficiência, flexibilidade e confiabilidade, quando comparado com as estruturas monolíticas convencionais, baseadas num único agente. Estas vantagens se tornam ainda mais proeminentes em aplicações marítimas, uma vez que veículos marítimos autônomos são muito mais baratos do que navios convencionais em termos de custos de capital e de operação, podem operar com segurança em regiões do mar outrora inacessíveis, são menos sujeitos aos efeitos deletérios associados ao mal tempo, e são mais discretos em termos de assinaturas acústica e magnética. Para resolver o problema de controle em tela, esta tese considera o emprego de uma estratégia de controle baseada em duas camadas de implementação. A camada inferior, baseada no princípio de controle de horizonte retrocedido (controle preditivo baseado em modelo e estimação baseada em horizonte móvel), é responsável por controlar o movimento individual dos veículos. A camada superior, baseada na teoria de consenso, é responsável por controlar o movimento da formação. O conceito de horizonte retrocedido é particularmente interessante para aplicações de controle de veículos oceânicos devido a sua capacidade de lidar com dinâmicas não-lineares, incertezas paramétricas, perturbações externas, além da sua inerente capacidade de lidar sistematicamente com restrições práticas nos sinais de controle e nos estados. A teoria de consenso é interessante para aplicações de controle de formação devido a simplicidade da lei de controle associada. O desempenho do sistema de controle projetado é avaliado através de simulações numéricas.

Palavras-chave: controle não-linear. controle cooperativo. seguimento de rota. controle preditivo baseado em modelo. estimação baseada em horizonte móvel.

TABLE OF CONTENTS

LIST OF FIGURES

LIST OF TABLES

ACRONYMS AND ABBREVIATIONS

2D	Two dimensional
AMV	Autonomous marine vehicle
AOSN	Autonomous ocean sampling network
ASC	Autonomous surface craft
ASW	Antisubmarine warfare
AUV	Autonomous underwater vehicle
C2	Command and control
CB	Centre of buoyancy
CC	Cooperative controller
CD-EKF	Continuous-discrete extended Kalman Filter
CG	Centre of gravity
CLOST	Cooperative line of sight target following
COLAV	Collision avoidance
CPF	Cooperative path following
DARPA	Defense advanced research projects agency
DMC	Dynamic matrix control
DOF	Degrees of freedom
WiMUST	Widely scalable mobile underwater sonar technology
EC	European comission

ETC	Event triggered communication
FLC	Feedback linearization control
FM	Formation manoeuvres
FP6	6th framework of the European commission
FRP	Formation reference point
GAS	Globally asymptotically stable
GES	Global exponential stable
GPC	Generalized predictive controller
GPS	Global positioning system
IDCOM	Identification command
IVHS	Intelligent vehicle/highway system
IVV	Integration – Verification – Validation
J-UCAS	Joint unmanned combat air systems
L	Linear
LBL	Long base line
L-MPC	Lyapunov-based model predictive control
LP	Linear programming
LQG	Linear quadratic gaussian
LQR	Linear quadratic regulator
LTI	Linear time invariant
MHE	Moving horizon estimator

MPC	Model predictive control
NATO	North Atlantic treaty organization
NASA	National Aeronautics and Space Administration
NL	Nonlinear
NLP	Nonlinear programming
OCSO	Ocean current state observer
OCP	Optimal control problem
PFC	Path following controller
PID	Proportional - Integral - Derivative
QDMC	Quadratic dynamic matrix control
QP	Quadratic programming
RB	Rigid body (subscript)
REF	Reference (subscript)
RH	Receding horizon
ROV	Remotely operated underwater vehicle
RPM	Rotations per minute
SISO	Single input single output
SNAME	Society of naval architects and marine engineers
TPF	Terrestrial planet finder
UAV	Unmanned aerial vehicle
UMV	Unmanned mobile robot

NOTATION

All mathematical variables used in this thesis are represented in italics. To reduce the math symbology and render the reading easier, they are written according to the following convention:

Matrices are represented in upper-case letters (M represents matrix $[M]$).

Vectors are represented in lower-case bold letters ($\boldsymbol{v}$ represents vector $\vec{\boldsymbol{v}}$).

Multidimensional functions are represented lower-case bold letters ($\boldsymbol{f}(.)$).

Unidimensional functions are represented lower-case letters ($f(.)$).

The use of subscript and superscript indexes does not follow a general rule, and for that reason, the adopted conventions are explained not in this section, but in the main text.

The sets of numbers are expressed by calligraphed letters, according to the common practice:

$\mathbb{N}$ is the natural number set.

$\mathbb{Z}$ is the integer number set.

$\mathbb{Z}^+$ is the non-negative integer number set.

$\mathbb{R}$ is the real number set.

The ship motions are named according to the Society of Naval Architects and Marine Engineers (SNAME) conventions, as indicated as follow:

Degree of Freedom	Motion	Direction	Operation
1	Surge	x	
2	Sway	y	Translation
3	Heave	z	
4	Roll	x	
5	Pitch	y	Rotation
6	Yaw	z	

SYMBOLS

A	Added mass (subscript)
$A(\mathcal{G})$	Adjacent matrix
$\mathbb{U}_v$	Allowable set of velocities
γ_{ij}	Along path distance between vehicles i and j
$\boldsymbol{v_2}$	Angular velocity vector of $\{B\}$
$\{B\}$	Body-Fixed frame $\{X_B, Y_B, Z_B\}$
$\bar{u}$	Common speed profile
$c(.)$	Cos (.)
$s(.)$	Sin (.)
C_i	Communication package
$\boldsymbol{u}(.)$	Control action vector
N_c	Control horizon
$\mathbb{U}$	Control set
$\boldsymbol{\xi}$	Coordination error vector
C	Coriolis and centripetal matrix
$\tilde{u}_c^i$	Correction speed (vehicle i)
$J(.)$	Cost function
D	Damping matrix
$D(\mathcal{G})$	Degree matrix

k	Discretized time
t_k^i	Discretized time (vehicle i)
$W(.)$	Disturbance set
$w(.)$	Disturbance vector
$\{I\}$	Earth-Fixed inertial frame $\{X_I, Y_I, Z_I\}$,
$\hat{\gamma}_i^i$	Estimate of parameter γ_i, by vehicle i
$\hat{\gamma}_j^i$	Estimate of parameter γ_j, by vehicle i
J	Euler angle rotation matrix
ε	Event trigger communication threshold
$\boldsymbol{\tau_1}$	External forces vector
$\boldsymbol{\tau_2}$	External torques vector
$J_N^0(.)$	Finite horizon cost function
$\boldsymbol{\tau_R}$	Forces and moments vector due to gravity and fluid density
$\boldsymbol{\tau_A}$	Forces and moments vector due to added mass
$\boldsymbol{\tau_D}$	Forces and moments vector due to hydrodynamic effects
$\boldsymbol{\tau_c}$	Forces and moments vector due to thrusters and surfaces
$\mathcal{G}$	Graph topology
Z	Heave force
w	Heave velocity
M	Inertia matrix

$J_\infty^0(.)$	Infinite horizon cost function
$\boldsymbol{x_0}(.)$	Initial state
K_d	Inner loop gain matrix
$\boldsymbol{v_1}$	Linear velocity vector of $\{B\}$
Q	L-MPC tuning matrix
R	L-MPC tuning matrix
x	Longitudinal position
V	Lyapunov function
T	Velocity correlation matrix
σ_r^2	Measurement covariance noise in r
σ_u^2	Measurement covariance noise in u
σ_y^2	Measurement covariance noise in y
σ_ψ^2	Measurement covariance noise in ψ
σ_x^2	Measurement noise covariance in x
n_r	Measurement noise in r
n_u	Measurement noise in u
n_x	Measurement noise in x
n_y	Measurement noise in y
n_ψ	Measurement noise in ψ
$\boldsymbol{h}(.)$	Measurement set

N_{MHE}	MHE measurement window horizon
$\boldsymbol{z}$	MHE measurement model
Q_*^{-1}	MHE tuning matrix
R_*^{-1}	MHE tuning matrix
$\mathcal{N}$	Normal distribution
L_D	Normalized graph Laplacian
$\boldsymbol{\eta_2}$	Orientation vector of $\{B\}$, (Euler Angles)
γ	Path parameter
θ	Pitch angle
q	Pitch angular velocity
M	Pitch moment
$\boldsymbol{\eta}$	Position and heading vector
$\boldsymbol{e}$	Position tracking error
$\boldsymbol{\eta_1}$	Position vector of $\{B\}$
$\boldsymbol{z_M}$	Position/heading measurement vector
$\boldsymbol{\eta_{u_d}}$	Position/heading vector for control input $\boldsymbol{u_d}$
N_p or N	Prediction horizon
$\boldsymbol{K_k}$	Reference controller gain matrix
$\boldsymbol{P_{Ref}}$	Reference position vector
$\boldsymbol{p_{Ref}}$	Reference position vector

$\boldsymbol{\eta}_{Ref}$	Reference position/heading vector
$\boldsymbol{u}_{Ref}$	Reference surge and yaw velocities vector
u^i_{Ref}	Reference surge speed (vehicle i)
u_{Ref}	Reference surge velocity
r^i_{Ref}	Reference yaw speed (vehicle i)
ϕ	Roll angle
p	Roll angular velocity
K	Roll moment
R^I_B	Rotation matrix from $\{B\}$ to $\{I\}$ (6 DOF)
$R(\psi)$	Rotation matrix from $\{B\}$ to $\{I\}$ (horizontal motion – 2 DOF)
$J(\psi)$	Rotation matrix from $\{B\}$ to $\{I\}$ (horizontal motion – 3 DOF)
ΔT	Sampling time
$\mathcal{N}$	Set of vehicles
$\mathcal{N}_i$	Set of vehicles that communicate with vehicle i
$\boldsymbol{u}_d$	Speed assignment
$\bar{\boldsymbol{u}}_d$	Speed assignment (reference controller)
$\widetilde{\boldsymbol{u}}$	Speed assignment tracking error
z	Speed assignment tracking error
$l(.)$	Stage cost
$\mathbb{X}$	State set

$\boldsymbol{x}(.)$	State vector
X	Surge force
u	Surge velocity
Y	Sway force
v	Sway velocity
$\boldsymbol{\gamma}$	Synchronization states vector
X_f	Terminal constraint set
$F(.)$	Terminal cost
y	Transversal position
$-\boldsymbol{g}$	Vector of gravity restoring loads
$\boldsymbol{u}_{Ref}^i$	Vector of reference speeds (vehicle i)
$\boldsymbol{u}_M$	Velocities measurement vector
$\boldsymbol{u}$	Velocity vector
$\boldsymbol{v}$	Velocity vector (u, v, r)
z	Vertical position
ψ	Yaw (heading) angle
r	Yaw angular velocity
N	Yaw moment
$\tilde{\boldsymbol{p}}$	Position error vector
$\boldsymbol{v}_r$	Vehicle velocity vector (related to the ocean current)
$\boldsymbol{v}_{ci}$	Ocean current velocity vector (related to $\{I\}$)

$\widehat{\boldsymbol{v}}_{\boldsymbol{ci}}$	Ocean current estimated velocity vector (related to $\{I\}$)
K_{p_obs}	Ocean current state observer gain matrix
K_{c_obs}	Ocean current state observer gain matrix
$\widetilde{\boldsymbol{v}}_{\boldsymbol{ci}}$	Ocean current velocity error vector
$\boldsymbol{v}_{\boldsymbol{c}}$	Ocean current velocity vector (related to $\{B\}$)
u_r	Vehicle surge velocity component (relative to the current)
v_r	Vehicle sway velocity component (relative to the current)
u_c	Ocean current longitudinal velocity component (relative to $\{B\}$)
v_c	Ocean current transversal velocity component (relative to $\{B\}$)

1 INTRODUCTION

This thesis addresses the problem of cooperative control of multi-agent systems. In this introductory chapter, the motivation and the main applications of this technology are presented. Afterwards, the concerned literature is reviewed, and the engineering control problem is formalized for a fleet of Autonomous Marine Vehicles (AMVs). Finally, the thesis' main contributions are identified, and its documental structure is presented.

1.1 Motivation

The objective of multi-agent systems performing cooperative tasks is to accomplish complex missions through the synchronized work of its networked agents. The idea of a monolithic structure replaced by a cluster of distributed agents has proved to be advantageous in terms of cost (mass production), efficiency (work repartition), flexibility (reconfiguration capability) and reliability (redundancy) (Ferri, Munafo, & LePage, 2018). This statement is supported not only by artificial systems assisted by active control, but also by natural biological systems where strict cooperation can be observed, resulting in benefits for groups' performance, as well as for individual's survivability (Kyrkjebø, 2007). Typical examples of cooperation in nature are bacteria swarming, fish schools and bird flocks (Figure 1-1).

Figure 1-1: Examples of cooperation in natural biological systems

Bacteria swarming[1]   Fish school[2]   Bird flock[3]

Boosted by recent developments in control techniques, computing power, communication capabilities and miniaturization technologies, the cooperative

---

[1] Scientists discover bacterial colonies warn the community of deadly threats | SYFY WIRE
[2] https://allthatsinteresting.com/schooling-fish
[3] https://pixabay.com/illustrations/sunset-birds-flock-nature-sky-4576884/

deployment of multi-agent systems has been pushing the attention of the scientific community, for applications in distinct areas such as military battle systems, mobile sensor networks, survey & inspection, transport systems, and others (Fax & Murray, 2004) and (Murray, 2007).

1.1.1 Military Battle Systems

Modern military systems are becoming increasingly sophisticated, combining the use of manned and unmanned vehicles in complex battlefield environments (Murray, 2007). It is expected that fully unmanned systems will be sufficiently robust until 2030, allowing them to significantly outnumber humans on the future battlefields (Verret, 2005).

This trend can already be observed in modern battlespace management systems which are increasingly considering solutions based on decentralized resource allocation followed by centralized execution, relying on the cooperative operation of large collections of distributed vehicles, with local computation, global communication and decentralized control actions (Murray, 2007).

The main tasks to be addressed by the military battle systems are (Murray, 2007):

1) **Vehicle´s formation**, where a set of vehicles, manned or unmanned, are requested to move in a desired geometric formation;

2) **Cooperative classification and surveillance**, consisting in acquiring maximal amounts of relevant information using a collection of vehicles, to maintain the knowledge of the state of a geographical area. If the vehicles can communicate with each other, the shared information can be used to determine their motion;

3) **Cooperative attack and rendezvous**, consisting in bringing a collection of vehicles to a common location, at a specific time, while minimizing their radar exposure through locally optimized individual paths; and

4) **Mixed initiative systems**, where a collection of unmanned vehicles and human operators must collectively perform a task or a mission.

Example 1-1 (Joint Unmanned Combat Air Systems (J-UCAS)): J-UCAS (Figure 1-2) is a "networked system of high performance, weaponized unmanned air vehicles to effectively and affordably perform 21st century combat missions, including Suppression of Enemy Air Defenses; Electronic Attack; Precision Strike; Surveillance/Reconnaissance; and, Persistent Global Attack within the emerging global command and control architecture" (Darpa, 2004).

Figure 1-2: Joint Unmanned Combat Air Systems
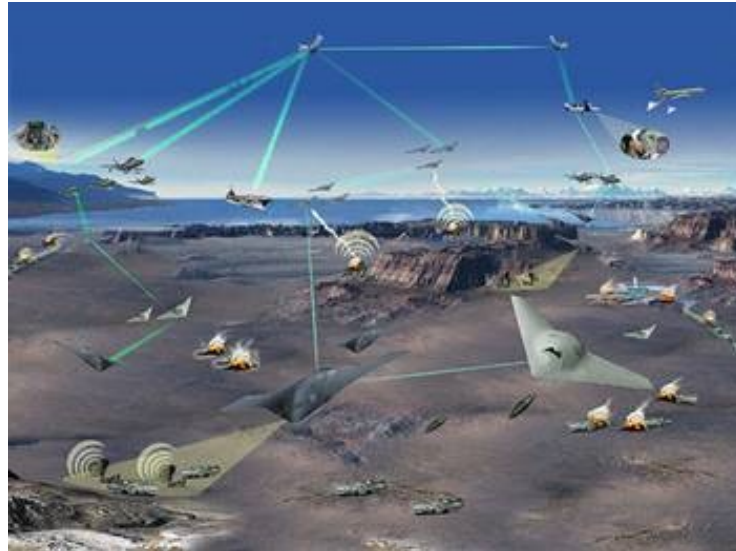
(Darpa, 2004)

Example 1-2 (Multistatic Antisubmarine Warfare Robotic Network): The Multistatic Antisubmarine Warfare (ASW) Robotic Network (Figure 1-3) is a NATO program developed as an alternative approach to conventional ASW surveillance, carried out by submarines and frigates with towed arrays. In the proposed architecture, one or more sonar sources installed on stationary buoys or surface ships, transmit a sonar signal which reflects from objects and is collected by hydrophone arrays towed by Autonomous Underwater Vehicles (AUVs). Once a possible threat is detected, the AUVs track its path and transmit the acquired data to the Command and Control (C2) center through a communication network composed by mobile Autonomous Surface Crafts (ASCs) (wave gliders) and fixed buoys (gateways) (Ferri, Munafo, & LePage, 2018).

Figure 1-3: Multistatic Antisubmarine Warfare Robotic Network
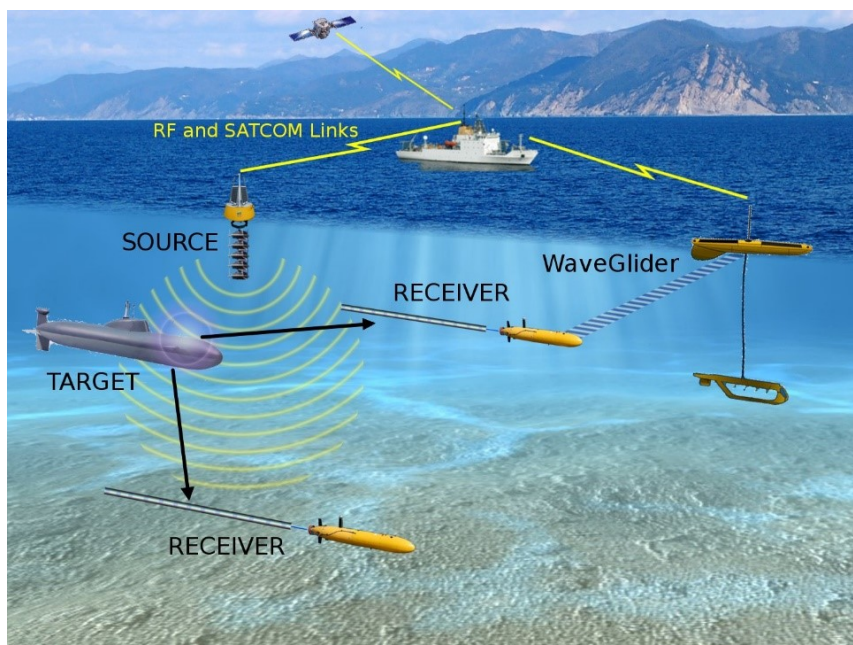
(Ferri, Munafo, & LePage, 2018)

1.1.2 Mobile Sensor Networks

The deployment of mobile networked sensors operating in cooperative mode aims to maximize the amount of information that they can gather, since the sensors can be repositioned to the most appropriate operating places.

Example 1-3 (Distributed Aperture Observing): a) TechSat 21 Microsatellites: TechSat 21 experiment, consisting of three microsatellites flying in formation to operate as a single larger conventional satellite, with a single and large aperture antenna (Figure 1-4 a)) (Martin, Klupar, Kilberg, & Winter, 2001)**. b) Terrestrial Planet Finder:** A NASA program aiming to detect Earth-like planets that orbit nearby stars and to study their atmosphere composition. It is based on a separated infrared interferometer composed by four spacecrafts equipped with telescopes that send their data to a fifth integrating data spacecraft (Figure 1-4 b) (US Naval observatory, 2017).

Figure 1-4: Distributed aperture observing – a) TechSat 21 microsatellites and b) TPF interferometers

(Martin, Klupar, Kilberg, & Winter, 2001)   (US Naval observatory, 2017)
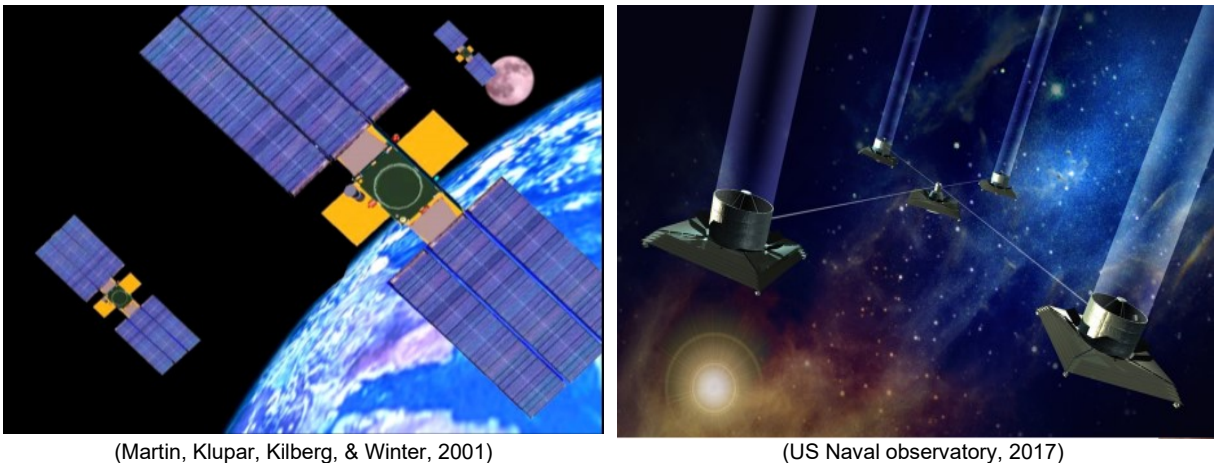
For the marine field, the deployment of fleets of autonomous marine vehicles (AMVs) operating in cooperative mode to sample environmental data presents advantages compared to the conventional use of research platform vessels. The AMVs demand less capital investment to be built (small units), have the potential to operate at lower costs, can explore previously impenetrable environments of the sea, are less subjected to be hampered by rough weather and are extremely quiet, consequently subjected less to self-noise interference (Fernandes, Stevenson, & Brierley, 2002).

Concerns related to the AMVs endurance are less prominent than before due to the rapid development of battery technology. The endurance, nowadays ranging from hours to several days, is expected to evolve for long-periods of deployments, ranging from weeks to months (Monk, et al., 2017).

Example 1-4 (Environmental Sampling): The Autonomous Ocean Sampling Network (AOSN), composed by a collection of smart and adaptive robotic vehicles (Figure 1-5) that move to areas in which they can maximize their gathering performance, as a function of previously acquired data (adaptive sampling). The gathered information is transmitted in near real-time to a shore facility to be processed by numerical models in order to predict the physical and biological state of the ocean in real time over sustained periods (Monterey Bay Aquarium Research Institute, 2016).

Figure 1-5: Autonomous Ocean Sampling Network (AOSN)
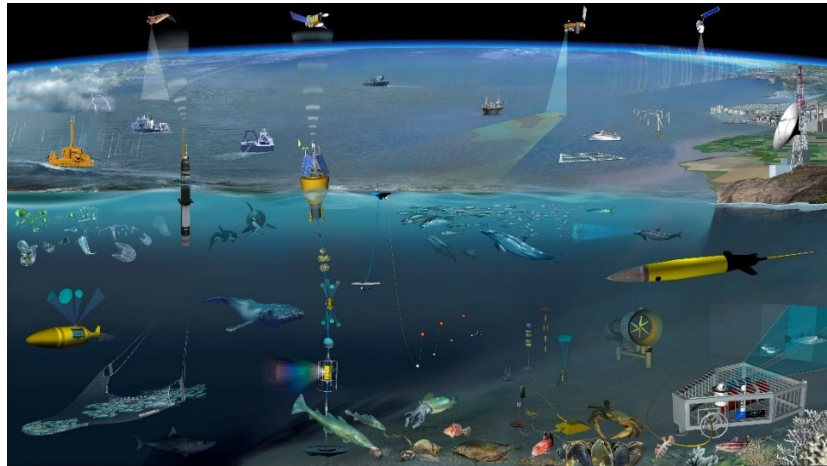
(Whitt & et. al, 2020)

1.1.3 Survey & Inspection

The deployment of AUVs supported by ASCs (Figure 1-6) offers a flexible and economical alternative to conduct underwater surveys and inspections by minimizing the need for surface support vessels, while performing more effectively the assigned tasks.

Figure 1-6: AUV and ASC conducting survey & inspection
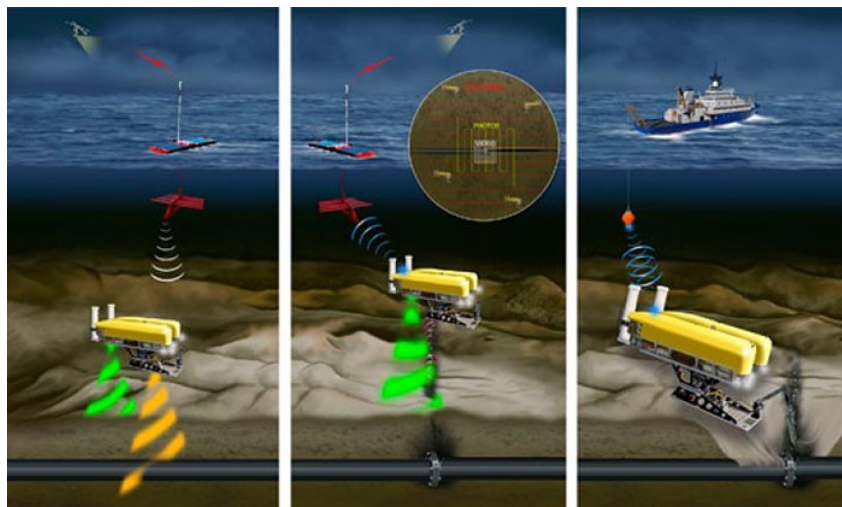
(Woods Hole Oceanographic Institution, 2019)

Example 1-5 (Survey & Inspection): a) Geophysical Surveys: marine habitat mapping (Figure 1-7 a) and **b) Subsea Inspections:** pipeline mapping and inspection (Figure 1-7 b).

Figure 1-7: Survey & Inspection – a) Marine habitat mapping and b) Pipeline mapping and inspection
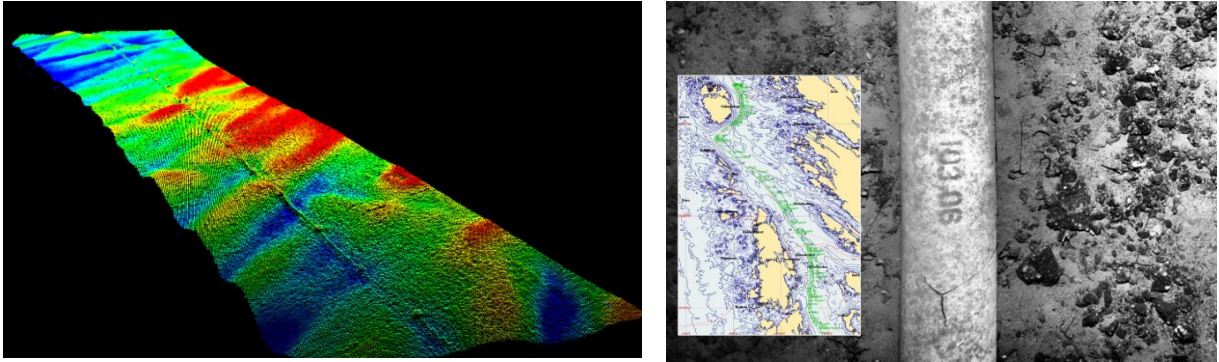
(Hagen P. E., 2016)

1.1.4 Transport Systems

Self-driving cars on intelligent highways can no longer be a futuristic fictional scenario. The "Intelligent Vehicle/Highway System" (IVHS) profits from recent developments in the fields of electronics, information processing, communications and control, many of them derived from military programs. This system considers bidirectional communications between vehicles (equipped with specialized sensors and wireless communications systems), as well as between the vehicles and the highway traffic-control centers. While the former intends to assure safer operations (collision warning and avoidance), the latter intends to coordinate the formation of the vehicles at closely spaced intervals (platoons) (Martin, Marini, & Tosunoglu, 1999). The same concept has been extended for marine shipping, where fully autonomous ships are foreseen for the next decade.

Example 1-6 (Transport Systems): a) Intelligent Highways: Futurist conception of intelligent airways at Coruscant planet (Figure 1-8 a) (http://starwars.wikia.com). **b) Autonomous Ships:** ROSATOM maritime autonomous surface ships in convoys following a nuclear-powered icebreaker to improve efficiency of shipping along the Northern Sea route (Figure 1-8 b) (Nielsen, 2018).

Figure 1-8: Transport system – a) Intelligent airways and b) Autonomous surface ships

(http://starwars.wikia.com)   (Nielsen, 2018)

1.2   Literature Review

The field of cooperative control of multi-agent systems dates to the late 1980s, initially in the area of mobile robotics. Prior to this time, research has never addressed the topics of robotic systems and distributed problem-solving systems together (Arai, Pagello, & Parker, 2002). In the 1990s, supported by the development of inexpensive and reliable wireless communication systems, research in this field increased significantly (Murray, 2007).

In the late 1990s and early 2000s, research related to cooperative control of multiple Unmanned Aerial Vehicles (UAVs) gained momentum in the United States, prompting further advances which have spread throughout new applications in several areas such as military battle systems, mobile sensor networks, survey & inspection, and transport systems (Murray, 2007).

In the 2000s, the scientific control community has increased its attention towards Autonomous Marine Vehicles (AMVs), with applications involving the deployment of Autonomous Underwater Vehicles (AUVs), Autonomous Surface Crafts (ASCs) and a combination of both. Although these applications present unique nuances linked to the constraints imposed by the marine environment, some control formation strategies derived from mobile robots and UAVs can be adapted and applied with minor changes (Li, Zhu, & Qian, 2014).

Originally conceived for military applications, the AMVs have also found use in the marine geoscience domain. The AUVs, particularly, have become the best oceanography research tool due to their ability to explore autonomously extreme sea environments, while providing higher quality data if compared with conventional research surface vessels, especially in deep water. The primary applications concern volcanism and hydrothermal vent studies, mapping and monitoring of low-temperature fluid escape features and chemosynthetic ecosystems, benthic habitat mapping in shallow and deep-water environments, and mapping of seafloor morphological features (Wynn, et al., 2014).

For didactical purposes, the present review will be conducted in four stages, according to the control problem focus of the reference literature:

- Individual Motion Control;
- Model Predictive Control;
- Formation Control Strategies; and
- Cooperative Control.

1.2.1 Individual Motion Control

The motion control problem for marine vehicles can be roughly categorized as point stabilization, trajectory tracking or path following. In point stabilization, the control objective is to stabilize the vehicle at a given point, with a desired orientation. In trajectory tracking, the objective is to track a geometric path with an associated timing specification. If the timing specification requirement is derogated, the problem reduces to path following (Encarnação & Pascoal, 2001). Therefore, trajectory tracking can be considered as a generalized case of point stabilization and path following can be considered as a relaxed case of trajectory tracking.

The degree of difficulty involved in solving these problems is highly dependent on the vehicle's configuration. For fully actuated systems, the problems are now reasonably well understood and can be solved by using the control allocation map. However, since it is usually costly or even unfeasible to fully actuate autonomous vehicles (due to weight, reliability, complexity, and efficiency considerations), most of these systems are underactuated and the design of their motion control system is subjected to challenging technical issues, normally associated with control performance and close-loop stability (Das, Subudhi, & Pati, 2016).

The point stabilization problem for underactuated vehicles concerns the inexistence of smooth (or even continuous) constant state-feedback stabilizing control laws. Approaches to overcome this theoretical issue consider the use of periodic time-varying control laws, hybrid switched seesaw control laws and virtual velocity controls, under the premise that underactuated vehicles are locally controllable on a smaller scale (Greytak & Hover, 2008). Dynamic positioning, which is beyond the scope of the present thesis, can be categorized as a typical problem of point stabilization.

The trajectory tracking problem for underactuated vehicles relies on the fact that most of these systems are not fully feedback linearizable and exhibit nonholonomic constraints, limiting the direct application of standard nonlinear control tools (Aguiar & Hespanha, 2003). Approaches to overcome these theoretical issues consider the use of local linearization combined with multi-variable model decoupling[4] (Pettersen & Nijmeijer, 2001) and (Lefeber, Pettersen, & Nijmeijer, 2003), linearization of the generalized vehicle error dynamics over the corresponding

---

[4] To steer the same number of degrees of freedom as the number of controls available.

trimming path[5] combined with gain scheduling techniques (Kaminer, Pascoal, Hallberg, & Silvestre, 1998), and nonlinear Lyapunov-based designs (Aguiar & Hespanha, 2003).

The use of path following control dates in the early 1990s, with applications in the field of ground robotics (Sansom, 1992). For marine applications, this topic has received relatively less attention than point stabilization and trajectory tracking until the early 2000s. The basic assumption in path following control is that the vehicle's forward speed tracks a desired speed profile, while the controller acts on the vehicle orientation to drive it to the path. Compared to trajectory tracking, smoother convergence to the path can be achieved and the control signals are less subjected to saturation, due to derogation of the time-parameterized path requirement (Encarnação & Pascoal, 2001). It is particularly interesting for oceanographic applications since the missions are not normally driven by restrictive temporal specifications.

The first methodologies to solve the path following problem in AUV applications relied on nonlinear Lyapunov-based control strategies as presented in (Encarnação & Pascoal, 2000) and (Encarnação, Pascoal, & Arcak, 2000), where a kinematic controller is merged into a standard integrator backstepping framework. The task of the kinematic controller consists in tracking the orthogonal projection of the vehicle position on the path (virtual target point).

However, this methodology imposes a severe restriction in the vehicle's initial position, which must lie inside a path centered tube with radius smaller than the path's smallest radius of curvature. If this condition is not observed, the position of the virtual target projection on the path is not well defined, and singularities occur in the control design.

This restriction is lifted in (Lapierre, Soetanto, & Pascoal, 2003b) by controlling the rate of progression of the virtual target along the path, thus introducing an extra degree of freedom that can be explored to avoid such singularities. Consequently, the problems that arise when the position of the virtual target point is simply defined by the projection of the actual vehicle on the path are bypassed. As in the previous work, the controller design starts at a kinematic level and evolves to a dynamic setting using backstepping techniques.

---

[5] To obtain a linear time invariant system.

In the previous works, the control design heavily relied on accurate knowledge of the vehicle dynamics. The effect of parametric modeling uncertainties is addressed in (Aguiar & Hespanha, 2004) and (Aguiar & Hespanha, 2007) for path following and trajectory tracking. Basically, a hybrid controller derived from the combination of an adaptive switching supervisory control with a nonlinear Lyapunov-based tracking control law was used. However, the effects of measurement noise and environmental disturbances were not considered in the analysis.

Such effects are addressed in (Aguiar & Pascoal, 2007b), which also solved the problem of input saturations by considering surge and yaw speeds as controls. Additionally, the problem of unmodeled dynamics was tackled by merging the dynamic and kinematic tasks through extended Lyapunov/backstepping based techniques, however at the expense of obtaining more complex control laws. To overcome this problem, the authors proposed to separate these tasks again in an inner-outer loop control structure, so that the inner loop deals with the vehicle dynamics (speed tracking scheme), and the outer loop deals with the control laws (guidance scheme).

This strategy is implemented by (Maurya, Aguiar, & Pascoal, 2009) for a path following controller. In this control architecture, the kinematic outer loop acts as a heading command generator, calculating the heading angle required to drive the vehicle along the desired path and issuing this information to the inner dynamic loop, composed by the feedback connection of the vehicle itself and a classical heading controller (autopilot). Since the two loops present decoupled dynamics and considering that the outer loop does not require in-depth knowledge of the vehicle's internal dynamics, it is possible to use it on a wide range of vehicles already equipped with a heading autopilot. This approach has been widely used in combination with cooperative controllers. Focusing mainly on the experimental results, this work does not present the stability proof of the inner-outer loop control structure.

This aspect is dealt with in (Morishita, 2018) and (Maurya, Morishita, Pascoal, & Aguiar, 2022). Taking advantage of nonlinear control concepts such as system's input-output stability (IOS) properties and the small-gain theorem, it was possible to characterize the closed loop stability, while obtaining quantitative relationships of the tuning parameters.

As expected, trajectory tracking and path following approaches present both advantages and disadvantages. As an attempt to mutualize the benefits of both approaches, an intermediate strategy denominated path maneuvering was conceived. In path manoeuvring, the time-dependence derived from trajectory tracking exists, but is flexible. Roughly stating, while path following focuses on the geometric task and trajectory tracking focuses on the dynamic task, path manoeuvring takes both into account. In this context, (Burger & Pettersen, 2010) developed a path manoeuvring controller, in which the behavior can be smoothly changed between both modes. Using a trajectory tracking control structure, the real time is substituted by a virtual time, for which the rate of change is set as a function of the distance between the vehicle itself and its individual virtual target.

An alternative control scheme mutualizing the advantages of PID and sliding mode control schemes is presented in (Burger, Pavlov, & Pettersen, 2009), where the use of conditional integrators is introduced. This approach inherits the robustness of integral action and sliding mode control, while avoiding their associated drawbacks such as chattering and integrator wind-up. The tuning process of the integrators is intuitive, taking advantage of the experience derived from these two well-known control methods.

Many control solutions for the motion control problem do not consider the existing input constraints, thus the associated control laws hold locally, in regions of attraction where such constraints are not violated. However, it is very difficult to characterize such regions in order to determine the possible starting positions/orientations of the vehicle.

In recent years, thanks to developments in computer technology and optimization theory, MPC has become one of the most popular control techniques also for fast dynamics applications such as motion control. Its ability to systematically handle physical constraints renders it particularly interesting to solve more challenging versions of the path following problem, while managing the previously mentioned issues (Said, 2018) and (Hung N. T., Rego, Crasta, & Pascoal, 2018).

Such approach is expected to outperform other path following strategies by pushing the actuators close to their limits. Additionally, it can easily deal with other tasks such as path planning (Shen, Shi, & Buckham, 2017) and obstacle avoidance (Hung N. , et al., 2022).

1.2.2 Model Predictive Control

The literature presents several publications reviewing MPC, covering historic developments, concepts, algorithms, recent progress and future perspectives as presented in (Garcia, Prett, & Morari, 1989), (Mayne, Rawlings, Rao, & Skokaert, 2000) and (Mayne, 2014).

Optimal control theory plays an important role in the design of modern control systems, and also in the field of applied mathematics. Its objective is the minimization of the cost of specific processes[6]. Pioneer theoretical results mainly include Bellman's principle of optimality and Pontryagin's minimum principle (Kirk, 2004).

In the late 1950s and early 1960s, the Smith Predictor (Smith, 1957), the Linear Quadratic Gaussian (LQG) / Linear Quadratic Regulator (LQR) algorithms (Kalman, 1960), the correlation of optimal control and linear programming (Zadeh & Whalen, 1962) and the RH control concept (Propoi, 1963) laid down the basis for the development of MPC (Garcia, Prett, & Morari, 1989). However, these control methods cannot handle system constraints[7] on state, output and control variables, limiting their use in practical applications[8].

Motivated by the need of the oil industry to maximize its profitability by optimizing its internal processes, the MPC concept was conceived in the late 1960s, and intensively developed through the 1970s, as a solution for the previously mentioned limitation. It is relevant to mention the predictive functional control technique proposed by Jacques Richalet and the application of the RH control concept for state-space models (Wang, 2009).

The first-generation of commercial MPC packages, dating back to the late 1970s and the 1980s, include the Model Predictive Heuristic Control[9] (Richalet, Rault, Testud, & Papon, 1978) and the Dynamic Matrix Control (DMC) (Cutler & Ramaker, 1980). In both algorithms, a dynamic model of the plant (respectively relying on impulse and step responses) is used to predict the effect of future control actions over the system outputs, and an algorithm is used to solve the open-loop optimal control problem (Garcia, Prett, & Morari, 1989). However, in both

---

[6] Or alternatively, the maximization of the return from specific processes.

[7] If the constraints are ignored in the problem formulation, the controller performance is endangered, demanding *ad hoc* fixups that also increase the commissioning costs of the system (Garcia, Prett, & Morari, 1989).

[8] The optimal solution can often be found near or on the boundary of the operational region defined by the system constraints. Consequently, it is mandatory to take them into account in order to assure the stability and performance of the control system, as well as the profitability of the controlled process.

[9] Later denominated "Identification Command" (IDCOM).

approaches, the treatment of control and output constraints is *ad hoc* (Mayne, Rawlings, Rao, & Skokaert, 2000).

This limitation was lifted in the second-generation package, with the Quadratic Dynamic Matrix Control (QDMC) (Garcia & Morshedi, 1986), where quadratic programming is used to exactly solve the constrained open-loop optimal control problem, when the system is linear, the cost is quadratic, and the control and state constraints are defined by linear inequalities. This technique also allows, if necessary, temporary violation of some output constraints, enlarging the set of states that can be properly controlled (Mayne, Rawlings, Rao, & Skokaert, 2000).

Different from these algorithms, the Generalized Predictive Controller (GPC) (Clarke, Mohtadi, & Tuffs, 1987) focused on adaptive control. Incorporating a transfer function model, this algorithm applies for SISO systems in the absence of constraints (Garcia, Prett, & Morari, 1989).

The third-generation package, dating the 1990s, considers several levels of constraints (hard, soft, ranked), provides mechanisms to recover from OCP recursive unfeasibility, addresses the issues related to time varying control structures, being able to deal with a wide range of process dynamics and controller specifications (Qin & Badgwell, 1997).

Afterwards, different kinds of MPC products with different features and improvements have been developed and marketed by a number of companies in process industries (Hashizume, 2015). However, the requirement of heavy computational burden[10] has limited MPC to applications with slow dynamics, with sample times measured in seconds or even in minutes (Wang & Boyd, 2009).

With recent developments of computer technology and optimization theory, the computational barriers have been largely lifted and MPC has become one of the few control techniques that has been receiving an increasingly interest from researchers in both the academic and industrial[11] sectors.

In this context, (Hung, Rego, Crasta, & Pascoal, 2018) developed two input-constrained nonlinear controllers, the first a Lyapunov-based control and the second a sample-data Lyapunov-Based MPC (L-MPC). The latter incorporates an additional constraint in the optimal control problem (OCP) that speeds up the convergence rate

---

[10] Associated with the online solution of the optimization problem.
[11] MPC is often cited as the **M**ost **P**opular advanced **C**ontrol method for industrial process applications. However, the PID controller is still the backbone of automatic control since it is industry proven, robust, transparent and simple, despite its inherent limitations (Wang, 2009).

of the Lyapunov function, when compared to the former. Both controllers are globally asymptotically stable, thus implying that the vehicles converge to and follow their assigned paths, regardless of their initial states. Similar approaches are found in (Budiyono, 2011) and (Steenson, et al., 2014).

However, motion control in a three-dimensional space requires the use of higher-order models which, in traditional MPC schemes, leads to computational complexity and loss of controllability. To solve this issue (Jagtap, et al., 2016) proposes to treat the horizontal and vertical motions separately and independently, replacing the initial higher-order model by two independent time-varying linearized reduced-order models. In this way, the MPC problem is formulated as two independent optimization problems.

The receding horizon (RH) principle in which MPC relies on can also be deployed to design high-performance state estimators and filters, as an alternative to the Extended Kalman Filter (EKF). Due to its relative simplicity and demonstrated efficacy, the EKF is widely used in control system applications. However, there are many barriers related to its practical implementation, some of them related to its inability to proper handle state constraints as well as its limitation to fully exploit the nonlinear internal model.

Recently, due to its inherent characteristics, the Moving Horizon Estimator (MHE) has been increasingly used as a tool to solve the state estimation problem while solving the issues previously mentioned (Haseltine & Rawlings, 2005). Additionally, according to comparative studies, MHE tends to outperform EKF also in terms of initialization, convergence and accuracy, however at the expense of computational burden (Said, 2018).

In fact, MHE can be understood as the dual of MPC and the development of both techniques has been strongly interconnected (Kuhl, Diehl, Kraus, Schloder, & Bock, 2011). As MPC, MHE is an optimization technique. It uses a series of past measurements, corrupted by noise and other inaccuracies, to produce precise estimates of unknown variables or parameters (Mehrez, 2019). The literature concerning MHE focuses mainly to UMR such the works of (Mehrez, 2019), (Brembeck, 2019) and (Jayasiri, Gros, & Mann, 2016), but a considerable number of strategies can be applied for AMV with minor adaptations.

An important aspect to point out is that MHE approach is a reformulation of the general optimization objective of the Kalman filter theory (Simon, 2010), since it can

be understood as a real-time calculable approximation of the full-information filter (Brembeck, 2019), leading to advantages such as improved estimates, greater robustness against external disturbances, poor guesses of the initial state, and tuning parameters (Haseltine & Rawlings, 2005). However, the associated price of such benefits is the computational burden required to solve the optimization problem online.

A challenging issue concerning the use of MHE refers to the definition of the arrival cost term in the OCP total cost function. This term is conceived to introduce information from past measurements into the current estimates, since the time window moves constantly. As stability and performance are strongly impacted by this term, research on this subject has gained significant momentum recently (Talla Ouambo, Boum, Imano, & Corriou, 2021).

Finally, it is important to point out that topics such as automatic obstacle tracking, and collision avoidance (COLAV) are still at early stages of development. However, preliminary results indicate that it is advantageous to tackle these issues in the MPC framework, since it is possible to consider the obstacles' motion, the evolution of the dynamic environment, and the different operational constraints. Thus, compared to other methods, it is possible to attain higher design flexibility combined with best performance (Hagen, Kufoalor, Brekke, & Johansen, 2018).

1.2.3 Formation Control Strategies

The literature concerning formation control strategies is vast, referring mainly to Unmanned Mobile Robots (UMRs) and Unmanned Aerial Vehicles (UAVs). Fortunately, a considerable number of strategies can be applied for Autonomous Marine Vehicles (AMVs) with minor adaptations (Li, Zhu, & Qian, 2014) and (Muchiri, Kamau, & Ikua, 2017).

An extensive analysis of such strategies is a laborious task since many variations can be obtained from the combination of the existing algorithms. Therefore, for practical reasons, the strategies will be grouped into four main categories: behavior-based methods, artificial potential field techniques, leader-follower schemes and virtual structure schemes (Hadi, Khosravi, & Sarhadi, 2021).

In behavior-based methods, each agent has several basic motor schemas representing different desired behaviors such as following-wall, collision and obstacle avoidance, source seeking and maintaining formation. Each motor schema generates

a vector to characterize the desired control response associated to the behavior. The resulting control action of the agent is the result of the hierarchization of the behaviors, obtained through the weighted average of the motor schema vectors. This approach is a simple and intuitive tool to achieve an adequate tradeoff between multiple competing objectives, however, due to the lack of a precise definition of the behaviors, it is difficult to formalize the problem mathematically, jeopardizing the formal proofs of convergence and stability. For that reason, this approach is normally associated with other control methods (Li, Zhu, & Qian, 2014).

In artificial potential field techniques, each agent in the formation is driven by a field of forces associated with artificial potentials assigned to its neighborhood entities (target points, other vehicles and obstacles). Each agent moves freely, subjected to attractive and repulsive forces, in a flexible geometric formation. To deal with environmental complexities, new strategies based on queues and artificial potential trenches have been proposed. In the latter, each agent is attracted to and moves along the bottom of a potential field, while achieving its relative position in the formation. These techniques inherit a natural ability to deal with obstacle avoidance and inter-agent collision, in a movable formation pattern. Different from behavior-based methods, this approach can be mathematically formalized, allowing the formal analysis of convergence and stability. However, designing potential field functions is not a straightforward task, and the classical problem of local minimum identification remains an issue to be dealt with (Li, Zhu, & Qian, 2014).

In leader-follower schemes, an agent is set to be the leader of the formation while the remaining ones are set to be the followers. The key concept is that the leader tracks a predefined referenced trajectory (sometimes given by a virtual target) and the followers track transformed versions of the leader's states, according to predefined plans. Conventionally, the information flow between agents is unidirectional, from the leader to the followers. This characteristic is particularly interesting for marine vehicles, which are subjected to underwater communication issues. The main advantage of this approach relies on its intuitiveness and simplistic implementation since the followers only need to maneuver according to the leader. However, in general, there is no feedback connection between the leader and the followers, so if the leader fails, the entire formation also fails (Li, Zhu, & Qian, 2014).

In virtual structure schemes, a rigid geometric structure is introduced as a reference and the agents act as if they were embedded particles of such structure.

The formation control is derived in three steps. The first step consists in defining the dynamics of the virtual structure. In the second step, the desired motion of the virtual structure is translated into desired motions for each agent. Finally, the third step consists in designing the individual track controllers for each agent. This approach is commonly used in spacecraft or small satellite formation flight control (Chen & Wang, 2005). Despite the simplicity to coordinate the behavior of the whole formation, the rigid body like motion of the virtual structure imposes several limitations on its potential applications. This approach is not indicated for time-varying formation patterns, subject to frequent reconfigurations. It is also not suitable for formations containing an elevated number of agents, due to the complexity induced by the inter-agent constraints. Additionally, applications requiring obstacle avoiding capacity cannot be properly addressed following this approach (Li, Zhu, & Qian, 2014) and (Xiang, 2011).

In (Ren, 2007), it is shown that the formation control algorithms previously mentioned can be unified in the general framework of consensus approach, which relies on the idea that each agent updates its synchronization state based on the synchronization states of its neighbors, so that they converge to a common value (consensus). By appropriately defining the synchronization states, and once consensus is achieved, the formation control problem is indirectly solved. Requiring only a communication topology among the agents, the main advantage of this approach concerns the simplicity of consensus control law (Olfati-Saber, Fax, & Murray, 2007) and (Gulzar, Rizvi, Javed, Munir, & Asif, 2018).

There are many other methods in formation control such as generalized coordinates, navigation-based approach, genetic algorithm, neural networks, fuzzy logic, reinforcement learning, flocking, rendezvous, cyclic pursuing, etc., (Chen & Wang, 2005), which are beyond the scope of this thesis. However, it is relevant to mention that Model Predictive Control (MPC) has recently also been adopted to obtain distributed flocking cooperative control strategies (Lyu, Hu, Chen, Zhao, & Pan, 2019).

There are no strict rules to choose the most suitable method for a given application. The designer is even free to combine several methods, as reported in (Beard, Lawton, & Hadaegh, 2001), which proposes a coordination architecture that combines leader-follower, behavior-based and virtual structure approaches, applied to multiple spacecraft formation control in deep space.

The ultimate goal of all of these strategies is to synchronize the formation. Inspired by the examples observed in nature, the synchronized motion of artificial systems assisted by active control dates to the 1980s in the academic and research domains, and to the 2000s in the commercial industry. Synchronization can be understood as a type of time conformity between systems and can be categorized into the concepts of cooperation and coordination. The choice of the synchronization strategy affects the systems behaviors (Kyrkjebø, 2007).

In cooperation, all agents are equally responsible for performing the motion paths/trajectories (group objective), while assuring the desired geometry formation (geometric objective). Since the agents must have some knowledge of the states of other agents, the information flow among them is bidirectional.

Differently, coordination requires that one agent (leader) takes the responsibility for achieving the group objective, while the other agents (followers) remain responsible only for attaining the geometric objective. The leader governs the motion of the followers, but its behavior is not influenced by them. Since the information flow is unidirectional, from the leader to the followers, the coordination strategy attenuates information flow issues (Kyrkjebø, 2007).

The degree of synchronization, ranging from strictly cooperative to strictly coordinated, determines the group behavior in case of individual faults. For example, in a strictly cooperative redundant group, if one agent fails, the group behavior is endangered. On the other hand, in a strictly coordinated redundant group, this problem does not happen.

However, the way in which the group behavior will respond to individual faults depends mainly on the control design itself. It is possible to design cooperative systems that disregard faulty agents, thus not impacting the group behavior or coordinated systems that keep a feedback connection between faulty followers and the leader, thus affecting the group behavior. Consequently, a nominally cooperative system may behave as a coordinated system in a situation of failure and vice-versa (Kyrkjebø, 2007).

Furthermore, the control scheme can be designed to reconfigure itself in case of failure. For example, if the leader fails in a cooperative control scheme, one of the remaining agents can be converted into leader (sleeping leader) to govern the motion of the group (Kyrkjebø, 2007).

The main technical issues associated with the synchronized motion of marine vehicles refer to their inherent dynamics characteristics, environmental complexity, and underwater communication constraints (Li, Zhu, & Qian, 2014).

The motion control problem of marine vehicles faces particular problems. Besides the high inertia-damping ratio, there are also difficulties related to the hydrodynamic aspects, reflected in a set of complex hydrodynamic coefficients that must be determined and taken into account in the associated formulation (Encarnação & Pascoal, 2000). However, some coefficients cannot be accurately measured or determined due to technological constraints (Li, Zhu, & Qian, 2014). Additionally, the assessed values may not hold during extreme maneuvers, when the vehicle experiences large angles of attack and sideslip, emphasizing nonlinearities and cross couplings (Aguiar & Hespanha, 2007). Consequently, control applications normally adopt simplified mathematical models, thus inheriting the drawbacks correlated to neglected dynamics (Li, Zhu, & Qian, 2014).

Another aspect that differentiates marine vehicle applications is the environmental complexity, reflected in two problems: obstacle avoidance and environmental disturbances. The former problem is commonly dealt with by behavior-based and/or artificial potential field techniques. An alternative method consists in modifying the formation structure (size and shape) when it passes through restricted areas, restoring its original configuration immediately after the passage. More recently, MPC has also been used to tackle this problem, for fixed and/or moving obstacles. Unfortunately, for the latter problem, many potential sea-proven solutions are still stagnating on theoretical stages due to its inherent complexity (Li, Zhu, & Qian, 2014).

The last issue concerns underwater communication constraints. Marine vehicles operating in synchronized mode need to exchange information such as position and velocity to accomplish the geometric task. Nowadays, underwater communications rely mainly on acoustic systems. However, underwater acoustic communications are plagued with intermittent failures, latency, and multipath effects. Additionally, they are limited in range and bandwidth. Different approaches have been proposed to overcome these constraints, most of them relying on the minimization of the information flow (Li, Zhu, & Qian, 2014) and (Gulzar M. M., Rizvi, Javed, Munir, & Asif, 2018).

Currently, from the aspect of communication technology, topics concerning marine wireless communication systems are gaining momentum, combined with key technologies of multi-agent cluster cooperation such as information fusion, mission planning and cooperative control (Ma, Liu, Zhao, & Zhao, 2022) and (Liu, Shan, Mao, & Wang, 2022).

1.2.4 Cooperative Control

Although cooperative control of AMVs dates back the early 1980s (Oh, Park, & Ahn, 2015) and (Das, Subudhi, & Pati, 2016), the migration of this application from academic to marine industry domain took place in the 2000s (Blidberg, 2001).

In this context, it is relevant to mention the pioneer ASIMOV project, a research and development effort started in 1998 with the help and support of the Commission of the European Communities, for marine data acquisition and transmission. The key concept of the project consists in the coordinated operation of an ASC and AUV (Pascoal, et al., 2000).

In this project, the cooperative control problem was firstly addressed in (Encarnação & Pascoal, 2001)[12], considering a leader-follower approach, where a slave vehicle (AUV) is forced to track the projection of the master vehicle (ASC) into the 2D nominal path. However, this strategy demands a significant amount of information exchange among the vehicles and can´t be easily generalized to more than two vehicles.

To attenuate this drawback, (Lapierre, Soetanto, & Pascoal, 2003a) proposes a leader-follower approach in which a Lyapunov-based backstepping control law steers two vehicles along identical parallel paths, while ensuring that the lateral distance among them remains constant. Executing the same path following algorithm, the leader travels along its assigned path, while the follower adjusts its speed based on the "along-path distance" gap related to the leader (the coordination variable). Consequently, only the leader "along-path distance" is required to be sent to the follower and the amount of information exchanges are kept to a minimum.

Based on the virtual structure method, (Skjetne, Moi, & Fossen, 2002) proposes a flexible backstepping-based control scheme in which the vehicles maneuver as a single unit, following a virtual Formation Reference Point (FRP) that tracks a predefined path (geometric task), complying with a predefined speed profile

---

[12] For the motion control problem, trajectory tracking and path following approaches were considered.

(dynamic task). In this case, the geometric and dynamic tasks rely on decentralized and centralized control systems, respectively.

However, as the centralized control system receives full state information of all vehicles and returns the path and speed information for each vehicle, the volume of communicated real-time signals is not irrelevant. This drawback is solved in (Skjetne, Ihle, & Fossen, 2003), where a decentralized dynamic control system was conceived to coordinate each vehicle based only on the scalar path variables of other vehicles, thus drastically reducing the volume of communicated signals.

Since the information flow plays an essential role in the formation control problem, it is necessary to define what information must be exchanged and how to enable this exchange. Concerning the first aspect, the definition of the coordination (or synchronization) variable does not have a straightforward answer, since its choice depends on path characteristics (Ghabcheloo, Pascoal, Silvestre, & Kaminer, 2005) and (Ghabcheloo, Pascoal, Silvestre, & Kaminer, 2007)[13]. Concerning the second aspect, a consecrated tool used to model the inter-vehicle communication topology is the Graph Theory, involving the elegant concept of Graph Laplacian, a matrix representation of the graph associated with a given communication network.

It is relevant to mention that the relationship between the location of the Laplacian eigenvalues and the graph structure can be used to identify desirable and undesirable formation interconnection topologies based on a Nyquist-like stability criterion as presented in (Fax & Murray, 2002) and (Fax & Murray, 2004). An overview of networked control systems is presented in (Zampieri, 2008).

In 2006, the 6th framework of the European Commission (FP6) launched the multinational GREX[14] project, entitled "Coordination and Control of Cooperating Heterogeneous Unmanned Systems in Uncertain Environments". Its main objective was to develop theoretical methods and practical tools for multiple vehicle cooperation. Emphasis was placed on the coordination of marine vehicles, the promising main tool for exploration and exploitation of the ocean (European Commission, 2008), (MC Marketing Consulting, n.d.), (Aguiar, et al., 2009), (Kalwa, 2009) and (Yao, 2013).

---

[13] In these references, the concept of path re-parametrization was introduced in applications of multiple wheeled vehicles following parallel straight lines and scaled circumference paths.
[14] Latin word for "herd".

In the field of marine geosciences, it is relevant to mention the EC WiMUST (Widely scalable Mobile Underwater Sonar Technology) project, supported by the European Commission under the Horizon 2020 Framework Program. Its main goal is to conceive and design an intelligent team of cooperative AMVs, acting as intelligent sensing and communicating nodes of a reconfigurable moving acoustic network, to perform geophysical and geotechnical acoustic surveys at sea (WiMUST Project, 2019). Under this project, (Abreu, Morishita, Pascoal, Ribeiro, & Silva, 2016) developed a cooperative controller for a fleet of streamer-vehicle systems.

For marine vehicles, a relatively common practice to solve the cooperative deployment problem is the adoption of a segregated control architecture, unfolded in two control layers. The lower layer is responsible for the individual motion control of the vehicles, while the higher layer is in charge of the collective motion control of the entire formation. This strategy is adopted in (Ghabcheloo, et al., 2009), by combining a path following controller and a consensus-based cooperative controller. In the consensus-based framework, the control laws adjust the vehicles' speeds around their nominal values to achieve the desired formation pattern (synchronization). Even considering the occurrence of time delays, this reference is based on the unrealistic premise that each vehicle transmits continuously its coordination state to a subset of other vehicles, according to a predefined communication topology.

This limitation is lifted in (Vanni, 2007), (Vanni, Aguiar, & Pascoal, 2007), (Aguiar & Pascoal, 2007a) and (Vanni, Aguiar, & Pascoal, 2008) by incorporating a logic-based communication module at the cooperative controller level. This architecture considers the fact that communication does not occur in a continuous manner[15], has an associated cost, and is subjected to non-homogeneous time delays. Essentially, each vehicle estimates, in a synchronized way, its own state[16] and the states of the other neighboring vehicles. When the difference between the actual and the estimated own states exceeds a certain threshold, the vehicle transmits its synchronization parameter to allow the other vehicles to update their estimates. Consequently, communication occurs asynchronously at discrete instants of time.

---

[15] It is important to quote that continuous communication is undesirable, and perhaps even not necessary in practice.
[16] Self-state estimation.

Another problem concerning underwater communication is data loss. This issue is properly addressed in (Rout & Subudhi, 2016), where an event-based communication algorithm, based on a continuous-discrete extended Kalman Filter (CD-EKF), is conceived to solve the problem of lack of information during communication failures. Using a Lyapunov-based backstepping approach in a leader-follower framework, when data loss occurs, the filter algorithm is activated for each follower vehicle to estimate the states of the leader.

Thus far, all the listed references considered only fixed reference paths. In (Jain, Alessandretti, Aguiar, & de Souza, 2018) the reference paths are time-varying, since the inertial reference frame moves. This approach is particularly interesting for applications such as convoy protection, underway replenishment, source seeking and autonomous landing on moving platforms. Additionally, the decentralized cooperative controller incorporates a self-triggered algorithm to reduce the frequency of communication in relation to traditional periodic transmission methods. However, practical issues such as communication losses and time delays are not considered.

In (Hung & Pascoal, 2018), a decentralized consensus-based cooperative controller was combined with the sampled-data L-MPC developed in (Hung, Rego, Crasta, & Pascoal, 2018). This strategy proved to be capable of handling practical constraints on vehicle inputs and the inter-vehicle communication topology network. The cooperative control module also incorporates an event triggered communication (ETC) mechanism to minimize the information flow among vehicles.

Besides its use in motion control problems, MPC has also been employed for marine cooperative applications. In (Lyu, Hu, Chen, Zhao, & Pan, 2019), MPC is used to obtain a distributed flocking control strategy for a fleet of AMV, with limited communication range.

In the domain of estimation, differently from MPC, the use of MHE in cooperative applications is still at early stages of development. As an example, in (Wang, Chen, Gu, & Hu, 2014), MHE is used to solve the cooperative localization problem of AUVs, based on range measurements from a single surface mobile beacon.

Nevertheless the advances in many modern control techniques such as backstepping and MPC, consensus still remains a popular strategy to solve cooperative control problems due to its simplicity and inherent ability to deal with inter-vehicle communication issues (Yu, Zeng, & Guo, 2022).

1.3 Objectives

The main objectives of this thesis are to design a path following controller fully based on the RH control concept, and to integrate it into the structure of an upper-level cooperative consensus-based controller. Additionally, it is also intended to investigate the closed-loop stability and robustness of the entire system through numerical simulations.

Due to the intricate nature of the optimization problem in which the RH concept is based, an in-depth mathematical analysis of stability and robustness is not dealt with in this thesis. This analysis is envisaged for future research, taking advantage of concepts such as Input-to-State-Stability (ISS) and Input-to-Output-Stability (IOS) combined with the small gain theorem (Appendix A).

1.3.1 Problem Statement

Under the perspective of systems engineering (NASA, 2016), the cooperative path following control problem can be stated considering the following requirements and constraints:

A) Requirements:

- **R1:** To steer a group of underactuated[17] AMV along given spatial paths, without time specification requirements (path following control problem)…

- **R2:** …while holding a desired time-varying inter-vehicle formation pattern (cooperative control problem).

B) Constraints:

- **C1:** The vehicles are collectively coupled.
- **C2:** The underwater inter-vehicle communications are plagued with intermittent failures, latency and multipath effects.
- **C3:** The vehicles are subjected to environmental disturbances.
- **C4:** The vehicles must avoid obstacles.
- **C5:** The vehicles must not collide before reaching their reference paths.

---

[17] Differently from fully actuated systems, the motion control of underactuated systems is still an active research topic due to challenges related to the design of stabilizing control law which combines performance and stability (Das, Subudhi, & Pati, 2016).

Thus, since the vehicles are collectively coupled (C1), they must communicate with each other to accomplish the common task. However, the underwater communications are subjected to severe restrictions (C2). In order to solve this paradox, it is mandatory to adopt a new control paradigm departing from classical centralized control strategies, in which a single controller possesses all the information required to achieve the desired control objectives (Ghabcheloo, et al., 2009).

1.3.2 Proposed Control Strategy

The proposed control strategy considers two distinct layers of implementation, as shown in Figure 1-9, to solve the cooperative path following control problem of marine vehicles. The lower-level layer, comprising the path following controller, is responsible for controlling the individual motion of the vehicles, while the higher-level layer, encompassing the consensus-based cooperative controller, is in charge of controlling the whole formation.

Figure 1-9: Control levels
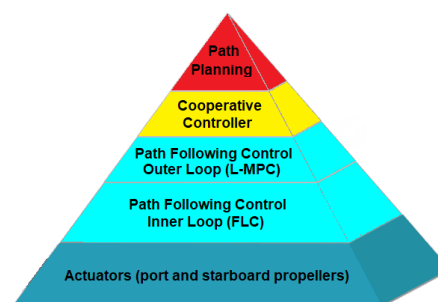
(From Author)

1.3.2.1 Individual Motion Control (lower layer)

The path following controller design is decoupled in an inner-outer loop structure. The outer loop acts as a guidance system, calculating and issuing the speeds required to drive the vehicle up to its predefined speed parameterized path (kinematic task). The inner loop acts as a speed tracker system, assuring that the propulsion system of the vehicle supplies the forces and moments required to attain the required speeds (dynamic task).

This architecture presents advantages for practical implementation. Since the kinematic and dynamic tasks are addressed independently, simpler control laws can be obtained, and the tuning process is simplified due to fast-slow temporal scale separation. Additionally, since the loops are decoupled, it is possible to use the same

outer loop in a wide range of vehicles already equipped with factory-assembled inner loops. (Maurya, Aguiar, & Pascoal, 2009). However, the control laws are more subjected to smoothness and saturation issues (Vanni, 2007).

The outer loop is fully based on the RH concept[18], comprising a Lyapunov-Based Model Predictive Control (L-MPC) and a Moving Horizon Estimator (MHE). This technique, initially conceived in the 1960s mainly for the petrochemical industry, is nowadays successfully used in different segments of the industry (Garcia, Prett, & Morari, 1989), (Wang, 2009) and (Seborg, Edgar, Mellichamp, & Doyle III, 2016).

This success is intrinsically linked to its specific ability to systematically handle practical constraints during the design and implementation phases of the system. This aspect results in transparent performance criteria specifications, avoiding *ad hoc* fixups which compromise the performance of the control system and increase its commissioning costs (Garcia, Prett, & Morari, 1989).

Besides this aspect, the capability to deal with nonlinear complex dynamics, parametric uncertainties, and external disturbances make it an interesting technique for the motion control of marine vehicles. The list of advantages and disadvantages of this technique is summarized as follows (Garcia, Prett, & Morari, 1989), (Wang, 2009) and (Seborg, Edgar, Mellichamp, & Doyle III, 2016):

Advantages:
- It relies on a multivariable control theory;
- The controller design is simple and directly related to the physics of the problem;
- Its implementing time is much shorter than other competing advanced control methods;
- It easily handles with complicated dynamics;
- It has an inherent ability to handle, easily and systematically, the applicable constraints;
- It has anticipation capability[19], allowing the controller to make better decisions at the current time to account for future possibilities;
- The tuning process is simplified, since the performance parameters of the controller are strongly related to well understood physical aspects;

---

[18] It includes also a state observer to provide estimates of the ocean current's velocity.
[19] Similar to feedforward control.

- It has the ability to manage different levels of the control hierarchy;

- It systematically handles multi-rate measurements and missed measurement points; and

- Its maintenance is simple. Modifications in the model or in the control specifications do not require a complete redesign of the system. If the plant changes, "on the fly" reconfiguration is sometimes possible.

Disadvantages:

- The characterization of the closed-loop system stability;

- The performance of the control law;

- The choice of the optimization horizon length; and

- The online numerical implementation.

The inner loop (which is normally supplied as a factory-assembled component of the vehicle) was conceived using the feedback linearization technique.

1.3.2.2 Formation Control (higher layer)

The formation control is based on a consensus-based decentralized cooperative controller. In this approach, the decision-making process is assigned directly to the vehicles, instead of a centralized single global controller.

Essentially, the vehicles exchange information over a communication network in order to achieve agreement (consensus) regarding a certain variable of interest. The main advantages and disadvantages are listed as follows (Olfati-Saber, Fax, & Murray, 2007):

Advantages:

- Control law simplicity;

- Less stringent communication requirements;

- Robustness; and

- Scalability.

Disadvantages:

- Limited to enforce desired behaviors; and

- General location issue (only relative position).

The proposed control architecture reflecting the adopted strategy is presented in Figure 1-10.

Figure 1-10: Proposed control strategy
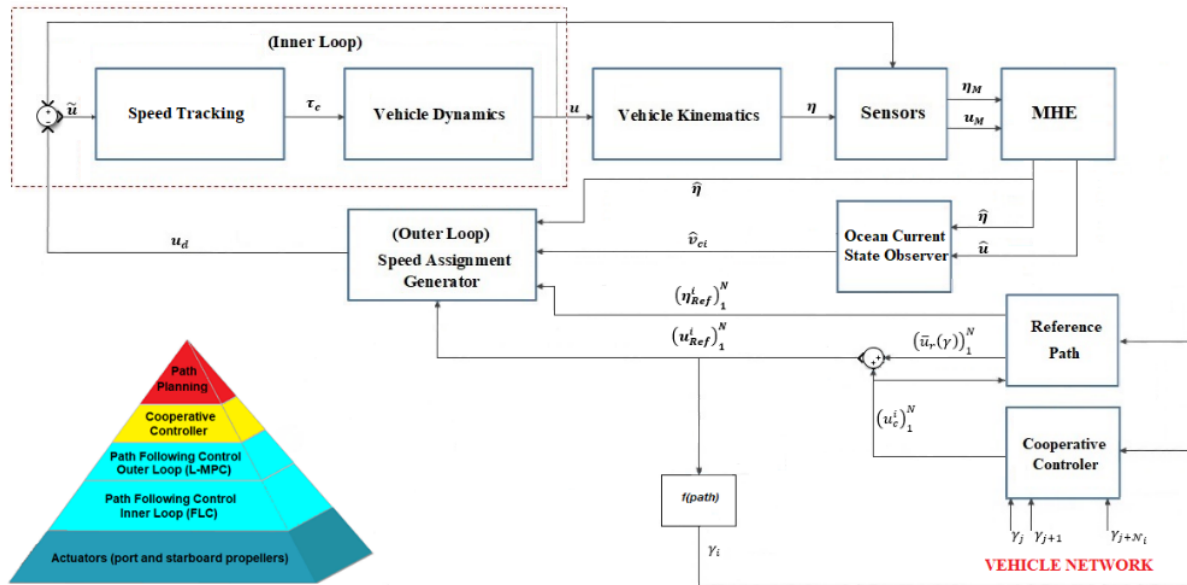
(From Author)

1.3.3 Application Case

The application case intends to reproduce three mission scenarios envisaged by the GREX project[20], consisting in the simultaneous operation of ASCs and/or AUVs performing a series of coordination tasks such as Cooperative Path Following (CPF), Formation Manoeuvres (FM), and Cooperative Line of Sight Target Following (CLOST).

In Cooperative Path Following (CPF), the vehicles run their own tracks while adjusting their speeds to reach the desired formation pattern.

If the pattern is time-varying, the problem is categorized as Formation Maneuvers (FM)[21].

Differently, in Cooperative Line of Sight Target Following (CLOST), the formation receives the location of a target through an acoustic channel and tracks it, while keeping the desired geometric pattern.

---

[20]The GREX project was launched in June 2006 within the 6th framework programme of the European Union. It´s main objective was to create conceptual and practical techniques to coordinate a swarm of diverse, heterogeneous physical robotic vehicles working in cooperation to achieve a defined practical goal in an optimized manner. Emphasis was placed on the coordination of marine vehicles, the promising main tool for the exploration and exploitation of the ocean (European Commission, 2008) and (MC Marketing Consulting, n.d.) .
[21] Also referenced as "Go to Formation".

Once such definitions are posed, the current thesis will consider three possible mission scenarios, comprising each type of task, respectively:

1.3.3.1 Scenario 1 (CPF): Quest for Hydrothermal Vents

Deep-water hydrothermal vents can be understood as natural plumbing systems that transport heat and chemicals from the interior of the Earth to the ocean, regulating its chemistry. Marine geologists and biologists have acquired considerable knowledge about such vents and their associated ecosystems and chemosynthetic life forms.

Besides their importance for the biotechnological industry, the vents also contain valuable clues about the evolution of life on Earth (Aguiar, et al., 2009). This subject also concerns the promising deep-water mining industry, since valuable mineral deposits are supposed to exist on the seafloor near hydrothermal vents.

The mission scenario for the *"Quest of Hydrothermal Vents"* (Figure 1-11) consists in the deployment of AUVs equipped with methane sensors, capable of cooperatively computing the spatial estimates of the methane concentration gradient. Based on such data, the formation heads towards the region of higher concentration until finding the vent source (Aguiar, et al., 2009).

Figure 1-11: Mission 1 – Quest for hydrothermal vents
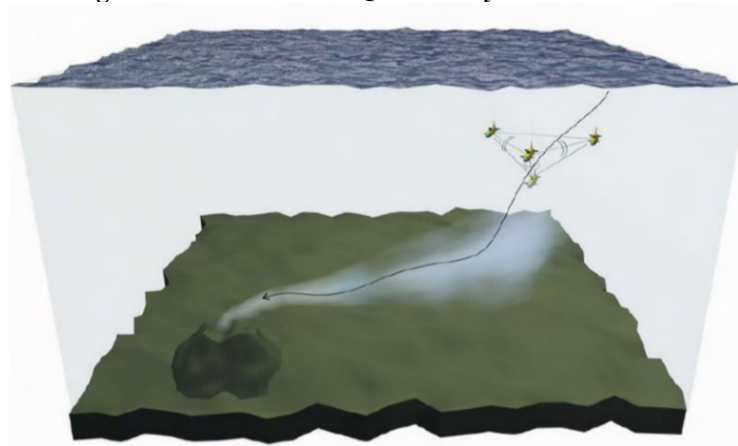
(Aguiar, et al., 2009)

1.3.3.2 Scenario 2 (FM): Marine Habitat Mapping

Mapping the marine environment in terms of biological life composition and distribution, bathymetry and seabed characteristics are essential to understand the marine habitats and to establish sensible approaches aiming for the conservation of such habitats and the rational and sustainable exploitation of the sea resources.

This subject is receiving increasing attention worldwide since guidelines, policies and directives for the study and preservation of marine environment strongly rely on the mapped data (Aguiar, et al., 2009).

The mission scenario for *"Marine Habitat Mapping"* (Figure 1-12) consists in an ASC connected to a ROV through a thin umbilical for fast data transmission. The ASC executes lawn-mowing maneuvers on the surface, followed by the ROV in a proper depth. The ROV transmits pictures of the seabed back to the support ship through a radio link installed on the ASC.

Once an interesting pattern on the seabed is identified by the scientific crew in the support ship, two dormant AUVs (on the seabed and/or at the surface) are activated[22] and dispatched to the spotted site in order to map the surrounding region. Meanwhile, the ASC/ROV continue to execute the lawn-mowing manoeuvres, searching other sites of interest (Aguiar, et al., 2009).

Figure 1-12: Mission 2 – Marine habitat mapping
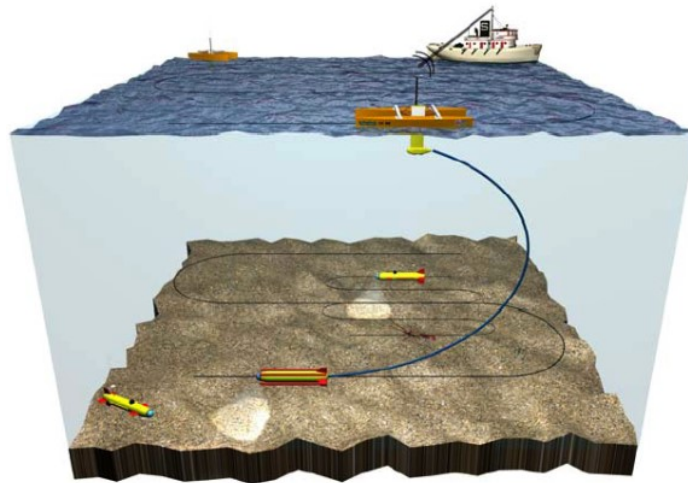
(Aguiar, et al., 2009)

1.3.3.3 Scenario 3 (CLOST): Fish Data Download

The use of passive and active telemetry devices to tag marine animals with data collecting devices is a practice that has been widely used by marine scientists in research concerning the dispersal, spawning dynamics and thermoregulatory mechanisms of such animals.

All these topics can be contextualized in the general framework of spatial management of marine living resources. Critical impacts include the use of spatial

---

[22] Via an acoustic communication link installed onboard the ASC.

behavior in fisheries stock assessment and the design of marine protected areas (Aguiar, et al., 2009).

The mission scenario for *"Fish Data Download"* (Figure 1-13) consists in the deployment of two ASCs equipped with acoustic receivers[23] and one AUV. While navigating in cooperative formation, the ASCs sweep the water column and search for sounds emitted by an acoustic tag.

Once the tag is detected and marked, one ASC communicates its position to the AUV which starts to track it. Once the fish data download task is concluded, the AUV manoeuvres back to the vicinity of the steadily moving ASCs to wait for further instructions (Aguiar, et al., 2009).

Figure 1-13: Mission 3 – Fish data download
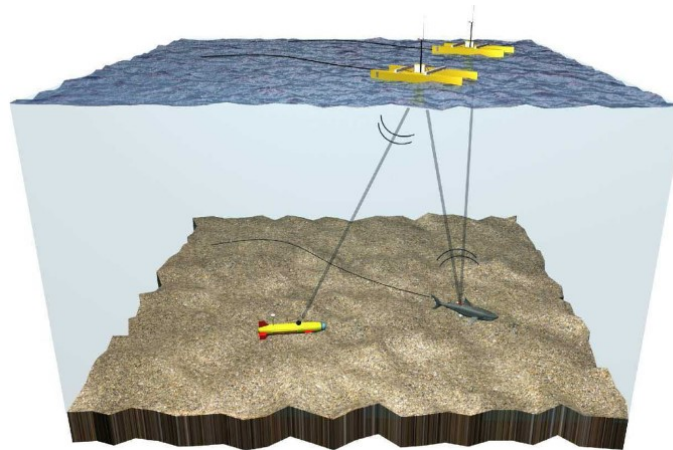
(Aguiar, et al., 2009)

1.4 Thesis Contributions

1.4.1 Contributions

The RH concept (MPC) is a powerful framework for solving a broad spectrum of control problems. Considered by many engineers as the **M**ost **P**opular **C**ontrol technique, its popularity derives from its ability to systematically handle multivariable constrained systems.

Besides the considerable progress achieved in recent years, this technique still suffers from a gap in the characterization of closed-loop stability and robustness for marine control systems. Despite the implicit nature of the optimization procedure, the intricate dynamics[24] of the vehicles combined with the restrictions imposed by the

---

[23] Using more than one ASC, the position of the tags can be determined more precisely.

[24] Characterized by a high inertia-damping ratio.

marine environment render this issue particularly challenging. This problem becomes even more noticeable when MPC is used in combination with other controllers and/or state observers, sometimes at different architectural levels, such as in cooperative applications.

The first contribution of this thesis is to design a Globally Asymptotically Stable (GAS) path following controller, fully based on the RH control concept. The control problem is solved by a sampled-data L-MPC (guidance system) combined with a feedback linearization controller (speed tracker system), in an inner-outer loop structure. The estimation problem is solved by an MHE.

The key point concerning GAS characterization is the incorporation of a contractive constraint in the L-MPC OCP formulation, derived from a GAS reference controller. This approach suppresses the need to incorporate a terminal cost and a terminal set in the associated OCP.

The second contribution, strictly linked to the main goal of this thesis, is to incorporate the path following controller in a distributed upper-level consensus-based cooperative controller, while pushing forward the numerical investigation related to the system closed-loop stability and robustness, in order to reduce the previously mentioned gap.

1.4.2 Limitations

The control system developed in this thesis is limited to the case of bidirectional communication, in the absence of time delays (latency) and information (data) loss. Additionally, it does not incorporate a module that avoids inter-vehicle collisions before reaching the reference trajectories, or during obstacle avoidance maneuvers.

1.5 Thesis Organization

This section provides a roadmap of this thesis in order to facilitate its reading and comprehension.

Chapter 1 initially introduces the thesis motivation and the associated literature review. Just after, it unfolds the thesis objectives by considering the problem statement, the proposed control strategy, and the application case. Additionally, it points out the thesis contributions, as well as its structural organization.

Chapter 2 reviews the fundamentals of the RH principle applied for control and estimation (MCP/MHE), presents the basic formulation applied to MIMO linear systems, and introduces some consideration concerning stability and robustness.

Chapter 3 presents the mathematical model of the AMV (AUV and ASC). The model is initially deduced for six degrees of freedom and then, after assuming some simplifying hypothesis, is reduced to three degrees of freedom. The chapter closes with the presentation of the reference vehicles to be used in the numerical simulations.

Chapter 4 develops the path following controller, decoupled in an inner-outer loop structure, combining a L-MPC (guidance system) and a feedback linearization controller (speed tracker system). This module also encompasses an MHE to provide noise attenuated estimates of position/heading and speed measurements. Additionally, the system comprises a state observer to estimate the ocean current velocity. Representing the lower level of the control architecture, this module is responsible for controlling the individual motion of the vehicles.

Chapter 5 develops the cooperative controller, designed based on consensus and Lyapunov theories. The controller also incorporates an event-based communication algorithm to assure that the inter-vehicle communication occurs on a discrete basis, only when strictly necessary. Additionally, it updates the formulation of the L-MPC OCP for cooperative application. Representing the higher level of the control architecture, this module is responsible for controlling the collective motion of the vehicles (formation).

Chapter 6 presents the numerical simulations performed to verify and validate the designed control system. This process is conducted on an incremental basis, considering a bottom-top approach (from the L-MPC based path following controller to the consensus-based cooperative controller).

Chapter 7 consolidates the conclusions obtained in the previous chapters and presents recommendations for future research.

Chapter 8 lists the reference bibliography.

Appendix A presents the mathematical tools and definitions required to support the reading of the main text, presenting topics concerning nonlinear system theory and graph theory.

Appendix B consolidates the numerical data used in the simulations (vehicle parameters and control gains).

2   PRELIMINARIES ON THE RECEDING HORIZON PRINCIPLE

This chapter presents a brief overview of the Receding Horizon (RH) control concept, encompassing MPC and MHE techniques. The basic formulation is reproduced[25], and some considerations about stability and robustness are presented. The key concept of MPC (MHE) is to predict, through a model, the future (the past) behavior of a system and select the best control action (the best state trajectory that fits the considered measurements window), according to a predefined optimization problem, while dealing systematically with constraints. Since both approaches are conceptually similar[26], this chapter will focus, without loss of generality, on the MPC framework.

2.1   General Overview

Essentially, the MPC framework has three stages: prediction, online optimization and control (RH implementation). A typical block diagram[27] is presented in Figure 2-1. An explicit dynamic model of the process/plant predicts its future behavior[28], and an optimization algorithm uses this information to calculate the best control sequence, according to a predefined Optimal Control Problem (OCP).

Figure 2-1: MPC basic block diagram
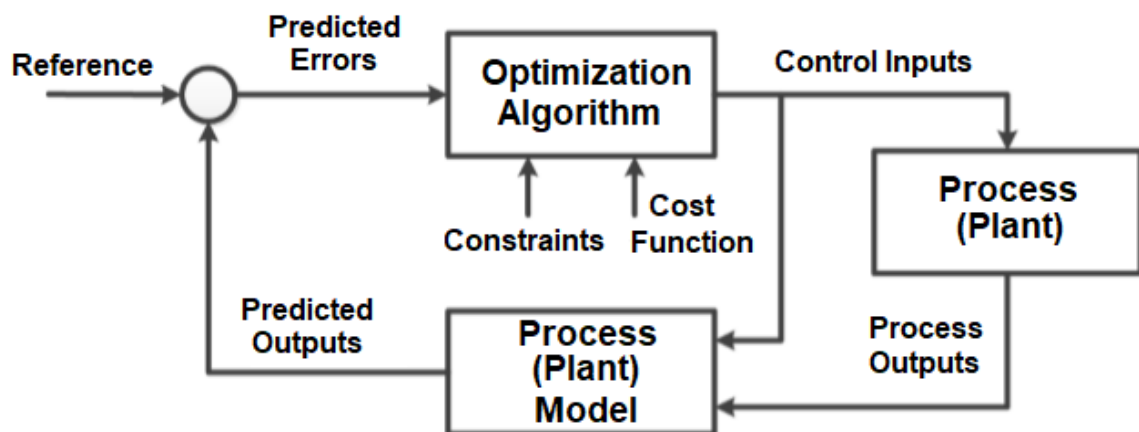
(From Author)

---

[25] A full derivation of the algorithm is presented in (Wang, 2009).
[26] MHE can be understood as a MPC deployed in the past instead of the future.
[27] In the literature, different configurations can be found, however the prediction model and the optimization algorithm are common to all of them.
[28] The behavior of the system is characterized by its state and output vectors.

2.2   The Receding Horizon Concept

The calculation of the best control sequence relies on the RH principle, in which the current control action is obtained by solving online, at each sampling instant, a finite horizon open-loop OCP, taking the current state of the plant as the initial state.

For the Figure 2-1 structure, the OCP considers N elements of predicted errors (the prediction horizon) as input data and yields an optimal control sequence of N_c elements (the control horizon), with $N_c \leq N$. Only the first control of this sequence is applied to the plant. This procedure is then repeated for future sampling times, resulting in a sampled data closed-loop feedback control law (Mayne, Rawlings, Rao, & Skokaert, 2000) and (Murray, et al., 2002).

Formally, consider a general discrete nonlinear system:

$$x(k + 1) = f\big(x(k), u(k)\big), \quad x(0) = x_0$$

where $f: \mathbb{R}^n x \mathbb{R}^m \to \mathbb{R}^n$ is the vector containing the system dynamics and x_0 is the system initial state.

Without loss of generality, the origin is assumed to be the equilibrium point, and the control objective is to assure that this point is GAS. Thus, the finite horizon OCP is defined as follow[29]:

$$\min_{u} \left[J(x, u) = \sum_{k=0}^{N-1} l\big(x(k), u(k)\big) + F(x_N) \right]$$

$$s.t$$

$$x_u(k + 1) = f\big(x_u(k), u(k)\big)$$

$$x_u(0) = x_0$$

$$x_N \in \chi_f$$

$$x_u(k) \in \mathbb{X}, \ \forall \, k \in [0, N-1]$$

$$u(k) \in \mathbb{U}, \ \forall \, k \in [0, N]$$

---

[29] Ideally, the OCP should be solved considering an infinite horizon, however it is not possible since it would lead to an "ill-behaved" cost function J. A customary practice is to truncate it up to a maximum number of samples N, and to consider, for $k > N$, the infinite horizon cost $F(x_N)$, starting from state x_N.

where $J(x, u)$ is the cost (or value) function, $l(x, u)$ is the stage (or running) cost[30], $F(x_N)$ is the nonnegative terminal cost[31] that penalizes the state attained at the terminal sample, and χ_f is the terminal set associated to the terminal constraint.

The compact sets $\mathbb{X}$ and $\mathbb{U}$ represent the system constraints on the states and on the controls, respectively.

The RH control concept is summarized as follow:

- Step 1: Sense the initial condition state vector x_0;

- Step 2: At the first sampling instant, compute a finite-time optimal trajectory x considering the initial condition state vector x_0, resulting in the solution curve $u(k)$, $k \in [0, N]$;

- Step 3: Only the first set of elements of $u(k)$ is implemented as a control input; and

- Step 4: At the next sampling instant, repeat Step 1 considering the plant state vector as the new initial condition state vector[32].

Many aspects must be considered when applying the RH concept. The sampling time must be long enough for step 2 to find an optimal trajectory. Second, the time window used in step 2 should be long enough to benefit from predictive feedforward, but not too long to make computational time exceed the sampling time. Third, for a finite-time optimal control problem, the terminal cost must be close to the optimization problem's value function, otherwise the system may not converge properly. Finally, the optimization method must be reliable[33]. Due to these aspects, any control/estimation technique based on the RH principle is difficult to be mathematically analyzed (Hauser, 2020).

For didactical purposes, Figure 2-2 and Figure 2-3 (Mehrez, 2019) reproduce the RH concept implementation for MPC and MHE, respectively.

---

[30] The designer is free to set the stage cost according to the control objectives. For example, if the objective is to penalize state errors and control efforts, one could set $l(x, u) = \left\| x_{u_d} - x_{ref} \right\|_Q^2 + \left\| u_d - u_{ref} \right\|_R^2$, where Q and R are ponderation matrices.

[31] As previously stated, the infinite horizon cost starting at x_N.

[32] MPC computes an open-loop trajectory to obtain a closed-loop feedback control law by means of the repeated replanning.

[33] Failures in step 2 can be tolerated to some extent simply by using the previous trajectory segment, but to achieve good performance Step 2 should succeed regularly.

Figure 2-2: RH concept for MPC

Single input single output simple example

$$x(k+1) = f(x(k), u(k))$$

- At **decision instant** k, measure the state $x(k)$
- Based on $x(k)$, compute the (**optimal**) **sequence of controls** over a **prediction horizon** N:

$$u^*(x(k)) := (u^*(k), u^*(k+1), \ldots u^*(k+N\text{-}1))$$

- **Apply** the control $u^*(k)$ on the sampling period $[k, k+1]$.
- Repeat the same steps at the next decision instant

(Mehrez, 2019)

Figure 2-3: RH concept for MHE

Disturbed SISO simple example

$$x(k+1) = f(x(k), u(k)) + v_x$$
$$y(k) = h(x(k)) + v_y = x(k) + v_y$$

- At a certain time step k, acquire past measurements over a **window** of size N_{MHE}.

- Find the **best** state trajectory that best fit the considered window of measurements.

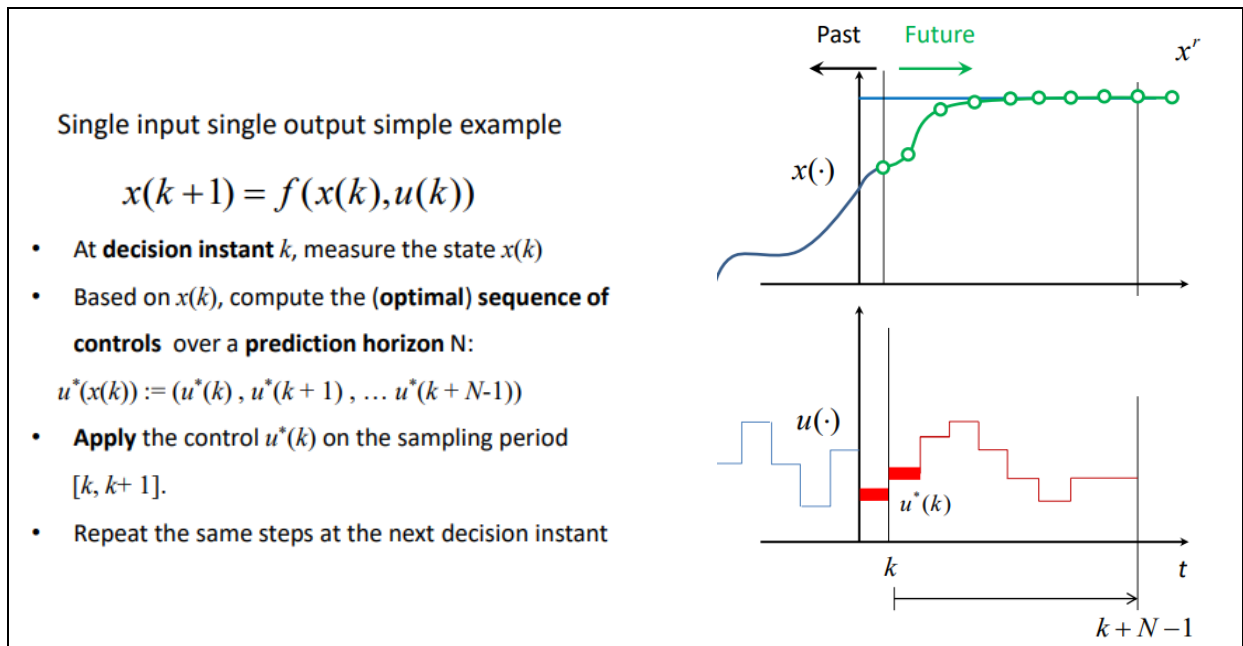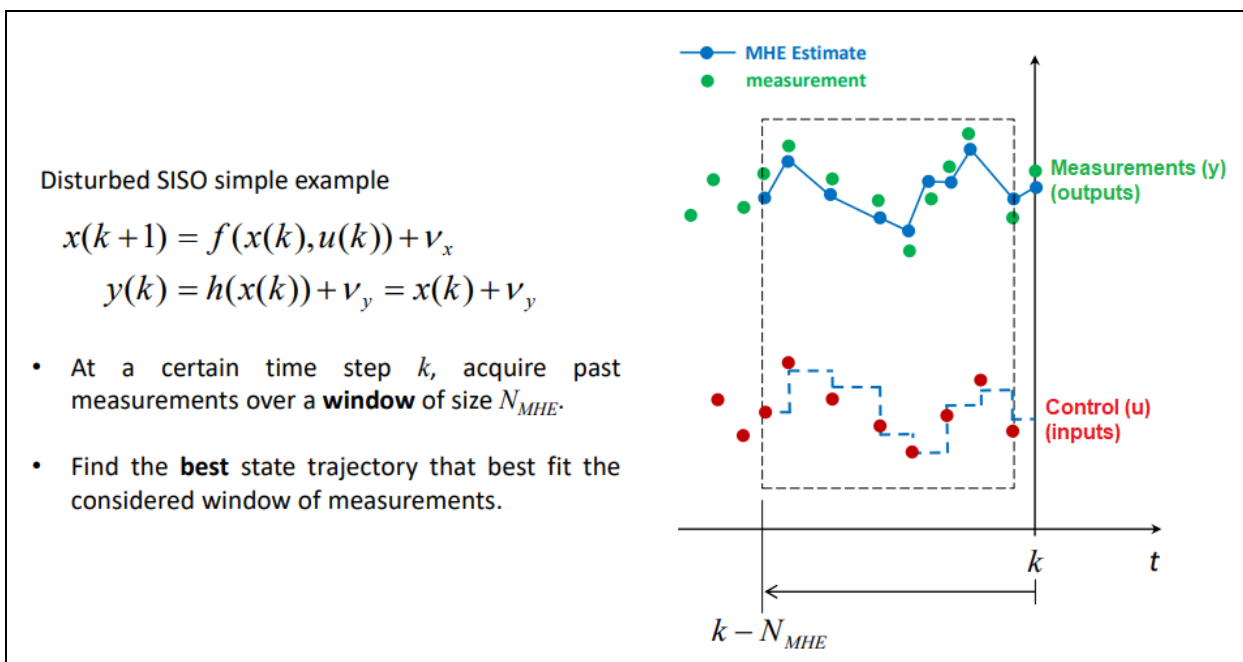(Mehrez, 2019)

2.3   MPC Formulation

For didactical purposes, this item introduces the MPC concept for linear MIMO systems, based on (Wang, 2009). However, without loss of generality, it can be extended for nonlinear systems[34].

---

[34] Linear or nonlinear MPC is linked to the characteristics of the internal prediction model.

2.3.1 Prediction Model

The first step in MPC design consists in formulating its internal plant model. For a given plant with m inputs, q outputs ($q \leq m$) and n states, the state-space model written on discrete basis is given by:

$$\boldsymbol{x_m}(k + 1) = A_m \boldsymbol{x_m}(k) + B_m \boldsymbol{u}(k) + B_d \boldsymbol{\omega}(k) \tag{2.1}$$

$$\boldsymbol{y}(k) = C_m \boldsymbol{x_m}(k) \tag{2.2}$$

where $A_m \in \mathbb{R}^{n \times n}$, $B_m \in \mathbb{R}^{n \times m}$, $C_m \in \mathbb{R}^{q \times n}$ are the system matrices, $\boldsymbol{u} \in \mathbb{R}^m$ is the vector containing the input (or manipulated) variables, $\boldsymbol{y} \in \mathbb{R}^q$ is the vector containing the plant outputs and $\boldsymbol{x} \in \mathbb{R}^n$ is the state vector[35]. Furthermore, a sequence of integrated zero-mean white noise is used to construct the disturbance vector $\boldsymbol{\omega} \in \mathbb{R}^n$, which is multiplied by an appropriate matrix $B_d \in \mathbb{R}^{n \times n}$. The incremental variation of this vector is given by:

$$\epsilon(k) = \boldsymbol{\omega}(k) - \boldsymbol{\omega}(k - 1) \tag{2.3}$$

Equation (2.1) can be written in a one-time step backwards as:

$$\boldsymbol{x_m}(k) = A_m \boldsymbol{x_m}(k - 1) + B_m \boldsymbol{u}(k - 1) + B_d \boldsymbol{\omega}(k - 1) \tag{2.4}$$

To incorporate integral action into the MPC algorithm, the design model must embed an integrator on its structure. The first step to carry out this task consists in defining the state and input vectors on an incremental basis:

$$\Delta \boldsymbol{x_m}(k) = \boldsymbol{x_m}(k) - \boldsymbol{x_m}(k - 1) \tag{2.5}$$

$$\Delta \boldsymbol{u}(k) = \boldsymbol{u}(k) - \boldsymbol{u}(k - 1) \tag{2.6}$$

By subtracting (2.4) from (2.1) yields:

$$\Delta \boldsymbol{x_m}(k + 1) = A_m \Delta \boldsymbol{x_m}(k) + B_m \Delta \boldsymbol{u}(k) + B_d \boldsymbol{\varepsilon}(k) \tag{2.7}$$

---

[35] In the RH control concept, it is assumed that the input $\boldsymbol{u}(k)$ does not affect the output $\boldsymbol{y}(k)$ at the same time, thus, $D_m = 0$ in the plant model.

Associating the output $y(k)$ to the incremental state variable $\Delta y(k)$, yields:

$$\Delta y(k+1) = y(k+1) - y(k) \tag{2.8}$$

Considering (2.2) and (2.7), the following equation is obtained:

$$\Delta y(k+1) = C_m \Delta x_m(k+1) = C_m A_m \Delta x_m(k) + C_m B_m \Delta u(k) + C_m B_d \varepsilon(k) \tag{2.9}$$

By replacing (2.9) into (2.8), the resulting equation can be lumped together with (2.7), resulting in the following state-space description:

$$\begin{bmatrix} \Delta x_m(k+1) \\ y(k+1) \end{bmatrix} = \begin{bmatrix} A_m & 0^T \\ C_m A_m & I \end{bmatrix} \begin{bmatrix} \Delta x_m(k) \\ y(k) \end{bmatrix} + \begin{bmatrix} B_m \\ C_m B_m \end{bmatrix} \Delta u(k) + \begin{bmatrix} B_d \\ C_m B_d \end{bmatrix} \varepsilon(k) \tag{2.10}$$

$$y(k) = \begin{bmatrix} 0 & I \end{bmatrix} \begin{bmatrix} \Delta x_m(k) \\ y(k) \end{bmatrix} \tag{2.11}$$

where $0 \in \mathbb{R}^{q \times n}$ and $I \in \mathbb{R}^{q \times q}$. By defining the new state vector $x \in \mathbb{R}^{n+q}$:

$$x(k) = [\Delta x_m(k)^T \quad y(k)^T]^T \tag{2.12}$$

equations (2.10) and (2.11) can be written as:

$$x(k+1) = Ax(k) + B\Delta u(k) + B_\varepsilon \varepsilon(k) \tag{2.13}$$
$$y(k) = Cx(k) \tag{2.14}$$

where A, B and C are matrices corresponding to the forms given in (2.10) and (2.11). The triplet (A, B, C) characterizes the augmented model to be used in the MPC design.

It is important to mention that controllability and observability are prerequisites for the augmented system, especially for unstable dynamics. While the former is essential to assure the closed-loop control performance, the latter is a precondition to assure the feasibility of the state observer design. However, if only closed-loop

stability is a matter of concern, these conditions may be relaxed to stabilizability and detectability, respectively.

Once the mathematical model is deduced, it is possible to calculate the predicted plant outputs, considering the future control inputs as the adjustable manipulated variables. The future incremental control trajectory, composed by N_c elements, is given by:

$$\boldsymbol{\Delta U} = [\boldsymbol{\Delta u}(k_i)^T \quad \boldsymbol{\Delta u}(k_i + 1)^T \quad ... \quad \boldsymbol{\Delta u}(k_i + N_c - 1)^T]^T \tag{2.15}$$

Assuming that the state vector $\boldsymbol{x}(k_i)$ is available at sampling instant $k_i > 0$, its future trajectory evolution along N_p elements can be computed considering the state-space model (A, B, C) and the future control trajectory $\boldsymbol{\Delta U}$ (2.15), comprising all controls $\boldsymbol{\Delta u}$ in the corresponding time instant:

$\boldsymbol{x}(k_i + 1\|k_i) = A\boldsymbol{x}(k_i) + B\boldsymbol{\Delta u}(k_i) + B_d\boldsymbol{\varepsilon}(k_i)$	(2.16)
$\boldsymbol{x}(k_i + 2\|k_i) = A\boldsymbol{x}(k_i + 1\|k_i) + B\boldsymbol{\Delta u}(k_i + 1) + B_d\boldsymbol{\varepsilon}(k_i + 1\|k_i)$	(2.17)
$= A^2 x(k_i) + AB\Delta u(k_i) + B\Delta u(k_i + 1) + AB_d\varepsilon(k_i) + B_d\varepsilon(k_i + 1\|k_i)$	
. . .	
$\boldsymbol{x}(k_i + N_p\|k_i) = A^{N_p}\boldsymbol{x}(k_i) + A^{N_p-1}B\boldsymbol{\Delta u}(k_i) + A^{N_p-2}B\boldsymbol{\Delta u}(k_i + 1) + \cdots$ $\qquad + A^{N_p-N_c}B\boldsymbol{\Delta u}(k_i + N_c - 1) + A^{N_p-1}B_d\boldsymbol{\varepsilon}(k_i)$ $\qquad + A^{N_p-2}B_d\boldsymbol{\varepsilon}(k_i + 1\|k_i) + \cdots + B_d\boldsymbol{\varepsilon}(k_i + N_p - 1\|k_i)$	(2.18)

where $\boldsymbol{x}(k_i + m\|k_i)$ is the predicted state variable at $k_i + m$ with given current plant information $\boldsymbol{x}(k_i)$.

With the hypothesis that $\boldsymbol{\varepsilon}(k)$ is a zero-mean white noise sequence, the predicted value of $\boldsymbol{\varepsilon}(k_i + 1\|k_i)$ at future sample i is assumed to be zero[36]. Consequently, for notational simplicity, this term will be omitted henceforward.

Considering (2.16) - (2.18), the output vector (2.14) can be expressed in a compact matrix form as:

---

[36] Null noise effect over the predicted values.

$$Y = Fx(k_i) + \phi \Delta U \tag{2.19}$$

where:

$$F = \begin{bmatrix} CA \\ CA^2 \\ CA^3 \\ \vdots \\ CA^{N_p} \end{bmatrix} \tag{2.20}$$

$$\phi = \begin{bmatrix} CB & 0 & 0 & \dots & 0 \\ CAB & CB & 0 & \dots & 0 \\ CA^2B & CAB & CB & \dots & 0 \\ \vdots & \vdots & \vdots & \vdots & \vdots \\ CA^{N_p-1}B & CA^{N_p-2}B & CA^{N_p-3}B & \dots & CA^{N_p-N_c}B \end{bmatrix} \tag{2.21}$$

2.3.2 Optimal Control Problem

The second step in the MPC design is to solve the OCP, according to a predefined control objective. Initially, the set-point signal at sampling time k_i, and the associated set-point reference vector are defined respectively as:

$$r(k_i) = [r_1(k_i) \quad r_2(k_i) \quad \cdots \quad r_q(k_i)] \tag{2.22}$$

$$R_s = [\mathbf{1}]^T r(k_i) = \overline{R}_s r(k_i) \tag{2.23}$$

where $r(k_i) \in \mathbb{R}^q$ and $[\mathbf{1}] = [1 \quad 1 \quad \cdots \quad 1] \in \mathbb{R}^{N_p}$.

The cost function, comprising the terms associated to the control objectives, is defined as:

$$J = (R_s - Y)^T (R_s - Y) + (\Delta U)^T \overline{R}(\Delta U) \tag{2.24}$$

where $\overline{R} \in \mathbb{R}^{mN_c \times mN_c}$ is a weight matrix to be tuned according to such objectives.

The incremental optimal control ΔU that minimizes J along one optimization window is given by:

$$\Delta U = (\phi^T \phi + \overline{R})^{-1} (\phi^T \overline{R}_s r(k_i) - \phi^T Fx(k_i)) \tag{2.25}$$

with the assumption that matrix $(\phi^T \phi + \overline{R})^{-1}$ exists.

Applying the RH control principle, only the first m elements in ΔU are taken to form the incremental optimal control:

$$\Delta u(k_i) = [I \quad 0 \quad \cdots \quad 0][(\phi^T \phi + \bar{R})^{-1}(\phi^T \bar{R}_s r(k_i) - \phi^T F x(k_i))] \tag{2.26}$$

where $I \in \mathbb{R}^{m \times m}$ and $0 \in \mathbb{R}^{m \times m}$.

The actual control signal applied to the plant is computed according to:

$$u(k_i) = u(k_i - 1) + \Delta u(k_i) \tag{2.27}$$

and the process is repeated for the next sampled time.

2.3.3 Constrained Case

Up to now, the OCP was solved without considering the physical constraints of the system. The third step in MPC design consists in incorporating such constraints in the formulation. They are normally encountered in the controls and in the states/outputs[37] as summarized in Table 2-1 (for a given sampling time k):

Table 2-1: Types of constraints[38]

	Rate of Change	Amplitude
Control	$\Delta u^{min} \leq \Delta u(k) \leq \Delta u^{max}$ $\vdots$ $\Delta u^{min} \leq \Delta u(k+n) \leq \Delta u^{max}$	$u^{min} \leq \Delta u(k) \leq u^{max}$ $\vdots$ $u^{min} \leq \Delta u(k+n) \leq u^{max}$
State/Output	Amplitude	
	$x^{min} \leq x(k) \leq x^{max}$ $\vdots$ $x^{min} \leq x(k+n) \leq x^{max}$	$y^{min} \leq y(k) \leq y^{max}$ $\vdots$ $y^{min} \leq y(k+n) \leq y^{max}$

After incorporating the constraints as part of the design requirements, it is necessary to translate them into linear inequalities. In this way, developing (2.27) for N_c elements, results:

---

[37] State and output constraints are intrinsically linked due to relation (2.14).
[38] The constraints are valid for the entire horizons. The constraint set is not unique. Other constraints can be added to it.

$$\begin{bmatrix} \boldsymbol{u}(k_i) \\ \boldsymbol{u}(k_i + 1) \\ \boldsymbol{u}(k_i + 2) \\ \vdots \\ \boldsymbol{u}(k_i + N_c - 1) \end{bmatrix} = \begin{bmatrix} I \\ I \\ I \\ \vdots \\ I \end{bmatrix} \boldsymbol{u}(k_i - 1) + \begin{bmatrix} I & 0 & 0 & \cdots & 0 \\ I & I & 0 & \cdots & 0 \\ I & I & I & \cdots & 0 \\ \vdots & \vdots & \vdots & \vdots & \vdots \\ I & I & I & \cdots & I \end{bmatrix} \begin{bmatrix} \Delta\boldsymbol{u}(k_i) \\ \Delta\boldsymbol{u}(k_i + 1) \\ \Delta\boldsymbol{u}(k_i + 2) \\ \vdots \\ \Delta\boldsymbol{u}(k_i + N_c - 1) \end{bmatrix} \qquad (2.28)$$

Re-writing (2.28) in a compact matrix form, with C_1 and C_2 corresponding to the appropriate matrices, yields:

$$\boldsymbol{U} = C_1\boldsymbol{u}(k_i - 1) + C_2\Delta\boldsymbol{U} \qquad (2.29)$$

The imposition of constraints in $\boldsymbol{U}$ yields:

$$\boldsymbol{U}^{min} \leq \boldsymbol{U} \leq \boldsymbol{U}^{max} \qquad (2.30)$$

which can be broken down as:

$$-\boldsymbol{U} \leq -\boldsymbol{U}^{min} \qquad (2.31)$$

$$\boldsymbol{U} \leq \boldsymbol{U}^{max} \qquad (2.32)$$

where $\boldsymbol{U}^{min}$ and $\boldsymbol{U}^{max}$ are column vectors with N_c elements of $\boldsymbol{u}^{min}$ and $\boldsymbol{u}^{max}$, respectively. Replacing (2.29) into (2.31) - (2.32), yields:

$$-(C_1\boldsymbol{u}(k_i - 1) + C_2\Delta\boldsymbol{U}) \leq -\boldsymbol{U}^{min} \implies -C_2\Delta\boldsymbol{U} \leq -\boldsymbol{U}^{min} + C_1\boldsymbol{u}(k_i - 1) \qquad (2.33)$$

$$(C_1\boldsymbol{u}(k_i - 1) + C_2\Delta\boldsymbol{U}) \leq \boldsymbol{U}^{max} \implies C_2\Delta\boldsymbol{U} \leq \boldsymbol{U}^{max} - C_1\boldsymbol{u}(k_i - 1) \qquad (2.34)$$

In the same way, the imposition of constraints in $\Delta\boldsymbol{U}$ yields:

$$-\Delta\boldsymbol{U} \leq -\Delta\boldsymbol{U}^{min} \qquad (2.35)$$

$$\Delta\boldsymbol{U} \leq \Delta\boldsymbol{U}^{max} \qquad (2.36)$$

where $\Delta\boldsymbol{U}^{min}$ and $\Delta\boldsymbol{U}^{max}$ are column vectors with N_c elements of Δu^{min} and Δu^{max}, respectively.

The imposition of constraints in $\boldsymbol{Y}$ derives from (2.19) and yields:

$$\boldsymbol{Y}^{min} \leq F\boldsymbol{x}(k_i) + \phi\Delta\boldsymbol{U} \leq \boldsymbol{Y}^{max} \qquad (2.37)$$

which can be broken down as:

$$-Fx(k_i) - \phi\Delta U \leq -Y^{min} \tag{2.38}$$

$$Fx(k_i) + \phi\Delta U \leq Y^{max} \tag{2.39}$$

Updating (2.24) with the constraints yields:

$$J = \left(R_s - Fx(k_i)\right)^T\left(R_s - Fx(k_i)\right) - 2\Delta U^T\phi^T\left(R_s - Fx(k_i)\right) + \Delta U^T(\phi^T\phi + \bar{R})\Delta U \tag{2.40}$$

subjected to the following inequality constraints:

$$\begin{bmatrix} M_1 \\ M_2 \\ M_3 \end{bmatrix} \Delta U \leq \begin{bmatrix} N_1 \\ N_2 \\ N_3 \end{bmatrix} \tag{2.41}$$

where:

$$M_1 = \begin{bmatrix} -C_2 \\ C_2 \end{bmatrix} \quad N_1 = \begin{bmatrix} -U^{min} + C_1 u(k_i - 1) \\ U^{max} - C_1 u(k_i - 1) \end{bmatrix}$$

$$M_2 = \begin{bmatrix} -I \\ I \end{bmatrix} \quad N_2 = \begin{bmatrix} -\Delta U^{min} \\ \Delta U^{max} \end{bmatrix}$$

$$M_3 = \begin{bmatrix} -\phi \\ \phi \end{bmatrix} \quad N_3 = \begin{bmatrix} -Y^{min} + Fx(k_i) \\ Y^{max} - Fx(k_i) \end{bmatrix}$$

The OCP solution consists in finding the incremental optimal control ΔU that minimizes (2.40), along one optimization window, considering the constraints (2.41). Since (2.40) is quadratic, and the constraints are linear inequalities, the problem resumes to find an optimal solution in the framework of a standard quadratic programming problem (Wang, 2009). For nonlinear MPC, the OCP can be solved by transforming it into a Nonlinear Program Problem (NLP) as detailed in item 4.2.1.2.

2.4 Stability and Robustness

2.4.1 Stability

Ideally, it would be desirable to solve an infinite horizon OCP in the MPC formulation, however this problem is rather "ill-behaved" since it would involve a summation of infinite terms which could lead to an infinite cost even for well-behaved trajectories.

A solution to overcome this problem consists in truncating the problem at some maximum number of samples N, leading to a finite horizon OCP. In this case, a terminal cost might be added to the finite horizon cost function in order to penalize the state attained at the terminal sample.

However, in general, it is not true that repeated minimizations over a finite receding horizon objective lead to the optimal solution of the associated infinite horizon problem[39]. Consequently, the actual closed-loop trajectories, obtained by means of repeated replanning[40], will differ from the predicted open-loop trajectories, thus there is no guarantee that the closed-loop system will be stable. Even optimality and recursive feasibility cannot be assured. (Mayne, Rawlings, Rao, & Skokaert, 2000).

The strategy originally adopted to overcome the stability issue in practical applications (normally with slow dynamics) was to consider a sufficiently large horizon. Because satisfactory results were obtained, research concerning formal conditions to assure stability did not receive attention in the industry and early academic literatures.

This limitation was lifted in (Mayne, 2014) and (Mayne, Rawlings, Rao, & Skokaert, 2000), which concluded that the imposition of a terminal cost and a terminal constraint set in the finite horizon OCP would render sufficient conditions to assure nominal stability in constrained MPC. This strategy is based on the fact that stability, under certain conditions[41], can be verified in finite horizon optimal controllers if an appropriate Lyapunov function, performing the function of a terminal cost, is added to the original finite horizon cost function. This approach is consistent with the fact that *"optimality does not imply stability"* (Kalman, 1960).

Ideally, the terminal cost $F(.)$ should be the infinite horizon cost function $J_\infty^0(.)$. In this hypothetical situation, $J_N^0(.) = J_\infty^0(.)$, thus the control sequence obtained in the first optimization would be applied for all future instants[42], while recursive feasibility[43], stability and robustness would be automatically assured. However, in practice, nonlinearities and/or constraints render this situation

---

[39] Even assuming a perfect model, in the absence of disturbances.
[40] MPC turns open-loop trajectory optimization into a closed-loop controller by means of repeated replanning.
[41] Stabilizability and detectability.
[42] In this situation, online optimization would be no longer necessary.
[43] The OCP is called recursively feasible, if for all feasible initial states, feasibility (existence of a feasible control sequence) is guaranteed at every state along the closed-loop trajectory.

impossible, but it is still possible to choose $F(.)$ so that it approximately matches $J_\infty^0(.)$ in a suitable neighborhood of the origin. So, the task consists in defining a proper set $X_f \in \mathbb{R}^n$ in this neighborhood (Mayne, Rawlings, Rao, & Skokaert, 2000).

Formally, if further minor assumptions are satisfied, nominal stability is assured if the following necessary conditions are attained, (Mayne, Rawlings, Rao, & Skokaert, 2000):

- A1: $X_f \subset \mathbb{X}$, X_f closed, $0 \in X_f$ (state constraint satisfied in X_f);
- A2: $\boldsymbol{u} \in \mathbb{U}$, for all $\boldsymbol{x} \in X_f$ (control constraint satisfied in X_f);
- A3: $\boldsymbol{f}(\boldsymbol{x}(k), \boldsymbol{u}(\boldsymbol{x}(k))) \in X_f$, for all $\boldsymbol{x} \in X_f$; and
- A4: $[l + F](\boldsymbol{x}(k), \boldsymbol{u}(\boldsymbol{x}(k))) \leq 0$ for all $\boldsymbol{x} \in X_f$, and $F(\boldsymbol{x}(k))$ is a local Lyapunov function.

However, besides the difficulties associated to the definition of the terminal cost and terminal constraint set, it is not possible to assure GAS convergence (Alessandretti, Aguiar, & Jones, 2013) and (Yu, Li, Chen, & Allgöwer, 2015). A solution to overcome this problem is to incorporate a contractive constraint in the OCP formulation.

This constraint is designed based on the knowledge of an existing global stabilizing control law, associated to a reference controller. Thus, the designed system inherits such global asymptotic stability. Since the contractive constraint represents a sufficient condition to assure stability, the terminal cost and the terminal constraint set can be derogated from the OCP formulation (Hung, Rego, Crasta, & Pascoal, 2018).

2.4.2 Robustness

The introduction of uncertainties in the system, lumped together in vector $\boldsymbol{w}(k)$[44] $\in W(\boldsymbol{x}(k), \boldsymbol{u}(k))$, raises questions concerning robustness[45], since the positive invariance property (A3) is no longer valid[46]. However, it can be

---

[44] Uncertainty can be a combination of additive disturbances, state estimation errors and model errors.
[45] Defined as the ability to keep certain properties such as stability and performance in the presence of uncertainty.
[46] Due to modeling uncertainty and exogenous disturbances, the actual state trajectory will deviate from the predicted trajectory.

recovered if all possible realizations of $w(k)$ in the OCP are considered, and the applicable constraints are satisfied.

The key parameters $F\big(x(k)\big)$, X_f and $u\big(x(k)\big)$ must satisfy, besides A1-A2, the following robust variations of requirements A3-A4 (Mayne, Rawlings, Rao, & Skokaert, 2000):

- A3r: $f(x(k), u(x(k)), w) \in X_f$, for all $x \in X_f$ and for all $w \in W(x, u(x))$;
- A4r: $[l + F](x(k), u(x(k)), w) \leq 0$ for all $x \in X_f$, for all $w \in W(x, u(x))$ and $F(x(k))$ is a robust terminal cost (Lyapunov function) in a neighborhood of the origin.

Most of the existing literature on the topic of robust MPC may be broadly categorized into three branches: inherent robustness, min-max formulations, and tube MPC approaches (Mayne, 2014).

Inherent robustness is the simple approach since it just neglects the uncertainties, *i.e.*, considers only the nominal model in the controller design. Under certain conditions, the resultant controller is robustly stable against sufficiently small additive disturbances (Mayne, 2014).

In the min-max formulation, open-loop performance is optimized assuming a worst-case uncertainty/disturbance realization. This leads to extremely conservative control policies and a small domain of feasibility[47], since the "diameter" of the tube that contains the nominal trajectory is not negligible (Mayne, 2014).

Alternatively, closed-loop min-max formulations (usually termed "feedback MPC")[48], while having improved feasibility properties, are prohibitively complex to implement since the optimization involves searching over control policies (Singh, Pavone, & Slotine). Additionally, as a consequence of feedback introduction, optimality is no longer guaranteed. (Mayne, 2014).

In the tube MPC approach, an auxiliary feedback controller acts to minimize the deviation between the actual and nominal state trajectories[49], therefore it ensures that even in the presence of uncertain dynamics and bounded exogenous disturbances, the deviation remains bounded. Normally it employs two parallel MPC

---

[47] In this case, there is no control sequence such that the constraints are satisfied.
[48] This technique employs local feedback around a nominal or reference trajectory so that the trajectories associated with the uncertainties' realizations remain in a possible small neighborhood of the nominal trajectory (in other words, it shrinks the "diameter" of the previously mentioned tube).
[49] It keeps the actual trajectory within an invariant "tube" around the nominal trajectory.

algorithms. The first algorithm generates a nominal state and control sequence assuming no disturbances. The second algorithm acts as an effective auxiliary controller by penalizing deviations from the nominal trajectory computed within the first algorithm. Differently from the previous approach, the online OCP is converted back into a search over control sequences rather than control policies, thereby reducing computational complexity (Singh, Pavone, & Slotine).

Concluding, for the sake of clarity, it is important to emphasize that as any other model-based control technique, the MPC robustness is intrinsically linked to the precision of its internal model. Consequently, MPC is not inherently more or less robust than classical feedback as has been falsely claimed. On the other hand, MPC can be tuned more easily for robustness than classic feedback controllers,[50] taking advantage of the future outputs predicted by the internal model[51] (Garcia, Prett, & Morari, 1989).

2.5　Summary

This chapter presented a brief overview of the RH principle, encompassing the MPC/MHE techniques, the basic formulation related to MIMO linear systems, and some considerations about stability and robustness.

The MPC optimization problem predicts an optimal state trajectory and supplies the corresponding open-loop control sequence for a finite time interval. In order to incorporate some feedback mechanism, it executes some small portion of the control sequence[52], senses the new state, and repeats the procedure again.

Its main advantages are the ability to take better decisions at the current time to account for future possibilities, as well as the capacity to systematically handle practical constraints.

It is relevant to stress that constrained MPC is intrinsically a nonlinear problem, even if the controlled plant is linear. While main aspects concerning nominal stability of deterministic systems are well understood, robustness of uncertain systems[53] still represents a major challenge, requiring substantial work in extending the associated theory.

---

[50] This fact might be responsible for the misconception regarding MPC robustness.
[51] Transparent online tuning.
[52] The open-loop manipulated input function.
[53] The trademark of modern control theory.

3 AUTONOMOUS MARINE VEHICLE MODEL

This chapter presents the Autonomous Marine Vehicle (AMV) model borrowed from (Fossen, 1999) and (Fossen, 2002), described by its kinematic and dynamic equations. Initially described in 6 DOF, the model is reduced to 3 DOF (horizontal motion) after assuming some simplifying hypothesis. The chapter also describes the reference vehicles used in the numerical simulations.

3.1 Reference Frames

To derive the vehicle's equations of motion, it is a common practice to define two reference frames: an Earth-Fixed inertial frame $\{I\}$, composed by the orthonormal axes $\{X_I, Y_I, Z_I\}$, and a Body-Fixed frame $\{B\}$, composed by the orthonormal axes $\{X_B, Y_B, Z_B\}$, as presented in Figure 3-1.

Figure 3-1: Earth-fixed and Body-Fixed reference frames

DOF	Forces and Moments	Velocities	Positions and Euler Angles
1. Surge	X	u	x
2. Sway	Y	v	y
3. Heave	Z	w	z
4. Roll	K	p	ϕ
5. Pitch	M	q	θ
6. Yaw	N	r	ψ

(Loc, Choi, You, Kim, & Kim, 2012)

To describe the vehicle motion, the following entities are defined according to SNAME nomenclature (Table 3-1).

Table 3-1: Describing vectors

Vector		Description	Referenced to:	Type:
$\boldsymbol{\eta} = \left[\boldsymbol{\eta}_1^T, \boldsymbol{\eta}_2^T\right]^T$	$\boldsymbol{\eta}_1 = [x, y, z]^T$	Position of the origin of $\{B\}$	$\{I\}$	Measurement
	$\boldsymbol{\eta}_2 = [\phi, \theta, \psi]^T$	Orientation of $\{B\}$, in Euler Angles	$\{I\}$	Measurement
$\boldsymbol{v} = \left[\boldsymbol{v}_1^T, \boldsymbol{v}_2^T\right]^T$	$\boldsymbol{v}_1 = [u, v, w]^T$	Linear velocities of the origin of $\{B\}$	$\{B\}$	Measurement
	$\boldsymbol{v}_2 = [p, q, r]^T$	Angular velocities of $\{B\}$	$\{B\}$	Measurement
$\boldsymbol{\tau} = \left[\boldsymbol{\tau}_1^T, \boldsymbol{\tau}_2^T\right]^T$	$\boldsymbol{\tau}_1 = [X, Y, Z]^T$	External forces	$\{B\}$	Actuation
	$\boldsymbol{\tau}_2 = [K, M, N]^T$	External torques	$\{B\}$	Actuation

3.2   Equations of Motion

3.2.1   Kinematic Equations

The kinematic equations (Fossen, 2002) can be written in compact form as

$$\dot{\boldsymbol{\eta}} = J(\boldsymbol{\eta})\boldsymbol{v} \tag{3.1}$$

with

$$J(\boldsymbol{\eta}) = \begin{bmatrix} R_B^I(\boldsymbol{\eta_2}) & 0_{3x3} \\ 0_{3x3} & T_{\eta_2}(\boldsymbol{\eta_2}) \end{bmatrix} \tag{3.2}$$

where

$$R_B^I(\boldsymbol{\eta_2}) = \begin{bmatrix} c\psi c\theta & -s\psi c\theta + c\psi s\theta s\phi & s\psi c\phi + c\psi s\theta c\phi \\ s\psi c\theta & c\psi c\theta + s\psi s\theta s\phi & -c\psi s\phi + s\psi s\theta c\phi \\ -s\theta & c\theta s\phi & c\theta s\phi \end{bmatrix} \tag{3.3}$$

is the rotation matrix from $\{B\}$ to $\{I\}$, defined by means of three successive rotations (Euler's angles - zyx convention), and

$$T_{\eta_2}(\boldsymbol{\eta_2}) = \begin{bmatrix} 1 & s\phi t\theta & c\phi t\theta \\ 0 & c\phi & -s\phi \\ 0 & s\phi/c\theta & c\phi/c\theta \end{bmatrix} \tag{3.4}$$

is the matrix[54] which correlates the Body-Fixed angular velocity vector (p, q, r) with roll, pitch and yaw rate vector $(\dot{\phi}, \dot{\theta}, \dot{\psi})$.

3.2.2   Dynamic Equations

For marine vehicles, it is convenient to express the dynamic equations in the Body-Fixed reference frame $\{B\}$, centered at the vehicle's center of gravity (CG).

The rigid-body dynamic equations can be expressed in vectorial form as

$$M_{RB}\dot{\boldsymbol{v}} + C_{RB}(\boldsymbol{v})\boldsymbol{v} = \boldsymbol{\tau}_{RB} \tag{3.5}$$

---

[54] This matrix is undefined for a pitch angle $(\theta) = \pm \pi/2$. However, for practical applications, the representation still remains valid since the marine vehicle will operate far from this singular point.

where M_{RB} is the rigid-body inertia matrix, $C_{RB}(\boldsymbol{v})$ is the rigid-body Coriolis and centripetal matrix and $\boldsymbol{\tau}_{RB}$ is a generalized vector of external forces and moments, which can be decomposed as

$$\boldsymbol{\tau}_{RB} = \boldsymbol{\tau}_A + \boldsymbol{\tau}_D + \boldsymbol{\tau}_R + \boldsymbol{\tau}_c \tag{3.6}$$

where:

- $\boldsymbol{\tau}_A$ is the force and moment vector due to hydrodynamic added mass

$$\boldsymbol{\tau}_A = -M_A\dot{\boldsymbol{v}} - C_A(\boldsymbol{v})\boldsymbol{v} \tag{3.7}$$

- $\boldsymbol{\tau}_D$ is the force and moment vector due to hydrodynamic effects (damping, lift and skin friction)

$$\boldsymbol{\tau}_D = -D(\boldsymbol{v})\boldsymbol{v} \tag{3.8}$$

- $\boldsymbol{\tau}_R$ is the force and moment vector due to gravity and fluid density (weight and buoyancy)

$$\boldsymbol{\tau}_R = C(\boldsymbol{\eta}) \tag{3.9}$$

- $\boldsymbol{\tau}_c$ is the force and moment vector due to thrusters and surfaces (normally considered as control input)

Combining (3.6) - (3.9) into (3.5), the 6 DOF dynamic equations can be expressed as

$$\underbrace{M_{RB}\dot{\boldsymbol{v}} + C_{RB}(\boldsymbol{v})\boldsymbol{v}}_{\text{Rigid-Body Terms}} + \underbrace{M_A\dot{\boldsymbol{v}} + C_A(\boldsymbol{v})\boldsymbol{v} + D(\boldsymbol{v})\boldsymbol{v}}_{\text{Hydrodynamic Terms}} + \underbrace{g(\boldsymbol{\eta})}_{\text{Restoring Term}} = \boldsymbol{\tau}_c \tag{3.10}$$

Or equivalently

$$M\dot{\boldsymbol{v}} + C(\boldsymbol{v})\boldsymbol{v} + D(\boldsymbol{v})\boldsymbol{v} + g(\boldsymbol{\eta}) = \boldsymbol{\tau}_c \tag{3.11}$$

where

$$M = M_{RB} + M_A \tag{3.12}$$

$$C = C_{RB}(\boldsymbol{v}) + C_A(\boldsymbol{v}) \tag{3.13}$$

The properties of these matrices are summarized in Table 3-2. Properties such as symmetry, skew-symmetry and positive-definiteness are intrinsically linked to the physical characteristics of the system and can be exploited in the control system design as well as in the associated stability analysis.

Table 3-2: Properties of the matrices[55]

Rigid-Body Matrices	Hydrodynamic Matrices
$M_{RB} = M_{RB}^T > 0$	$M_A = M_A^T > 0$
$\dot{M}_{RB} = 0$	$\dot{M}_A = 0$
$C_{RB}(\boldsymbol{v}) = -C_{RB}^T(\boldsymbol{v})$[56]	$C_A(\boldsymbol{v}) = -C_A^T(\boldsymbol{v})$[39]
-	$D(v) > 0$

3.2.3 Simplified Model

The AMV simplified mathematical model is obtained considering the following assumptions[57]

- A1: The vehicle motion is restrained to a horizontal plane[58], in an even keel condition (heave and pitch negligible);
- A2: Negligible roll;
- A3: The vehicle presents neutral buoyancy, and the center of buoyancy (CB) coincides with the center of gravity (CG); and
- A4: The axes of the body-fixed reference frame are chosen to coincide with the vessel's principal axis.

Under these assumptions, the 6 DOF kinematic and dynamic models reduces respectively to

---

[55] The extended expressions of these matrices are presented in (FOSSEN, 1994) and (FOSSEN, 2011).
[56] This matrix can be parameterized to be skew-symmetrical.
[57] Under these assumptions, the model is valid for AUVs and ASCs.
[58] The depth and the pitch angle can be controlled by a specific and independent control system.

- **Kinematic Model:**

$$\dot{\boldsymbol{\eta}} = J(\psi)\boldsymbol{v} \implies \begin{bmatrix} \dot{x} \\ \dot{y} \\ \dot{\psi} \end{bmatrix} = \begin{bmatrix} \cos\psi & -\sin\psi & 0 \\ \sin\psi & \cos\psi & 0 \\ 0 & 0 & 1 \end{bmatrix} \begin{bmatrix} u \\ v \\ r \end{bmatrix} \tag{3.14}$$

Defining

$$\boldsymbol{p} = \begin{bmatrix} x \\ y \end{bmatrix} \tag{3.15}$$

$$R(\psi) = \begin{bmatrix} \cos\psi & -\sin\psi \\ \sin\psi & \cos\psi \end{bmatrix} \tag{3.16}$$

equation (3.14) can be rewritten as

$$\dot{\boldsymbol{\eta}} = \begin{bmatrix} \dot{\boldsymbol{p}} \\ \dot{\psi} \end{bmatrix} = \begin{bmatrix} R(\psi) & 0_{2x1} \\ 0_{1x2} & 1 \end{bmatrix} \begin{bmatrix} u \\ v \\ r \end{bmatrix} \tag{3.17}$$

- **Dynamic Model:**

$$M\dot{\boldsymbol{v}} + C(\boldsymbol{v})\boldsymbol{v} + D(\boldsymbol{v})\boldsymbol{v} = \boldsymbol{\tau}_c \tag{3.18}$$

where

$$M = \begin{bmatrix} m - X_{\dot{u}} & 0 & 0 \\ 0 & m - Y_{\dot{v}} & -Y_{\dot{r}} \\ 0 & -N_{\dot{v}} & I_{Z-N_{\dot{r}}} \end{bmatrix} \tag{3.19}$$

$$C(\boldsymbol{v}) = \begin{bmatrix} 0 & 0 & -(m - Y_{\dot{v}})v \\ 0 & 0 & (m - X_{\dot{u}})u \\ (m - Y_{\dot{v}})v & -(m - X_{\dot{u}})u & 0 \end{bmatrix} \tag{3.20}$$

$$D(\boldsymbol{v}) = D_L(\boldsymbol{v}) + D_{NL}(\boldsymbol{v}) \tag{3.21}$$

where the linear and nonlinear damping matrices are given by

$$D_L(\boldsymbol{v}) = -\begin{bmatrix} X_u & 0 & 0 \\ 0 & Y_v & Y_r \\ 0 & N_v & N_r \end{bmatrix} \tag{3.22}$$

$$D_{NL}(\boldsymbol{v}) = -\begin{bmatrix} X_{u|u|}|u| & 0 & 0 \\ 0 & Y_{v|v|}|v| & Y_{r|r|}|r| \\ 0 & N_{v|v|}|v| & N_{r|r|}|r| \end{bmatrix} \tag{3.23}$$

and the vector of control forces and moments is given by

$$\boldsymbol{\tau} = \begin{bmatrix} \tau_u \\ \tau_v \\ \tau_r \end{bmatrix} \tag{3.24}$$

To support the control system design[59], an additional simplification can be made. For an underactuated low-speed vehicle, without lateral actuation, presenting port/starboard and fore/aft symmetries, the off-diagonals elements of matrices M and D can be neglected, resulting in a decoupled model. Thus, if only the actuated dynamics is considered, the dynamic model (3.18) can neglect the sway DOF resulting

$$M\dot{\boldsymbol{u}} + C(\boldsymbol{u})\boldsymbol{u} + D(\boldsymbol{u})\boldsymbol{u} = \boldsymbol{\tau}_c \tag{3.25}$$

where $\boldsymbol{u} = [u \quad r]^T$. For the sake of simplicity, the notations of the associated inertia, Coriolis/centripetal and damping new matrices $\in \mathbb{R}^{2x2}$ are kept as M, C and D, respectivelly.

3.2.4 Ocean Current Model

In the presence of constant irrotational ocean current $\boldsymbol{v}_c = [u_c \quad v_c]^T$, related to the Body-Fixed reference frame $\{B\}$, the kinematic model (3.14) holds if the following adjustments are made

$$\begin{bmatrix} \dot{x} \\ \dot{y} \\ \dot{\psi} \end{bmatrix} = \begin{bmatrix} \cos\psi & -\sin\psi & 0 \\ \sin\psi & \cos\psi & 0 \\ 0 & 0 & 1 \end{bmatrix} \begin{bmatrix} u_r + u_c \\ 0 + +v_c \\ r \end{bmatrix} \tag{3.26}$$

where

---

[59] Not plant simulation.
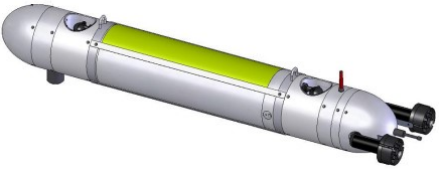
$$u = u_r + u_c$$
$$v = v_r + v_c$$

where the sub-index r denotes the vehicle's velocity relative to the ocean current, and the sub-index c denotes the ocean current's velocity relative to the Body-Fixed reference frame $\{B\}$.

In the dynamic model (3.25), the velocity vector must consider $\boldsymbol{u} = [u_r \quad r]^T$. Moreover, matrices C and D must consider u_r and v_r instead of u and v.

3.3 The Reference Vehicles

In order to perform the numerical simulations, two reference vehicles were chosen; the ASC Medusa and the AUV Mares. Their physical and functional characteristics are presented in Table 3-3:

Table 3-3: AMV physical and function characteristics

Characteristic	ASC Medusa	AUV Mares
Hull Diameter	150 mm	200 mm
Width	350 mm	200 mm
Length	1035 mm	1500 mm
Height	875 mm	200 mm
Dry Weight	27 kg	32 kg
Max. Depth	0 m[49]	100 m
Velocity Range	0,0 - 1,5 m/s	0,0 - 1,5 m/s
Typical Endurance	12 hours @ 1,0 m/s	10 hours @ 1,0 m/s
Photo		

3.3.1 ASC Medusa

The reference ASC is the Medusa[60] vehicle developed by Instituto Superior Técnico (IST) of Lisbon, Portugal (IST Lisboa, 2020). The vehicle is composed of two

---

[60] Medusa can be deployed as ASC and AUV.

acrylic cylinder hulls, covered in both ends by aluminum caps, and attached to a central aluminum framework.

The lower submerged hull houses the batteries, sensors, a hi-resolution camera, and an acoustic modem. The upper semi-submerged hull houses sensors, computers and a low-resolution camera, and connects to a mast equipped with GPS and radio frequency antennas.

It is propelled by two stern axial thrusters that control surge and yaw motions. In terms of automation, the Medusa is equipped with an inner loop for speed and heading control (Abreu, et al., 2016).

Combined with AUVs, the ASC Medusa can be used in research and commercial applications, deployed in missions such as data download and water column profiling, resource exploration and mapping, and high-resolution habitat mapping (Cardeira, 2017).

The numerical simulations employing ASC Medusa borrow the inertia properties and hydrodynamic coefficients from (Abreu P. C., 2014), as summarized in Table 3-4.

Table 3-4: ASC Medusa inertia and hydrodynamic properties at the surface[61].

Inertia	Added Mass	Linear damping	Nonlinear damping
$m = 17\,kg$	$X_{\dot{u}} = -20\,kg$	$X_u = -0.2\,kg/s$	$X_{|u|u} = -25\,kg/m$
$I_z = 1\,kg.m^2$	$Y_{\dot{v}} = -30\,kg$	$Y_v = -50\,kg/s$	$Y_{|v|v} = -0.01\,kg/m$
	$N_{\dot{r}} = -8.69\,kg.m^2$	$N_r = -4.14\,kg.m^2/s$	$N_{|r|r} = -6.23\,kg.m$
	$N_{\dot{v}} = 0\,kg.m$	-	$N_{v|v|} = 0\,kg$
	$Y_{\dot{r}} = 0\,kg.m$	-	$Y_{r|r|} = 0\,kg.m$

3.3.2 AUV Mares

The reference AUV is the Mares[62] vehicle, designed and built by Ocean Systems Group (Auvac - Autonomous Undersea Vehicle Applicantions Center, n.d.). It is a torpedo shaped vehicle constructed in a modular framework, composed by a central hull and several interchangeable and reconfigurable sections, most of them manufactured in acetal copolymer.

---

[61] For horizontal motion, if the vessel presents port/starboard and fore/aft symmetries, them the off-diagonals elements of matrices *M* and *D* can be neglected for low-speed applications.
62 Modular Autonomous Robot for Environment Sampling.

It can be configured to carry a wide variety of sensors, collecting data while following predefined trajectories. Major application areas include pollution monitoring, scientific data collection, sonar mapping, and mine countermeasures.

The electronic circuits and the batteries are located in the central hull. The main computer is a PC-104 stack, with a power supply, the CPU, a communications board and a solid-state disk. The navigation system is based on a LBL acoustic network. The vehicle software continuously fuses range (from the acoustic beacons), compass heading, and thruster RPM to compute the estimated position.

It is propelled by two stern axial thrusters that control surge and yaw motions and, differently from similar-sized vehicles, it also has vertical thrusters to control surge and pitch motions. This arrangement permits operations in very confined areas, with virtually independent horizontal and vertical motion, for near zero speeds.

The numerical simulations employing AUV Mares borrow the inertia properties and hydrodynamic coefficients from (Ferreira, Pinto, Matos, & Cruz, 2009), as summarized in Table 3-5.

Table 3-5: AUV Mares inertia and hydrodynamic properties

Inertia	Added Mass	Linear damping	Nonlinear damping
$m = 32\,kg$	$X_{\dot{u}} = -1.74\,kg$	$X_u = 0\,kg/s$	$X_{|u|u} = -4.05\,kg/m$
$I_z = 4.73\,kg.m^2$	$Y_{\dot{v}} = -42.8\,kg$	$Y_v = 0\,kg/s$	$Y_{|v|v} = -113\,kg/m$
	$N_{\dot{r}} = -6.32\,kg.m^2$	$N_r = 0\,kg.m^2/s$	$N_{|r|r} = -1.57\,kg.m2$
	$N_{\dot{v}} = 0.0289\,kg.m$	-	$N_{v|v|} = 2.38\,kg$
	$Y_{\dot{r}} = 0.0289\ kg.m$	-	$Y_{r|r|} = 1.88\ kg.m$

3.4 Summary

In this chapter, the mathematical model of the AMV (AUV or ASC) was developed, considering its kinematic and dynamic components.

The kinematic model is of particular importance since it is also used as the MPC internal predictive model. Important model properties, reflected on its matrices' properties, were highlighted in order to support the control system design. Initially described in 6 DOF, the model was reduced to 3 DOF after assuming some simplifying hypothesis.

Finally, the sea proven ASC Medusa and AUV Mares were selected as reference vehicles to support the numerical simulations.

4 PATH FOLLOWING CONTROLLER

In this chapter, the path following controller is developed. Representing the lower level of the control architecture, this module is responsible for controlling the individual motion of the vehicles, ensuring that they converge to a predefined speed parameterized path. Its design is decoupled in an inner-outer loop structure. The outer loop comprises a Lyapunov-Based Model Predictive Control (L-MPC) responsible to calculate and issue the speed assignment (the guidance system). The inner loop consists in a feedback linearized controller responsible to execute the speed assignment (the speed tracker system). This module also encompasses a Moving Horizon Estimator (MHE) to provide noise attenuated estimates of position and heading measurements, and a state observer to provide estimates of the ocean current's velocity.

4.1 Problem Statement

Let $\boldsymbol{p}(t) \in \mathbb{R}^2$ be the vector containing the position of an underactuated vehicle with no lateral thrusters, and $\boldsymbol{p}_{Ref}(\gamma(t)) \in \mathbb{R}^2$ be the desired path, parameterized by $\gamma(t) \in \mathbb{R}$, with $\partial \boldsymbol{P}_{Ref}/\partial \gamma$ bounded. Let $u_{Ref}(\gamma(t)) \in \mathbb{R}$ be the speed assignment associated with the desired path. As proposed by (Vanni, Aguiar, & Pascoal, 2008), the control problem can be stated in two parts[63]

DEFINITION 4.1: (***Constrained Path Following Problem***): *Let $\boldsymbol{p}_{Ref}(\gamma) \in \mathbb{R}^2$ be the desired path parameterized by $\gamma \in \mathbb{R}$, and $u_{Ref}(\gamma) \in \mathbb{R}$ be its associated positive speed assignment. Considering the input constrained set $\mathbb{U}_v := \{(u,r): 0 \leq u \leq u_{max}, |r| \leq r_{max}\}$, derive control laws for $\boldsymbol{u} = [u \quad r]^T$ and $\dot{\gamma}$ such that all closed-loop signals are bounded and both $\|\boldsymbol{e}\|$ and $\|z\|$ converge asymptotically to a neighborhood of the origin of radius δ.*

where $\boldsymbol{e}$ and z are the path following and speed assignment tracking errors, given by

$$\boldsymbol{e} := \boldsymbol{p} - \boldsymbol{p}_{Ref}(\gamma) \tag{4.1}$$

$$z = \dot{\gamma} - u_{Ref}(\gamma) \tag{4.2}$$

---

[63] For notational simplicity, the time dependency is dropped in the incoming formulation.

It can be noticed that forcing $\|z\|$ to converge to the origin, implicitly defines the path following strategy $(\dot{\gamma} = u_{Ref}(\gamma))$[64]. In this case, the speed assignment u_{Ref} expresses the rate of change of γ. Thus, the speed of the virtual reference point is given by $\frac{\partial \boldsymbol{p}_{Ref(\gamma)}}{\partial \gamma} \dot{\gamma} = \frac{\partial \boldsymbol{p}_{Ref(\gamma)}}{\partial \gamma} u_{Ref}$[65].

DEFINITION 4.2: (**Speed Tracking Problem**): *Supposing that $\boldsymbol{u}_d$ is sufficiently smooth and its time derivative is bounded, derive a feedback control law $\boldsymbol{\tau} = [\tau_u \quad \tau_r]^T$ such that $\boldsymbol{u}$ converges asymptotically to $\boldsymbol{u}_d$.*

The path following controller basic structure is decoupled in two independent control loops (Maurya, Aguiar, & Pascoal, 2009), as presented in Figure 4-1. The outer (kinematic) loop calculates and issues the speed assignment required to drive the vehicle into the desired path, while respecting the associated speed assignment (guidance scheme – Definition 4.1). In turn, the inner (dynamic) loop assures that the speed assignment is properly tracked (speed tracker scheme – Definition 4.2).

Figure 4-1: Basic inner-outer loop structure
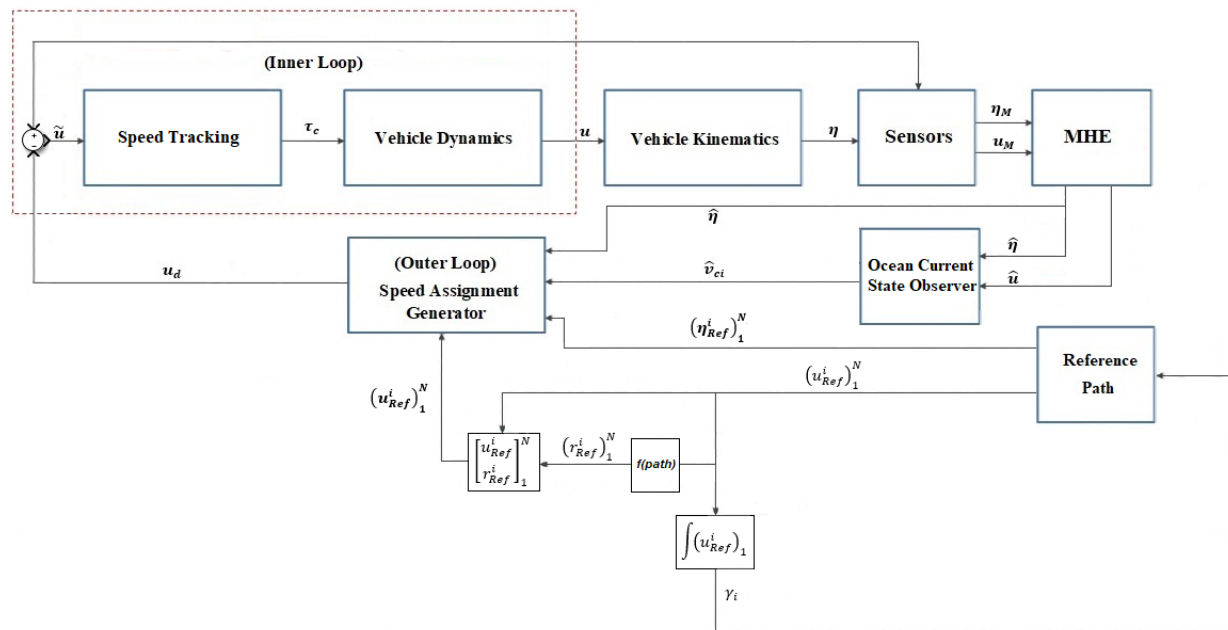
(From Author)

---

[64] The path following strategy is not unique. In this strategy, the virtual reference point is forced to move at the desired speed, by assigning $\dot{\gamma} = u_{Ref}(\gamma)$. Another strategy could envisage the introduction of an additional control variable, by setting a control law for $\ddot{\gamma}$ (using backstepping, for example). Differently from the first strategy, the virtual reference point would move faster/slower if the vehicle is ahead/behind it.

[65] Note that if $\frac{\partial \boldsymbol{p}_{Ref(\gamma)}}{\partial \gamma} = 1$, then the speed of the virtual reference point coincides with the speed assignment.

This architecture presents advantages for practical implementation such as simpler control laws, and fast-slow temporal scale separation which simplifies the tuning process. Additionally, since the loops are dynamically decoupled and considering that the outer loop does not require an in-depth knowledge of the vehicle's internal dynamics, it is possible to use the same outer loop in a wide range of vehicles already equipped with factory-assembled speed control systems (Maurya, Aguiar, & Pascoal, 2009)[66]. However, the control laws are more subjected to smoothness and saturation issues (Vanni, 2007).

4.2   Path Following Controller

4.2.1   Outer (Kinematic) Loop

The outer (kinematic) loop comprises a sampled-data L-MPC. As mentioned in item 2.4.1, the adoption of a terminal cost and a terminal constraint set in the OCP formulation assures recursive feasibility and stability of the controller. However, these two figures can be neglected in the OCP formulation if a contractive constraint is adopted instead. This constraint is constructed based on a global Lyapunov function and its associated stabilizing constrained control law, which both of them inherited from a generic reference controller. So, the outer loop design is performed in two steps. Firstly, the contractive constraint is formulated, and after the L-MPC is designed considering this constraint in the OCP.

4.2.1.1   Contractive Constraint Formulation

The contractive constraint is derived from the feedback linearization controller developed in (Vanni, 2007) and (Vanni, Aguiar, & Pascoal, 2008). Once incorporated into the OCP formulation, the contractive constraint assures that the MPC inherits global asymptotic stability of the reference controller. In this way, regardless of any initial position and orientation, the vehicle always converges to the path asymptotically (global region of attraction).

The path following tracking error, expressed in the Body-Fixed frame {B}, and its associated time derivative are given by

---

[66] The outer loop is designed separately from the whole loop, assuming that its output variables can be tracked instantaneously by the inner loop. This premise is unrealistic since the inner loop also has its own dynamics. For this reason, in practice, the outer loop must be tuned considering the characteristics of the inner loop (Maurya, Aguiar, & Pascoal, Marine vehicle path following using inner-outer loop control, 2009).

$$e(t) := R^T(\psi)(p - p_{Ref}) \tag{4.3}$$

$$\dot{e}(t) := \dot{R}^T(\psi)(p - p_{Ref}) + R^T(\psi)(\dot{p} - \dot{p}_{Ref}) \tag{4.4}$$

where

$$\dot{R}^T(\psi) = -S(r)R^T(\psi) \text{ with } S(r) = \begin{bmatrix} 0 & -r \\ r & 0 \end{bmatrix} \tag{4.5}$$

and

$$\dot{p}_{Ref} = \frac{\partial p_{Ref}}{\partial \gamma} \dot{\gamma} \tag{4.6}$$

Substituting (4.5) and (4.6) into (4.4) yields

$$\dot{e} := -S(r)R^T(\psi)(p - p_{Ref}) + R^T(\psi)\left(\dot{p} - \frac{\partial p_{Ref}}{\partial \gamma} \dot{\gamma}\right) \tag{4.7}$$

Replacing (3.14) and (4.3) into (4.7), and introducing the vector δ yields

$$\dot{e} := -S(r)(e - \delta) - S(r)\delta + R^T(\psi)\left(R(\psi)\begin{bmatrix} u_r + u_c \\ v_r + v_c \end{bmatrix} - \frac{\partial p_{Ref}}{\partial \gamma} \dot{\gamma}\right) \tag{4.8}$$

$$\dot{e} := -S(r)(e - \delta) + \begin{bmatrix} 0 & r \\ -r & 0 \end{bmatrix}\begin{bmatrix} \delta \\ 0 \end{bmatrix} + \begin{bmatrix} u_r \\ v_r \end{bmatrix} + \begin{bmatrix} u_c \\ v_c \end{bmatrix} - R^T(\psi)\frac{\partial p_{Ref}}{\partial \gamma} \dot{\gamma} \tag{4.9}$$

where $\delta = [\delta \quad 0]^T$, with δ being an arbitrarily small negative constant, is a constant vector introduced to incorporate the angular velocity r in the error dynamics formulation. Developing (4.9) yields

$$\dot{e} := -S(r)(e - \delta) + \begin{bmatrix} 0 \\ -r\delta \end{bmatrix} + \begin{bmatrix} u_r \\ v_r \end{bmatrix} + v_c - R^T(\psi)\frac{\partial p_{Ref}}{\partial \gamma} \dot{\gamma} \tag{4.10}$$

$$\dot{e} := -S(r)(e - \delta) + \begin{bmatrix} u_r \\ -r\delta \end{bmatrix} + \begin{bmatrix} 0 \\ v_r \end{bmatrix} + v_c - R^T(\psi)\frac{\partial p_{Ref}}{\partial \gamma} \dot{\gamma} \tag{4.11}$$

$$\dot{e} := -S(r)(e - \delta) + \begin{bmatrix} 1 & 0 \\ 0 & -\delta \end{bmatrix}\begin{bmatrix} u_r \\ r \end{bmatrix} + \begin{bmatrix} 0 \\ v_r \end{bmatrix} + v_c - R^T(\psi)\frac{\partial p_{Ref}}{\partial \gamma} \dot{\gamma} \tag{4.12}$$

By setting

$$\Delta = \begin{bmatrix} 1 & 0 \\ 0 & -\delta \end{bmatrix} \text{ and } \bar{u}_d = \begin{bmatrix} u_r \\ r \end{bmatrix} \tag{4.13}$$

equation (4.12) can be written as

$$\dot{e} := -S(r)(e - \delta) + \Delta\bar{u}_d + \begin{bmatrix} 0 \\ v_r \end{bmatrix} + v_c - R^T(\psi)\frac{\partial p_{Ref}}{\partial \gamma}\dot{\gamma} \tag{4.14}$$

A stabilizing control law for the path following error dynamics (4.14), imported from the GAS reference controller (Vanni, 2007), is given by

$$\bar{u}_d := \Delta^{-1}\left[-K_k \tanh(e - \delta) - \begin{bmatrix} 0 \\ v_r \end{bmatrix} - v_c + R^T(\psi)\frac{\partial p_{Ref}}{\partial \gamma}\dot{\gamma}\right] \tag{4.15}$$

where

$$K_k = \begin{bmatrix} K_{kx} & 0 \\ 0 & K_{kr} \end{bmatrix} \tag{4.16}$$

Defining the following Lyapunov function

$$V(e) = \frac{1}{2}(e - \delta)^T(e - \delta) \tag{4.17}$$

its time derivative is given by

$$\dot{V}(e) = (e - \delta)^T \dot{e} \tag{4.18}$$

Replacing (4.15) into (4.14) yields

$$\dot{e} := -S(r)(e - \delta) - K_k \tanh(e - \delta) \tag{4.19}$$

Replacing (4.19) into (4.18) yields

$$\dot{V}_{\bar{u}_d}(e) = -(e - \delta)^T S(r)(e - \delta) - (e - \delta)^T K_k \tanh(e - \delta) \tag{4.20}$$

Since $S(r)$ is skew-symmetric, results

$$\dot{V}_{\bar{u}_d}(e) = -(e - \delta)^T K_k \tanh(e - \delta) \tag{4.21}$$

So, the contractive constraint can be stated as

$$\dot{V}_{u_d}(e) \le \dot{V}_{\bar{u}_d}(e) = -(e - \delta)^T K_k \tanh(e - \delta) \tag{4.22}$$

4.2.1.2 Lyapunov-Based MPC (L-MPC)

The introduction of the contractive constraint in the MPC formulation leads to the Lyapunov-Based MPC (L-MPC). Initially, the controller is designed considering the kinematic model as the system reference internal model. From (3.14), imposing no sway motion, results

$$
\begin{bmatrix} \dot{x} \\ \dot{y} \\ \dot{\psi} \end{bmatrix} = \begin{bmatrix} \cos\psi & -\sin\psi & 0 \\ \sin\psi & \cos\psi & 0 \\ 0 & 0 & 1 \end{bmatrix} \begin{bmatrix} u_r \\ 0 \\ r \end{bmatrix} + \begin{bmatrix} u_{ci} \\ v_{ci} \\ 0 \end{bmatrix}
$$

$$
\dot{\boldsymbol{\eta}}(t) \overset{def}{=} f(\boldsymbol{\eta}(t), \boldsymbol{u}(t), \boldsymbol{v_{ci}}(t))
$$

(4.23)

To implement the L-MPC, (4.23) must be discretized. Applying Euler's method with sampling time ΔT yields

$$
\begin{bmatrix} x(k+1) \\ y(k+1) \\ \psi(k+1) \end{bmatrix} = \begin{bmatrix} x(k) \\ y(k) \\ \psi(k) \end{bmatrix} + \Delta T \begin{bmatrix} u_r(k)\cos\psi(k) + u_{ci}(k) \\ u_r(k)\sin\psi(k) + v_{ci}(k) \\ r(k) \end{bmatrix}
$$

$$
\boldsymbol{\eta}(k+1) \overset{def}{=} f(\boldsymbol{\eta}(k), \boldsymbol{u}(k), \boldsymbol{v_{ci}}(k))
$$

(4.24)

The L-MPC controller is them formulated as an OCP, incorporating the cost function $J(.)$ and all applicable constraints, including the contractive constraint. The optimization window is limited to a predefined length N of future time instances and is shifted in every sample step (Hung, Rego, Crasta, & Pascoal, 2018)

$$
\min_{u_d} \left[J(\boldsymbol{\eta_0}, \boldsymbol{u_d}) = \sum_0^{N-1} l\left(\boldsymbol{\eta_{u_d}}(\gamma(k)), \boldsymbol{u_d}(k) \right) \right]
$$

(4.25)

$s.t$

$$
\boldsymbol{\eta_{u_d}}(\gamma(k+1)) = f(\boldsymbol{\eta_{u_d}}(\gamma(k)), \boldsymbol{u_d}(k), \boldsymbol{v_{ci}}(k))
$$

(4.26)

$$
\boldsymbol{\eta_{u_d}}(0) = \boldsymbol{\eta_0}
$$

(4.27)

$$
\dot{\gamma}(k) = u_{Ref}(k)
$$

(4.28)

$$
\boldsymbol{\eta_{u_d}}(\gamma(k)) \in \mathbb{X}, \forall\, k \in [0, N-1]
$$

(4.29)

$$
\boldsymbol{u_d}(k) \in \mathbb{U}, \forall\, k \in [0, N]
$$

(4.30)

$$
\dot{V}_{u_d}\left(e(\gamma(k)) \right) \leq \dot{V}_{\bar{u}_d}\left(e(\gamma(k)) \right)
$$

(4.31)

where the stage cost $l(\boldsymbol{\eta}_{u_d}, \boldsymbol{u}_d)$ is given by:

$$l(\boldsymbol{\eta}_{u_d}, \boldsymbol{u}_d) = \left\| \boldsymbol{\eta}_{u_d} - \boldsymbol{\eta}_{ref} \right\|_Q^2 + \left\| \boldsymbol{u}_d - \boldsymbol{u}_{ref} \right\|_R^2 \tag{4.32}$$

and the weighing (tuning) matrices Q and R are given respectively by

$$Q = \begin{bmatrix} q_x & 0 & 0 \\ 0 & q_y & 0 \\ 0 & 0 & q_\psi \end{bmatrix} \tag{4.33}$$

$$R = \begin{bmatrix} r_u & 0 \\ 0 & r_r \end{bmatrix} \tag{4.34}$$

For the current application, the OCP does not foresee the use of slack variables[67] since the applicable constraints can be categorized as "hard constraints" such as minimum and maximum speeds (associated to the limitations of the propulsion system) as well as forbidden positions (to avoid collisions with obstacles).

The OCP (4.25) - (4.31) can be solved by three basic approaches (Diehl, Bock, Diedam, & Wieber, 2006):

- Dynamic Programing (relying on the optimality principle associated to the Hamilton-Jacobi-Bellman equation);
- Indirect Methods (relying on a boundary value problem solved by variational calculus, Euler-Lagrange differential equations or Pontryagin's maximum principle); and
- Direct Methods (relying on the transformation of the original infinite OCP into a finite dimensional NLP.

Direct Methods are nowadays the most successful approach used to solve constrained OCP. The main advantage of this approach consists in its ability to easily treat inequality constraints subjected to structural changes during the optimization process. Generally, Direct Methods can be categorized into sequential and simultaneous approaches (Diehl, Bock, Diedam, & Wieber, 2006).

In the sequential approach, the state trajectory is considered as an implicit function of the controls, and of the initial state. Simulation and optimization steps run

---

[67] The system can be eventually driven into a region where the MPC problem is infeasible and hence no control action can be computed. Feasibility can be recovered by softening the constraints using slack variables, during intermediate stages of the process.

sequentially, and the discretized control is the only decision variable in the optimization process.

The most popular variant of this approach is direct single shooting (Diehl, Bock, Diedam, & Wieber, 2006). Besides its advantage concerning simplicity, direct single shooting is not suitable for nonlinear and/or unstable systems, in long prediction horizon applications, due to nonlinearity propagation (Mehrez, 2019).

Differently, in the simultaneous approach, the parameterized state trajectory is also a decision variable in the optimization process, being computed as an equality constraint. In this way, the effect of nonlinearity propagation is reduced compared to the sequential approach. Simulation and optimization steps run simultaneously, and only the NLP solution that complies with the equality constraints imposed by the system dynamics represents a valid control.

The most popular variant of this approach is direct multiple shooting, considered to be the best choice to solve nonlinear OCP in robotics. (Diehl, Bock, Diedam, & Wieber, 2006). The key idea is to break down the system integration into short time intervals, i.e., to use the system model as a state constraint at each optimization step. It exhibits good convergence properties and can be easily parallelized (Andersson, Gillis, Horn, Rawlings, & Diehl, 2019). Adopting such approach, the OCP (4.25) - (4.31) can be transcribed into a direct multiple shooting NLP as:

$$\min_{w} \Phi(w) \tag{4.35}$$

$$s.t$$

$$\boldsymbol{g_1}(w) = \begin{bmatrix} g_1(\boldsymbol{x_0}, \boldsymbol{u_0}) \\ \vdots \\ g_1(\boldsymbol{x_{N-1}}, \boldsymbol{u_{N-1}}) \\ g_1(\boldsymbol{x_N}) \end{bmatrix} \leq 0 \tag{4.36}$$

$$\boldsymbol{g_2}(w) = \begin{bmatrix} \overline{x}_0 - x_0 \\ f(\boldsymbol{x_0}, \boldsymbol{u_0}) - \boldsymbol{x_1} \\ \vdots \\ f(\boldsymbol{x_{N-1}}, \boldsymbol{u_{N-1}}) - \boldsymbol{x_N} \end{bmatrix} = 0 \tag{4.37}$$

where $\boldsymbol{\Phi}$ is the objective function, $w = [\boldsymbol{u_0} \quad \cdots \quad \boldsymbol{u_{N-1}} \quad , \quad \boldsymbol{x_0} \quad \cdots \quad \boldsymbol{x_N}]$ is the decision variable, $\boldsymbol{g_1}$ are the inequality constraints and $\boldsymbol{g_2}$ are the equality constraints.

4.2.2 Inner (Dynamic) Loop

Once issued the speed assignment, the next task consists in assuring its tracking. For that, let's consider the speed assignment tracking error

$$\tilde{\boldsymbol{u}}(t) := \boldsymbol{u}(t) - \boldsymbol{u}_d(t) \tag{4.38}$$

where $\boldsymbol{u}$ and $\boldsymbol{u}_d \in \mathbb{R}^2$ are the vectors of real and assigned speeds, respectively. Thus, the speed assignment tracking error dynamics is given by

$$\dot{\tilde{\boldsymbol{u}}}(t) := \dot{\boldsymbol{u}}(t) - \dot{\boldsymbol{u}}_d(t) \tag{4.39}$$

Inserting (3.25) into (4.39) results

$$\dot{\tilde{\boldsymbol{u}}} = M^{-1}(-C(\boldsymbol{u})\boldsymbol{u} - D(\boldsymbol{u})\boldsymbol{u} + \boldsymbol{\tau}_c) - \dot{\boldsymbol{u}}_d \tag{4.40}$$

The control objective consists in assuring that $\tilde{\boldsymbol{u}}$ converges asymptotically to the origin, which can be accomplished by setting the following control law

$$\boldsymbol{\tau}_c = -K_D(\boldsymbol{u} - \boldsymbol{u}_d) + M\dot{\boldsymbol{u}}_d + C(\boldsymbol{u})\boldsymbol{u} + D(\boldsymbol{u})\boldsymbol{u}_d \tag{4.41}$$

where $K_d \in \mathbb{R}^{2\times2}$. If the terms $C(\boldsymbol{u})\boldsymbol{u}$[68] and $\dot{\boldsymbol{u}}_d$[69] are neglected and considered as input perturbations, them (4.41) reduces to

$$\boldsymbol{\tau}_c = -K_d(\boldsymbol{u} - \boldsymbol{u}_d) + D(\boldsymbol{u})\boldsymbol{u}_d \tag{4.42}$$

and (4.40) reduces to

$$\dot{\tilde{\boldsymbol{u}}} = -M^{-1}(D(\boldsymbol{u})\tilde{\boldsymbol{u}} + K_D\tilde{\boldsymbol{u}}) \tag{4.43}$$

So, since $D(\boldsymbol{u})$ is positive-definite, and K_d can be set to be diagonal positive-definite, them the origin $\tilde{\boldsymbol{u}} = \boldsymbol{0}$ is globally asymptotically stable.

---

[68] To avoid the need of a sway sensor.
[69] To decouple the dynamics of inner and outer loops.

4.3   Moving Horizon Estimator (MHE)

The design of high-performance state estimators for robotics applications has become a key issue due to increasing complexity and more stringent operational safety requirements (Brembeck, 2019). To solve the state estimation problem, this thesis anticipates the use of an MHE. The MHE, differently from EKF, supplies its estimates based on the most recent windows of previous states and control actions[70].

The MHE acts as a filter, providing noise attenuated estimates of position and heading measurements for the L-MPC. The optimization window is limited to a predefined length of previous time instances (N_{MHE}) and is shifted in every sample step. The length of the sliding window is intrinsically linked to the estimates' smoothness.

To deal with measurement noise, it is necessary to consider a measurement model in the MHE structure

$$\begin{bmatrix} z_x \\ z_y \\ z_\psi \end{bmatrix} = \begin{bmatrix} x \\ y \\ \psi \end{bmatrix} + \begin{bmatrix} n_x \\ n_y \\ n_\psi \end{bmatrix} \Rightarrow z = h(\eta) + n_\eta \tag{4.44}$$

where sensor noises are distributed as $n_x \sim \mathcal{N}(0, \sigma_x^2)$, $n_y \sim \mathcal{N}(0, \sigma_y^2)$ and $n_\psi \sim \mathcal{N}(0, \sigma_\psi^2)$, resulting in the following covariance matrix

$$Q_* = \begin{bmatrix} \sigma_x^2 & 0 & 0 \\ 0 & \sigma_y^2 & 0 \\ 0 & 0 & \sigma_\psi^2 \end{bmatrix} \tag{4.45}$$

Additionally, the MPC motion model must be adjusted to take into account the presence of noise in the velocity measurements

$$\begin{bmatrix} z_u \\ z_r \end{bmatrix} = \begin{bmatrix} u \\ r \end{bmatrix} + \begin{bmatrix} n_u \\ n_r \end{bmatrix} \Rightarrow u_M = u + n_u \tag{4.46}$$

where z_u and z_r are the control commands measured by dedicated sensors.

The associated noises are modeled as $n_u \sim \mathcal{N}(0, \sigma_u^2)$ and $n_r \sim \mathcal{N}(0, \sigma_r^2)$, resulting in the following covariance matrix

---

[70] In EKF, the most recent estimate depends on the previous state and last control action (Markov assumption).

$$R_* = \begin{bmatrix} \sigma_u^2 & 0 \\ 0 & \sigma_r^2 \end{bmatrix} \tag{4.47}$$

The MHE is them formulated as an OCP, incorporating the cost function $J(.)$ and all applicable constraints. The optimization window is limited to a predefined length N_{MHE} of previous time instances and is shifted in every sample step: (Mehrez, 2019)

$$\min_{\eta,u} \left[J(\boldsymbol{\eta},\boldsymbol{u}) = \sum_{i=k-N_{MHE}}^{k} \|z_M(i) - h(\eta(i))\|_{Q_*^{-1}}^2 + \sum_{i=k-N_{MHE}}^{k-1} \|u_M(i) - u(i)\|_{R_*^{-1}}^2 \right] \tag{4.48}$$

$s.t$

$$\boldsymbol{\eta_u}(i+1) = f(\boldsymbol{\eta_u}(i), \boldsymbol{u}(i)) \tag{4.49}$$

$$\boldsymbol{\eta_u}(i) \in \mathbb{N}, \forall i \in [k - N_{MHE}, k] \tag{4.50}$$

$$\boldsymbol{u}(i) \in \mathbb{U}, \forall i \in [k - N_{MHE}, k-1] \tag{4.51}$$

where z_M and u_M are the vectors containing the measurement of position/heading and velocities, respectively, and the weighing (tuning) matrices Q_*^{-1} and R_*^{-1} are the inverse of the covariance matrices (4.45) and (4.47)[71].

4.4   Ocean Current State Observer

In the presence of an ocean current, the L-MPC needs to receive information about its velocity, in order to issue the proper speed assignment. However, to avoid the need of a dedicated sensor, the system encompasses an ocean current state observer.

The ocean current state observer is designed based on the kinematic model (3.17), corrected with the velocity components of the ocean current (3.26), referenced to the Earth-Fixed inertial frame $\{I\}$

$$\dot{\boldsymbol{p}} = R(\psi)\boldsymbol{v_r} + \boldsymbol{v_{ci}} \tag{4.52}$$

The following ocean current observer is borrowed from (Aguiar & Pascoal, 2007b):

[71] If the measurement covariance is high, the associated penalizing factor will be low and the contribution of such measurement in the OCP will be reduced, and vice versa.

$$\dot{\boldsymbol{p}} = R(\psi)\boldsymbol{v}_r + \widehat{\boldsymbol{v}}_{ci} + K_{p\_obs}\widetilde{\boldsymbol{p}} \tag{4.53}$$

$$\dot{\widehat{\boldsymbol{v}}}_{ci} = K_{c\_obs}\widetilde{\boldsymbol{p}} \tag{4.54}$$

where K_{p_obs} and K_{c_obs} are the observer diagonal gain matrices. The estimation errors are given by:

$$\widetilde{\boldsymbol{p}} = \boldsymbol{p} - \widehat{\boldsymbol{p}} \tag{4.55}$$

$$\widetilde{\boldsymbol{v}}_{ci} = \boldsymbol{v}_{ci} - \widehat{\boldsymbol{v}}_{ci} \tag{4.56}$$

For constant current ($\dot{\boldsymbol{v}}_{ci} = 0$), the estimation errors dynamics are:

$$\dot{\widetilde{\boldsymbol{p}}} = -K_{p\_obs}\widetilde{\boldsymbol{p}} + \widetilde{\boldsymbol{v}}_{ci} \tag{4.57}$$

$$\dot{\widetilde{\boldsymbol{v}}}_{ci} = -K_{c\_obs}\widetilde{\boldsymbol{p}} \tag{4.58}$$

If the observer gain matrices are tuned to be strictly positive, then the estimation errors will converge asymptotically to zero.

4.5   Summary

In this chapter, the Path-Following Controller responsible for the individual motion control of the vehicles was designed, split in an inner-outer loop structure. The outer loop, composed by a L-MPC, solved the kinematic task (guidance scheme), while the inner loop, composed by a Feedback Linearization controller, solved the dynamic task (speed tracking scheme). The controller also encompasses a MHE and an ocean current state observer.

To assure L-MPC recursive feasibility and stability, a contractive constraint, inherited from a reference globally asymptotically stable controller, was included in the associated OCP formulation. This approach suppressed the need to adopt a terminal cost and a terminal constraint set in the associated OCP.

In order to provide noise attenuates estimates of position and heading measurements for the L-MPC, the system also foresees an MHE. Fully based on the receding horizon concept, it can handle the applicable physical constraints while fully exploiting its own internal model. Another advantage concerns the simplicity of its tuning process, relying exclusively on the knowledge of measurement noise covariances. Additionally, an ocean current state observer was designed to avoid the need to measure the ocean current's velocity.

5   COOPERATIVE CONTROLLER

In this chapter, the cooperative controller is developed. Representing the higher layer of the control architecture, this module is responsible for controlling the collective motion of the vehicles, assuring that a desired geometric pattern (formation) is reached. It relies on a decentralized consensus strategy in which the vehicles exchange information over a communication network, to agree on a certain variable of interest. The controller also incorporates a logic-based communication algorithm to assure that communication occurs only when strictly necessary, on a discrete basis.

5.1   Problem Statement

Technical issues associated with underwater communication such as limited bandwidth and range, latency, intermittent failures and multipath effects (Ghabcheloo, et al., 2009) impose severe restrictions on the information flow among the vehicles, leading to the need to reduce it as much as possible. For that reason, a centralized control system based on the knowledge of all coordination parameters of all vehicles is not a practical solution for this type of application[72] (Vanni, 2007).

An alternative to minimize the information flow is to adopt a decentralized control strategy at the vehicle level. In this approach, for a given vehicle, the control action is obtained locally, based only on the knowledge of the coordination parameters of the neighboring vehicles that communicate with it. Due to the simplicity of the control law, consensus theory[73] has normally been chosen to tackle the problem.

To solve the formation control problem in the framework of consensus strategy, it is necessary to synchronize the formation (more specifically, to synchronize some pre-defined states of the vehicles). Once the synchronization states reach agreement, the formation control problem is indirectly solved, and the desired geometric pattern is achieved (Ghabcheloo, et al., 2009).

Consider a group of n vehicles $\mathcal{N} := \{1, \ldots, n\}$, each with its own parameterized path $\boldsymbol{p}_{Ref}^{i}(\gamma_i)$, $i \in \mathcal{N}$. Additionally, let $\mathcal{N}_i$ be the set of vehicles that

---

[72] Every vehicle would have to receive, either directly or through other vehicles, information about the rest of the formation, resulting in a significant information flow (Vanni, 2007).

[73] Supported by graph theory, to model the communication network.

vehicle i communicates with (the neighboring vehicles). By setting γ_i as the synchronization states of the vehicles, consensus (or agreement) among such states is reached when the following condition is attained (Ghabcheloo, et al., 2009)

$$\gamma_{ij}(t) := \gamma_i(t) - \gamma_j(t) \to 0 \ \forall \ i,j \ \in \ \mathcal{N} \tag{5.1}$$

where the term γ_{ij}, denominated "along-path distance", represents an appropriate measure of the distance between vehicles i and j in the formation[74].

To achieve its goal, the cooperative controller must adjust the desired speeds of the vehicles (u_{Ref}^i) according to the "along-path distances". The key concept behind its implementation is to set a common speed profile $(\bar{u}_r(\gamma))$ to all paths, and to introduce a control variable for each vehicle, in the form of a correction speed term $(\tilde{u}_c^i)$

$$u_{Ref}^i = \bar{u}_r(\gamma) + \tilde{u}_c^i \tag{5.2}$$

where the correction speed term $\tilde{u}_c^i$ is determined based on the "along-path distances" among vehicle i and the vehicles that communicate with it[75]. After reaching consensus, $\gamma_i(t) = \gamma_j(t) = \gamma$, and $\tilde{u}_c^i = 0$, which means that the whole formation travels synchronized at an assigned speed profile $\bar{u}_r(\gamma)$.

DEFINITION 5.1: (*Cooperative Control Problem*): *For each vehicle $i \in \mathcal{N}$, derive a control law for the correction speed $\tilde{u}_c^i = f(\gamma_i, \gamma_j)$, with $j \in \mathcal{N}_i$, such that $\lim_{t \to \infty}[\gamma_i(t) - \gamma_j(t)] = 0, \quad \forall \ i, \ j \ \in \ \mathcal{N}, \ and \ \lim_{t \to \infty}[\dot{\gamma}_i(t) - \bar{u}_r(\gamma(t))] = 0, \quad \forall \ i \ \in \ \mathcal{N}. The former condition imposes that all synchronization errors converge to zero, while the latter imposes that the formation speed converges to the common speed assignment* (Ghabcheloo, et al., 2009) and (Vanni, Aguiar, & Pascoal, 2008)*.*

To implement the inter-vehicle communication, the communication topology is modeled using Graph Theory (Appendix A2). The vehicles are represented by vertices in a graph, and the communication links are represented by its edges. It is

---

[74] The "along-path distance" definition is intrinsically linked to the path parametrization, as detailed in (Ghabcheloo, et al., 2009).

[75] This strategy is categorized as a decentralized one, since the calculation of $\tilde{v}_{di}$ relies exclusively on information available to vehicle i, *i.e.*, its own synchronization state and the synchronization states of the vehicles that communicate with it.

assumed that each vehicle is capable of communicating bidirectionally with their neighboring vehicles (bidirectional interconnection network, represented by undirected edges).

The Cooperative Control scheme, already incorporated in the whole control system, is illustrated in Figure 5-1.

Figure 5-1: Path following controller + cooperative controller

(From Author)
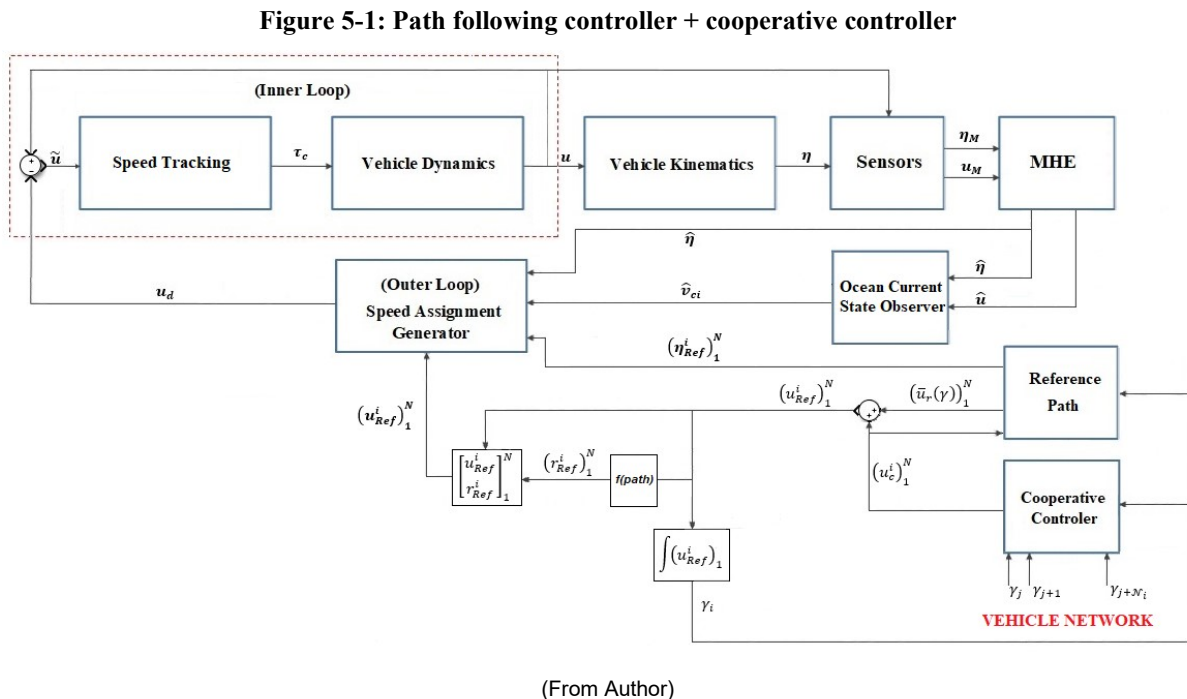
5.2 Cooperative Controller

The cooperative controller design is performed in two steps. Firstly, considering continuous communication[76], and after considering discrete communication through the implementation of a logic-based communication algorithm.

5.2.1 Continuous Communication

Let the communication network topology be represented by Graph $G(v, \varepsilon)$. The error vector describing its restrictions is given by

$$\xi = L_D \gamma \tag{5.3}$$

where $\xi \in \mathbb{R}^n$ is the error vector, $L_D = D^{-1}(D - A) \in \mathbb{R}^{n \times n}$ is the normalized Graph Laplacian associated to the communication network topology and $\gamma \in \mathbb{R}^n$ is the vector

---

[76] Performed at constant predefined time intervals.

containing the synchronization states of the vehicles. The elements of the error vector ξ are defined as

$$\xi_i = \gamma_i - \frac{1}{|\mathcal{N}_i|} \sum_{j \in \mathcal{N}_i} \gamma_j \qquad (5.4)$$

The dynamics of the error vector is given by

$$\dot{\xi} = L_D \dot{\gamma} \qquad (5.5)$$

The dynamics of the synchronization state vector is given by

$$\dot{\gamma} = \bar{u}_r(\gamma) + \tilde{u}_c \qquad (5.6)$$

PROPOSITION 5.1 *(Cooperative Control – Continuous Communications): The error vector converges asymptotically to the origin (synchronization) if the following decentralized control law is imposed over the correction speed term vector:*

$$\tilde{u}_c = -K_\xi \tanh(L_D \gamma) \qquad (5.7)$$

5.2.2 Event-Based Communication

Continuous communication is a costly and even an unnecessary practice. Particularly for underwater applications, it is unfeasible due to the technical issues previously mentioned. In this step, the cooperative control law is adjusted considering the inclusion of a logic-based communication algorithm, so that communication occurs on a discrete basis, strictly when really necessary.

Based on (Aguiar & Pascoal, 2007a) and (Vanni, Aguiar, & Pascoal, 2008) each vehicle is equipped with a supervisory logic-based communication algorithm that decides the moment to update and broadcast an information pack to the neighbors, based on a predefined criterion. During the time interval between two consecutive broadcasts, each vehicle runs estimates of the synchronization states of its neighbors as well as of its own state (self-state estimation). If the self-estimation error reaches a predefined threshold, the communication is triggered, and the associated information pack is broadcasted.

Let t_k^i for all $k \in \mathbb{Z}^+$ be the time instants in which vehicle i updates its cooperative control signal $\tilde{u}_c^i(t) = \tilde{u}_c^i(t_k^i)$ for all $t \in \left[t_k^i, t_{k+1}^i\right]$ and transmits the

information pack $C_i(t_k^i) := [t_k^i \quad \gamma_i(t_k^i) \quad \tilde{u}_c^i(t_k^i)]$ to its neighbors. Based on such information, the state of vehicle i is estimated by vehicle i itself (self-state estimation) and by vehicles $j \in \mathcal{N}_i$, according to:

$$\hat{\gamma}_i^i(t) = \hat{\gamma}_i^j(t) = \gamma_i(t_k^i) + (t - t_k^i)\left[\bar{u}_r + \tilde{u}_c^i(t_k^i)\right] \tag{5.8}$$

Vehicle i communicates its information pack to its neighbors if the following Event-Trigger Condition (ETC) is violated[77]:

$$\text{ETC} = \tilde{\gamma}_i^i(t) = \left|\gamma_i(t) - \hat{\gamma}_i^j(t)\right| \geq \varepsilon^2 \tag{5.9}$$

PROPOSITION 5.2 *(Cooperative Control – Discrete Communications): The error vector converges asymptotically to the origin (synchronization) if the following decentralized control law is imposed over the correction speed term vector:*

$$\tilde{\boldsymbol{u}}_c = -K_\xi \tanh(\boldsymbol{\gamma} - D^{-1}A\hat{\boldsymbol{\gamma}}) \tag{5.10}$$

The logic-based communication algorithm for an individual vehicle is presented in Table 5-1:

Table 5-1: Logic-based communication algorithm

Input: Information received $C_j(t_k^j) \; \forall j \in \mathcal{N}_i$ and γ_i
Output: Communication Pack C_i and control output $\tilde{v}_{di}$
1: Initialization
2: Define $K \leftarrow 0$; $t_k^i \leftarrow t$; $\tilde{u}_c^i(t_k) \leftarrow 0$; $\gamma_i(t_k) \leftarrow \gamma_i$
3: Transmit $C_i(t_k^i)$
4: For $t = h\tau_s$ where $h \in \mathbb{Z}^+$
5:     Estimate $\hat{\gamma}_i^j \; \forall j \in \mathcal{N}_i$, using (5.8)
6:     Compute ETC using (5.9)
7:   If $\xi = \left\|\gamma_i - \hat{\gamma}_i^i\right\| \leq \varepsilon^2$ them
8:     $K \leftarrow K + 1$; $t_k^i \leftarrow t$; $\gamma_i(t_k^i) \leftarrow \gamma_i(t)$
9:     Compute $\tilde{u}_c^i(t_k^i)$ using (5.10)
10:     Reset $\xi(t_k^i)$ to zero
11:     Transmit $C_i(t_k^i)$
12:   End If
13: Output $\tilde{u}_c^i(t) = \tilde{u}_c^i(t_k^i)$
14: End For

---

[77] Lower tolerance ε^2 reduces the neighborhood of the origin to which ξ converges but increases the number of messages exchanged among

5.3   Adjustment of the L-MPC Formulation

In cooperative mode, the OCP (4.25) - (4.31) associated to vehicle i must be adjusted to take into account the correction speed term $\tilde{u}_c^i$. To accomplish that, the OCP must predict, over the prediction horizon N, the value of the path parameter γ_i ($\hat{\gamma}_i^i$) driven by the path following input u_d^i, as well as the values of the path parameter γ_j ($\hat{\gamma}_j^i$) of its neighboring vehicles (Hung & Pascoal, 2018). In this way, the adjusted OCP results

$$\min_{u_d^i}\left[J^i\left(\boldsymbol{\eta}_0^i,\boldsymbol{u}_d^i\right)=\sum_0^{N-1}l\left(\boldsymbol{\eta}_{u_d}^i(\gamma(k)),\boldsymbol{u}_d^i(k)\right)\right] \tag{5.11}$$

$s.t$

$$\boldsymbol{\eta}_{u_d}^i(\gamma(k+1))=f^i(\boldsymbol{\eta}_{u_d}^i(\gamma(k)),\boldsymbol{u}_d^i(k),\tilde{u}_c^i,\boldsymbol{v}_{ci}(k)) \tag{5.12}$$

$$\boldsymbol{\eta}_{u_d}^i(0)=\boldsymbol{\eta}_0^i \tag{5.13}$$

$$\dot{\gamma}_i^i(k)=u^i=\bar{u}_r^i(k)+\tilde{u}_c^i \tag{5.14}$$

$$\dot{\gamma}_j^i(k)=u^j=\bar{u}_r^j(k)+\tilde{u}_c^j \quad \forall\, j\in\mathcal{N}_i \tag{5.15}$$

$$\boldsymbol{\eta}_{u_d}^i(\gamma(k))\in\mathbb{X},\forall\, k\in[0,N-1] \tag{5.16}$$

$$\boldsymbol{u}_d^i(k)\in\mathbb{U},\forall\, k\in[0,N] \tag{5.17}$$

$$\dot{V}_{u_d^i}^i\left(e(\gamma(k))\right)\le\dot{V}_{\bar{u}_d^i}^i\left(e(\gamma(k))\right) \tag{5.18}$$

where the stage cost $l\left(\boldsymbol{\eta}_{u_d}^i,\boldsymbol{u}_d^i\right)$ is given by

$$l\left(\boldsymbol{\eta}_{u_d}^i,\boldsymbol{u}_d^i\right)=\left\|\boldsymbol{\eta}_{u_d}^i-\boldsymbol{\eta}_{ref}^i\right\|_Q^2+\left\|\boldsymbol{u}_d^i-\boldsymbol{u}_{ref}^i\right\|_R^2 \tag{5.19}$$

5.4   Summary

In this chapter, the cooperative controller responsible for the vehicles' collective motion (formation) was designed. The cooperative control problem was solved in a decentralized framework at vehicle level, based on consensus and Lyapunov theories. The inter-vehicle communication network was modeled using graph theory, considering that each vehicle was capable of communicating with its neighbors and vice versa. The controller was initially designed considering the premise of continuous communication and then, by incorporating a logic-based communication algorithm, it was adjusted for discrete communication, assuring that the vehicles communicate only when strictly necessary.

6   NUMERICAL RESULTS

The simulations were performed utilizing the interior-point optimization method, provided by the IPOPT (Interior Point Optimizer) package[78] (Wächter & Biegler, 2006), coupled with MATLAB/SIMULINK via the CasADi toolbox (Andersson, Gillis, Horn, Rawlings, & Diehl, 2019).

CasADi (CasADi Software, 2018) is an open-source symbolic framework for algorithmic differentiation and numerical optimization. This tool provides a low-level framework for rapid and efficient implementation of algorithms for nonlinear numerical optimization such as nonlinear model predictive control[79] and other online and offline techniques.

The control scheme adopted in the simulations is presented in Figure 5-1 (for circular paths, the cooperative control scheme must be adjusted as shown in Figure 6-2). For one specific simulation case, this scheme was adapted to allow the suppression of dedicated speed sensors, as shown in Figure 6-1. In this case, the L-MPC outer loop signal (blue line) was used to feed directly the MHE and the ocean current state observer.

Figure 6-1: Adapted control scheme for speed sensors suppression
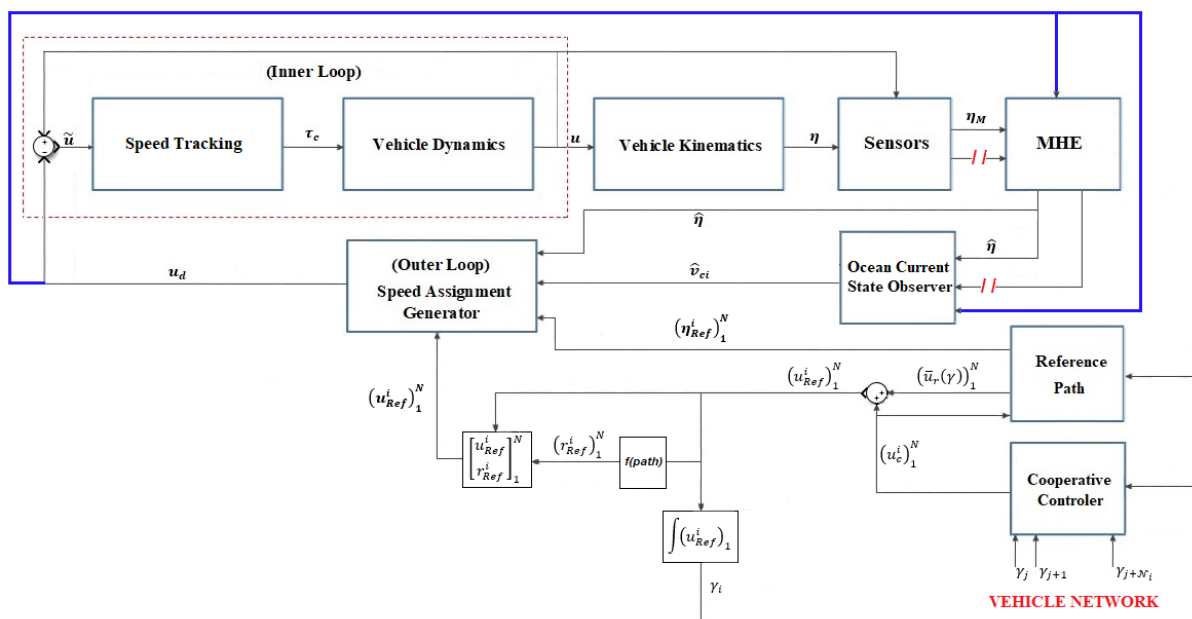
(From Author)

---

[78] IPOPT is an open-source software package for large-scale nonlinear optimization.
[79] CasADi in fact doesn't solve the problems but facilitates the implementation of different methods for numerical optimal control, by allowing post-installation addition of solvers and plugins.

Figure 6-2: Cooperative control scheme correction (circular paths)
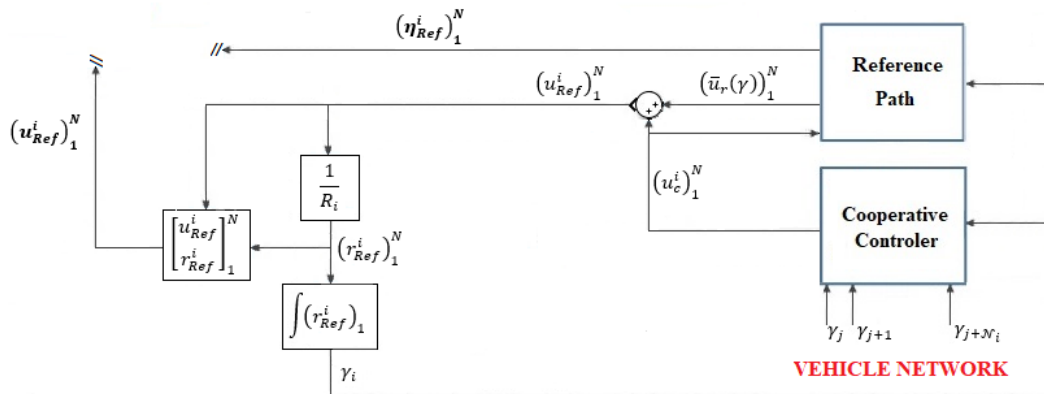
(From Author)

The system gains are summarized in Appendix B.

6.1   Simulation Description

In general terms, the main objective of this set of simulations is to assess recursive feasibility, stability and performance. To conduct this verification and validation step, five (5) simulation scenarios were envisaged:

- **Scenario 1:** Intends to assess the path following controller (MPC and L-MPC) convergence, compared to the reference feedback linearization path following controller (FLC). Intends also to evaluate the effect of the contractive constraint in the OCP solution.

- **Scenario 2:** Intends to verify the path following controller convergence (MPC x L-MPC) combined with obstacle avoidance capabilities, in single non-cooperative missions.

- **Scenario 3:** Intends to assess the performance of the cooperative path following controller, in multi-vehicle cooperative missions, however without considering measurement noise and ocean currents.

- **Scenario 4:** Intends to verify the performance of the cooperative path following controller, in multi-vehicle cooperative missions, however considering the presence of measurement noise and ocean currents. Thus, in this scenario, the estimators (MHE and ocean current observer) are included into the control loop. Particularly for this setting, the L-MPC outer loop signal is used to feed the estimators.

- **Scenario 5:** Similar to scenario 4, however incorporating the dynamics of the actuators and using the speed measurements to feed the estimators.

Each scenario is conceived considering particular cases in order to check the effects of different initial conditions and path types, as summarized in Table 6-1.

Table 6-1: Simulation summary

Scenario		Path	Speed Profile	Mode	Vehicles	Current (0,2 m/s)	Obstacle Avoidance	Noise
1	a	Straight	Constant	Single	1 ASC	x	x	x
	b	Circular	Constant	Single	1 ASC	x	x	x
2	a	Straight	Constant	Single	1 ASC	x	√	x
	b	Sinusoidal	Variable	Single	1 ASC	x	√	x
3	a	Circular	Variable	Cooperative	1 ASC / 2 AUV	x	x	x
	b	Mooring	Variable	Cooperative	3 AUV	x	x	x
4	a	Circular	Constant	Single	1 AUV	x	x	√
	b	Circular	Variable	Cooperative	3 AUV	√	√	√
5[80]	-	Circular	Variable	Cooperative	3 AUV	√	√	√

The speed limits of the vehicles (physical hard constraints) are presented in Table 6-2. The OCP $(t, x(\gamma(t)), T_p)$ parameters are summarized in Table 6-3.

Table 6-2: Speed limits

Vehicle	u (m/s)	r (rad/s)
ASC / AUV	$0,00 \leq u \leq 1,50$	$|r| \leq 0.50$

Table 6-3: OCP parameters

Cases		Module	t_s(s)	T_p(s)	N_p	N_c
1, 2 and 3	-	MPC	0,2	2,0	10	9
4a	i /ii	MPC	0,2	2,0	10	9
	i	MHE	0,2	1,0	5	4
	ii	MHE	0,1	1,0	10	9
4b	-	MPC	0,1	1,0	10	9
	-	MHE	0,1	1,0	10	9
5	-	MPC	0,1	1,0	10	9
	-	MHE	0,1	1,0	10	9

[80] Similar to 4b, however incorporating the dynamics of the actuators and using speed measurements to feed the estimators (MHE and ocean current observer).

In the path figures, the vehicle's position/heading is represented by a filled arrow (out of scale to improve visualization), and the trajectory by a dashed line. For path zoomed figures, the vehicles' predicted positions are represented by asterisks and their associated boundaries are represented by circles.

6.1.1 Scenario 1

In this scenario, the convergence of the path following controller is compared with the feedback linearization controller given by (4.15). Two cases were envisaged:

a) Starting at $(x = 55, \ y = 10, \ \psi = -\pi/2)$, the vehicle is supposed to follow a straight-line reference path, parameterized by $P_d(\gamma(t)) = (30 + 0.7\gamma(t), 30 + 0.7\gamma(t))$, with constant speed of 1 m/s; and

b) Starting at $(x = 35, \ y = 35, \ \psi = 0)$, the vehicle is supposed to follow a circular reference path, parameterized by $P_d(\gamma(t)) = (30\cos(\gamma(t)), 30\sin(\gamma(t)))$, with a constant speed of 1 m/s.

6.1.2 Scenario 2

In this scenario, the obstacle avoidance capability of the path following controller is analyzed. Two cases were envisaged:

a) Starting at $(x = 10, \ y = 55, \ \psi = -\pi)$, the vehicle is supposed to follow a parameterized straight-line reference path $P_d(\gamma(t)) = (30 + 0.7\gamma(t), 30 + 0.7\gamma(t))$, with constant speed of 1 m/s, while avoiding collision with a 5 m diameter circular obstacle; and

b) Starting at $(x = 10, \ y = 25, \ \psi = -\pi)$, the vehicle is supposed to follow a parameterized sinusoidal reference path $P_d(\gamma(t)) = 10\sin(0.1\gamma(t))$, with a variable speed profile $u(\gamma(t)) = 1 + 0.5\sin(0.1\gamma(t))$, while avoiding collision with a 5 m diameter circular obstacle.

6.1.3 Scenario 3

In this scenario, the cooperative path following controller is tested in multi-vehicle cooperative missions, without considering measurement noise and ocean currents. Two cases were envisaged to check the effect of adopting different parametrizations of the synchronization state γ, according to the path characteristics:

a) Considering concentric circular paths, as summarized in Table 6-4; and

b) Considering lay-mooring "U" paths, as summarized in Table 6-5.

Table 6-4: Scenario 3 – Case A (mission characteristics)

Vehicle	Starting Position	Circular Radius (m)	Graph Laplacian (L)	Formation Pattern ("s")	
				1st / 2nd Q	3rd / 4th Q
AUV1	$(x = 25, y = 0, \psi = \pi/2)$	30	$\begin{bmatrix} 2 & -1 & -1 \\ -1 & 2 & -1 \\ -1 & -1 & 2 \end{bmatrix}$	0	0,2
ASC1	$(x = 30, y = 0, \psi = \pi/2)$	35		0,2	0,2
AUV2	$(x = 45, y = 0, \psi = \pi/2)$	40		0	0,2
ASC1 (leader) Speed Assignment (rad/s)				0,020	0,033

Table 6-5: Scenario 3 – Case B (mission characteristics)

Vehicle	Starting Position	Semicircular Radius (m)	Graph Laplacian (L)	Formation Pattern ("s")	
				1st Part	2nd Part
AUV1	$(x = 25, y = -5, \psi = 0)$	10	$\begin{bmatrix} 2 & -1 & -1 \\ -1 & 2 & -1 \\ -1 & -1 & 2 \end{bmatrix}$	0	0
AUV2	$(x = 20, y = -10, \psi = 0)$	15		0	2
AUV3	$(x = 35, y = -25, \psi = 0)$	20		0	0
AUV2 (leader) Speed Assignment (m/s)				1,0	

6.1.4 Scenario 4

In this scenario, the MHE is tested according to the following cases:

a) Single mission, varying the OCP parameters, according to Table 6-3; and

b) Cooperative mission, considering three AUV deployed along concentric circular paths, where only AUV2 is equipped with MHE and subjected to measurement noise. The measurement noises were set as ($\sigma_x^2 = 0.1\,m$, $\sigma_y^2 = 0.1\,m$, $\sigma_\psi^2 = 0.01\,rad$, $\sigma_u^2 = 0\,m/s$, $\sigma_r^2 = 0\,rad/s$)[81] . Additionally, a 3 m circular obstacle is considered in the AUV2 path to check its obstacle avoidance capability. The initial conditions and the formation patterns are the same as scenario 3 – case a) (Table 6-4).

6.1.5 Scenario 5

Similar to scenario 4-b, however emulating the dynamics of the actuators (using a Simulink rate limiter dynamic block). Additionally, differently from the previous case, the MHE and the ocean current observer were fed with speed measurements instead of outer loop signals ($\sigma_x^2 = 0.1\,m$, $\sigma_y^2 = 0.1\,m$, $\sigma_\psi^2 = 0.01\,rad$, $\sigma_u^2 = 0.1\,m/s$, $\sigma_r^2 = 0.01\,rad/s$).

---

[81] To suppress the need for speed sensors, the speed measurements required to run the MHE, and the ocean current state observer were replaced by the L-MPC speed outputs, thus measurement noise does not apply for them.

6.2   Simulation Results

6.2.1   Scenario 1

The simulation has shown that, for the considered initial conditions, MPC is stable and presents better performance than FLC, since it converges faster to the reference path. On the other hand, L-MPC which is globally asymptotically stable due to the contractive constraint, presents intermediate performance compared to MPC and FLC.

In this way, a clear compromise is noticed between global asymptotic stability and performance. This fact is consistent with the contractive constraint concept, which limits L-MPC Lyapunov function time derivative, producing the same effect of a terminal constraint.

Case A

The paths are presented in Figure 6-3. It can be noticed that both MPC and L-MPC converge to the path much faster than FLC. However, the difference between MPC and L-MPC is not so significant. The outer-loop control signals are presented in Figure 6-4, showing that linear speeds attain its maximum allowable value (1,5 m/s) during path approaching phase and, after that, converge for the assigned speed (1,0 m/s). The position error norm is presented in Figure 6-5, indicating that L-MPC presents an intermediate convergence time, if compared to MPC and FLC. The effect of the contractive constraint (FLC blue curve) limiting the outer-loop Lyapunov function time derivative can be noticed in Figure 6-6.

Case B

The paths are presented in Figure 6-7. It can be noticed that both MPC and L-MPC converge to the path much faster than FLC. However, contrary to the previous case, the difference between MPC and L-MPC is not negligible. The outer-loop control signals are presented in Figure 6-8. The linear speed attains its maximum allowable value (1,5 m/s) during the path approaching phase and, after that, it converges for the assigned speed (1,0 m/s). The position error is presented in Figure 6-9, indicating that L-MPC shows an intermediate convergence time if compared to MPC and FLC. The effect of the contractive constraint (FLC blue curve) limiting the outer-loop Lyapunov function time derivative can be noticed in Figure 6-10.
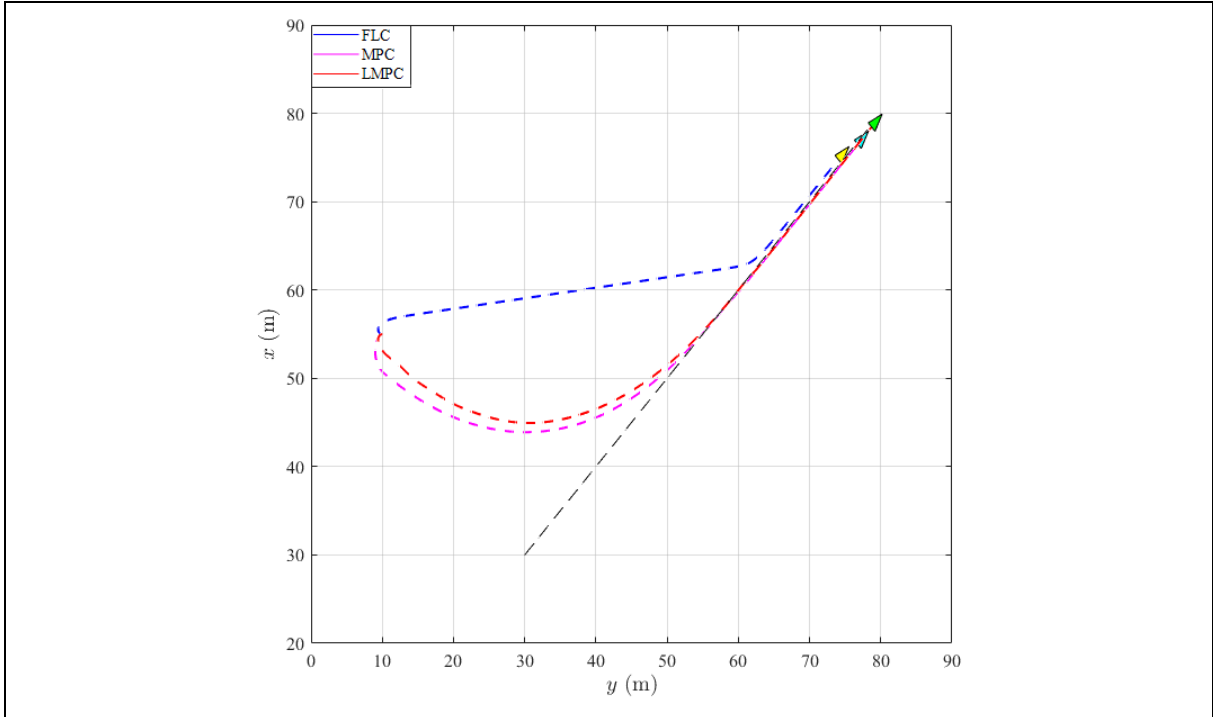
Figure 6-3: Scenario 1 (Case A) – Paths

FLC

MPC
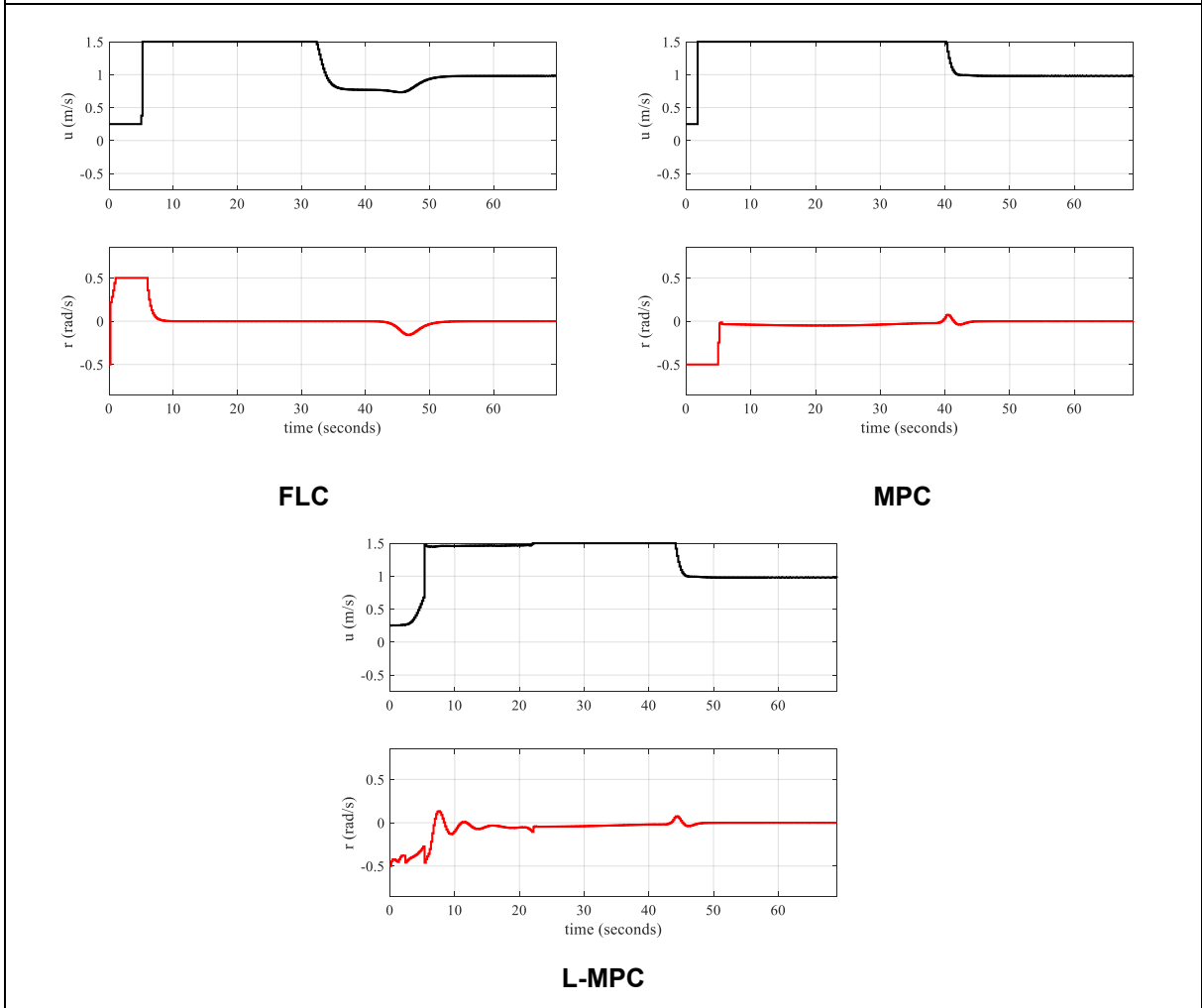
L-MPC

Figure 6-4: Scenario 1 (Case A) – FLC/MPC/L-MPC control signals (outer loop)
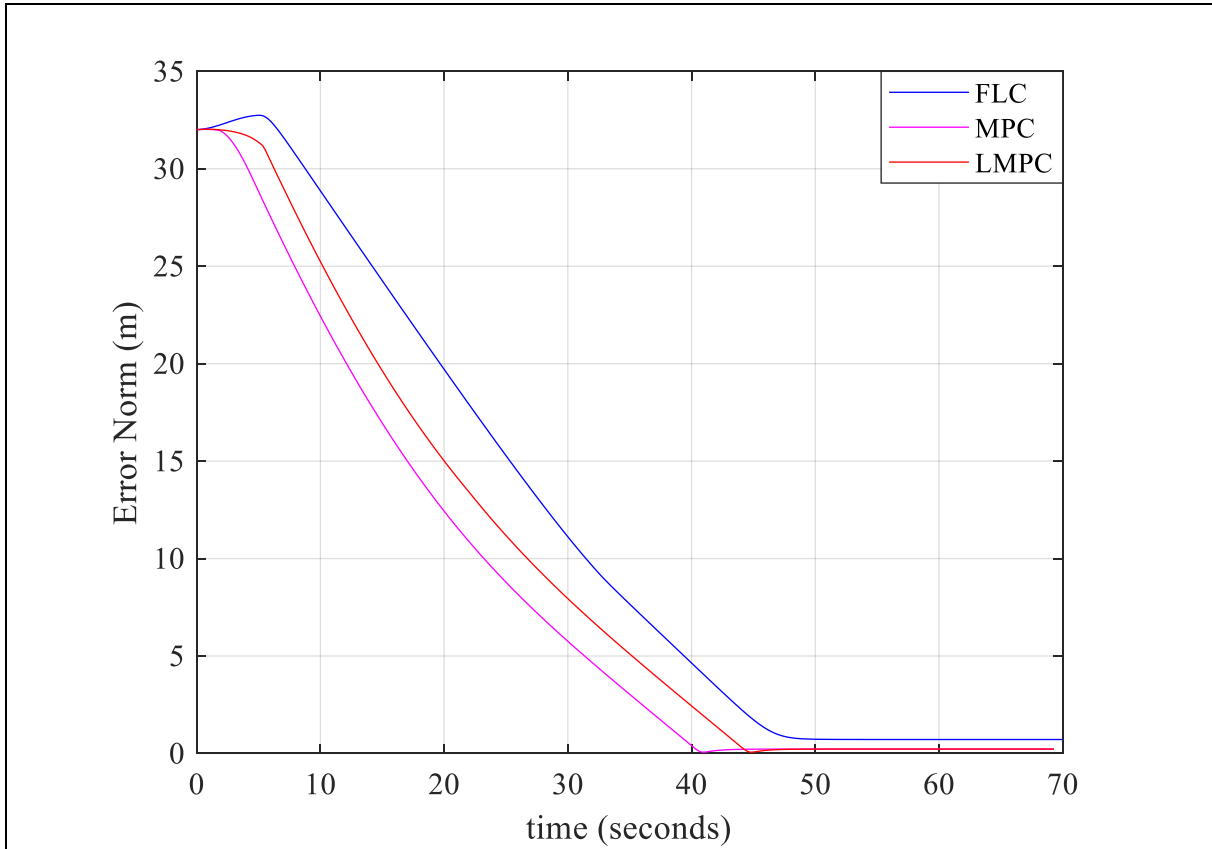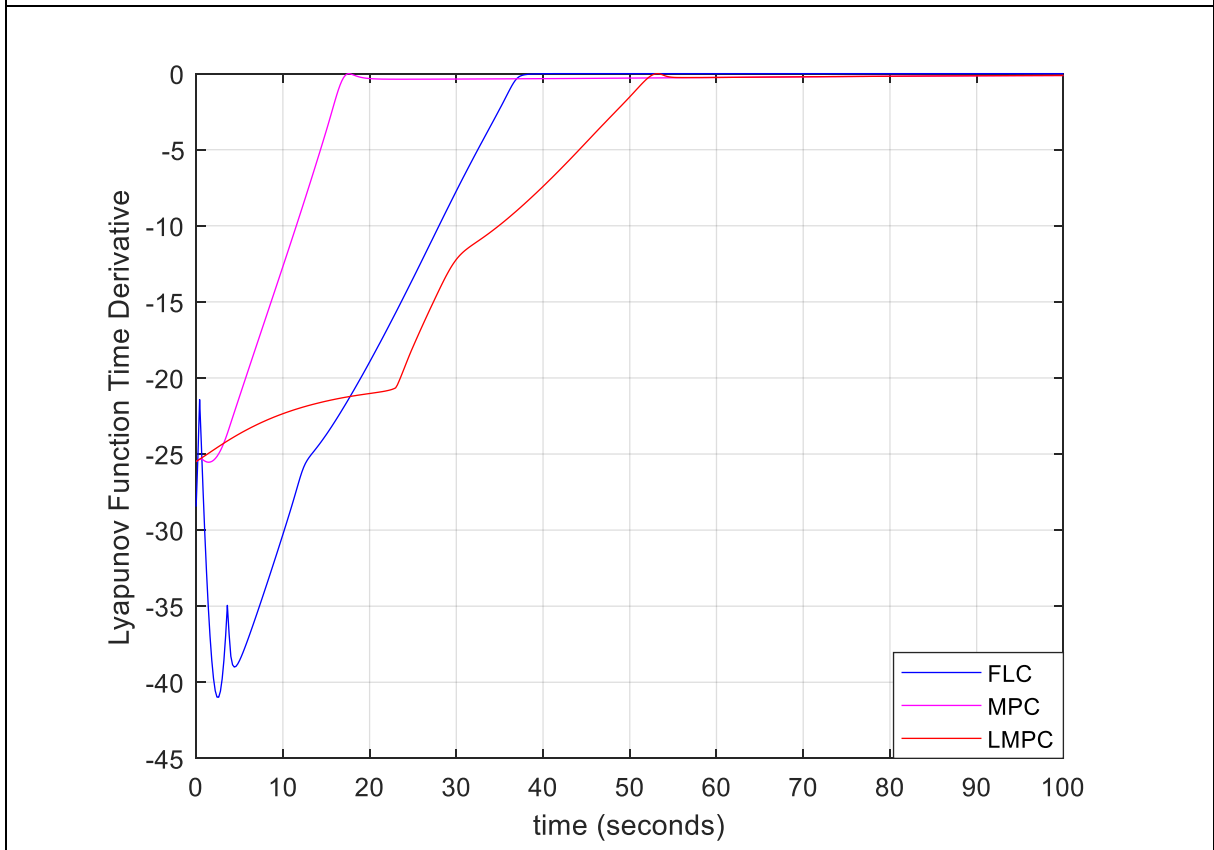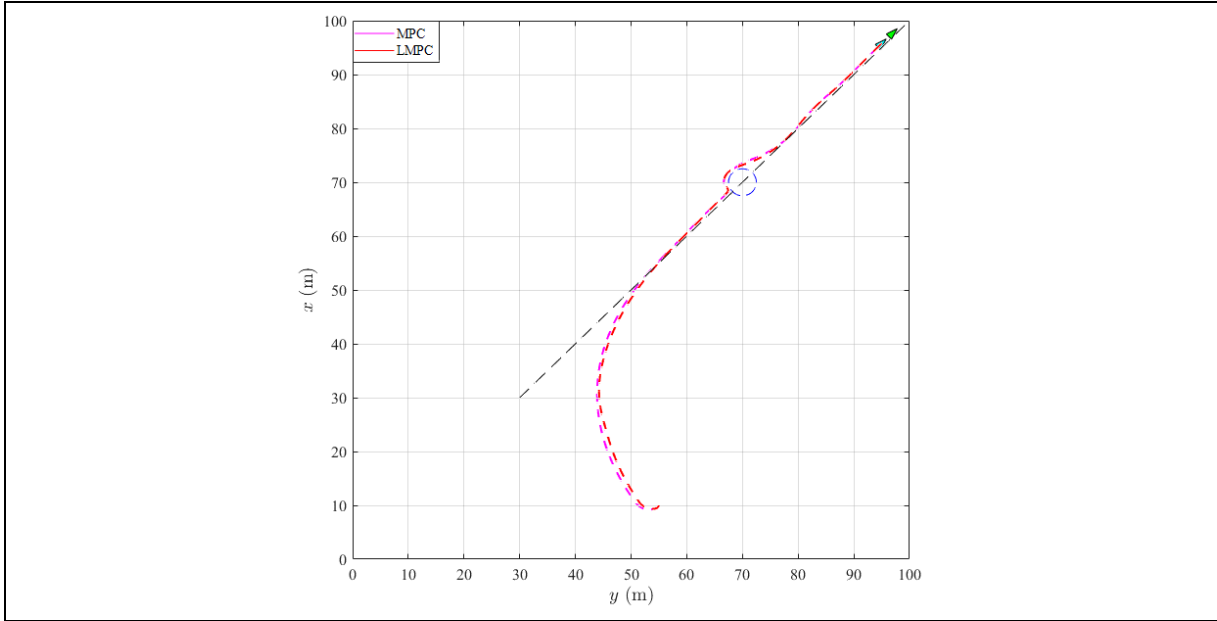
Figure 6-5: Scenario 1 (Case A) – Position error norms
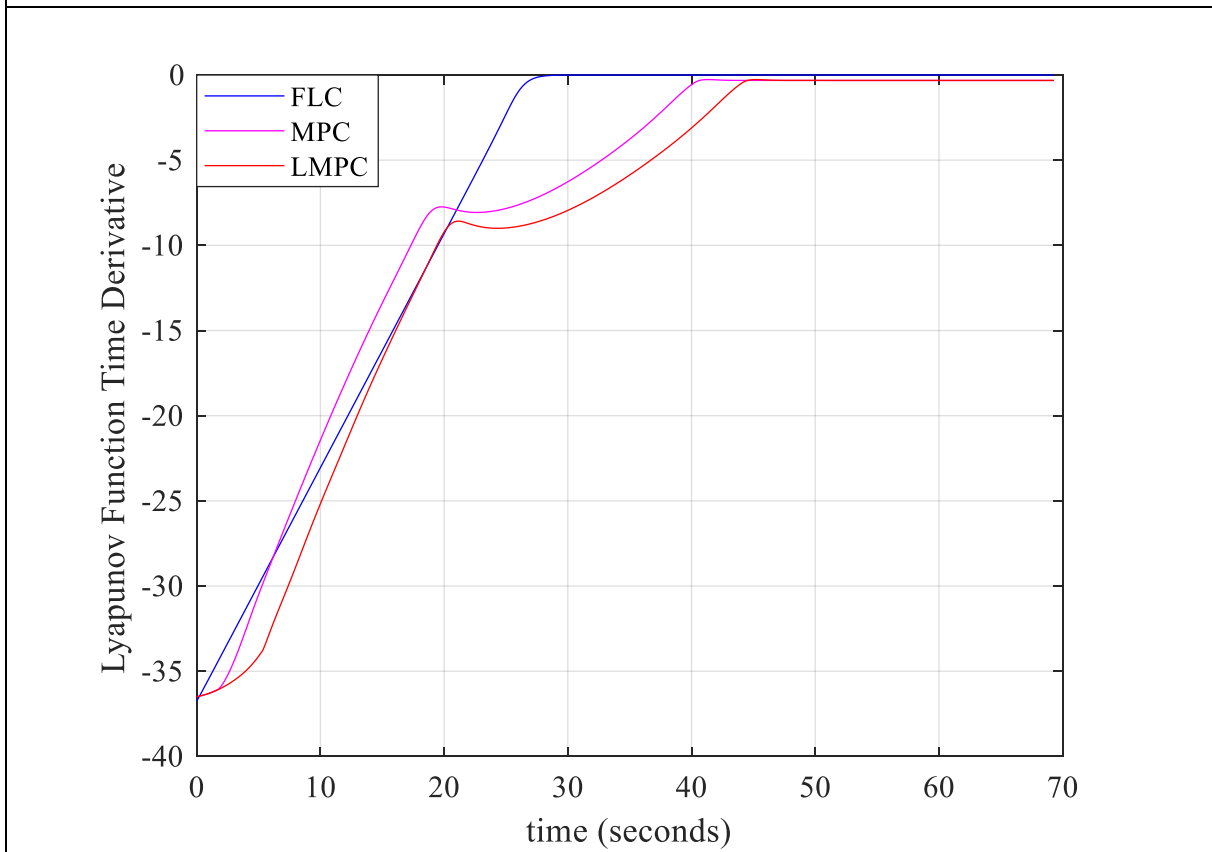
Figure 6-6: Scenario 1 (Case A) – Contractive constraint (blue curve)
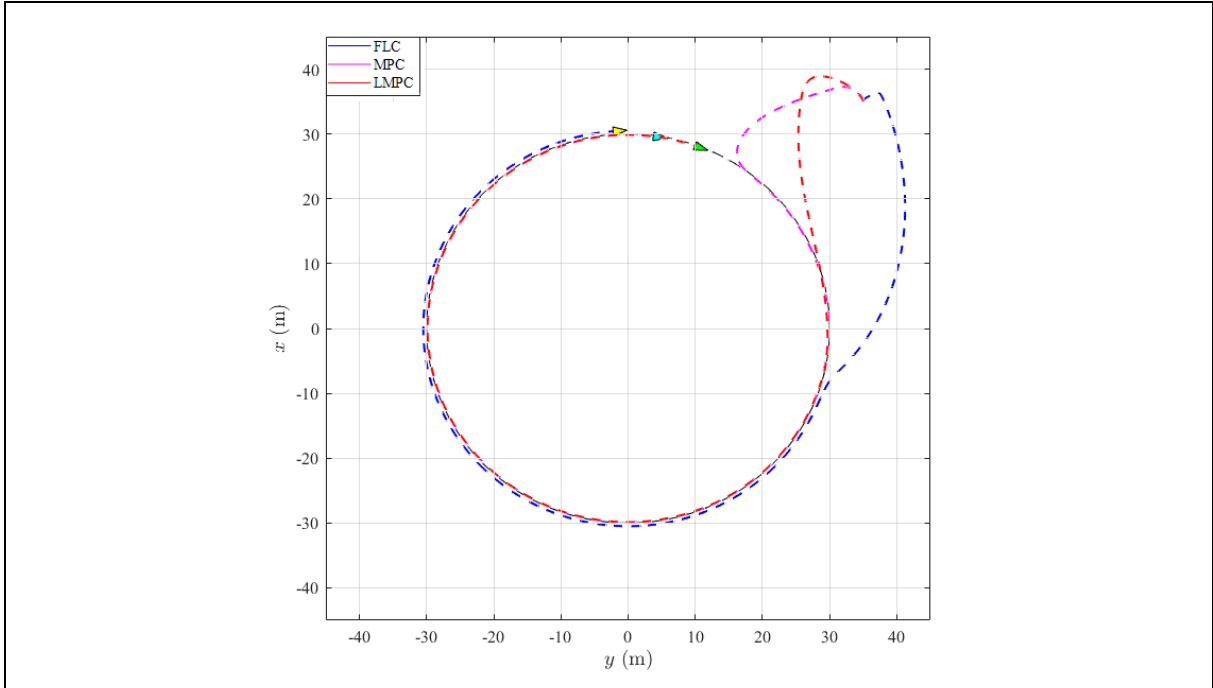
Figure 6-7: Scenario 1 (Case B) – Paths

FLC

MPC
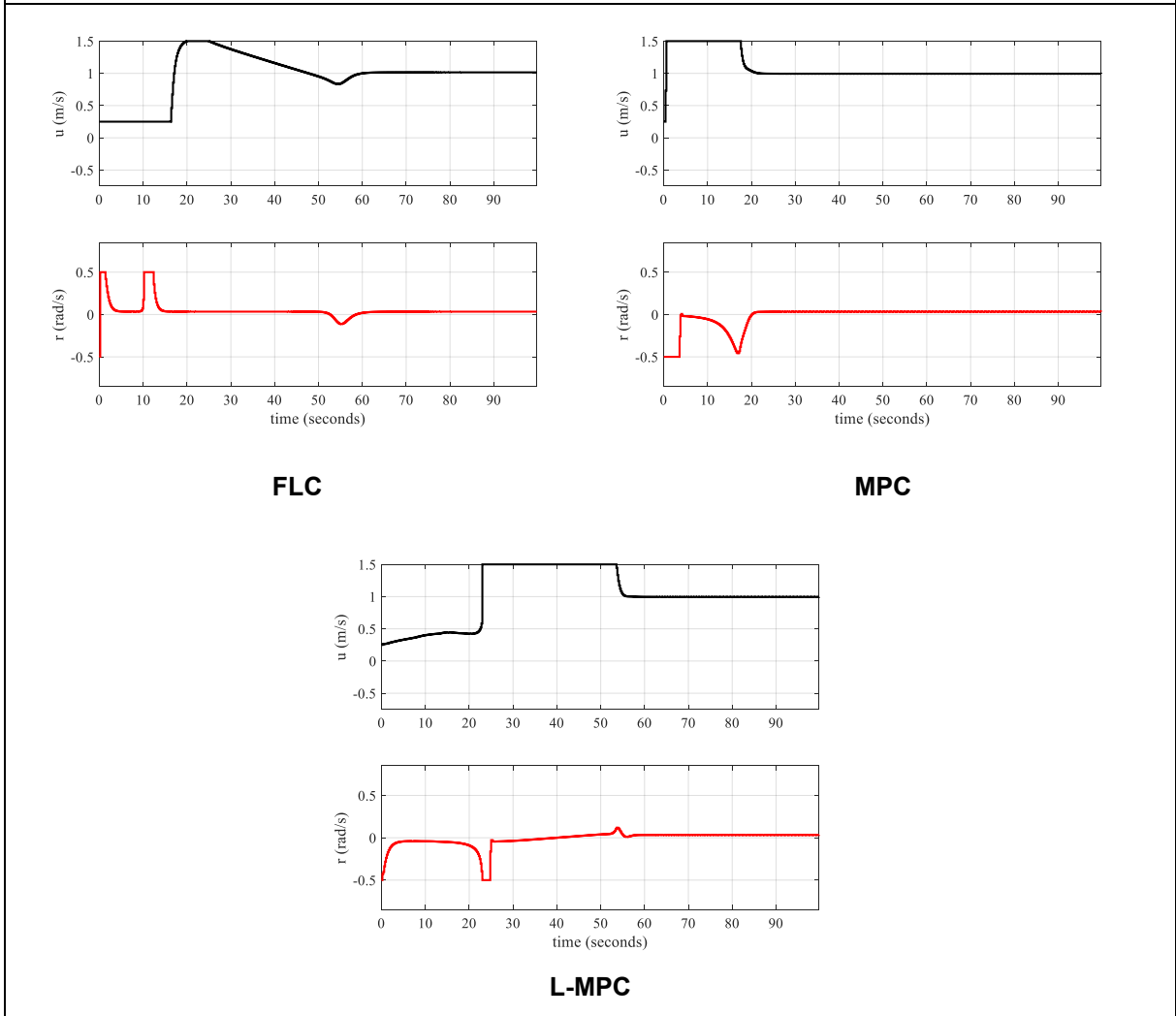
L-MPC

Figure 6-8: Scenario 1 (Case B) – FLC/MPC/L-MPC control signals (outer loop)
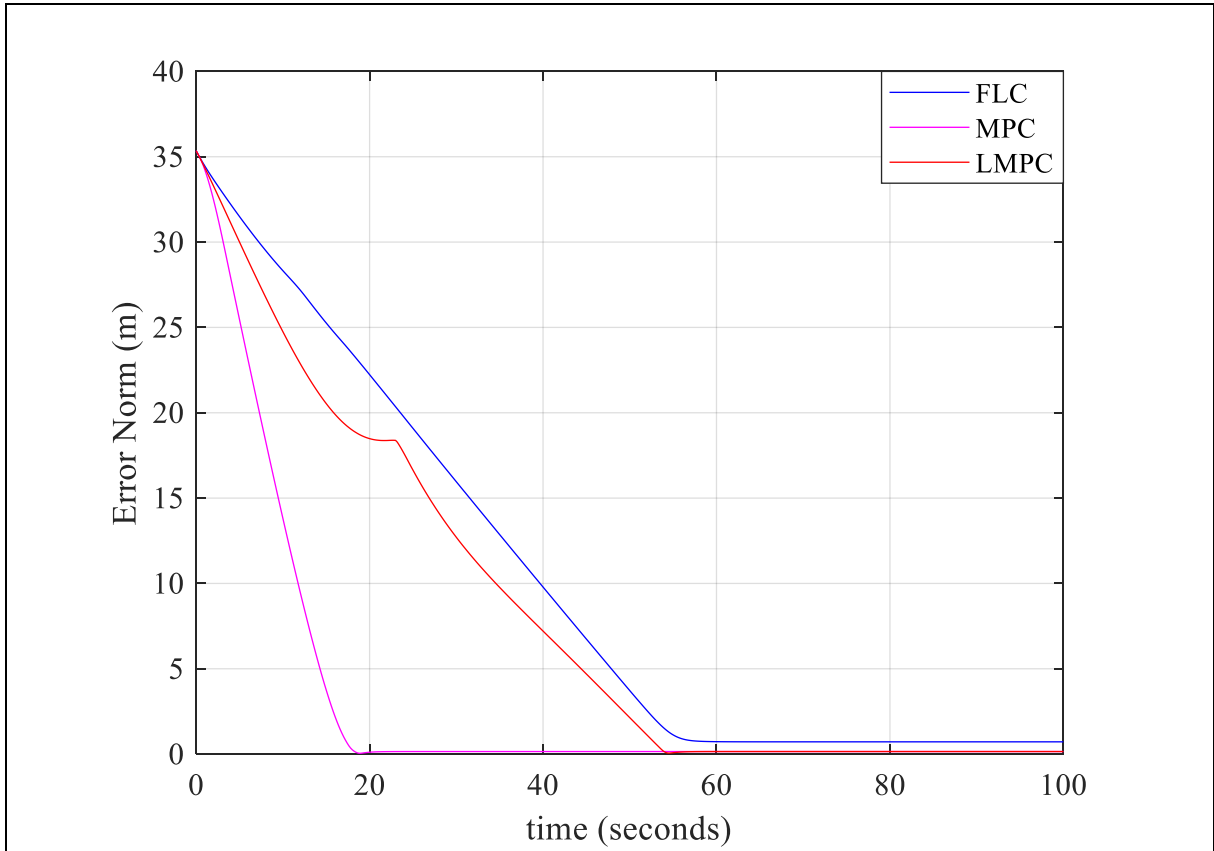
Figure 6-9: Scenario 1 (Case B) – Position error norms

Figure 6-10: Scenario 1 (Case B) – Contractive constraint (blue curve)

6.2.2 Scenario 2

The simulation has shown that, for the considered initial conditions, MPC is stable and presents a better performance than L-MPC, since it converges faster to the reference path. On the other hand, due to the contractive constraint, L-MPC is globally asymptotically stable.

Again, it can be noticed that there is a compromise between global asymptotic stability and performance. This fact is consistent with the contractive constraint concept, which limits L-MPC Lyapunov function time derivative.

Case A

The paths are presented in Figure 6-11 and Figure 6-12. It can be noticed that MPC converges slightly faster to the path than L-MPC. However, after reaching the path, the performance of both controllers is practically the same, even during the obstacle avoidance phase. The outer-loop control signals are presented in Figure 6-13. The linear speed attains its maximum allowable value (1,5 m/s) during path approaching phase and, after that, it converges for the assigned speed (1,0 m/s). The same occurs during the obstacle avoidance phase. The comparison between L-MPC inner-outer loop control signals is presented in Figure 6-14, where proper inner-loop tracking can be observed. The position error norm is presented in Figure 6-15. The effect of the contractive constraint (FLC blue curve) limiting the outer-loop Lyapunov function time derivative can be noticed in Figure 6-16.

Case B

The paths are presented in Figure 6-17 and Figure 6-18. It can be noticed that MPC converges faster to the path than L-MPC. However, after reaching the path, the performance of both controllers is practically the same, even during the obstacle avoidance phase. The outer-loop control signals are presented in Figure 6-19. The linear speed attains its maximum allowable value (1,5 m/s) during path approaching phase and, after that, it converges for the assigned sinusoidal speed. The same occurs during the obstacle avoidance phase. The comparison between L-MPC inner-outer loop control signals is presented in Figure 6-20, where proper inner-loop tracking can be observed. The position error norm is presented in Figure 6-21. The effect of the contractive constraint (FLC blue curve) limiting the outer-loop Lyapunov function time derivative can be noticed in Figure 6-22.
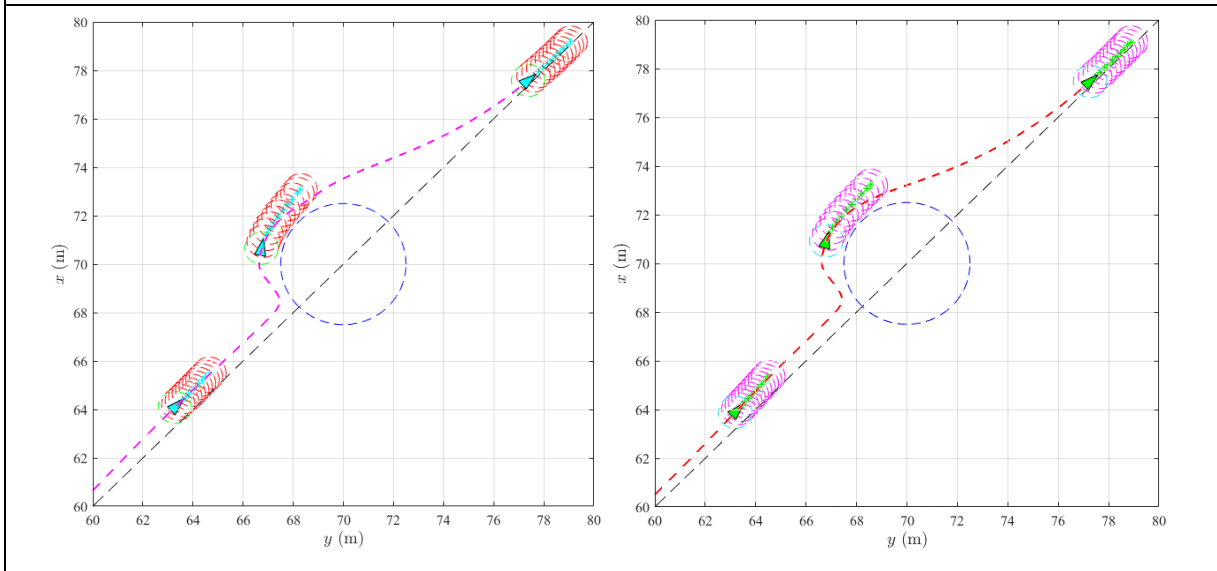
Figure 6-11: Scenario 2 (Case A) – Paths

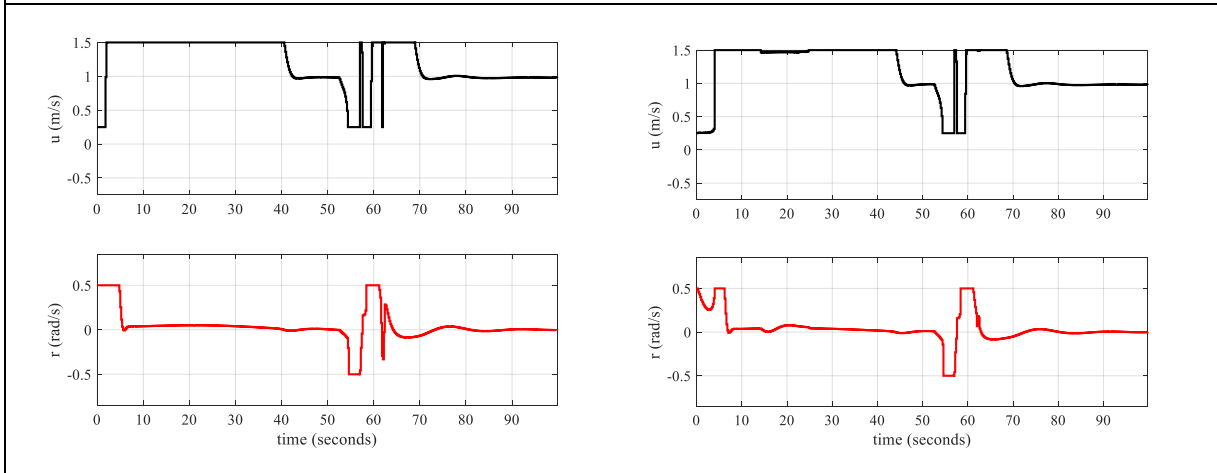**Figure 6-12: Scenario 2 (Case A) – MPC / L-MPC paths (zoom)**

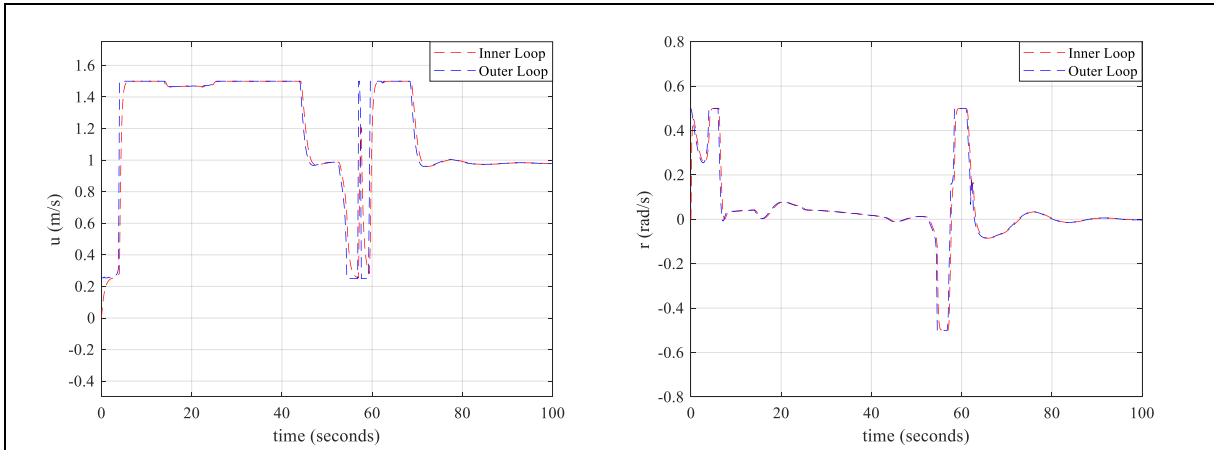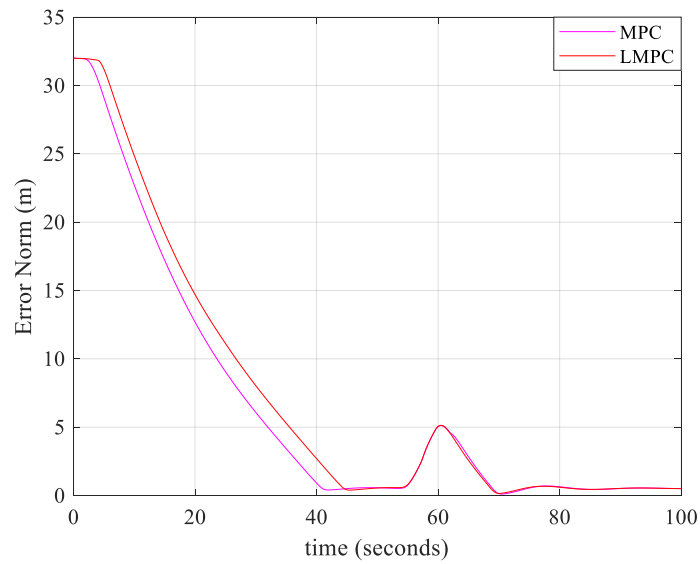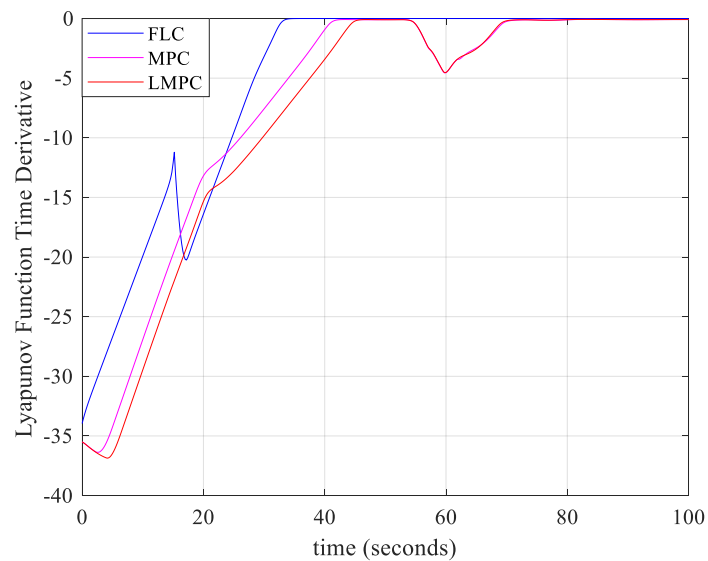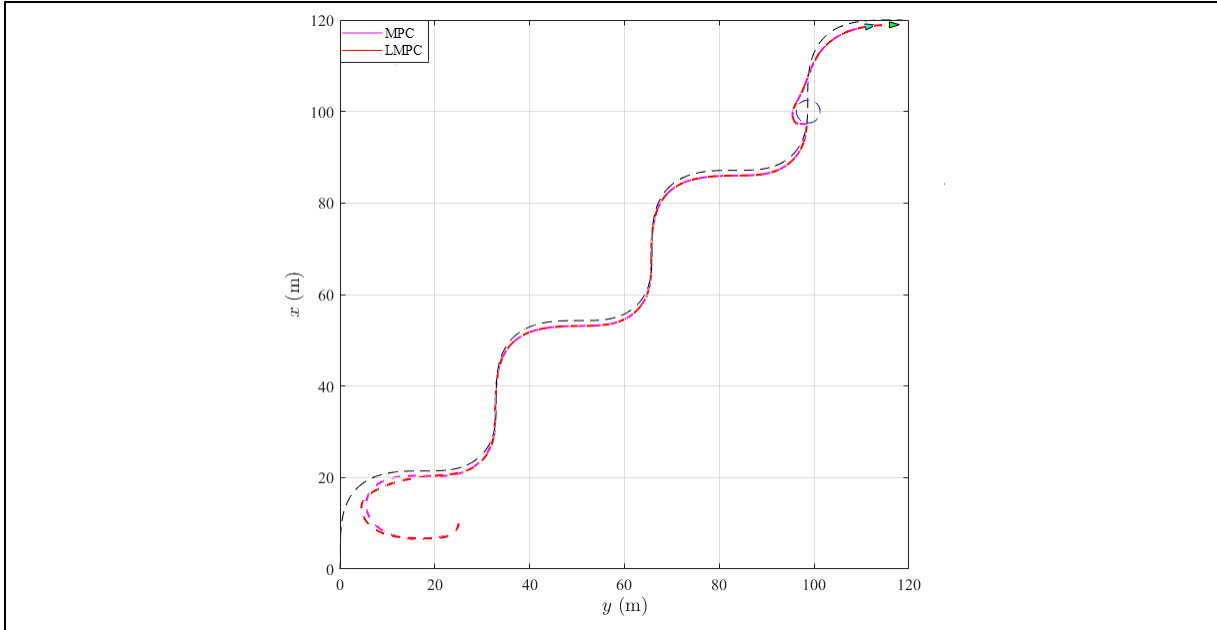**Figure 6-13: Scenario 2 (Case A) – MPC / L-MPC control signals (outer loop)**

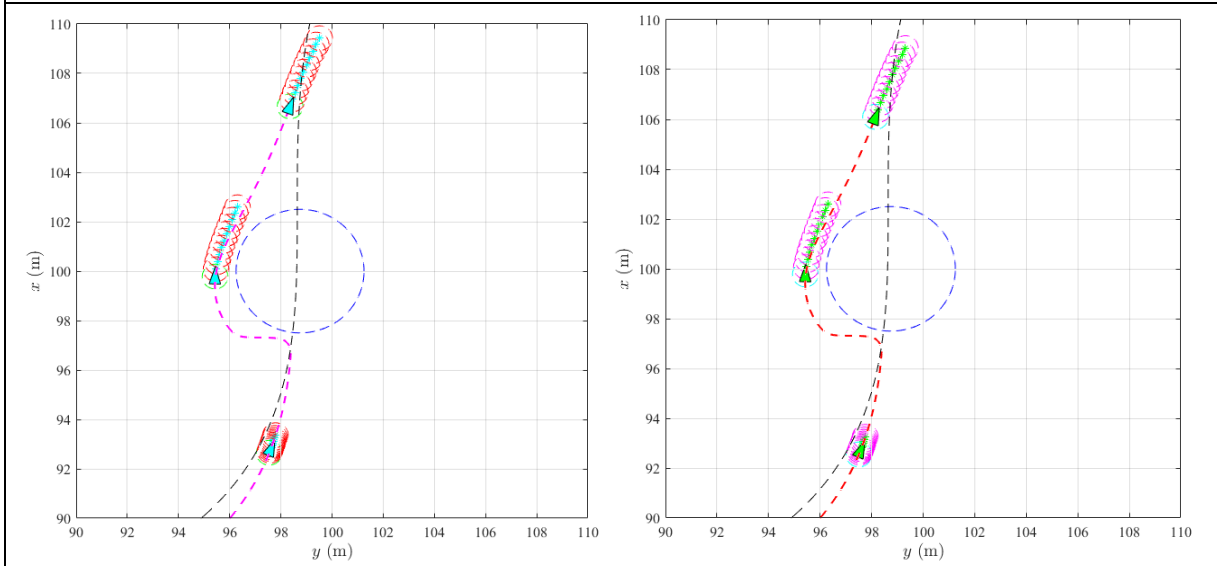**Figure 6-14: Scenario 2 (Case A) – L-MPC control signals**

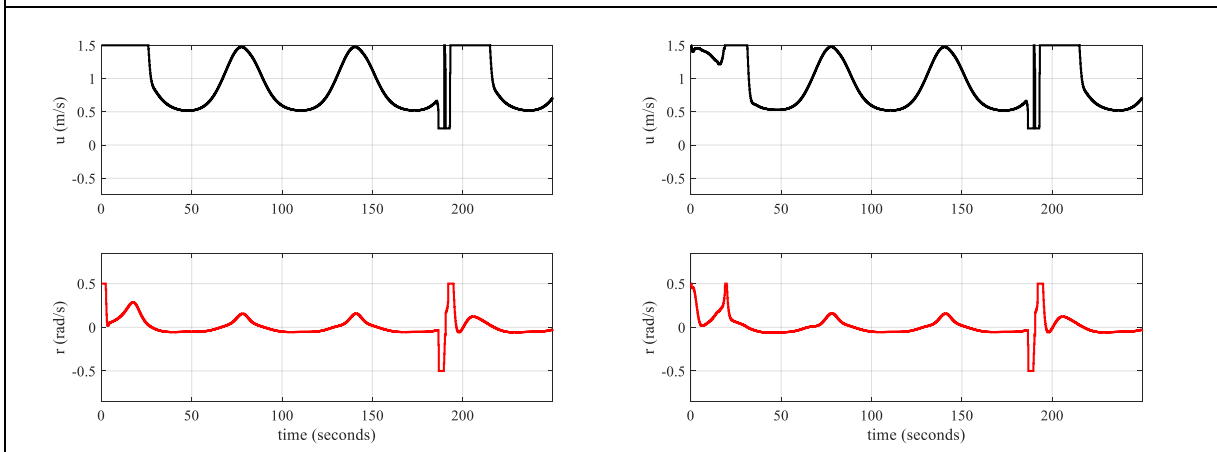**Figure 6-15: Scenario 2 (Case A) – Position error norm**

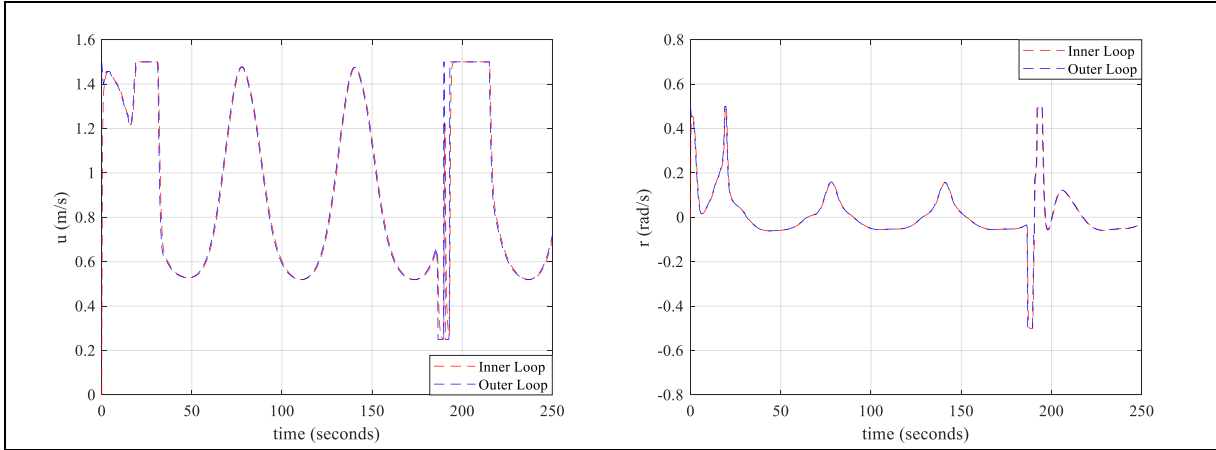**Figure 6-16: Scenario 2 (Case A) – Contractive constraint (blue curve)**
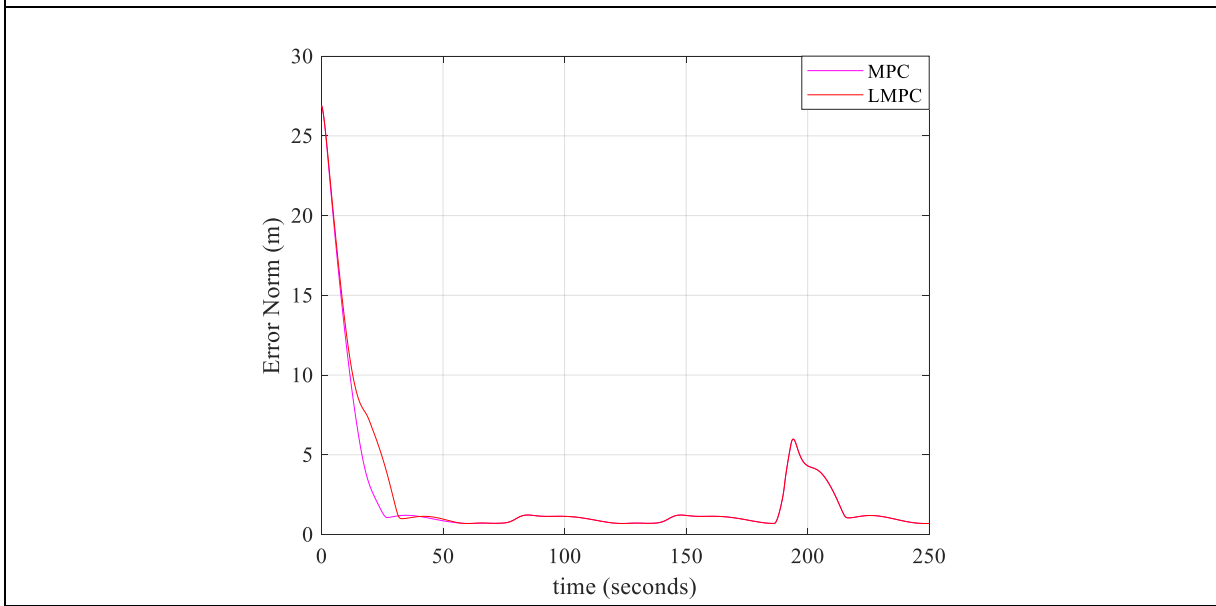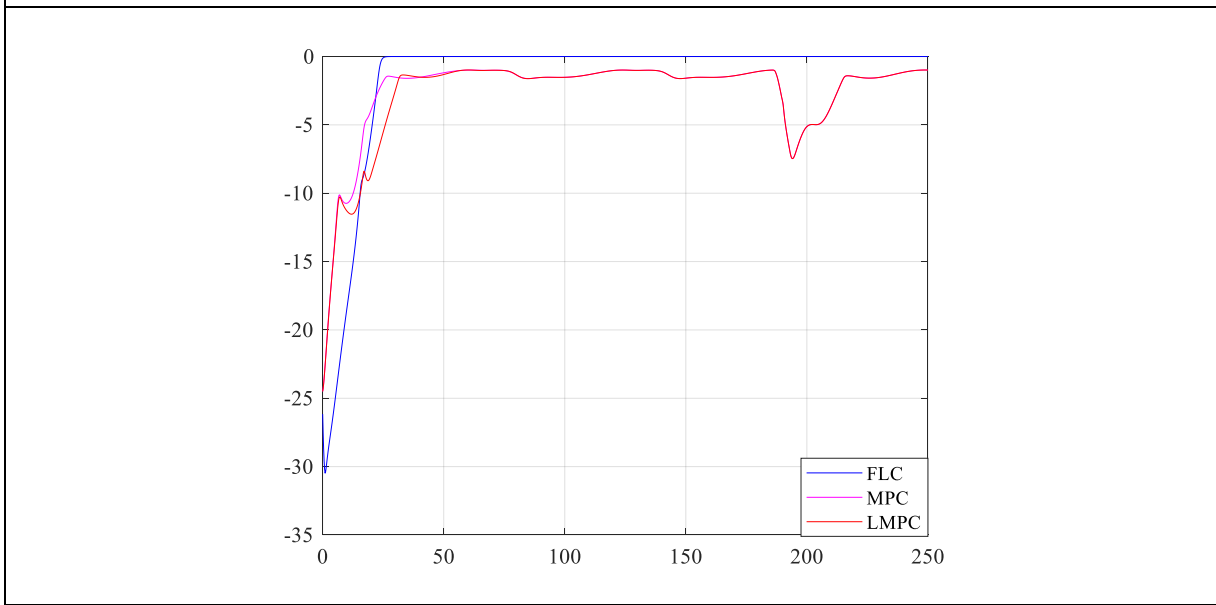
Figure 6-17: Scenario 2 (Case B) – Paths

Figure 6-18: Scenario 2 (Case B) – MPC / L-MPC paths (zoom)

Figure 6-19: Scenario 2 (Case B) – MPC / L-MPC control signals (outer loop)

Figure 6-20: Scenario 2 (Case B) – L-MPC control signals

Figure 6-21: Scenario 2 (Case B) – Position error norms

Figure 6-22: Scenario 2 (Case B) – Contractive constraint (blue curve)

6.2.3 Scenario 3

The performance of the cooperative path following controller in a multi-vehicle mission was assessed, without considering measurement noise.

Case A

One (1) ASC (yellow) and 2 AUV (green) are assigned to follow concentric circular paths, with a variable speed profile, while adopting two different formation patterns (triangular in the 1st / 2nd quadrants and aligned in the 3rd / 4th quadrants). The paths are presented in Figure 6-23 and Figure 6-24, where a path convergence and formation pattern compliance can be noticed. The vehicles' outer loop control signals are presented in Figure 6-25, where the speed assignment change can be observed. The path convergence can also be seen in Figure 6-26, since error norms vanish to zero. The last two figures concern the performance of the cooperative controller. Figure 6-27 presents the correction speeds and the coordination parameter (γ). Initially, to implement the triangular pattern, the cooperative controller increases the speed of the ASC and reduces the speeds of the AUV. Later, when the aligned pattern is activated, the opposite occurs. The communication events are presented in Figure 6-29, showing that inter-vehicle communication practically vanishes when the path parameters reach consensus.

Case B

Three (3) AUV (green) are assigned to follow parallel mooring paths, also with a variable speed profile. In the upwards path, the formation is set to be aligned, while in the downwards path it is set to be triangular. The paths are presented in Figure 6-30 and Figure 6-31 where a path convergence and formation pattern compliance can be noticed. The vehicles' outer loop control signals are presented in Figure 6-32, where the speed assignment change can be observed. The path convergence can also be seen in Figure 6-33, since error norms vanish to zero. The performance of the cooperative controller is exhibited by the last two figures. Figure 6-35 presents the correction speeds and the coordination parameter (γ). Starting with the aligned formation, the cooperative controller acts only when the triangular pattern is activated, increasing the speed of the central AUV and reducing the speed of the others. The communication events are presented in Figure 6-36, showing that inter-vehicle communication practically vanishes when the path parameters reach consensus.
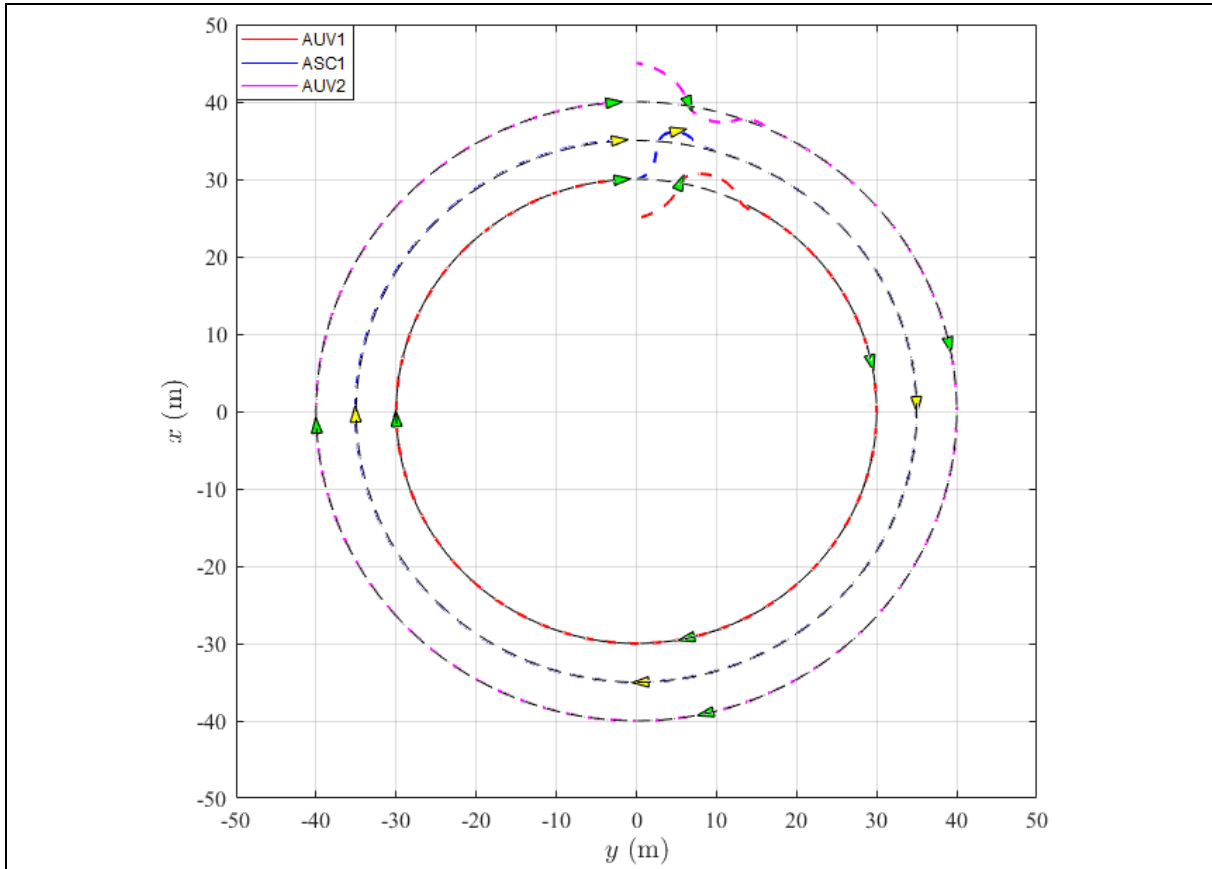
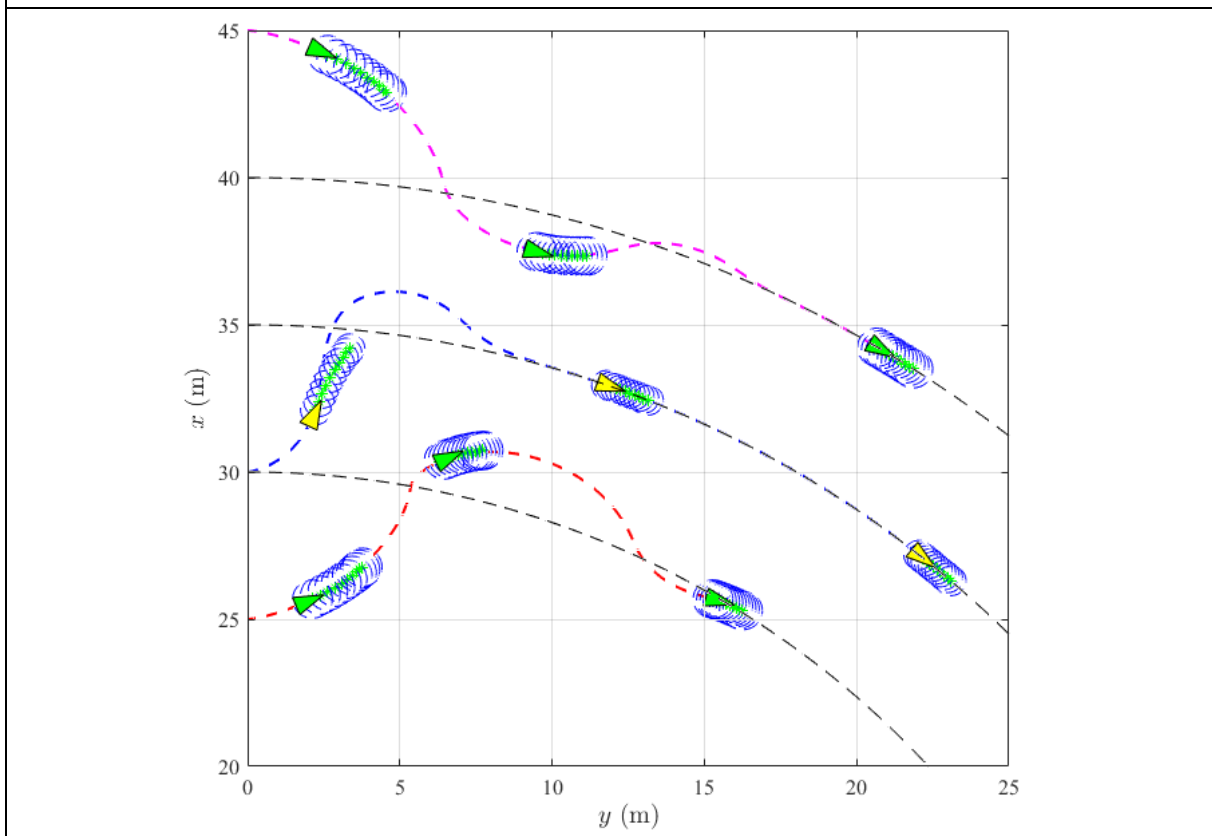**Figure 6-23: Scenario 3 (Case A) – Cooperative L-MPC path**

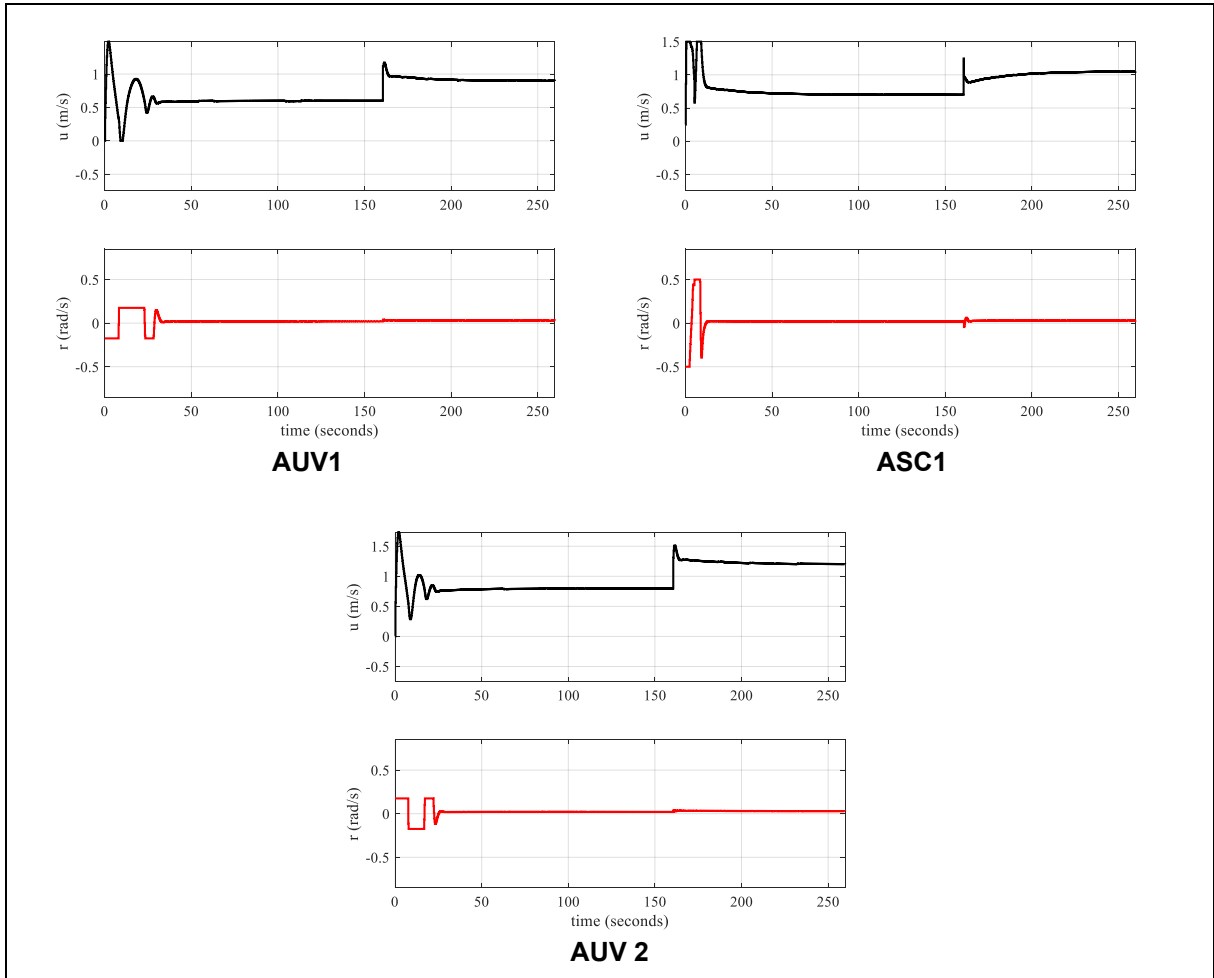**Figure 6-24: Scenario 3 (Case A) – Cooperative L-MPC path (zoom)**

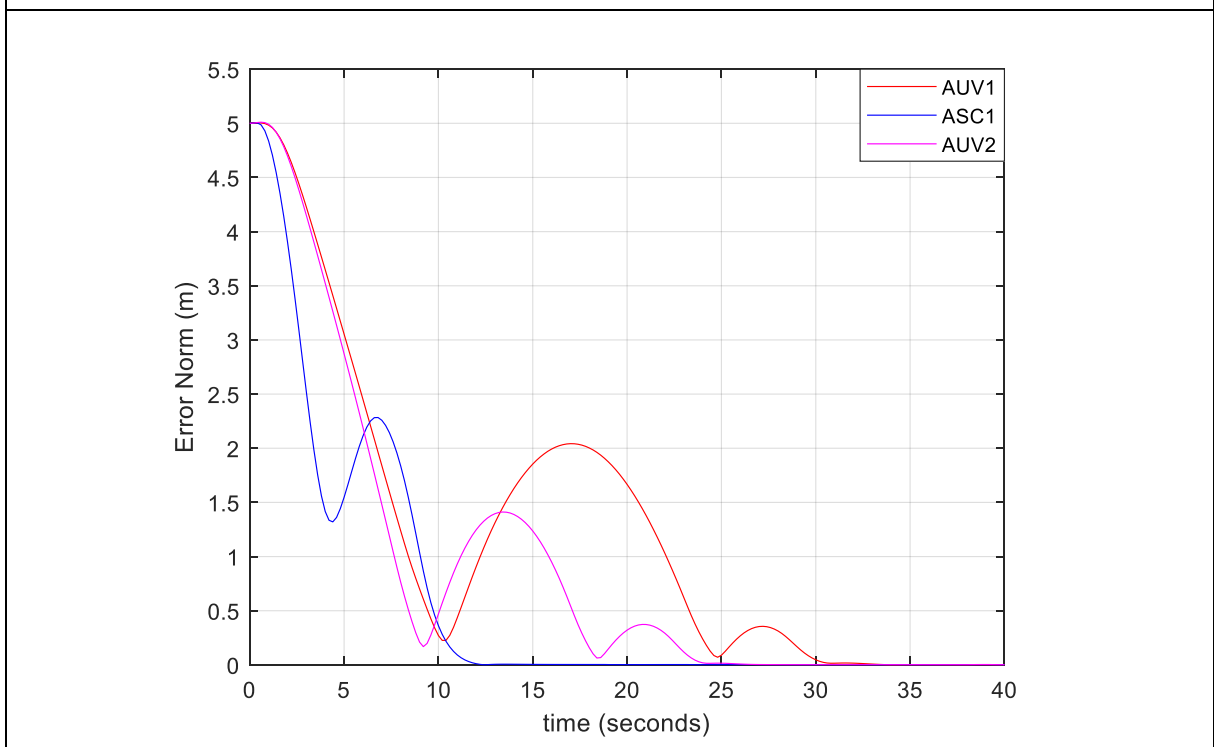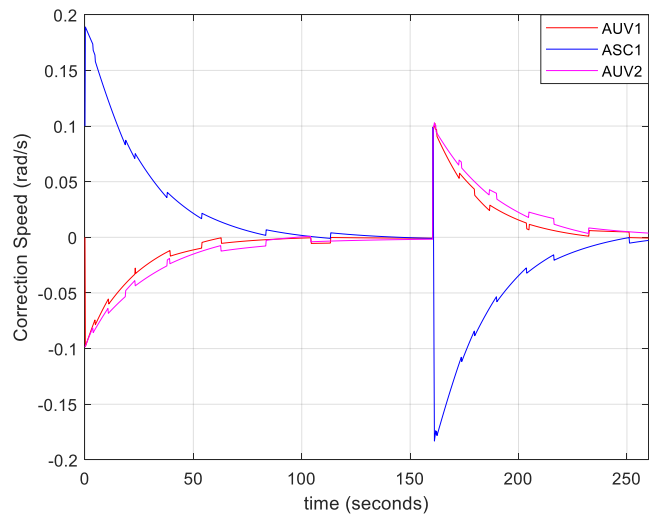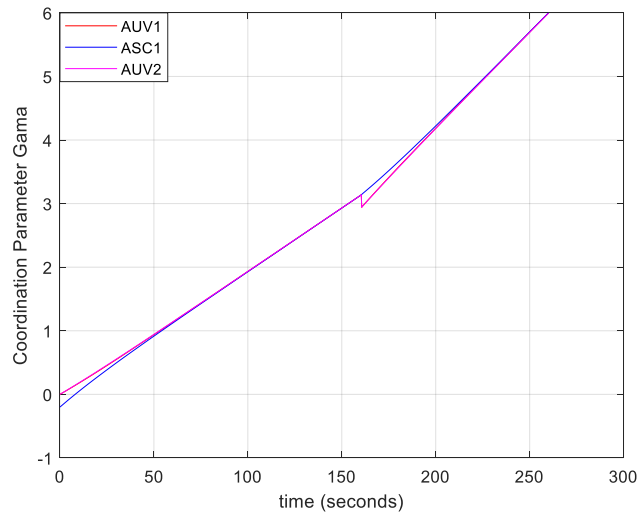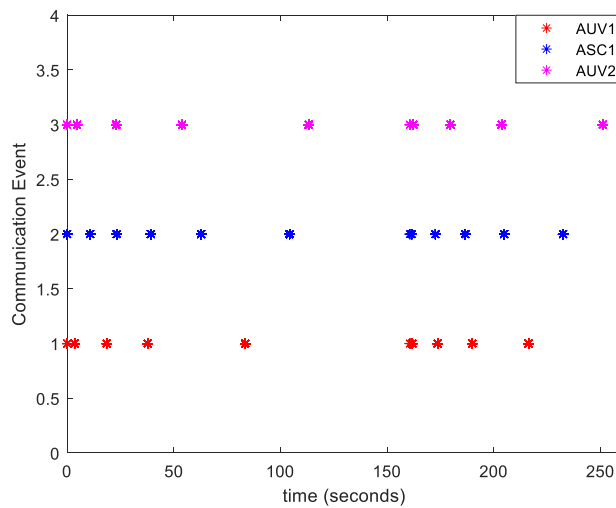**Figure 6-25: Scenario 3 (Case A) – L-MPC control signals (outer loop)**

Figure 6-26: Scenario 3 (Case A) – Position error norms

Figure 6-27: Scenario 3 (Case A) – Correction speeds

Figure 6-28: Scenario 3 (Case A) – Synchronization parameter γ

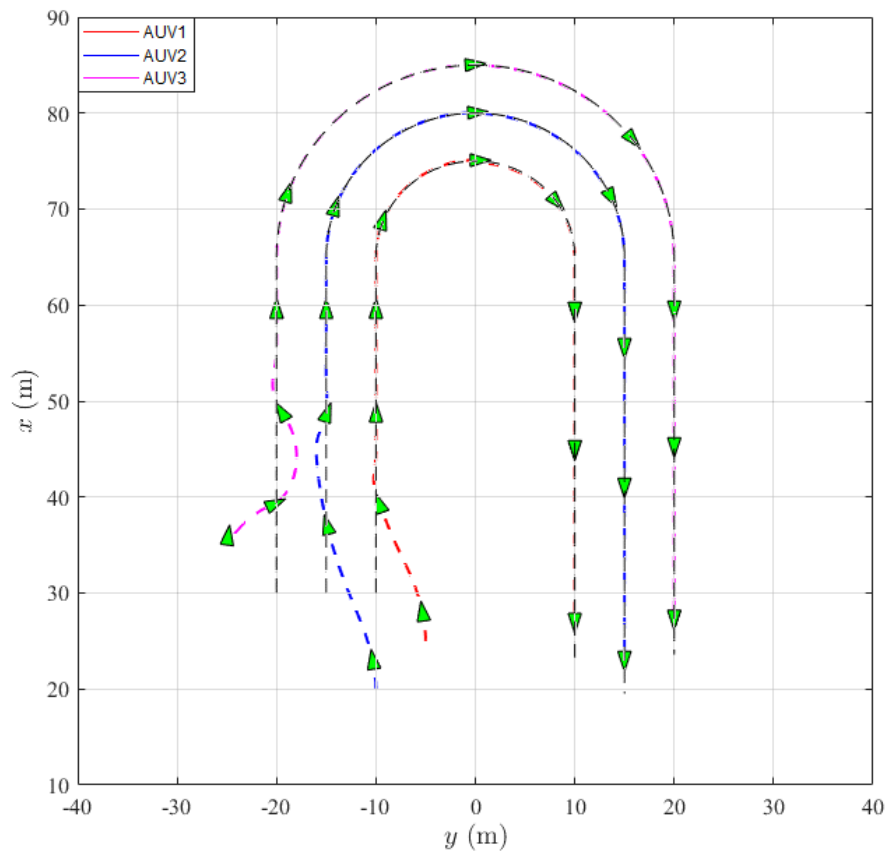**Figure 6-29: Scenario 3 (Case A) – Communication events**
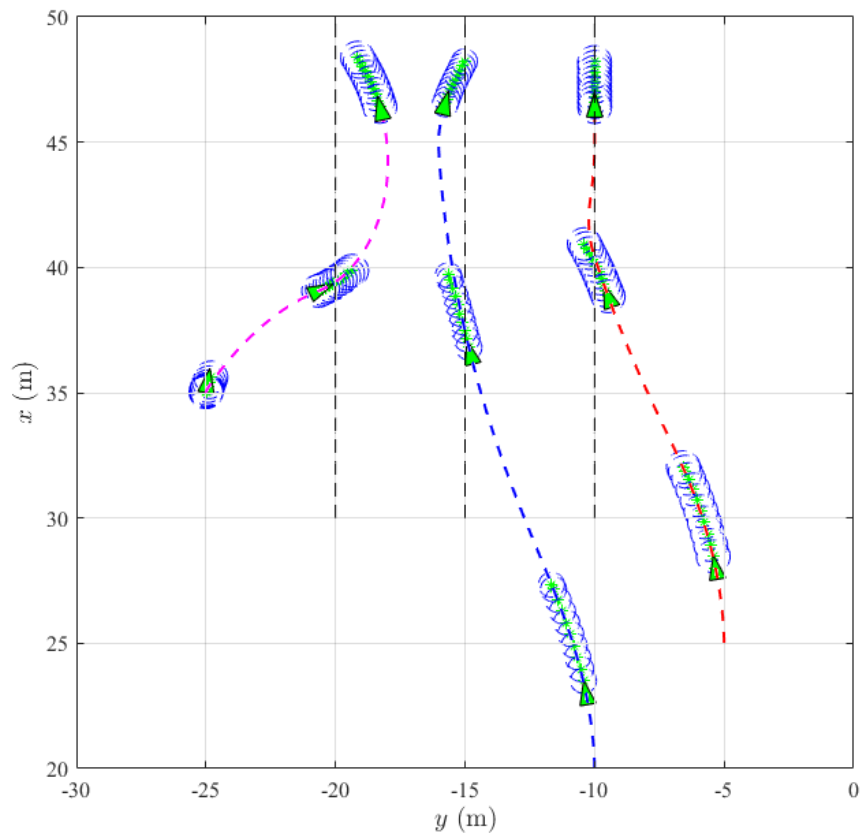
Figure 6-30: Scenario 3 (Case B) – Cooperative L-MPC path

Figure 6-31: Scenario 3 (Case B) – Cooperative L-MPC path (zoom)

AUV1

AUV2

AUV3
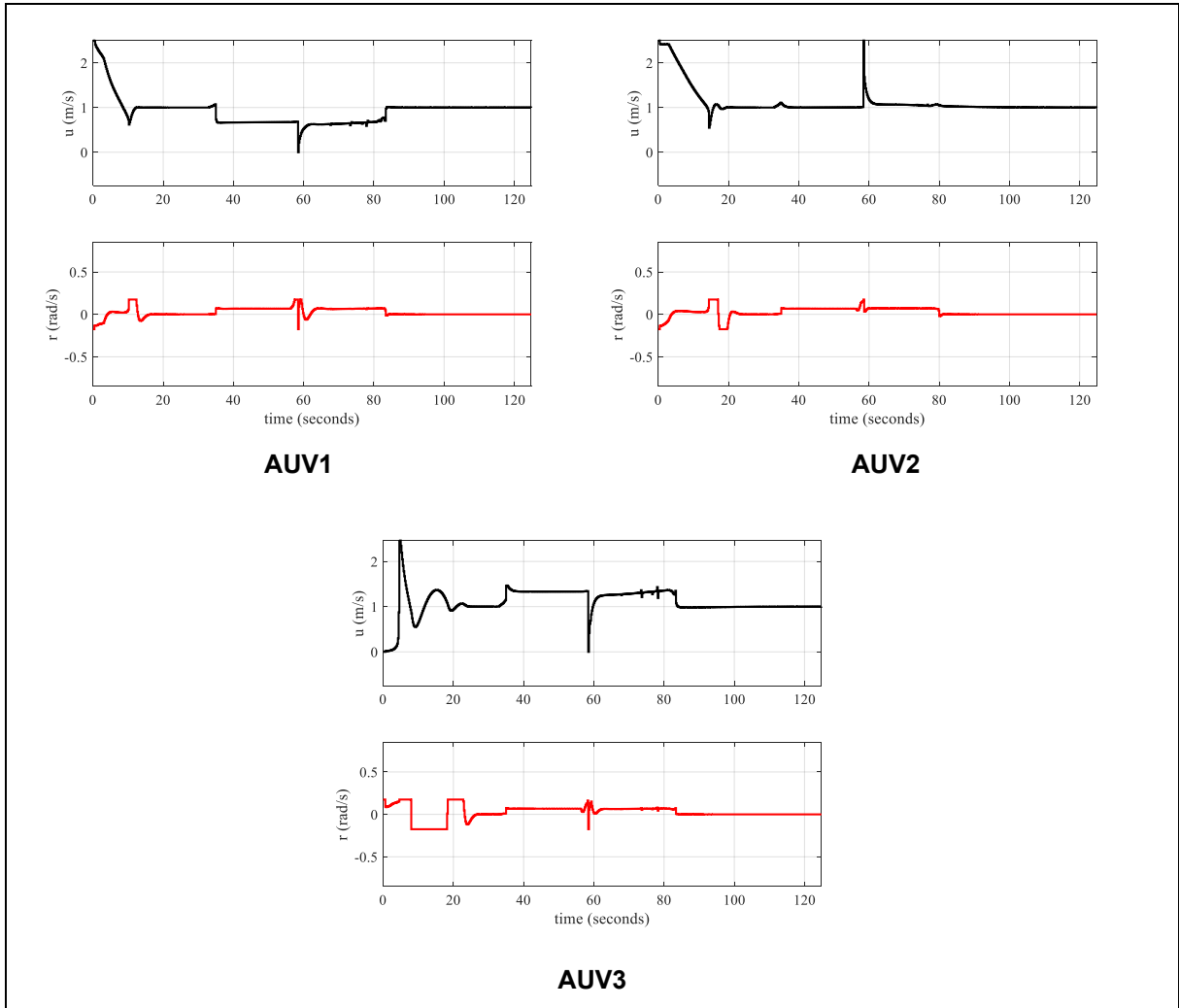
Figure 6-32: Scenario 3 (Case B) – L-MPC control signals (outer loop)
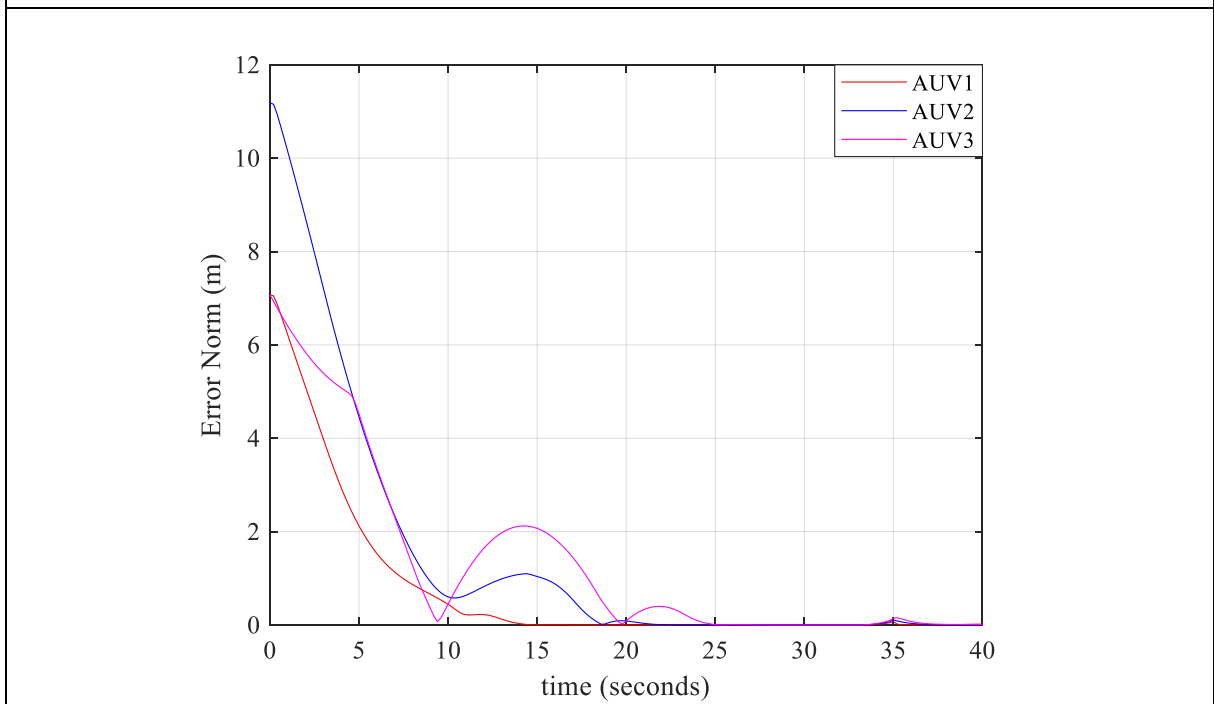
Figure 6-33: Scenario 3 (Case B) – Position error norms
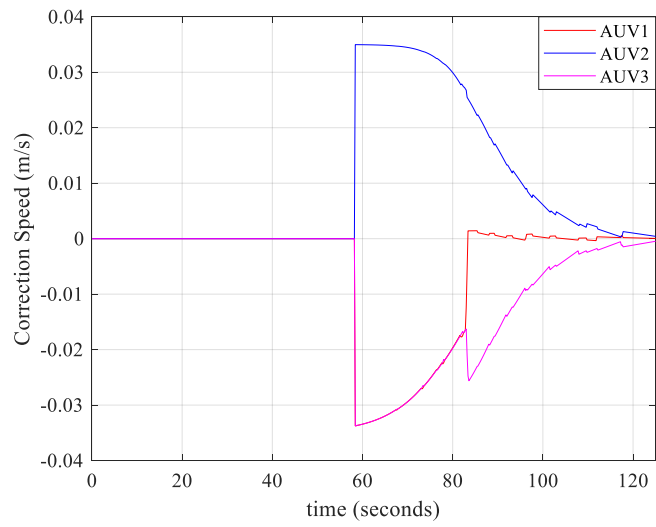
Figure 6-34: Scenario 3 (Case B) – Correction speeds

Figure 6-35: Scenario 3 (Case B) – Synchronization parameter γ

Figure 6-36: Scenario 3 (Case B) – Communication events

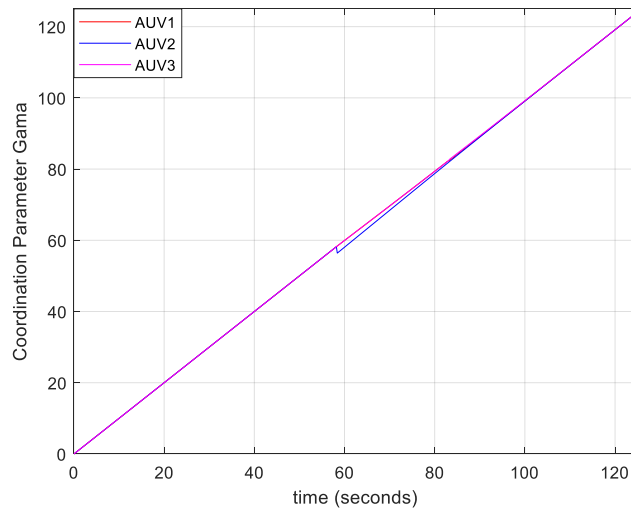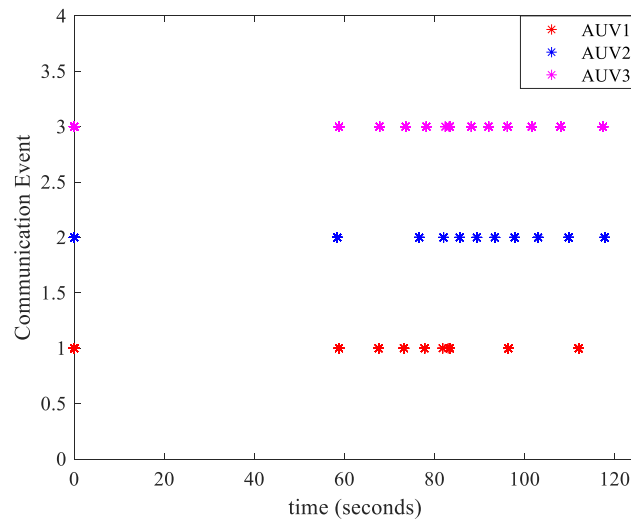6.2.4   Scenario 4

The performance of the cooperative path following controller in a multi-vehicle mission was assessed, considering the presence of measurement noise. The second case considered also the presence of a constant irrotational ocean current.

Case A

The AUV was able to follow its path as presented in Figure 6-37 and Figure 6-38. The effect of the OCP parameters over the MHE performance can be observed in Figure 6-39 (filtered measurements), Figure 6-40 (noise attenuation), and Figure 6-41 (L-MPC output signals). It can be noticed that Case A-ii outperforms Case A-I, which is on the verge of instability.

Concerning this aspect, it was noticed that the quality of the MHE estimates increases with the number of samples, but the closed loop stability is jeopardized if the time window associated with the prediction horizon increases. This occurs because the higher the time window is, the slower the MHE responds, and if the MHE is not fast enough to couple the system dynamics, the system destabilizes. Consequently, reducing the sample time coherently with the system dynamics proved to be a solution, however, at the expense of computational burden. For the current application, a prediction horizon of 2 s combined with a sampling time of 0,1 s proved to be a good trade-off between stability, quality and recursive feasibility.

Case B

The AUVs were able to follow the concentric circular paths, while respecting the desired formation pattern and complying with the path assigned speeds, as shown in Figure 6-42 and Figure 6-43, respectively. Intentionally, the vehicles departed from different initial conditions in order to check the occurrence of convergence issues, but they reached their assigned paths without problems. The "triangular" pattern was attained in the middle of the 1st quadrant, lost during the obstacle avoidance phase, but recovered again in the middle of the 2nd quadrant. At the beginning of the 3rd quadrant, the formation pattern was changed to "aligned" which was attained just after the beginning of the 4th quadrant.

The compliance with the path assigned speeds can be noticed in Figure 6-43[82]. At around $t = 160\,s$ the vehicles reached the 3rd quadrant and the path assigned speeds were increased as previously described. These speeds do not

---

[82] In this figure, the angular speeds were already converted into linear speeds.

present periodic components, indicating that the L-MPC compensated properly the kinematic effect of the ocean current. Considerations about the cooperative correction speeds are presented in the next paragraphs.

The path following error norms (Figure 6-44) indicate convergence to near zero values for all vehicles. The steady state error for AUV2 is slightly larger compared to the others but it remains acceptable (< 0,5 m). This behavior is expected since AUV2 is the only vehicle subjected to measurement noise. Even during the obstacle avoidance phase, the error remained acceptable, considering the size of the obstacle.

Particularly in this phase, AUV2 was able to avoid the obstacle (Figure 6-42). It can be noticed that the L-MPC, zeroed the u signal as soon as the vehicle reached the obstacle but not the r signal (Figure 6-45). Consequently, the vehicle turned anticlockwise and drifted slightly westwards due to the current. After that, the L-MPC resumed to issue non null values of u and the vehicle started to properly circumvent the obstacle.

The speed tracking performance of the inner loop is displayed in Figure 6-46, where close adherence among the outer loop commanded speeds and the vehicle real speeds can be noticed. Due to this fact, it was possible to use the outer loop signals (linear and angular speeds) as input data for the MHE and for the ocean current state observer, thus suppressing the need for dedicated sensors. The close adherence can be justified by neglected dynamics in the vehicle's mathematical model.

It is known that in practical experiments, this level of adherence will not be attained. However, as long as the inner loop is properly tuned and there is an adequate time scale separation among both loops, the obtained inner loop results, even not being fully realistic, do not compromise the considerations about the L-MPC design (Hung N. , et al., 2022).

The effect of the contractive constraint over vehicles' trajectories is summarized in Figure 6-47. It can be seen that only the AUV2 trajectory was impacted during the maneuver's initial stages. This behavior can be better understood when analyzing the associated Lyapunov function time derivatives.

For this particular scenario, it can be noticed that the system would be stable even if the contractive constraint was not considered in the OCP formulation (MPC -

green curve). This characteristic can be associated with the adopted prediction horizon length.

When it is considered (L-MPC), the system converges slowly since the contractive constraint (red curve) pushes its Lyapunov function time derivative (blue curve) down, attempting to limit it. After reaching zero, the red curve acts as a stability barrier (such as a terminal set), avoiding the blue curve to become positive, if it would be the case.

The MHE performance can be inferred in Figure 6-48, which presents its estimates and the associated noise attenuation levels (filtering), respectively. The quality of the estimates was satisfactory enough to assure the proper functioning of the closed loop control system.

The performance of the cooperative controller is summarized in Figure 6-49. Initially, to implement the "triangular" pattern, the cooperative controller increases the speed of the AUV2 and reduces the speeds of AUV 1 and 3. Later, when the "aligned" pattern is commanded, the opposite occurs. It can be clearly noticed that correction speeds vanish to zero after the coordination parameters reach consensus (Figure 6-50).

The communication events are presented in Figure 6-51, showing that inter-vehicle communication is necessary only during the synchronization phases, since it practically vanishes as soon as the coordination parameters reach consensus.
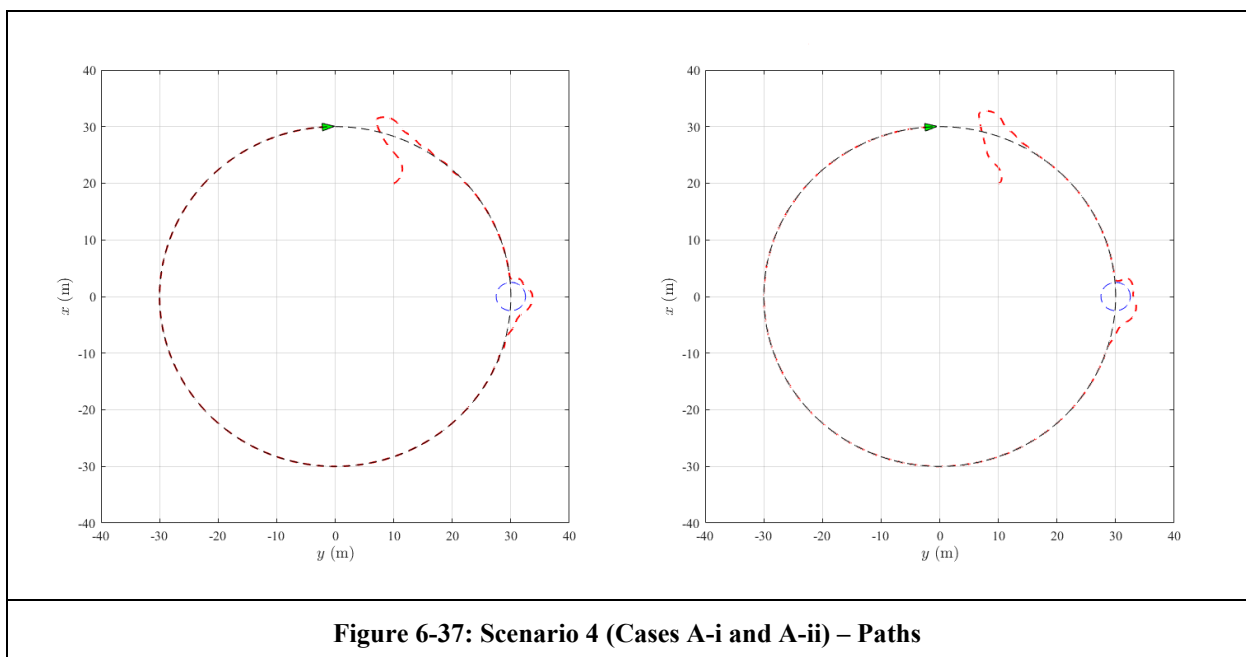
Figure 6-37: Scenario 4 (Cases A-i and A-ii) – Paths
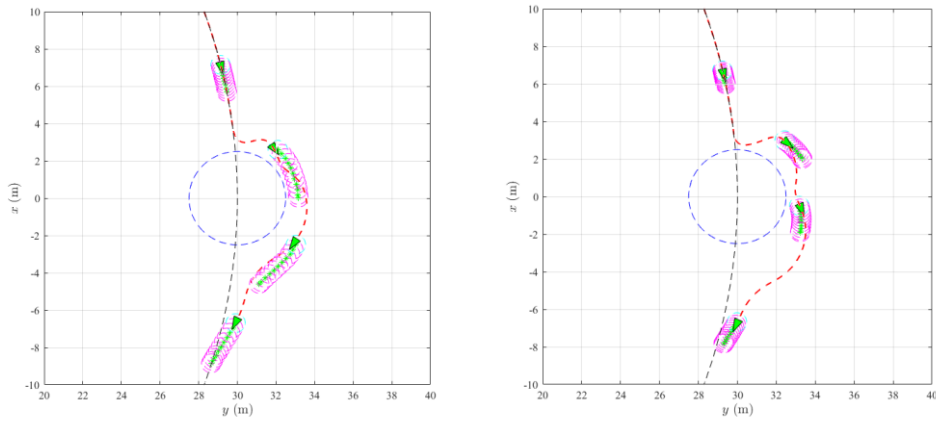
Figure 6-38: Scenario 4 (Cases A-i and A-ii) – Paths (zoom)
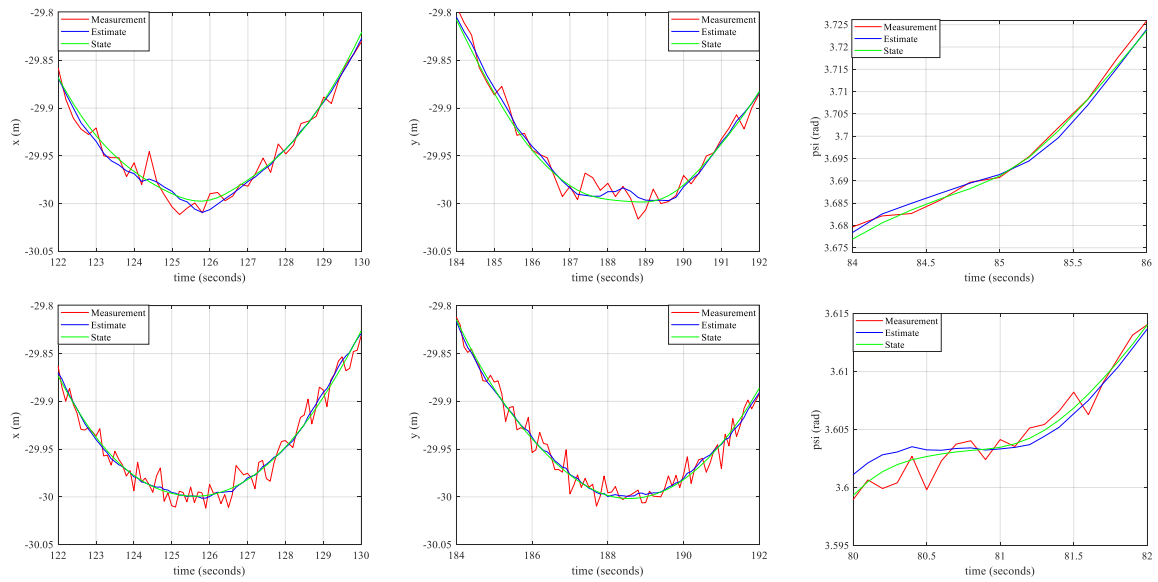
Figure 6-39: Scenario 4 (Cases A-i and A-ii) – MHE filtering
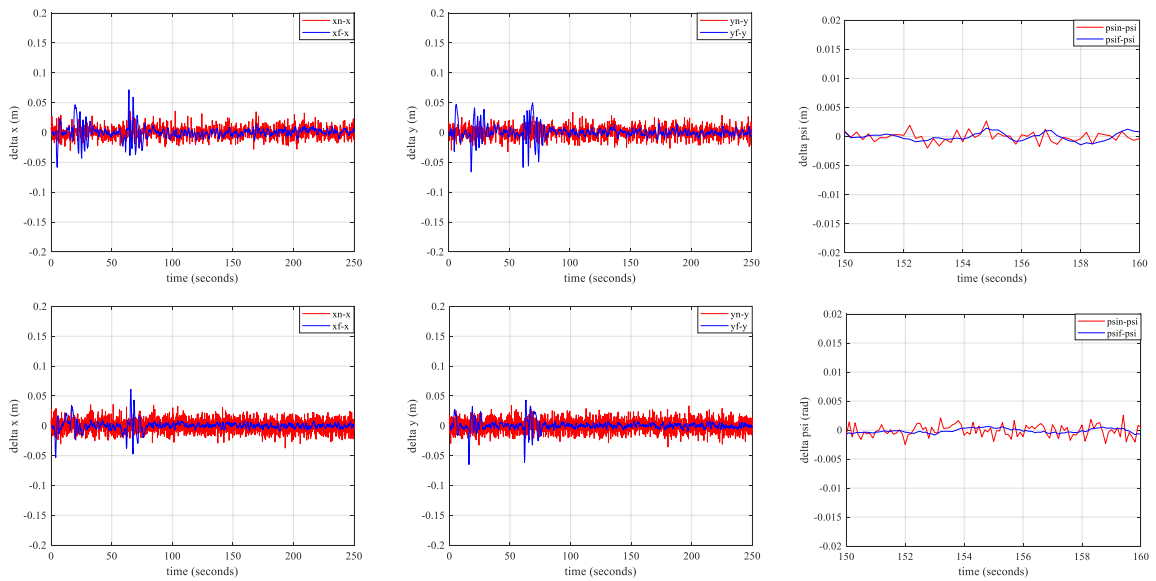
Figure 6-40: Scenario 4 (Cases A-i and A-ii) – MHE noise attenuation
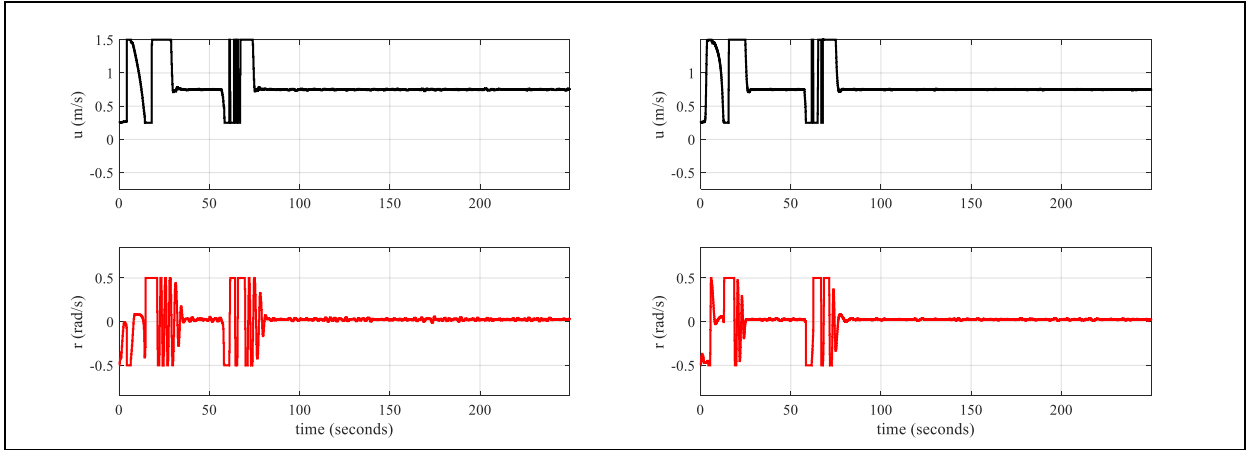
Figure 6-41: Scenario 4 (Cases A-i and A-ii) – Outer loop control signals
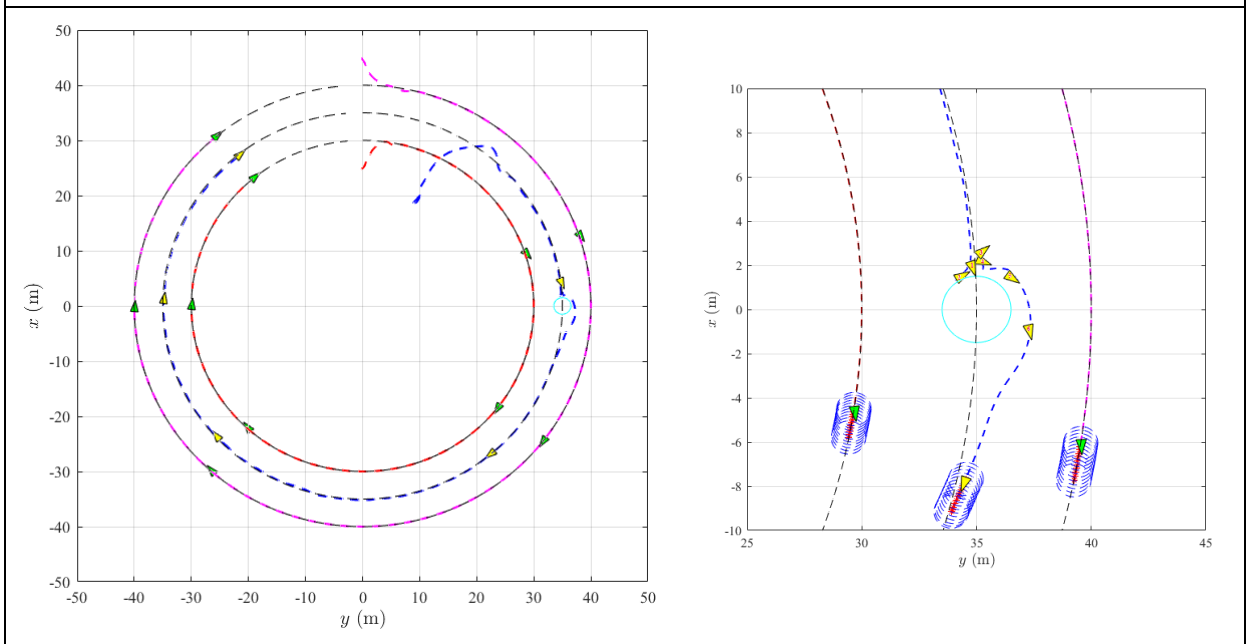
Figure 6-42: Scenario 4 (Case B) – Paths
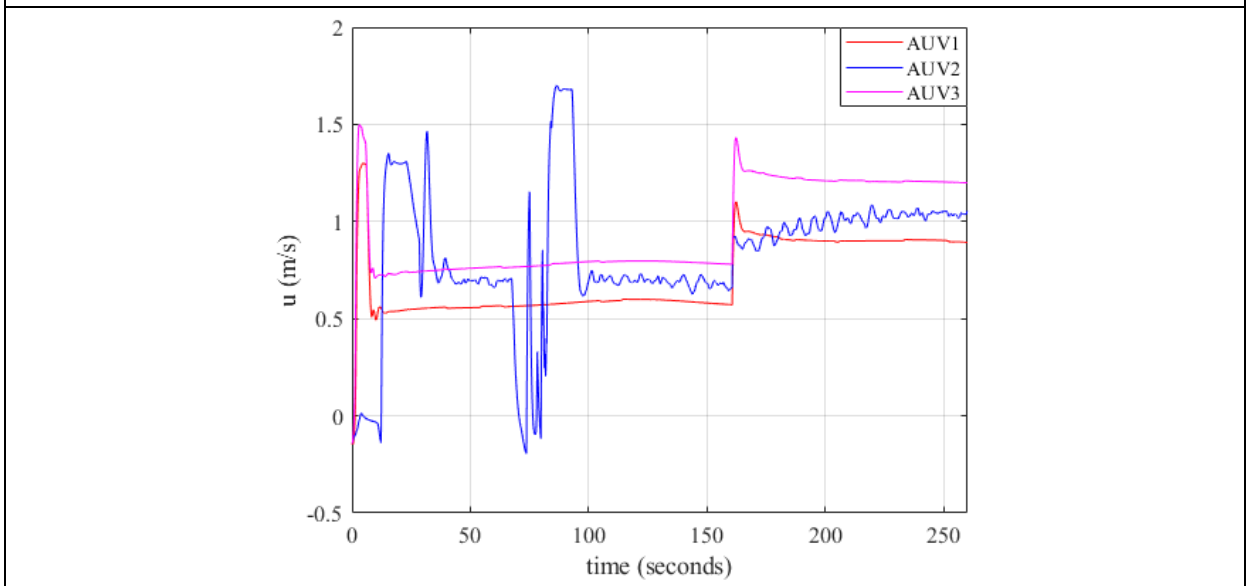
Figure 6-43: Scenario 4 (Case B) – Speed assignments
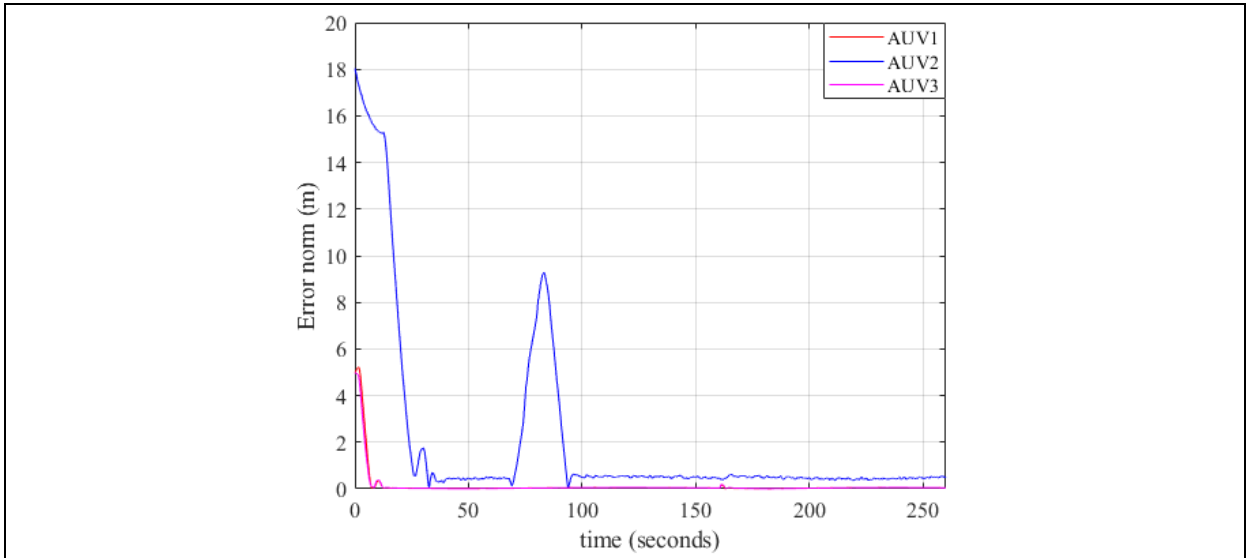
Figure 6-44: Scenario 4 (Case B) – AUV error norms
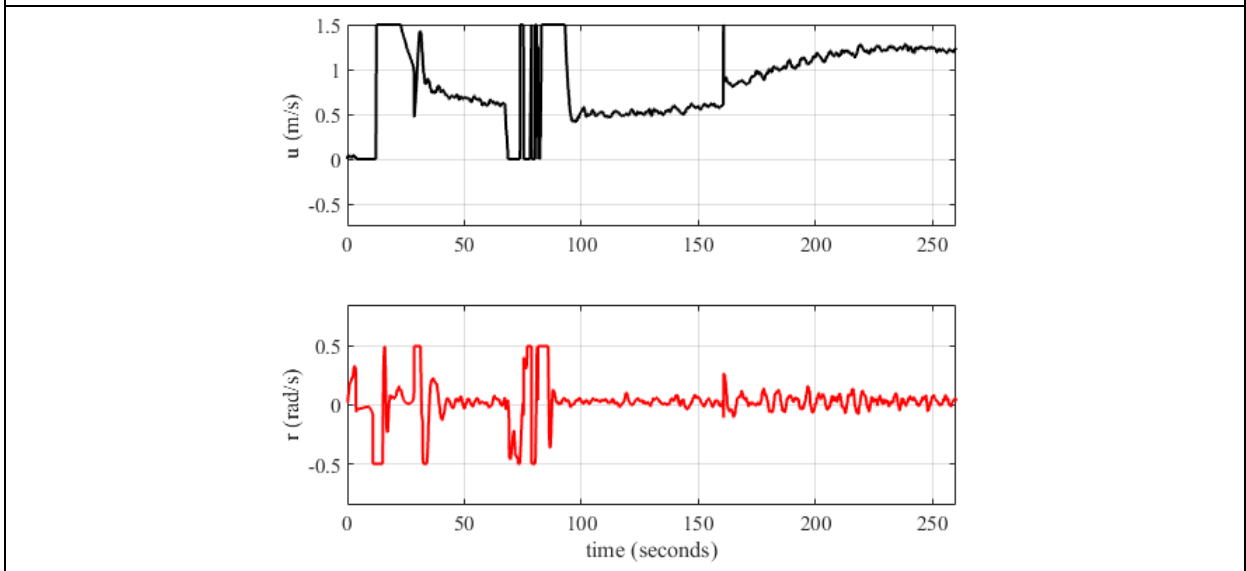
Figure 6-45: Scenario 4 (Case B) – AUV2 outer loop performance
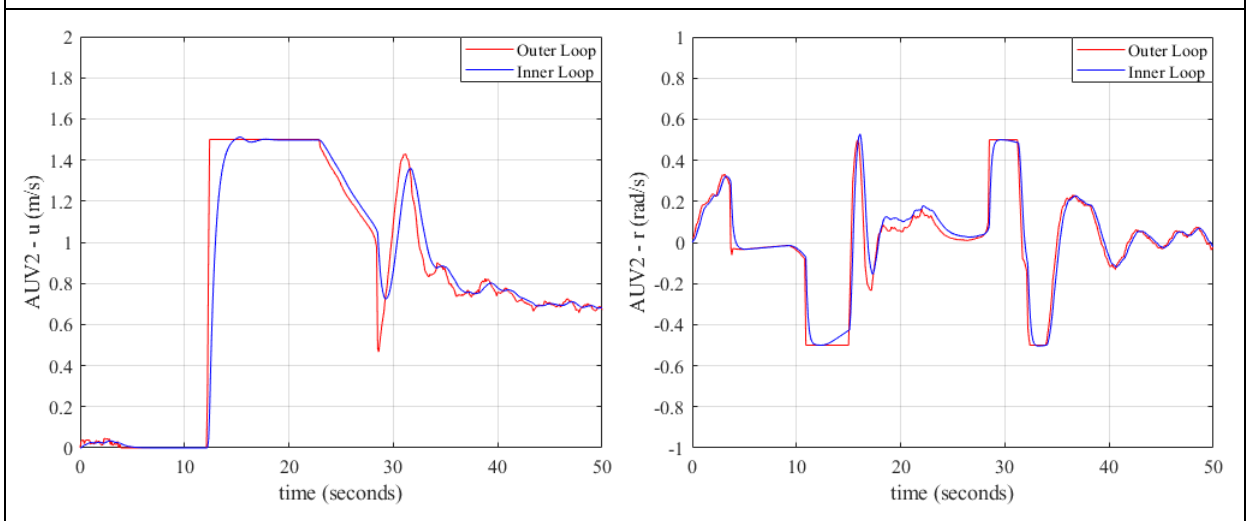
Figure 6-46: Scenario 4 (Case B) – Inner loop performance
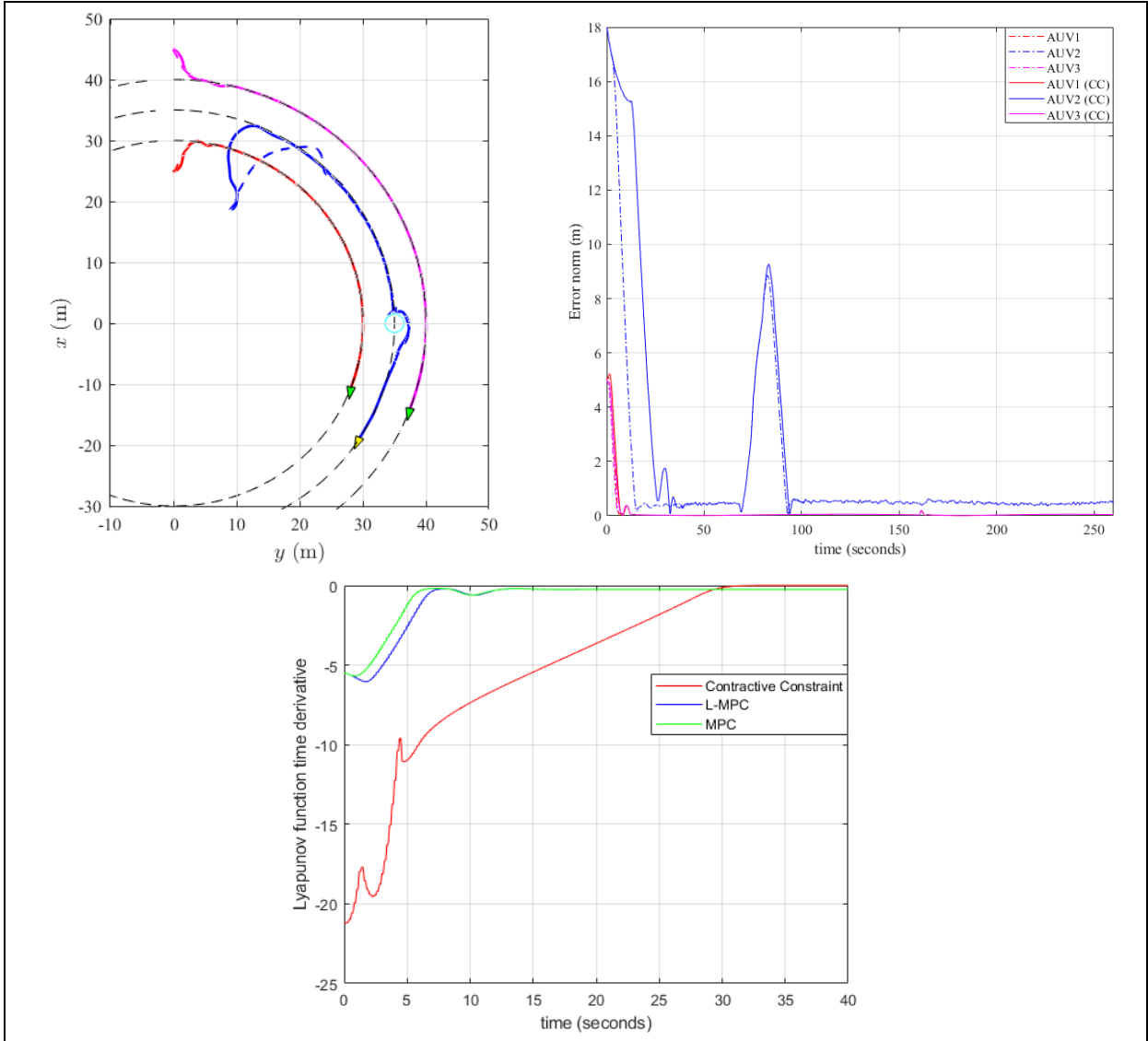
Figure 6-47: Scenario 4 (Case B) – Effect of the contractive constraint
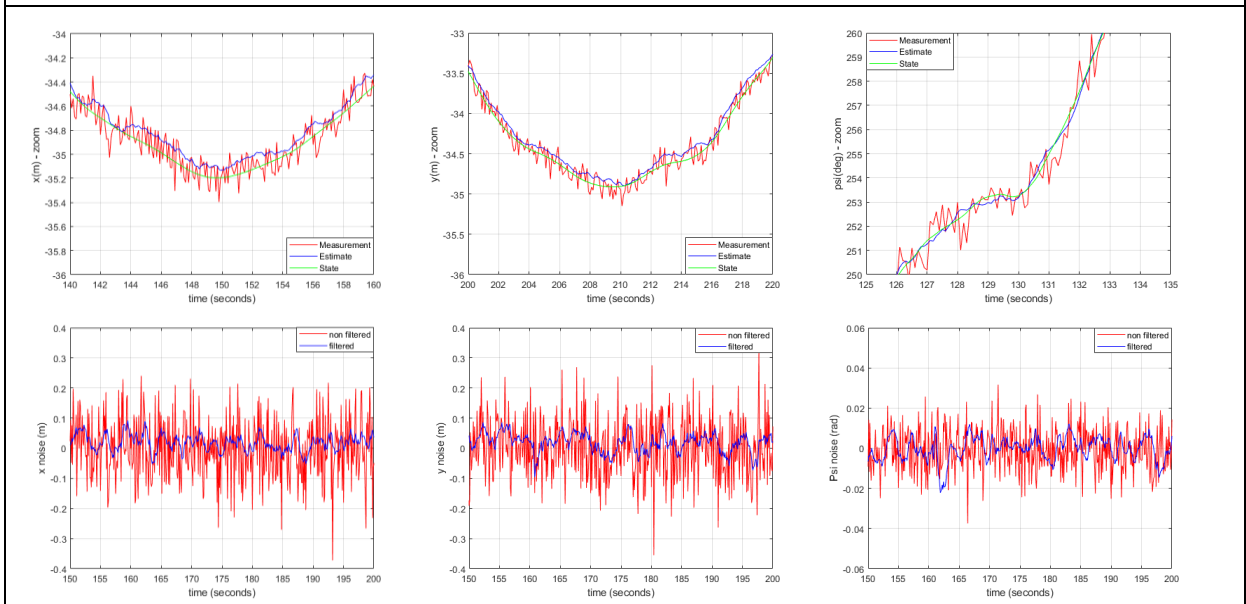
Figure 6-48: Scenario 4 (Case B) – MHE filtering performance
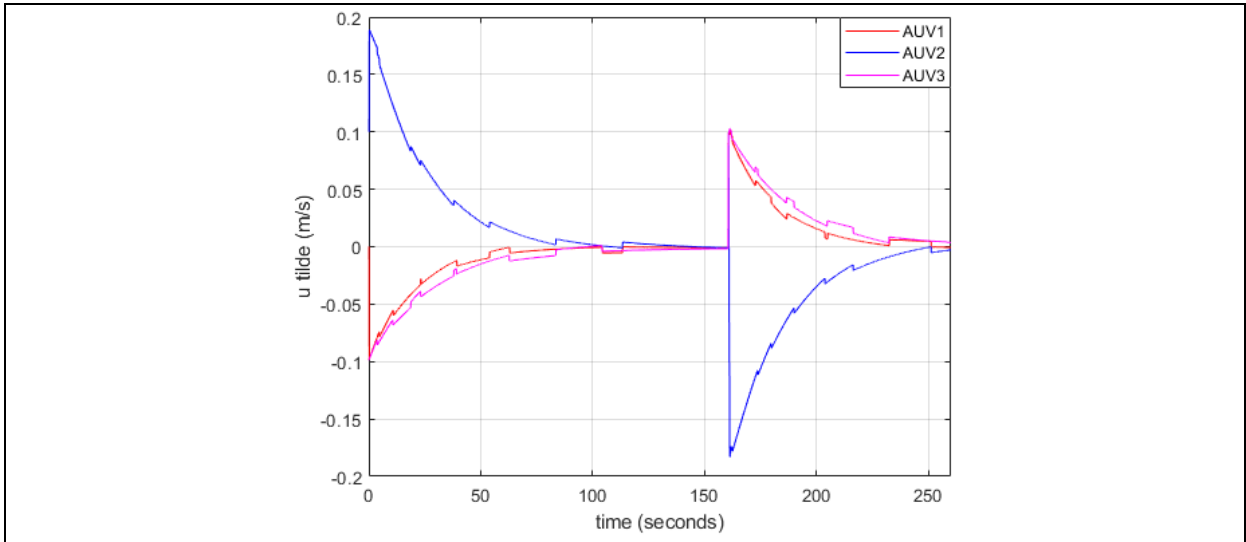
Figure 6-49: Scenario 4 (Case B) – Correction speeds
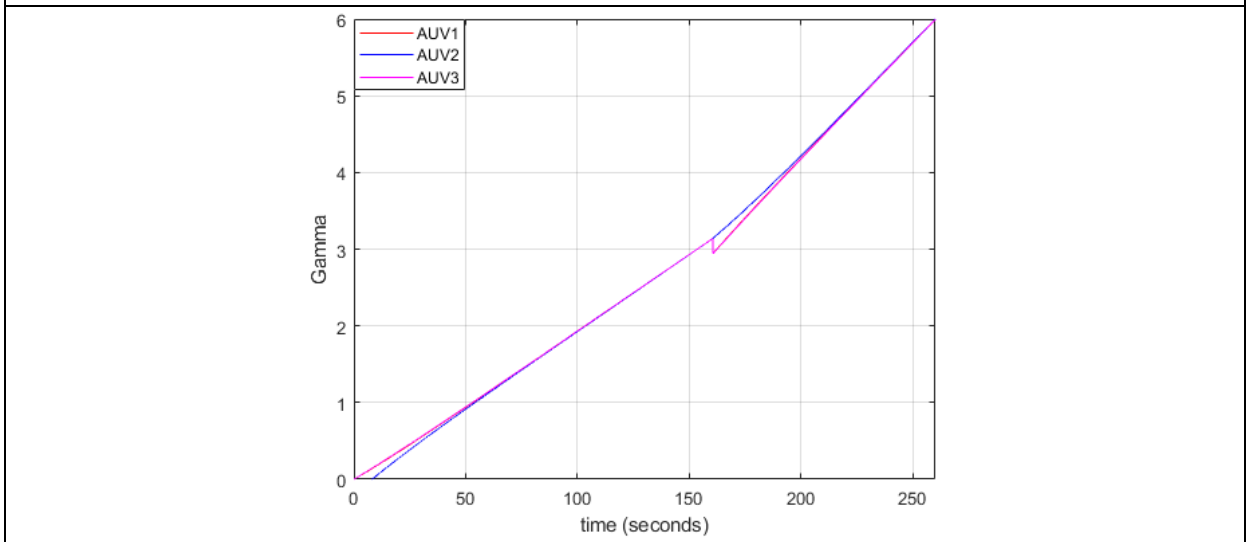
Figure 6-50: Scenario 4 (Case B) – Synchronization parameter γ
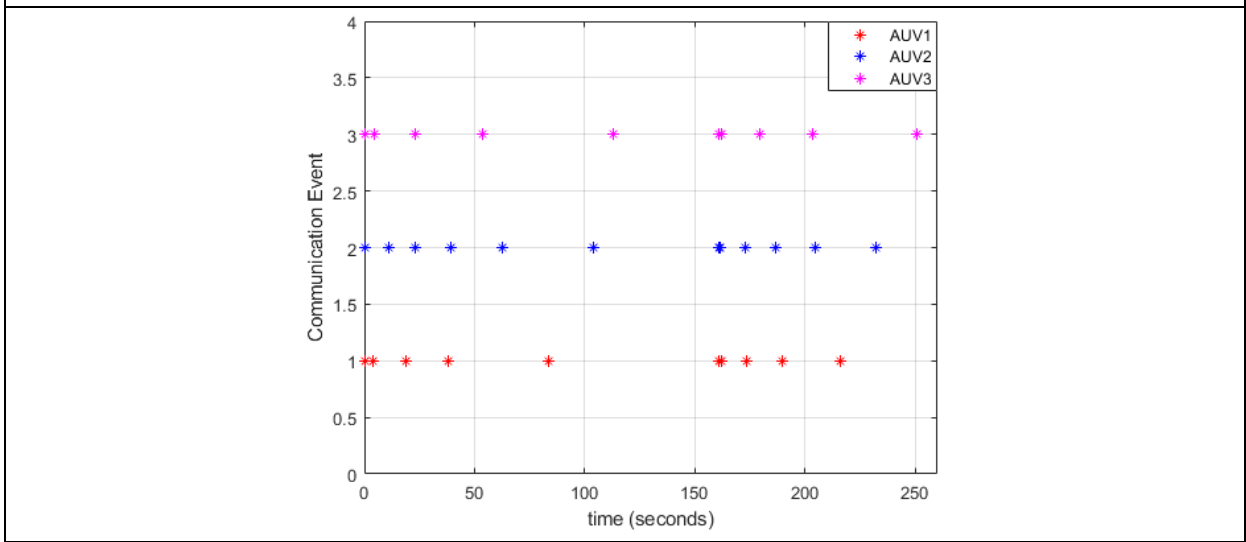
Figure 6-51: Scenario 4 (Case B) – Communication events

6.2.5 Scenario 5

This scenario, even considering the dynamics of the actuators, presents results that are quite similar to the previous one. Additionally, feeding the MHE and the ocean current state observer with speed measurements instead of outer loop signals did not significantly change the performance of the system.

The AUVs were able to follow the concentric circular paths, while respecting the desired formation pattern and complying with the path assigned speeds, as shown in Figure 6-52 and Figure 6-53, respectively. Intentionally, the vehicles departed from different initial conditions in order to check the occurrence of convergence issues, but they reached their assigned paths without problems. The "triangular" pattern was attained in the middle of the 1st quadrant, lost during the obstacle avoidance phase, but recovered again in the middle of the 2nd quadrant. At the beginning of the 3rd quadrant, the formation pattern was changed to "aligned" which was attained just after the beginning of the 4th quadrant.

The compliance with the path assigned speeds can be noticed in Figure 6-53[83]. At around $t = 160\ s$ the vehicles reached the 3rd quadrant and the path assigned speeds were increased as previously described. These speeds do not present periodic components, indicating that the L-MPC compensated properly the kinematic effect of the ocean current (Figure 6-54). Considerations about the cooperative correction speeds are presented in the next paragraphs.

The path following error norms (Figure 6-55) indicate convergence to near zero values for all vehicles. The steady state error for AUV2 is slightly larger compared to the others but it remains acceptable (< 0,5 m). This behavior is expected since AUV2 is the only vehicle subjected to measurement noise. Even during the obstacle avoidance phase, the error remained acceptable, considering the size of the obstacle.

Particularly in this phase, AUV2 was able to avoid the obstacle (Figure 6-52). It can be noticed that the L-MPC, zeroed the u signal as soon as the vehicle reached the obstacle but not the r signal (Figure 6-56). Consequently, the vehicle turned anticlockwise and drifted slightly westwards due to the current. After that, the L-MPC resumed to issue non null values of u and the vehicle started to properly circumvent the obstacle.

---

[83] In this figure, the angular speeds were already converted into linear speeds.

The speed tracking performance of the inner loop is displayed in Figure 6-57, where close adherence among the outer loop commanded speeds and the vehicle real speeds can be noticed, even considering the actuators' dynamics. The associated delay, for the current case, did not significantly change the performance of the system.

The effect of the contractive constraint over vehicles' trajectories is summarized in Figure 6-58. It can be seen that only the AUV2 trajectory was impacted during the maneuver's initial stages. This behavior can be better understood when analyzing the associated Lyapunov function time derivatives.

For this particular scenario, it can be noticed that the system would be stable even if the contractive constraint was not considered in the OCP formulation (MPC - green curve). This characteristic can be associated with the adopted prediction horizon length.

When it is considered (L-MPC), the system converges slowly since the contractive constraint (red curve) pushes its Lyapunov function time derivative (blue curve) down, attempting to limit it. After reaching zero, the red curve acts as a stability barrier (such as a terminal set), avoiding the blue curve to become positive, if it would be the case.

The MHE performance can be inferred in Figure 6-59, which presents its estimates and the associated noise attenuation levels (filtering), respectively. The quality of the estimates was satisfactory enough to assure the proper functioning of the closed loop control system. However, the L-MPC output signals (Figure 6-56) presented an oscillatory behavior (chattering) linked to the MHE estimates, indicating that performance improvements must still be pursuit.

The performance of the cooperative controller is summarized in Figure 6-60. Initially, to implement the "triangular" pattern, the cooperative controller increases the speed of the AUV2 and reduces the speeds of AUVs 1 and 3. Later, when the "aligned" pattern is commanded, the opposite occurs. It can be clearly noticed that correction speeds vanish to zero after the coordination parameters reach consensus (Figure 6-61).

The communication events are presented in Figure 6-62, showing that inter-vehicle communication is necessary only during the synchronization phases, since it practically vanishes as soon as the coordination parameters reach consensus.
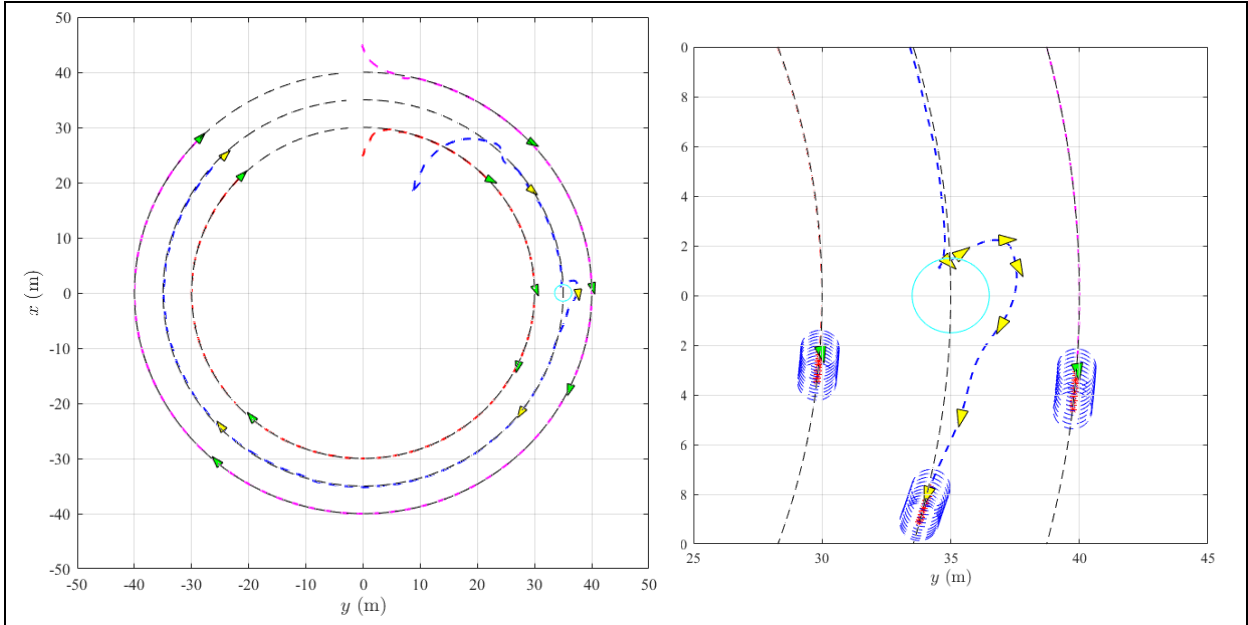
Figure 6-52: Scenario 5 – Paths
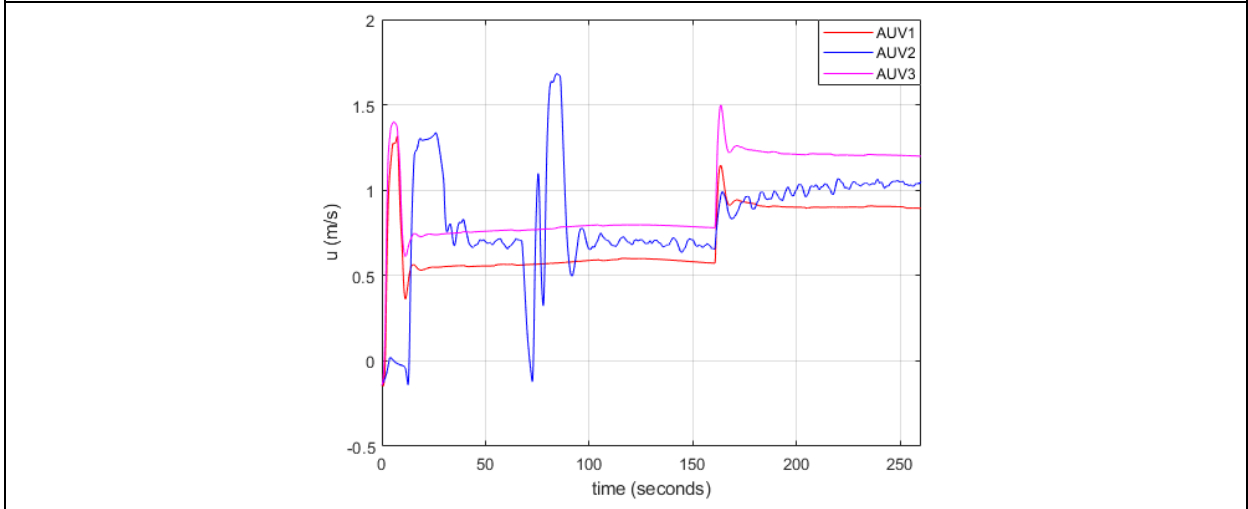
Figure 6-53: Scenario 5 – Speed assignments
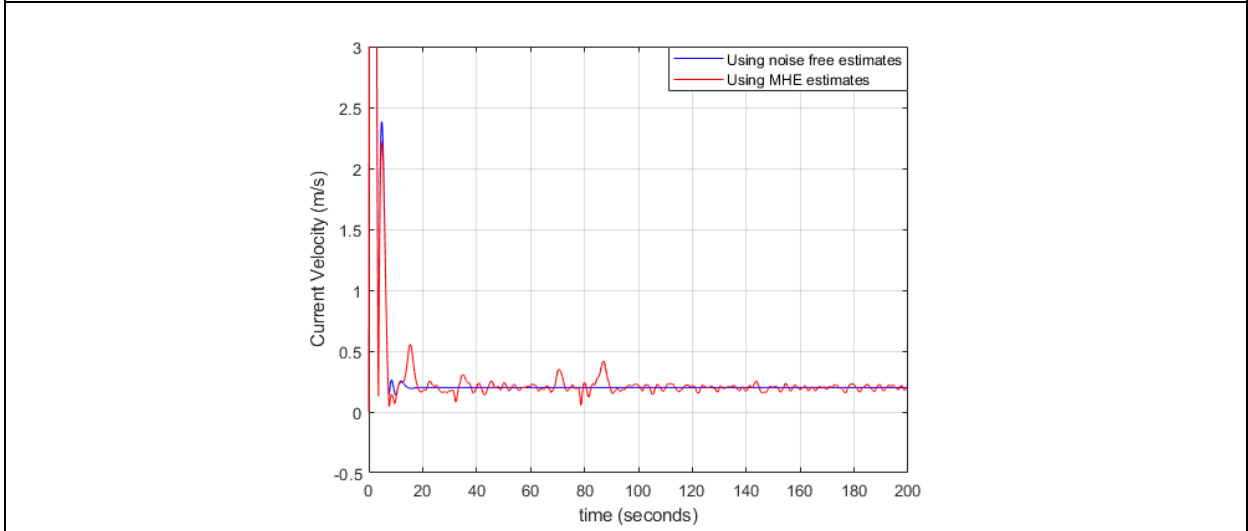
Figure 6-54: Scenario 5 – Ocean current state observer performance
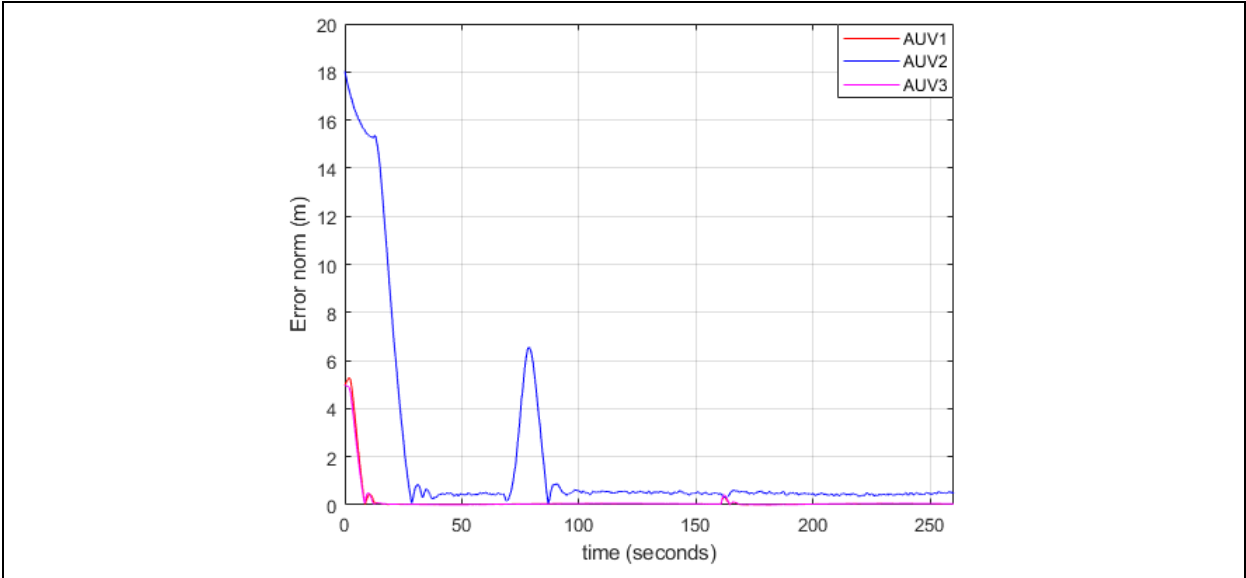
Figure 6-55: Scenario 5 – AUV error norms
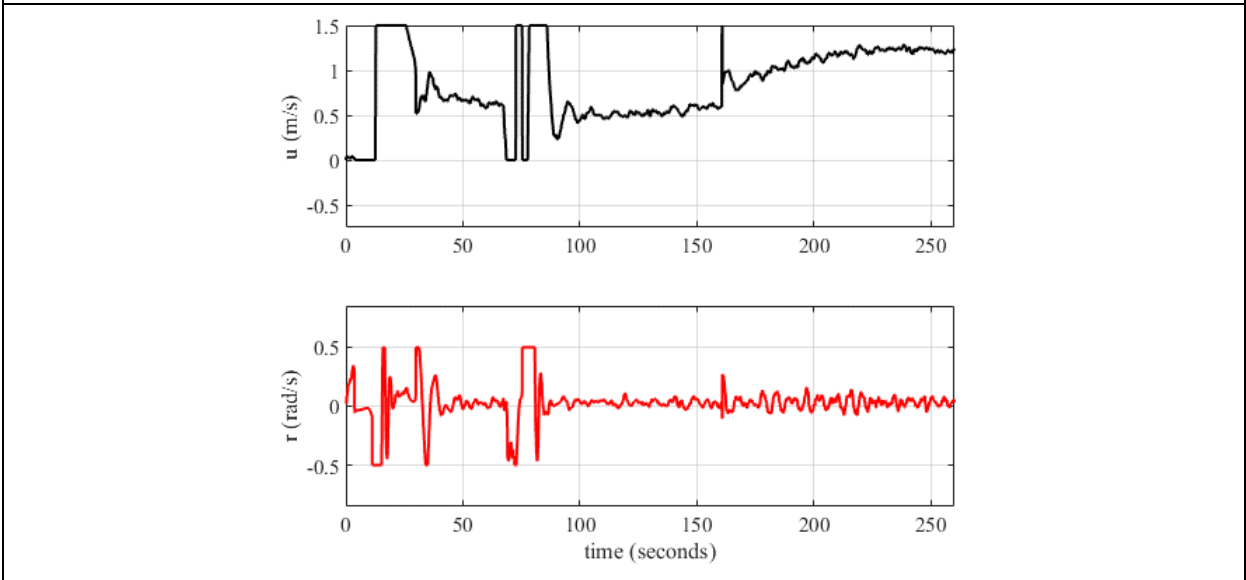
Figure 6-56: Scenario 5 – AUV2 outer loop performance
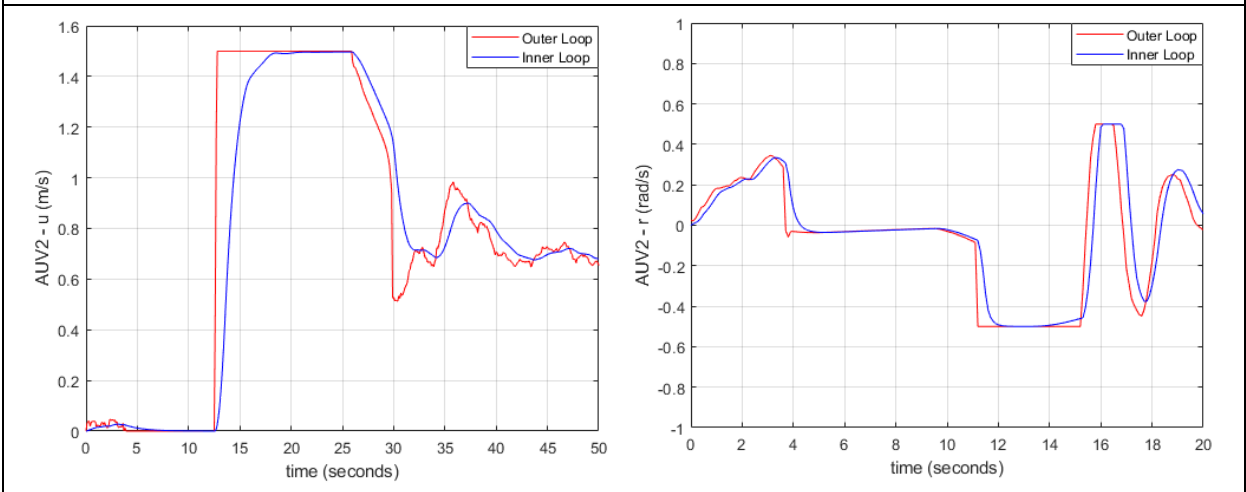
Figure 6-57: Scenario 5 – Inner loop performance
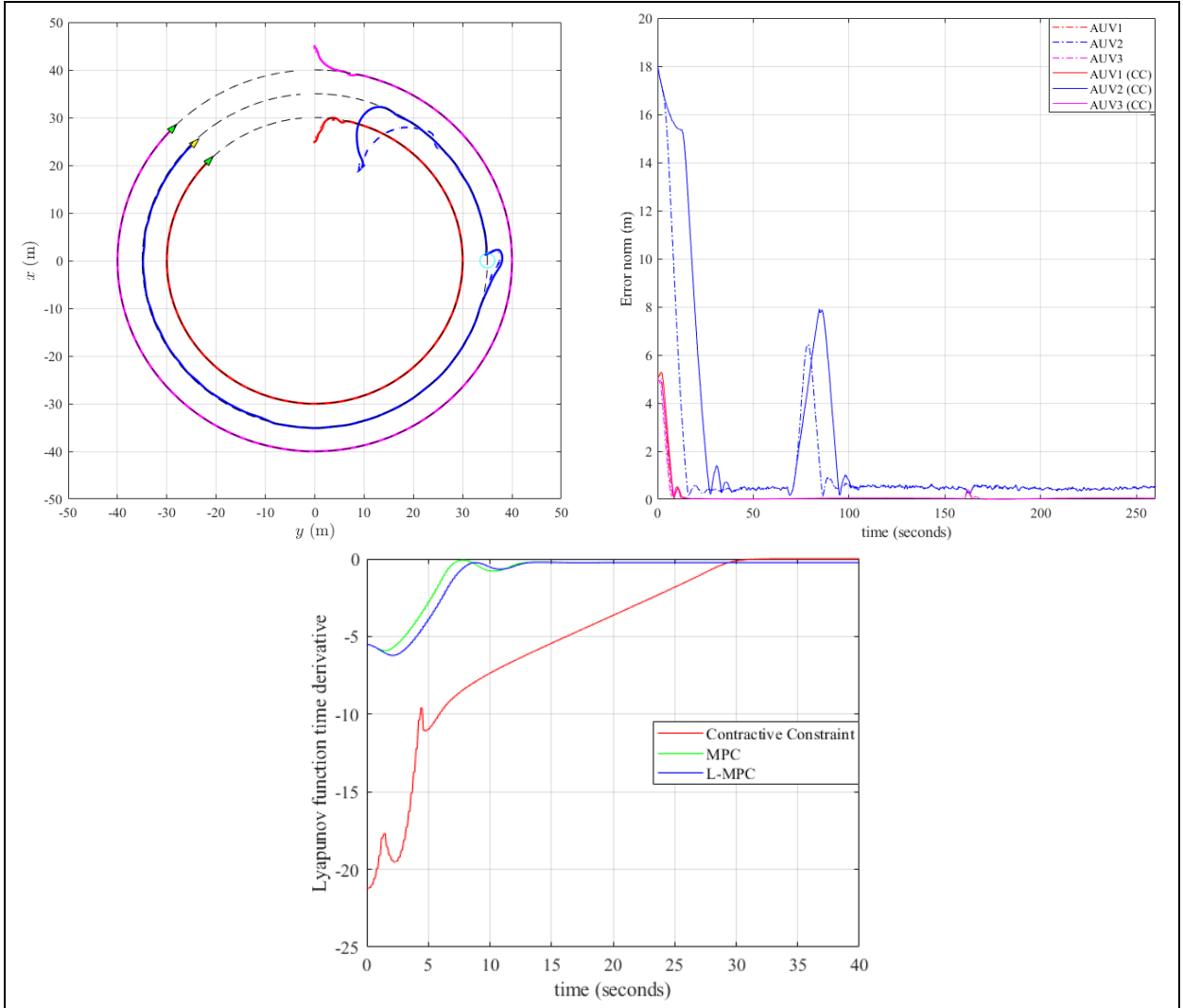
**Figure 6-58: Scenario 5 – Effect of the contractive constraint**
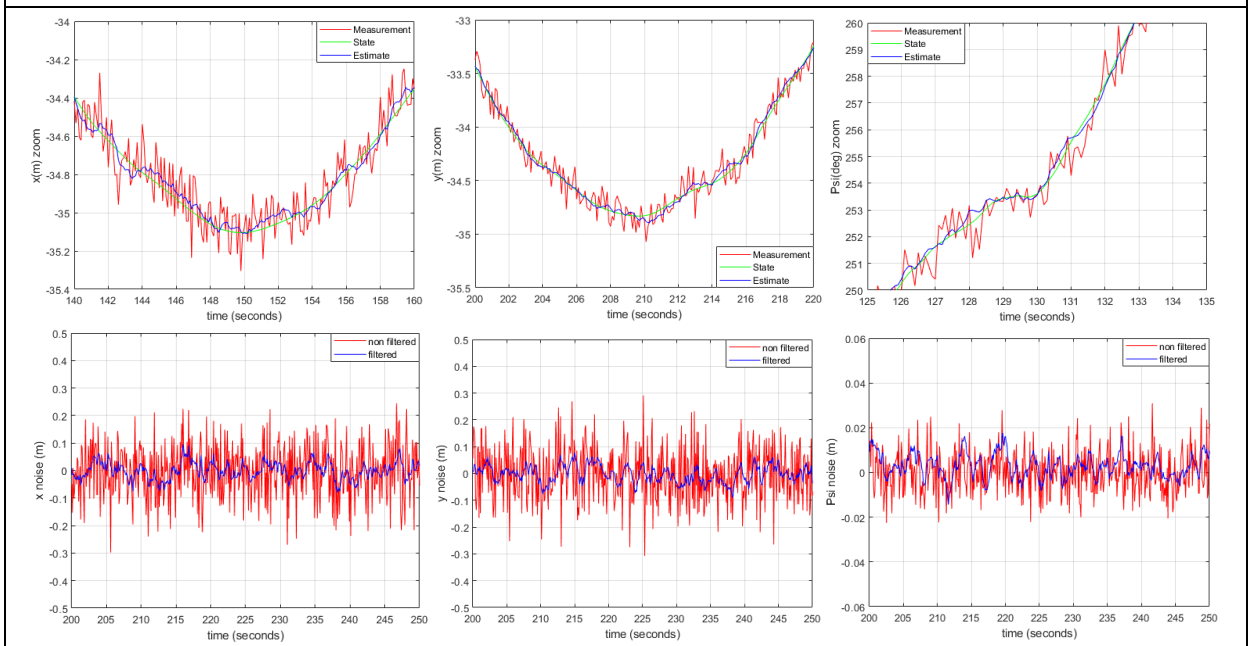
Figure 6-59: Scenario 5 – MHE filtering performance
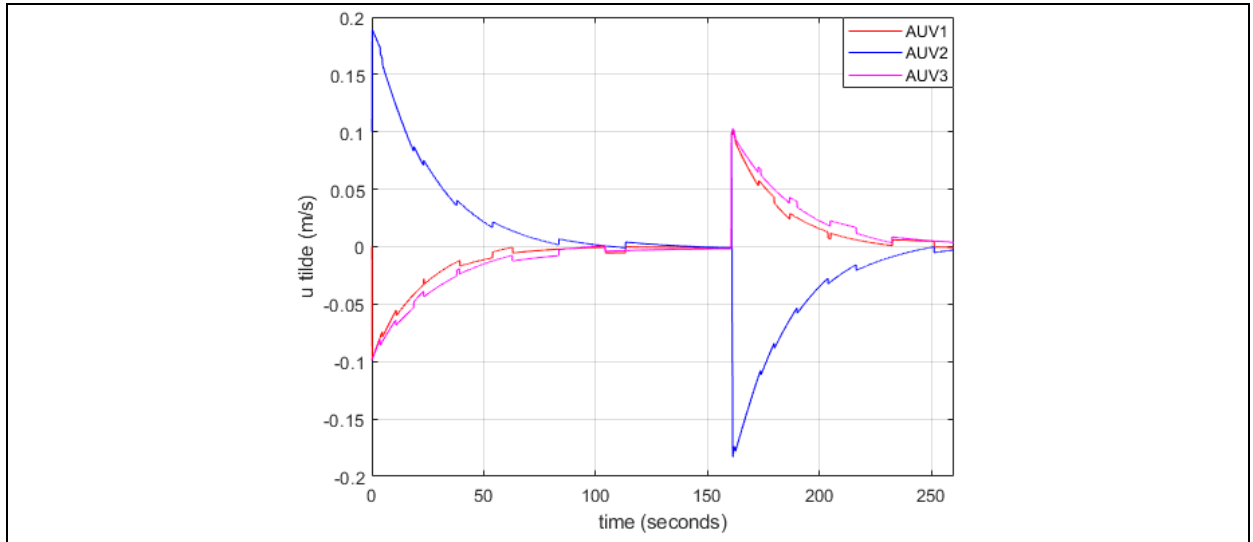
Figure 6-60: Scenario 5 – Correction speeds
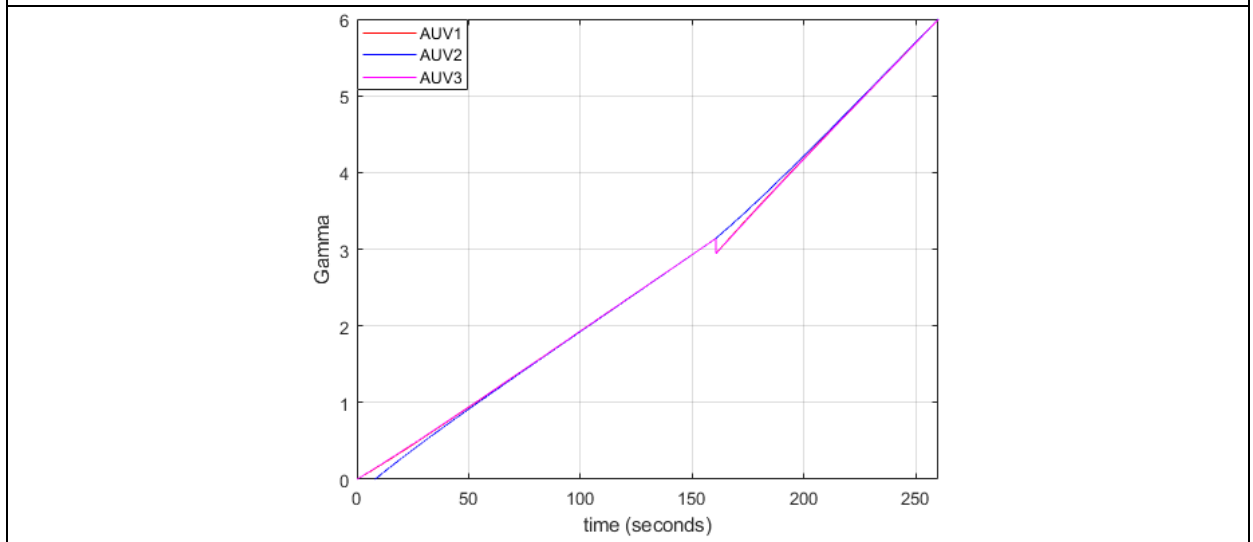
Figure 6-61: Scenario 5 – Synchronization parameter γ
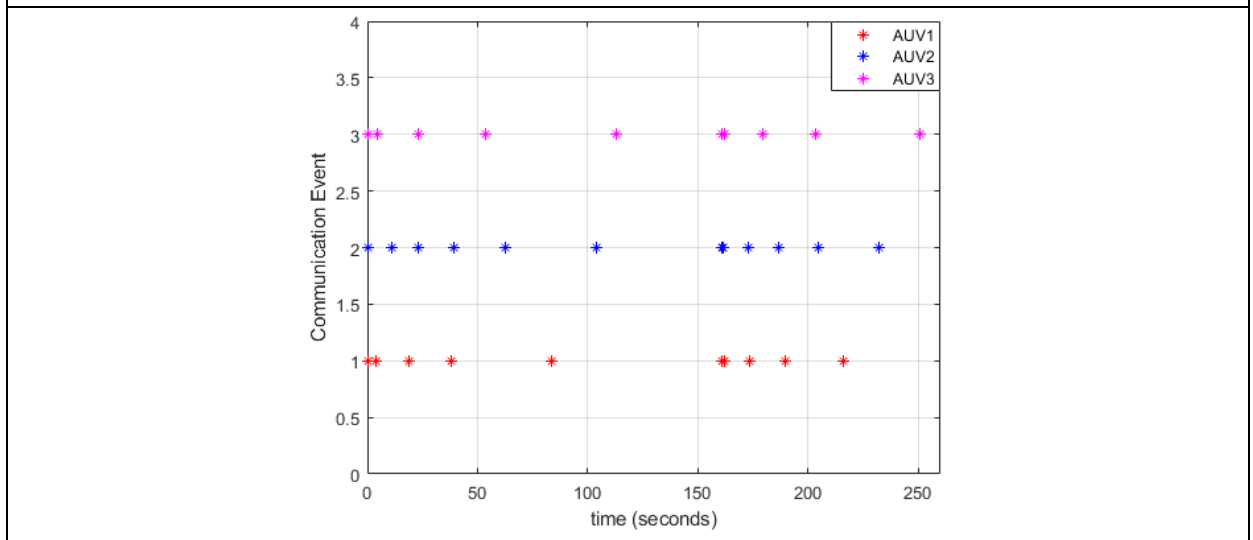
Figure 6-62: Scenario 5 – Communication events

6.3 Sensitivity Analysis for Robustness

The proposed sensitivity analysis intends to check the robustness of the developed control system[84] by varying the plant parameters. In the current analysis, the plant parameters were subjected to random variations of up to ±50% of their nominal values, following a uniform probability distribution, as presented in Figure 6-63. The number of samples was set as 30, as showed in Table 6-6.

Figure 6-63: Plant parameters distribution
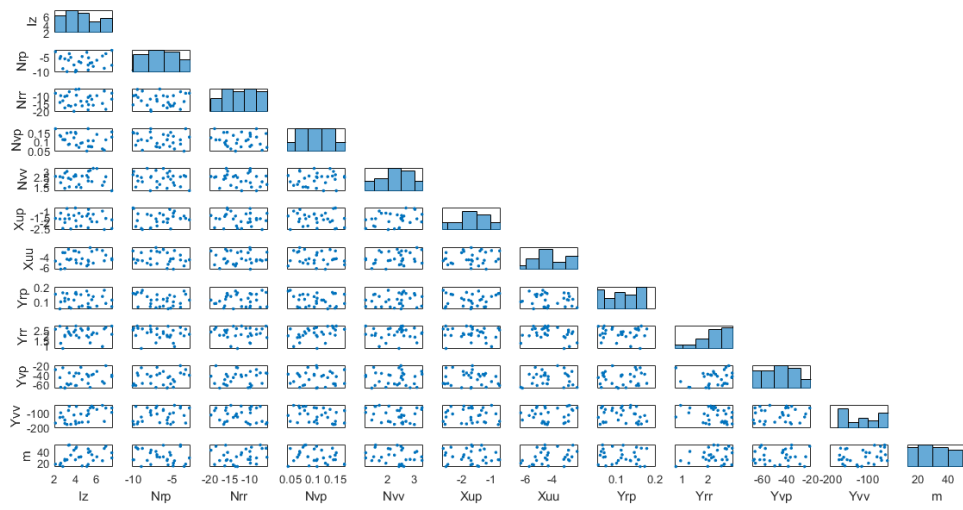
Table 6-6: Plant samples (30)

| Iz	Nrp	Nrr	Nvp	Nvv	Xup	Xuu	Yrp	Yrr	Yvp	Yvv	m
2.0770	-3.2796	-8.3180	0.1694	2.5073	-1.6466	-4.7901	0.1524	2.6002	-28.9827	-168.3486	17.9430
5.0774	-3.4843	-13.6482	0.0454	2.5876	-1.4324	-5.7510	0.1739	1.9630	-38.6169	-117.3423	13.9862
6.8975	-3.9596	-18.6377	0.1079	2.4771	-1.6484	-3.6316	0.0896	2.7734	-20.8018	-66.8627	48.8630
5.6902	-8.2376	-16.0029	0.1027	3.2679	-1.2785	-5.2060	0.1362	2.2619	-38.6866	-63.9493	24.3702
2.9729	-5.6753	-17.6951	0.1077	1.3860	-1.6930	-6.2640	0.1047	2.0118	-67.6951	-147.9750	24.1485
3.9860	-10.0671	-15.7849	0.1496	2.6649	-0.7091	-2.8110	0.1582	2.5226	-62.2727	-156.5822	25.5848
4.5071	-6.9740	-13.3987	0.0889	1.4558	-2.3274	-5.3001	0.1495	2.6623	-24.1712	-106.9548	30.7354
7.4638	-7.8383	-12.0929	0.1516	1.1572	-2.5631	-4.3299	0.0679	2.9036	-43.6065	-96.4686	37.6908
2.7798	-8.9998	-13.1386	0.1091	2.4043	-2.5550	-3.1373	0.1621	0.7331	-25.0882	-127.5496	13.7688
6.7479	-8.8671	-6.8694	0.0500	2.0026	-2.6512	-4.7342	0.1794	2.6325	-57.7250	-156.9282	45.1407
5.5517	-6.9922	-12.2292	0.0690	2.0245	-1.9392	-2.9014	0.1150	2.0772	-40.1143	-53.6477	34.2668
4.0277	-9.5163	-5.8457	0.1431	2.5439	-1.8478	-4.5617	0.1651	2.9059	-36.1292	-174.1757	45.5974
2.9757	-5.6433	-10.4344	0.1094	2.8208	-2.0202	-3.1586	0.1249	1.8908	-66.8369	-170.8852	26.1586
4.3228	-6.6233	-5.6346	0.0659	1.7472	-1.1898	-3.0583	0.0662	1.7850	-36.9083	-165.8279	29.9274
4.6280	-4.8951	-16.3894	0.0915	2.5441	-1.4730	-4.3304	0.0723	2.4918	-49.8665	-162.4287	14.8828
2.5766	-4.8649	-9.8582	0.1276	1.9157	-1.1721	-6.3849	0.1004	1.2323	-65.9360	-99.1626	19.6009
5.2380	-5.3361	-15.6640	0.0712	3.0040	-0.8362	-4.8720	0.1467	1.8258	-43.3357	-105.7396	38.2518
3.1758	-9.9819	-9.9229	0.1453	2.9809	-0.7529	-4.4179	0.1571	2.7103	-58.5927	-178.3508	25.5038
4.0751	-9.7116	-9.5729	0.0781	1.5075	-2.3830	-5.1665	0.1523	1.9940	-62.1584	-55.9768	47.3019
5.2010	-7.7855	-18.9801	0.1696	2.4200	-2.4940	-5.5223	0.0884	2.5880	-57.9258	-84.1703	17.3372
3.3213	-6.1630	-16.1781	0.0817	2.3402	-1.3302	-2.4864	0.1176	2.3541	-60.9550	-82.8924	50.7552
3.5405	-5.2139	-16.6394	0.1490	2.2341	-2.5881	-4.3906	0.0574	2.0188	-58.7693	-176.7741	33.5353
5.3946	-7.1095	-9.9825	0.0708	3.0756	-1.6870	-2.1654	0.0603	1.2738	-66.2894	-65.8267	39.9456
3.3977	-3.9425	-7.3341	0.0842	1.5288	-1.6766	-4.5789	0.0637	2.1955	-35.8562	-55.5308	51.1805
6.5712	-4.7230	-14.8331	0.0576	1.6650	-0.9859	-2.7421	0.1372	0.9153	-54.0033	-48.5718	23.8534
7.4696	-2.8008	-8.2922	0.1233	1.1567	-1.7716	-4.5516	0.1123	2.1066	-40.8177	-66.0357	28.7177
6.0369	-6.1594	-9.8700	0.1379	3.2542	-1.9625	-2.5506	0.0709	2.1834	-32.7764	-76.2502	30.6499
3.8438	-7.7429	-19.8993	0.1193	2.5020	-1.3821	-2.8103	0.1123	2.3345	-42.8454	-114.1379	42.1360
5.2072	-9.4288	-10.9674	0.1029	2.0775	-1.2363	-4.6459	0.0652	2.6881	-40.9613	-160.8777	44.2190
2.5037	-5.5478	-14.1984	0.1326	2.4861	-1.6981	-5.4301	0.0527	2.8891	-45.6154	-130.1163	16.6485

[84] More specifically the robustness of the inner (dynamic) loop. The outer (kinematic) loop and the cooperative controller are fully independent of the plant, therefore they are not subjected to parametric uncertainty.

The target function evaluated in the analysis was the path following error norm signal matching, as presented in Figure 6-64.

Figure 6-64: Cost function plot[85]
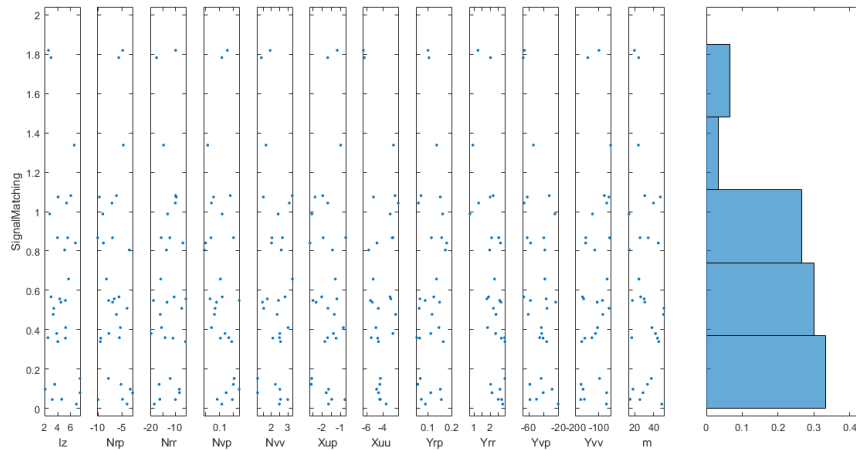
The path following error norms related to the nominal plant (blue curve) and sampled plants (red curves) are presented in Figure 6-65. It shows that the control system keeps its efficacy even in the presence of the considered parametric uncertainties, however, as expected, at the expense of the performance. These results demonstrate that the control system is robust up to this level of parameter incertitude.

Figure 6-65: Path following error norms (nominal and sampled plants)

---
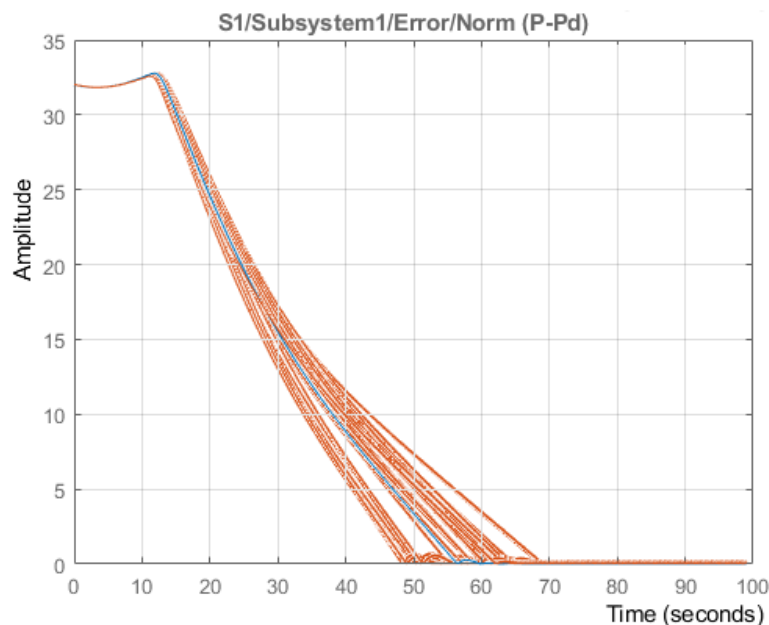
[85] The plot displays the evaluated target function value as a function of each parameter in the parameter set. The last column of subplots displays histograms of the probability distribution of the evaluated target function values.

6.4 Summary

In this chapter, the proposed control system was verified and validated through numerical simulations, on an incremental basis, considering a bottom-top approach (NASA, 2016).

Initially, the path following controller outer loop (L-MPC) was tested and compared with a feedback linearized controller, considering a straight invariable speed parameterized path. The effect of the contractive constraint over the controller performance was assessed. Even being slower than MPC in the considered scenarios, the L-MPC approach is recommended because there is no guarantee that MPC is recursively feasible and stable for other initial conditions. The results confirmed the effectiveness of the controller in terms of recursive feasibility, stability and convergence. Just in the sequence, the L-MPC was tested considering a sinusoidal speed parameterized path, with a fixed obstacle, in the presence of ocean currents, and consistent results, like the previous ones, were attained.

In parallel, the path following controller inner loop (feedback linearization speed tracker controller) was also assessed, and its tracking performance was confirmed. Due to the close adherence between commanded speeds and real vehicle's speeds, it was concluded that the outer loop speed assignment could eventually replace the surge and yaw speed measurements required to run the MHE and the ocean current state observer.

In the next step, the path following controller was integrated with the cooperative controller and the combined system was tested considering multi-vehicle mission scenarios. The system was capable of controlling the formation pattern, along their speed parameterized assigned paths. Its logic-based communication algorithm was capable of keeping the communication flow among the vehicles at a minimum level.

Finally, the MHE and the ocean current state observer were integrated to the cooperative path following controller, and the resulting system was tested in similar conditions as it had been tested before, however considering the presence of measurement noise and ocean currents. The performance of the system was preserved, thanks to the quality of the estimated feedback states (position/heading and speeds) supplied by the MHE, however improvements must be pursuit in order to reduce the chattering effect in the outer loop control signals.

Concerning the MHE performance, it was noticed that the quality of its estimates increases with the number of samples, but the closed loop stability is jeopardized if the time window associated with the prediction horizon increases. This occurs because the higher the time window is, the slower the MHE responds, and if the MHE is not fast enough to couple the system dynamics, the system destabilizes. Reducing the sample time coherently with the system dynamics proved to be a solution, however, at the expense of computational burden.

The ocean current state observer was able to provide estimates of the irrotational and constant ocean current velocity. However, for ASCs, this figure could be easily obtained using measurements of the vehicle's relative velocity with respect to the fluid (for example, using a Doppler log working in water locked mode), combined with the position measurements supplied by the GPS. Differently, for AUVs, estimating/measuring the ocean current speed poses considerable challenges due to the unavailability of the GPS signal.

Concerning the simulation environment, for the sake of fairness, it must be pointed out that it still suffers from the lack of some important realistic phenomena like a more precise model for the actuators' dynamics and the inclusion of an acoustic underwater communications algorithm that takes into account time delays and data loss[86]. These issues must be solved before starting the experimental phase, combined with a formal characterization of the control system overall stability[87].

Additionally, it must be registered that certain behaviors in the control signals are still not acceptable from the experimental perspective. In general, these signals are too large and aggressive, indicating that a better tuning set[88] must be pursuit. The same conclusion applies to the estimator signals. In some parts of the simulations, the gap between real and estimated values would not be acceptable for practical applications.

The system's robustness was assessed by considering variations in the plant parameters up to 50% of their nominal values, along 30 combination samples. The results indicate that the control system was able to keep its stability and convergence properties however, as expected, at the expense of performance.

---

[86] For an "experimental-free" validation, the simulation environment shall be as realistic as possible.

[87] A control solution without stability proof, even valid for very stringent conditions, would never be reasonably experimented in real life applications.

[88] Including the OCP parameters such as the prediction horizon and the sample time.

7   CONCLUSIONS AND FURTHER RESEARCH

This thesis addressed the motion control problem of multiple ocean vehicles operating in cooperative mode to accomplish common missions. Its main contribution was to design a path following controller fully based on the receding horizon principle, combining L-MPC and MHE, and to integrate it with a consensus-based distributed cooperative controller. The numerical performance of the designed system demonstrated its good behavior in terms of recursive feasibility, stability, convergence and robustness, indicating its potential for future experimental implementation.

7.1   Conclusions

The main conclusion of this work refers to the successful coupling of L-MPC and MHE, resulting in a path following controller (the guidance system) fully based on the receding horizon principle. Even not performing quantitative comparisons with many other path following strategies, the receding horizon approach (MPC/MHE) is expected to outperform them. Besides its unique capability to deal with obstacle avoidance scenarios, this strategy has also an inherent ability to allow the system to operate near to or at the boundaries of the allowable state-space region, where the (sub)optimal solution can normally be found, thus maximizing performance and avoiding the occurrence of actuators' saturation.

The MHE, even relying on its simplest form, without an arrival cost in the associated OCP cost function formulation, was able to provide estimates precise enough to assure the proper functioning of the closed loop system at numerical level. Consequently, there is margin for performance improvements if such term is incorporated into the formulation.

The strategy to use a contractive constraint in the L-MPC finite horizon OCP formulation as a sufficient condition to assure stability, besides its theoretical appeal, proved to be unnecessary. The results indicated that it can be derogated for the sake of simplicity if the prediction horizon is chosen large enough to assure stability (approximating the effect of the infinite horizon OCP).

The receding horizon approach applied for control and estimation resulted in a reduced number of gains which proved to be easily tuned. The L-MPC (outer loop) gains (5) were tuned by trial-and-error at once, while the MHE gains (5) were tuned

by conceptual rules of thumb. Additionally, the feedback linearized controller (inner loop) gains (2) were also easily tuned due to the fast-slow temporal scale separation verified among both loops. However, certain behaviors in the controller/estimator signals are still not acceptable from the experimental perspective, demanding additional tuning efforts.

Concerning the simulation environment, there are still some aspects that must be developed in order to improve its level of representativeness. The main points to be considered refer to actuators' dynamics and acoustic underwater communications.

These issues must be properly solved before starting the experimental phase, combined with a formal characterization of stability.

7.2 Future Research

Future works, besides experimental implementation, envisages:

- The development of stability proof demonstrations, even considering that any control/estimation technique based on the receding horizon principle is difficult to be analyzed and, when employed in practice, it usually does not satisfy many theoretical stability/convergence properties;
- A formal investigation of robustness;
- The use of an MHE based on active range-only beacon measurements, while dealing with the observability problem at near zero surge speeds;
- The investigation of arrival cost approximations in the MHE OCP;
- The incorporation of an MPC-based path planning module for set-point assignment.
- An ocean current state observer fully integrated in the MHE framework;
- The incorporation of an inter-vehicle collision avoidance module in the path following controller using Distributed Model Predictive Control, where each vehicle shares its predicted trajectory so that the others can avoid it;
- The update of the cooperative controller logic-based communication algorithm, considering time delays, data loss and communication sequencing; and
- To develop a path following controller using learning-based techniques such as learning-MPC or reinforcement learning, in order to better deal with uncertainty in vehicle and actuator models.

8 BIBLIOGRAPHY

Abreu, P. C. (2014). Sensor-based formation control of autonomous underwater vehicles. *(Master thesis)*. Lisbon, Portugal: Instituto Superior Técnico.

Abreu, P. C., Botelho, J., Góis, P., Pascoal, A., Ribeiro, J., Ribeiro, M., . . . Silva, H. (2016). The MEDUSA class of autonomous marine vehicles and their role in EU projects. *IEEE OCEANS 2016*, (pp. 1-10).

Abreu, P., Morishita, H. M., Pascoal, A., Ribeiro, J., & Silva, H. (2016). Marine vehicles with streamers for geotechnical surveys: modeling, positioning, and control. *IFAC-PapersOnLine, 49*(23), 458-464.

Aguiar, A. P., & Hespanha, J. P. (2003). Position tracking of underactuated vehicles. *Proceedings of the 2003 IEEE American Control Conference*, *3*, pp. 1988-1993.

Aguiar, A. P., & Hespanha, J. P. (2004). Logic-based switching control for trajectory-tracking and path-following of underactuated autonomous vehicles with parametric modeling uncertainty. *Proceedings of the 2004 IEEE American Control Conference*, *4*, pp. 3004-3010.

Aguiar, A. P., & Hespanha, J. P. (2007). Trajectory-tracking and path-following of underactuated autonomous vehicles with parametric modeling uncertainty. *IEEE Transactions on Automatic Control, 52(8)*, pp. 1362 - 1379.

Aguiar, A. P., & Pascoal, A. M. (2007a). Coordinated path-following control for nonlinear systems with logic-based communication. *2007 IEEE 46th Conference on Decision and Control*, (pp. 1473-1479).

Aguiar, A. P., & Pascoal, A. M. (2007b). Dynamic positioning and way-point tracking of underactuated AUVs in the presence of ocean currents. *International Journal of Control, 80(7)*, pp. 1092-1108.

Aguiar, A., Almeida, J., Bayat, M., Cardeira, B., Cunha, R., Haussler, A., . . . Vanni, F. (2009). Cooperative autonomous marine vehicle motion control in the scope of the EU GREX project: Theory and practice. *OCEANS 2009*, (pp. 1-10).

Alessandretti, A., Aguiar, A. P., & Jones, C. N. (2013). Trajectory-tracking and path-following controllers for constrained underactuated vehicles using model predictive control. *2013 IEEE European Control Conference*, (pp. 1371-1376).

Andersson, J. A., Gillis, J., Horn, G., Rawlings, J. B., & Diehl, M. (2019). CasADi - a software framework for nonlinear optimization and optimal control. *Mathematical Programming Computation, (11)(1)*, 1-36.

Arai, T., Pagello, E., & Parker, L. E. (2002). Editorial: Advances in multi-robot systems. *IEEE Transactions on Robotics and Automation, 18*(5), pp. 655-661.

Auvac - Autonomous Undersea Vehicle Applicantions Center. (n.d.). *AUV System Spec Sheet*. Retrieved 11 06, 2021, from Auvac - Autonomous Undersea Vehicle Applications Center: https://auvac.org/136-2/

Beard, R. W., Lawton, J., & Hadaegh, F. Y. (2001). A coordination architecture for spacecraft formation control. *IEEE Transactions on Control Systems Technology, 9(6)*, pp. 777-790.

Blidberg, D. R. (2001). The development of autonomous underwater vehicles (AUV); a brief summary. *2001 IEEE ICRA*, *4(1)*, pp. 1-12.

Brembeck, J. (2019). Nonlinear constrained moving horizon estimation applied to vehicle position estimation. *Sensors, 19(10), 2276.*

Budiyono, A. (2011). Model predictive control for autonomous underwater vehicle. *Indian Journal of Geo-Marine Sciences, 40(2)*, pp. 191-199.

Burger, M., & Pettersen, K. Y. (2010). Smooth transitions between trajectory tracking and path following for single vehicles and formations. *IFAC Proceedings Volumes*, *43(19)*, pp. 115-120.

Burger, M., Pavlov, A., & Pettersen, K. Y. (2009). Conditional integrators for path following and formation control of marine vessels under constant disturbances. *IFAC Proceedings Volumes*, *42(18)*, pp. 179-184.

Cardeira, B. (2017). The Medusa deep sea and fusion AUVs: when research and business get together. *Workshop on EU-funded marine robotics and applications.*

CasADi Software. (2018). Retrieved 12 20, 2019, from CasADi: https://web.casadi.org/

Chen, Y. Q., & Wang, Z. (2005). Formation control: a review and a new consideration. *2005 IEEE/RSJ International Conference on Intelligent Robots and Systems*, (pp. 3181-3186).

Clarke, D. W., Mohtadi, C., & Tuffs, P. S. (1987). Generalized predictive control. Part 1: The basic algorithm. Part 2: Extensions and interpretations. *23*, pp. 137-160.

Cutler, C. R., & Ramaker, B. L. (1980). Dynamic matrix control - a computer control algorithm. *Joint Automatic Control Conference, (No. 17*, p. 72).

Darpa. (2004, November). *J-UCAS Overview.* Retrieved November 19, 2018, from DARPA: http://archive.darpa.mil/j-ucas/J-UCAS_Overview.htm

Das, B., Subudhi, B., & Pati, B. B. (2016). Cooperative formation control of autonomous underwater vehicles: An overview. *International Journal of Automation and Computing, 13(3)*, 199-225.

Diehl, M., Bock, H. G., Diedam, H., & Wieber, P. B. (2006). Fast direct multiple shooting algorithms for optimal robot control. In *Fast Motions in Biomechanics and Robotics: Optimization and Feedback Control* (pp. 65-93).

Encarnação, P., & Pascoal, A. (2000). 3D path following for autonomous underwater vehicle. *Proceedings of the 39th IEEE Conference on Decision and Control*, *3*, pp. 2977-2982.

Encarnação, P., & Pascoal, A. (2001). Combined trajectory tracking and path following: an application to the coordinated control of autonomous marine craft. *Proceedings of the 40th IEEE conference on decision and control*, *1*, pp. 964-969.

Encarnação, P., Pascoal, A., & Arcak, M. (2000). Path following for autonomous marine craft. *IFAC Proceedings Volumes, 33(21)*, pp. 117-122.

European Commission. (2008, April 09). *Coordination and control of cooperating heterogeneous unmanned systems in uncertain environments*. Retrieved May 04, 2019, from CORDIS EU Research Results: https://cordis.europa.eu/project/rcn/79338/factsheet/en

Fax, J. A., & Murray, R. M. (2002). Graph laplacians and stabilization of vehicle formations. *IFAC Proceedings Volumes*, *35(1)*, pp. 55-60.

Fax, J. A., & Murray, R. M. (2004). Information flow and cooperative control of vehicle formations. *IEEE Transactions on Automatic Control, 49(9)*, pp. 1465-1476.

Fernandes, P. G., Stevenson, P., & Brierley, A. S. (2002). AUVs as research vessels: the pros and cons. *ICES ASC2002. Theme session J: Use of marine research vessels in ICES. Options for the future*, (p. 11).

Ferreira, B., Pinto, M., Matos, A., & Cruz, N. (2009). Hydrodynamic modeling and motion limits of auv mares. In IEEE (Ed.), *2009 35th Annual Conference of IEEE Industrial Electronics*, (pp. 2241-2246).

Ferri, G., Munafo, A., & LePage, K. D. (2018). An autonomous underwater vehicle data-driven control strategy for target tracking. *IEEE Journal of Ocean Engineering, 43(2)*, 323-343.

Fossen, T. I. (1999). *Guidance and control of ocean vehicles.* (J. W. Sons, Ed.) Chichester, England.

Fossen, T. I. (2002). *Marine control systems - guidance, navigation and control of ships, rigs and underwater vehicles.* Marine Cybernetics AS.

Garcia, C. E., & Morshedi, A. M. (1986). Quadratic programming solution of dynamic matrix control (QDMC). *Chemical Engineering Communication, 46(1-3)*, 73-87.

Garcia, C. E., Prett, D. M., & Morari, M. (1989). Model predictive control: theory and practice - A survey. *Automática, 25(3)*, 335-348.

Ghabcheloo, R., Aguiar, A. P., Pascoal, A., Silvestre, C., Kaminer, I., & Hespanha, J. (2009). Coordinated path-following in the presence of communication losses and time delays. *Journal on Control and Optimization, 48(1)*, 234-265.

Ghabcheloo, R., Pascoal, A., Silvestre, C., & Kaminer, I. (2005). Coordinated path following control of multiple wheeled robots with directed communication links. *Proceedings of the 44th IEEE Conference on Decision and Control*, (pp. 7084-7089).

Ghabcheloo, R., Pascoal, A., Silvestre, C., & Kaminer, I. (2007). Non-linear coordinated path following control of multiple wheeled robots with bidirectional communication constraints. *International Journal of Adaptive Control and Signal Processing, 21(2-3)*, 133-157.

Greytak, M., & Hover, F. (2008). Underactuated point stabilization using predictive models with application to marine vehicles. In IEEE (Ed.), *2008 IEEE/RSJ International Conference on Intelligent Robots and Systems*, (pp. 3756-3761).

Gulzar, M. M., Rizvi, S. H., Javed, M. Y., Munir, U., & Asif, H. (2018). Multi-agent cooperative control consensus: A comparative review. *Electronics, 7(20)*, pp. 1-22.

Gulzar, M. M., Rizvi, S. T., Javed, M. Y., Munir, U., & Asif, H. (2018). Multi-agent cooperative control consensus: A comparative review. *Electronics, 7(2), 22*.

Hadi, B., Khosravi, A., & Sarhadi, P. (2021). A review of the path planning and formation control for multiple autonomous underwater vehicles. *Journal of Intelligent & Robotic Systems, 101*, pp. 1-26.

Hagen, I. B., Kufoalor, D. K., Brekke, E. F., & Johansen, T. A. (2018). MPC-based collision avoidance strategy for existing marine vessel guidance systems. *2018 IEEE International Conference on Robotics and Automation*, (pp. 7618-7623).

Hagen, P. E. (2016). Pipeline Inspection with AUV: Operational Experience and Lessons Learned.

Haseltine, E. L., & Rawlings, J. B. (2005). Critical evalation of extended kalman filtering and moving-horizon estimation. *Industrial and Engineering Chemistry Research, 44(8)*, 2451-2460.

Hashizume, S. (2015). *Development of a predictive functional control technique and practical applications to chemical processes.* Sumitomo Chemical Co., Ltd., Production & Safety Fundamental Technology Center. Sumitomo Kagaku R&D Report.

Hauser, K. (2020, 12 28). *Section IV. Dynamic Control - Chapter 17. Optimal Control.* Retrieved 08 16, 2022, from Robotic Systems (draft): http://motion.cs.illinois.edu/RoboticSystems/OptimalControl.html

Hung, N. T., & Pascoal, A. M. (2018). Cooperative path following of autonomous vehicles with model predictive control and event triggered communications. *IFAC - PapersOnLine, 51(20)*, pp. 562-567.

Hung, N. T., Rego, F., Crasta, N., & Pascoal, A. M. (2018). Input-constrained path following for autonomous marine vehicles with a global region of attraction. *IFAC - PapersOnLine, 51(29)*, pp. 348-353.

Hung, N., Rego, F., Quintas, J., Cruz, J., Jacinto, M., Souto, D., . . . Pascoal, A. (2022). A review of path following control strategies for autonomous robotic vehicles: theory, simulations, and experiments. *arXiv preprint arXiv:2204.07319*.

IST Lisboa. (2020). *AUV MEDUSA*. Retrieved May 25, 2020, from DSOR - Dynamical Systems and Ocean Robotics Laboratory: http://dsor.isr.ist.utl.pt/vehicles/medusa/

Jagtap, P., Raut, P., Kumar, P., Gupta, A., Singh, N. M., & Kazi, F. (2016). Control of autonomous underwater vehicle using reduced order model predictive control in three dimensional space. *IFAC - PapersOnLine, 49(1)*, pp. 772-777.

Jain, R. P., Alessandretti, A., Aguiar, A. P., & de Souza, J. B. (2018). Cooperative moving path following using event based control and communication. *2018 IEEE 13th APCA International Conference on Automatic Control and Soft Computing*, (pp. 189-194).

Jayasiri, A., Gros, S., & Mann, G. K. (2016). Tracking control and state estimation of a mobile robot based on NMPC and MHE. *2016 IEEE American Control Conference*, (pp. 1999-2004).

Kalman, R. E. (1960). Contribution to the theory of optimal control. *Bol. Soc. Mat. Mexicana, 5(2)*, pp. 102-119.

Kalwa, J. (2009). The GREX-Project: Coordination and control of cooperating heterogeneous unmanned systems in uncertain environments. *OCEANS 2009 - EUROPE*, (pp. 1-9).

Kaminer, I., Pascoal, A., Hallberg, E., & Silvestre, C. (1998). Trajectory tracking for autonomous vehicles: An integrated approach to guidance and control. *Journal of Guidance, Control and Dynamics, 21(1)*, 29-38.

Khalil, H. K. (2002). *Nonlinear Systems.* New Jersey: Prentice Hall.

Kirk, D. E. (2004). *Optimal control theory - An introduction.* Courier Corporation.

Kuhl, P., Diehl, M., Kraus, T., Schloder, J., & Bock, H. G. (2011). A real-time algorithm for moving horizon state and parameter estimation. *Computers and Chemical Engineering, 35(1)*, 71-83.

Kyrkjebø, E. (2007). Motion coordination of mechanical systems. Leader follower synchronization of Euler-Lagrange systems using output feedback control. *PhD Thesis*.

Lapierre, L., Soetanto, D., & Pascoal, A. (2003a). Coordinated motion control of marine robots. *IFAC Proceedings Volumes, 36(21)*, pp. 217-222.

Lapierre, L., Soetanto, D., & Pascoal, A. (2003b). Nonlinear path following with applications to the control of autonomous underwater vehicles. *Proceedings of the 42nd IEEE Conference on Decision and Control, (2)*, pp. 1256-1261.

Lefeber, E., Pettersen, K. Y., & Nijmeijer, H. (2003). Tracking control of an underactuated ship. *IEEE Transactions on Control Systems Technology, 11(1)*, pp. 52-61.

Li, X., Zhu, D., & Qian, Y. (2014). A survey on formation control algorithms for multi-AUV system. *Unmanned Systems, 2(04)*, 351-359.

Liu, W., Shan, Q., Mao, Y., & Wang, J. (2022). Review of improved cooperative control of unmanned surface vehicle based on multi-agent system. *4th IEEE International Conference on Data-driven Optimization of Complex Systems (DOCS)*, (pp. 1-6).

Loc, M. B., Choi, H. S., You, S. S., Kim, J., & Kim, Y. H. (2012). Mu-synthesis depth controller design for a small autonomous underwater vehicle. *Advanced Science Letters, 15(1)*, pp. 202-209.

Lyu, Y., Hu, J., Chen, B. M., Zhao, C., & Pan, Q. (2019). Multivehicle flocking with collision avoidance via distributed model predictive control. *IEEE Transactions on Cybernetics, 51(5)*, pp. 2651-2662.

Ma, Y., Liu, Y., Zhao, L., & Zhao, M. (2022). A review on cooperative control problems of multi-agent systems. *Proceedings of the 41st IEEE Chinese Control Conference (CCC)*, (pp. 4831-4836).

Martin, A., Marini, H., & Tosunoglu, S. (1999). Intelligent vehicle/highway system: a survey, part1. *Florida Conference on Recent Advances in Robotics, (p.6.)*.

Martin, M., Klupar, P., Kilberg, S., & Winter, J. (2001). Techsat 21 and revolutionizing space missions using microsatellites. *American Institute of Aeronautics and Astronautics*, pp. 1-3.

Maurya, P., Aguiar, A., & Pascoal, A. (2009). Marine vehicle path following using inner-outer loop control. *IFAC Proceedings Volumes*, *42(18)*, pp. 38-43.

Maurya, P., Morishita, H. M., Pascoal, A., & Aguiar, A. P. (2022). A path-following controller for marine vehicles using a two-scale inner-outer loop approach. *Sensors, 22(11)*, 4293.

Mayne, D. Q. (2014). Model predictive control: recent developments and future promise. *Automatica, 50(12)*, 2967-2986.

Mayne, D. Q., Rawlings, J. B., Rao, C. V., & Skokaert, P. O. (2000). Constrained model predictive control: stability and optimality. *Automatica, 36(6)*, pp. 789-814.

MC Marketing Consulting. (n.d.). *EU research project GREX: Marketing Consulting - Michael Jarowinsky*. Retrieved May 04, 2019, from MC Marketing Consulting - Michael Jarowinsky: www.grex-project.eu

Mehrez, M. W. (2019). *Optimization based solutions for control and state estimation in dynamical systems (implementation to mobile robots) - A Workshop.* University of Waterloo, Ontario.

Monk, J., Barrett, N., Bridge, T., Carroll, A., Friedman, A., Hill, N., . . . Lucieer, V. (2017). Marine sampling field manual for autonomous underwater vehicles (AUVs). In R. Przeslawski, & S. Foster, *Field Manuals for Marine Sampling to Monitor Australian Waters* (pp. 65-81).

Monterey Bay Aquarium Research Institute. (2016, January 8). *Autonomous Ocean Sampling Network*. Retrieved November 21, 2018, from Monterey Bay Aquarium Research Institute: https://www3.mbari.org/aosn/

Morishita, H. M. (2018). *ISS and IOS proofs for an AUV.* Universidade de São Paulo, Department of Naval Architecture and Ocean Engineering, São Paulo, Brazil.

Muchiri, N., Kamau, S. I., & Ikua, B. W. (2017). Architectures and algorithms for multiple UAV cooperative control: A review. *Proceedings of the Sustainable Research and Innovation Conference*, (pp. 180-183).

Murray, R. M. (2007). Recent research in cooperative control of multi-vehicle systems. *Journal of Dynamic Systems, Measurements, and Control (ASME), 129*, pp. 571-583.

Murray, R. M., Hauser, J., Jadbabaie, A., Milam, M. B., Petit, N., Dunbar, W. B., & Franz, R. (2002). Online control customization via optimization-based control. *Software-Enabled Control: Information Technology for Dynamical Systems*, pp. 149-174.

NASA. (2016). *Nasa/SP-2007-6105 Rev2 - System Engineeering handbook.*

Nielsen, T. (2018, April 05). *Russia to develop unmanned ships for the Arctic.* Retrieved April 15, 2023, from The Barents Observer: https://thebarentsobserver.com/en/arctic/2018/04/russia-develop-unmanned-ships-arctic

Oh, K. K., Park, M. C., & Ahn, H. S. (2015). A survey of multi-agent formation control. (Elsevier, Ed.) *Automática, 53*, 424-440.

Olfati-Saber, R., Fax, J. A., & Murray, R. M. (2007). Consensus and cooperation in networked multi-agent systems. *Proceedings of the IEEE, 95(1)*, 215-233.

Pascoal, A., Oliveira, P., Silvestre, C., Sebastião, L., Rufino, M., Barroso, V., . . . Dando, P. (2000). Robotic ocean vehicles for marine science applications: the european Asimov project. *Proceedings of the OCEANS 2000 MTS/IEEE Conference and Exhibition, 1*, pp. 409-415.

Pettersen, K. Y., & Nijmeijer, H. (2001). Underactuated ship tracking control: theory and experiments. *International Journal of Control, 74(14)*, 1435-1446.

Propoi, A. I. (1963). Application of linear programming methods for the synthesis of automatic sampled-data systems. *Avtomat. I Telemekh, 24(7)*, pp. 912-920.

Qin, S. J., & Badgwell, T. A. (1997). An overview of industrial model predictive control technology. *Fifth International Conference on Chemical Process Control - AIChE Symposium Series, 93(316)*, pp. 232-256.

Ren, W. (2007). Consensus strategies for cooperative control of vehicle formations. *IET Control Theory & Applications, 1(2)*, 505-512.

Richalet, J., Rault, A., Testud, J. L., & Papon, J. (1978). Model predictive heuristic control: application to industrial processes. *Automatica, 14*(5), 413-428.

Rout, R., & Subudhi, B. (2016). A backstepping approach for the formation control of multiple autonomous underwater vehicles using a leader-follower strategy. *Journal of Marine Engineering & Technology*, 15(1), 38-46.

Said, M. M. (2018). Optimization based solutions for control and state estimation in non-holonomic mobile robots: stability, distributed control, and relative localization. *arXiv preprint arXiv:1803.06928*.

Sansom, C. (1993). Time-varying feedback stabilization of car-like wheeled mobile robots. *The International Journal of Robotics Research, 12(1)*, pp. 55-64.

Seborg, D. E., Edgar, T. F., Mellichamp, D. A., & Doyle III, F. J. (2016). *Process dynamic and control.* John Wiley & Sons.

Shen, C., Shi, Y., & Buckham, B. (2017). Integrated path planning and tracking control of an AUV: A unified receding horizon optimization approach. *IEEE/ASME Transactions on Mechatronics, 22(3)*, pp. 1163-1173.

Simon, D. (2010). Kalman filtering with state constraints: a survey of linear and nonlinear algorithms. *IET Control Theory & Applications, 4*(8), 1303-1318.

Singh, S., Pavone, M., & Slotine, J. J. (n.d.). Tube-based MPC: a contraction theory approach.

Skjetne, R., Ihle, F., & Fossen, T. I. (2003). Formation control by synchronizing multiple maneuvering systems. *IFAC Proceedings Volumes*, *36(21)*, pp. 241-246.

Skjetne, R., Moi, S., & Fossen, T. I. (2002). Nonlinear formation control of marine craft. *Proceedings of the 2002 41st IEEE Conference on Decision and Control*, *2*, pp. 1699-1704.

Smith, O. M. (1957). Closer control of loops with dead time. *Chemical Engineering Progress, 53*(5), pp. 217-219.

Steenson, L. V., Turnock, S. R., Phillips, A. B., Harris, C., Furlong, M. E., Rogers, E., & Evano, D. W. (2014). Model predictive control of a hybrid autonomous underwater vehicle with experimental verification. *Proceedings of the Institution of Mechanical Engineers Part M: Engineering for the Maritime Environment, 228(2)*, 166-179.

Talla Ouambo, S. A., Boum, A. T., Imano, A. M., & Corriou, J. P. (2021). Enhancement of the moving horizon estimation performance based on an adaptive estimation algorithm. *Journal of Control Science and Engineering*, pp. 1-14.

US Naval observatory. (2017). *Terrestrial planet finder interferometer (TPF-1) whitepaper for the AAAC exoplanet task force.*

Vanni, F. (2007). Coordinated motion control of multiple autonomous underwater vehicles. *Master Thesis*. Lisbon, Portugal: Instituto Superior Técnico.

Vanni, F., Aguiar, A. P., & Pascoal, A. M. (2007). Nonlinear motion control of multiple autonomous underwater vehicles. *IFAC Proceedings Volumes*, *40(17)*, pp. 75-80.

Vanni, F., Aguiar, A. P., & Pascoal, A. M. (2008). Cooperative path-following of underactuated autonomous marine vehicles with logic-based communication. *IFAC Proceedings Volumes*, *41(1)*, pp. 107-112.

Verret, S. (2005). *Technical Memorandun 2005-241: Current state of the art in multirobot systems.* Suffield, Alberta, Canada: Defence R&D Canada – Suffield.

Wächter, A., & Biegler, T. L. (2006). On the implementation of an interior-point filter line-search algorithm for large-scale nonlinear programming. *Mathematical Programming, 106(11)*, pp. 25-57.

Wang, L. (2009). *Model predictive control system design and implementation using MATLAB.* Springer Science & Business Media.

Wang, S., Chen, L., Gu, D., & Hu, H. (2014). An optimization based moving horizon estimation with application to localization of autonomous underwater vehicles. *Robotics and Autonomous Systems, 62(10)*, 1581-1596.

Wang, Y., & Boyd, S. (2009, March). Fast model predictive control using online optimization. *IEEE Transactions on Control Systems Technology, 18*(2), pp. 267-278.

Whitt, C., & et. al. (2020). Future vision for autonomous ocean observations. *Frontiers in Marine Science*.

WiMUST Project. (2019). *WiMUST Widely Scalable Mobile Underwater Sonar Technology*. Retrieved June 26, 2019, from WiMUST: http://www.wimust.eu/

Woods Hole Oceanographic Institution. (2019). *Consortium for Marine Robotics*. Retrieved April 14, 2023, from Woods Hole Oceanographic Institution: https://www2.whoi.edu/site/marinerobotics/research-portfolio/hybrid-auv-inspection-monitoring-and-intervention-of-seafloor-and-sub-seafloor-pipelines/

Wynn, R. B., Huvenne, V. I., Le Bas, T. P., Murton, B. J., Connelly, D. P., Bett, B. J., . . . Hunt, J. E. (2014). Autonomous Underwater Vehicles (AUVs): Their past, present and future contributions to the advancement of marine geoscience. *Marine Geology, 352*, 451-468.

Xiang, X. (2011). Coordinated motion control of underactuated autonomous underwater vehicles. *PhD Thesis*. Université Montpellier II.

Yao, Y. (2013). Cooperative navigation system for multiple unmanned underwater vehicles. *IFAC Proceedings Volumes*, *46(20)*, pp. 719-723.

Yu, H., Zeng, Z., & Guo, C. (2022). Coordinated formation control of discrete-time autonomous underwater vehicles under alterable communication topology with time-varying delay. *Journal of Marine Science and Engineering, 10:712*.

Yu, S., Li, X., Chen, H., & Allgöwer, F. (2015). Nonlinear model predictive control for path following problems. *25(8)*, pp. 1168-1182.

Zadeh, L., & Whalen, B. (1962). On optimal control and linear programming. *IRE Transactions on Automatic Control, 7*(4), pp. 45-46.

Zampieri, S. (2008). Trends in networked control systems. *IFAC Proceedings Volumes*, *41(2)*, pp. 2886-2894.

APPENDIX A – MATHEMATICAL TOOLS AND DEFINITIONS

A1) Nonlinear System Theory

The theorems and definitions presented in the current item were borrowed from (Khalil, 2002), without the associated proofs.

A1.1) Types of Functions

A system composed by n first order differential equations can be represented by the following vectorial equation, with the associated initial conditions vector (initial-value problem):

$$\frac{d\vec{x}}{dt} = \dot{\vec{x}} = \vec{f}(t, \vec{x}), \quad \vec{x}(t_0) = \vec{x}_0 \tag{A1.1}$$

where $\vec{x} \in \mathbb{R}^n$ is the state vector, $\vec{f} \in \mathbb{R}^n$ is the system velocity field vector and $\vec{x}(t_0) = \vec{x}_0 \in \mathbb{R}^n$ is the initial conditions vector. For notation simplicity, the system (A1.1) can be written as:

$$\dot{x} = f(t, x), \quad x(t_0) = x_0 \tag{A1.2}$$

To predict the evolution of the state vector $x(t)$ from its initial conditions vector $x(t_0) = x_0$, the initial value problem given by (A1.2) must have a unique solution. The solution existence and uniqueness can be assured if a key constraint, named Lipschitz condition, is imposed on the function $f(t, x)$.

Definition A1.1 (Lipschitz function): A function $f(t, x)$ satisfying the Lipschitz condition:

$$\|f(t, x) - f(t, y)\| \le L\|x - y\| \tag{A1.3}$$

for all (t, x) and (t, y) in some neighborhood of (t_0, x_0) is said to be Lipschitz in x and the positive constant L is called the Lipschitz constant.

Theorem A1.1 (Local Existence and Uniqueness): For the initial-value problem (A1.2), let $f(t, x)$ be a piecewise continuous function in t, satisfying the Lipschitz condition (A1.3) $\forall\, x, y \in B = \{x \in \mathbb{R}^n \mid \| x - x_0 \| \le r\}$, with $r > 0$, and for all $t \in [t_0, t_0 + \delta]$, with $\delta > 0$. Then (A1.2) has unique solution over $[t_0, t_0 + \delta]$.

Notice that the result of theorem A1.1 holds only locally, in the interval $[t_0, t_0 + \delta]$, where δ can be significantly small. To assure a global result, holding beyond the time interval $[t_0, t_0 + \delta]$, it is necessary to define a globally Lipschitz function.

Theorem A1.2 (Global Existence and Uniqueness): For the initial-value problem (A1.2), let $f(t, x)$ be piecewise continuous in t and satisfy the Lipschitz condition (A1.3) $\forall\, x, y \in \mathbb{R}^n$ and for all $t \in [t_0, t_1]$. Then (A1.2) has unique solution over $[t_0, t_1]$.

Due to the restrictiveness nature of the global Lipschitz condition, it would be useful to obtain a global result considering the local Lipschitz condition instead. As presented in the next theorem, this can be attained if further knowledge of the system solution is known.

Theorem A1.3 (Global Existence and Uniqueness for Locally Lipschitz Functions): For the initial-value problem (A1.2), let $f(t, x)$ be piecewise continuous in t and locally Lipschitz in x, for all $t \ge t_0$ and all x in a domain $D \subset \mathbb{R}^n$. Let W be a compact subset of D, assume that $x_0 \in W$, and every solution of (A1.2) remains entirely in W. Then, (A1.2) has unique solution for all $t > t_0$.

Definition A1.2 ($\mathcal{K}$ Class Function): A continuous function $\alpha \colon [0, a) \to [0, \infty)$ is said to belong to class $\mathcal{K}$, if it is strictly increasing and $\alpha(0) = 0$. It is said to belong to class K_∞ if $a = \infty$ and $\alpha(r) \to \infty$ as $r \to \infty$.

Definition A1.3 ($\mathcal{KL}$ Class Function): A continuous function $\beta \colon [0, a) \times [0, \infty) \to [0, \infty)$ is said to belong to class $\mathcal{KL}$ if, for each fixed s, the mapping $\beta(r, s)$ belongs to class $\mathcal{K}$, with respect to r, and for each fixed r, the mapping $\beta(r, s)$ is decreasing with respect to s and $\beta(r, s) \to 0$ as $s \to \infty$.

A1.2) Lyapunov Stability

The objective of this item is to present the Lyapunov Direct Method, by which, sometimes, it´s possible to assess the stability of an equilibrium point, without the need to proceed the linearization of the system around this point or to apply the central manifolds theory. The Lyapunov Direct Method allows to get a set of initial conditions whose trajectories converge to the equilibrium point, if it is asymptotically stable. In this way, it´s possible to assess the extension of its attraction domain.

Definition A1.4 (Stability of autonomous systems): For the initial-value problem (A1.2), assume that $f(t, x) = f(x)$. Without loss of generality[89], assume that $x = 0$ is an equilibrium point of (A1.2) so that $f(0) = 0$. Them, the equilibrium point $x = 0$ is:

- Stable if, for each $\delta > 0$, there is some $\varepsilon(\delta) > 0$ such that

$$\|x(0)\| < \varepsilon \Rightarrow \|x(t)\| < \delta, \qquad \forall\, t > 0 \tag{A1.4}$$

- Instable, if it is not stable; and

- Asymptotically stable, if it is stable and δ can be chosen such that:

$$\|x(0)\| < \varepsilon \Rightarrow \lim_{t \to \infty} x(t) = 0, \qquad \forall\, t > 0 \tag{A1.5}$$

Theorem A1.4 (Lyapunov Direct Method for autonomous systems): Let $x = 0$ be an equilibrium point for (A1.2) and $D \subset \mathbb{R}^n$ be a domain containing $x = 0$. Let $V: D \to \mathbb{R}$ be a continuously differentiable function such that:

$$V(0) = 0 \text{ and } V(x) > 0 \text{ in } D - \{0\} \tag{A1.6}$$

Them, the equilibrium point $x = 0$ is:

- Stable if,

$$\dot{V}(x) \leq 0, \qquad \forall\, x \in D \tag{A1.7}$$

- Asymptotically stable if,

$$\dot{V}(x) < 0, \qquad \forall\, x \in D \tag{A1.8}$$

---

[89] Any equilibrium point can be shifted to the origin by a coordinate change, without affecting its stability properties.

- Globally asymptotically stable if:

$$\dot{V}(x) < 0, \qquad \forall\, x \in D = \mathbb{R}^n \qquad\qquad\text{(A1.9)}$$

As can be noticed in the method, if $\dot{V}(x) \leq 0$, it's not possible to assure the asymptotic stability of the origin. However, if the only trajectory belonging to the set in which $\dot{V}(x) = 0$ is the origin, its asymptotic stability is assured, according to the following theorems.

Theorem A1.5 (Barbashin's Theorem): Let $x = 0$ be an equilibrium point for (A1.2). Let $V: D \rightarrow \mathbb{R}$ be a continuously differentiable positive definite function on a domain $D \subset \mathbb{R}^n$ containing the origin $x = 0$, such that $\dot{V}(x) \leq 0$ in D. Let $S = \{x \in D \mid \dot{V}(x) = 0\}$ and suppose that no solution can stay identically in S, other than the trivial solution $x(t) \equiv 0$. Them, the origin is asymptotically stable.

Theorem A1.6 (Krasovskii's Theorem): Let $x = 0$ be an equilibrium point for (A1.2). Let $V: \mathbb{R}^n \rightarrow \mathbb{R}$ be a continuously differentiable, radially bounded, positive definite function, such that $\dot{V}(x) \leq 0$ for all $x \in \mathbb{R}^n$. Let $S = \{x \in \mathbb{R}^n \mid \dot{V}(x) = 0\}$ and suppose that no solution can stay identically in S, other than the trivial solution $x(t) \equiv 0$. Them, the origin is globally asymptotically stable.

Definition A1.5 (Stability of non-autonomous systems): For the initial-value problem (A1.2), $x = 0$ is an equilibrium point if:

$$f(t, 0) = 0 \ \forall\, t > 0 \qquad\qquad\text{(A1.10)}$$

This equilibrium point is:

- Stable if, for each $\varepsilon > 0$, there exists some $\delta(\varepsilon, t_0) > 0$ such that

$$\|x(t_0)\| < \delta \Rightarrow \|x(t)\| < \varepsilon, \qquad \forall\, t \geq t_0 \geq 0 \qquad\qquad\text{(A1.11)}$$

- Uniform stable if, for each $\varepsilon > 0$, there exists some $\delta(\varepsilon) > 0$, independent of t_0, such that (A1.11) is satisfied;
- Instable, if it is not stable;
- Asymptotically stable, if it is stable and there exists a constant $c(t_0) > 0$ such that:

$$\|x(t_0)\| < c \Rightarrow \lim_{t \to \infty} x(t) = 0 \qquad\qquad\text{(A1.12)}$$

- Uniformly asymptotically stable if it is uniformly stable and there exists a positive constant c, independent of t_0, such that for all $\|x(t_0)\| < c \Rightarrow \lim_{t \to \infty} x(t) = 0$ uniformly in t_0; that is, for each $\eta > 0$, there is $T(\eta) > 0$ such that

$$\|x(t)\| < \eta, \quad \forall \, t \geq t_0 + T(\eta), \quad \forall \|x(t_0)\| < c \tag{A1.13}$$

- Globally uniformly asymptotically stable, if it is stable, $\delta(\varepsilon)$ can be chosen such that $\lim_{\varepsilon \to \infty} \delta(\varepsilon) = \infty$ and, for each pair of positive numbers η and c, there exists $T(\eta, c) > 0$ such that

$$\|x(t)\| < \eta, \quad \forall \, t \geq t_0 + T(\eta, c), \quad \forall \|x(t_0)\| < c \tag{A1.14}$$

For non-autonomous systems, it is more convenient to refine de definitions of stability and asymptotic stability using the comparison functions $\mathcal{K}$ and $\mathcal{KL}$, previously defined.

Theorem A1.7 (Lyapunov Direct Method for non-autonomous systems): Let $x = \mathbf{0}$ be an equilibrium point for (A1.10) and $D \subset \mathbb{R}^n$ be a domain containing $x = 0$. Let $V: [0, \infty) \, x \, D \to \mathbb{R}$ be a continuously differentiable function such that:

$$W_1(x) \leq V(t, x) \leq W_2(x) \tag{A1.15}$$

$$\frac{\partial V}{\partial t} + \frac{\partial V}{\partial x} f(t, x) \leq 0 \tag{A1.16}$$

$\forall \, t \geq 0$ and $\forall \, x \in D$, where $W_1(x)$ and $W_2(x)$ are continuous positive definite functions on D. Them, the equilibrium point $x = 0$ is stable.

If (A1.16) can be replaced by a more stringent inequality such as:

$$\frac{\partial V}{\partial t} + \frac{\partial V}{\partial x} f(t, x) \leq -W_3(x) \tag{A1.17}$$

$\forall \, t > 0$ and $\forall \, x \in D$, where $W_3(x)$ is continuous positive definite function on D, them, the equilibrium point $x = 0$ is uniformly asymptotically stable. Additionally, if $D = \mathbb{R}^n$ and $W_1(x)$ is radially unbounded, them the equilibrium point $x = 0$ is globally uniformly asymptotically stable.

In (Khalil, 2002), additional results for proving exponential stability using Lyapunov functions are presented.

A1.3) Boundedness

Even when the origin is not an equilibrium point, the Lyapunov analysis can be used to demonstrate the boundedness of the system trajectories.

Definition A1.6 (Boundedness): For the initial-value problem (A1.2), its solutions are:

- Uniformly bounded if there exists a positive constant c, independent of $t_0 \geq 0$, and for every $a \in (0,c)$, there is $\beta = \beta(a) > 0$, independently of t_0, such that:

$$\|x(t_0)\| \leq \alpha \implies \|x(t)\| \leq \beta , \forall \ t \geq t_0 \tag{A1.18}$$

- Globally uniformly bounded if (A1.18) holds for an arbitrarily large a.

- Uniformly ultimately bounded with ultimate bound b if there exist positive constants b and c, independently of $t_0 \geq 0$, and for every $a \in (0,c)$, there is $T = T(a, b) \geq 0$, independently of t_0, such that:

$$\|x(t_0)\| \leq \alpha \implies \|x(t)\| \leq \beta , \forall \ t \geq t_0 + T \tag{A1.19}$$

- Globally uniformly ultimately bounded if (A1.19) holds for an arbitrarily large a.

For autonomous systems, the term "uniform" can be dropped since the solution depends only on $t - t_0$.

A1.4) Input-to-State-Stability (ISS) / Input-to-Output-Stability (IOS) / Input-to-Output Practically Stable (IOpS)

Consider the system

$$\dot{x} = f(t, x, u) \tag{A1.20}$$

where $f : [0, \infty) \ x \ \mathbb{R}^n \ x \ \mathbb{R}^m \to \mathbb{R}^n$ is piecewise continuous in t and locally Lipschitz in x. The input $u(t)$ is a piecewise continuous bounded function of t for all $t \geq 0$. Supposed that the unforced system

$$\dot{x} = f(t, x, 0) \tag{A1.21}$$

has a globally uniformly asymptotically equilibrium point at the origin $x = 0$.

Definition A1.7 (Input-to-State-Stability): the system (A1.20) is said to be input-to-state-stable if there exist a class $\mathcal{KL}$ function β and a class $\mathcal{K}$ function γ such that for any initial state $x(t_0)$ and any bounded input $u(t)$, the solution $x(t)$ exists for all $t \geq t_0$ and satisfies:

$$\|x(t)\| \leq \beta(\|x(t_0)\|, t - t_0) + \gamma\left(\sup_{t_0 < \tau < t} \|u(\tau)\|\right) \tag{A1.22}$$

Definition A1.8 (Input-to-Output-Stability): the system (A1.20) is said to be input-to-output-stable if there exist a class $\mathcal{KL}$ function β and a class $\mathcal{K}$ function γ such that for any initial state $x(t_0)$ and any bounded input $u(t)$, the solution $x(t)$ exists for all $t \geq t_0$ and satisfies:

$$\|y(t)\| \leq \beta(\|x(t_0)\|, t - t_0) + \gamma\left(\sup_{t_0 < \tau < t} \|u(\tau)\|\right) \tag{A1.23}$$

Definition A1.9 (Input-to-Output Practically Stability): the system (A1.20) is said to be input-to-output-practically stable if there exist a class $\mathcal{KL}$ function β and a class $\mathcal{K}$ function γ such that for any initial state $x(t_0)$ and any bounded input $u(t)$, the solution $x(t)$ exists for all $t \geq t_0$ and satisfies:

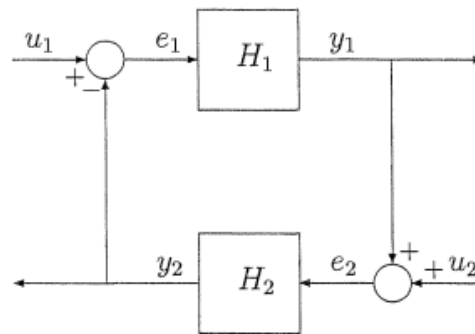$$\|y(t)\| \leq \beta(\|x(t_0)\|, t - t_0) + \gamma\left(\sup_{t_0 < \tau < t} \|u(\tau)\|\right) + d \tag{A1.24}$$

A1.5) Small Gain Theorem

Consider the two systems H_1 and H_2 (Figure A1), supposed to be finite gain $\mathcal{L}$ stable, thus holding the following properties:

$$\|y_1\|_{\mathcal{L}} \leq \gamma_1 \|e_1\|_{\mathcal{L}} + \beta_1 \tag{A1.25}$$

$$\|y_2\|_{\mathcal{L}} \leq \gamma_2 \|e_2\|_{\mathcal{L}} + \beta_2 \tag{A1.26}$$

Figure A1: Feedback connected systems


(Khalil, 2002)

Theorem A1.8 (Small Gain Theorem): Under the preceding assumptions, the feedback connection of systems H_1 and H_2 is finite gain $\mathcal{L}$ stable if $\gamma_1\gamma_2 < 1$.

A2) Graph Theory

The coordinated motion of a multi-agent system requires that the individual agents (vehicles, in the current case) exchange their states through a communication network. The constraints imposed by the communication topology among them can be modeled using the graph theory. The concepts and definitions presented in the current item were borrowed from (Ghabcheloo, et al., 2009))[90].

Definition A2.1 (Graph): A graph, induced by the intervehicle communication network, is a set $\mathcal{G}(v, \varepsilon)$, where $v = \{v_1, \dots, v_n\}$ denotes the set of n nodes (each corresponding to a vehicle) and $\varepsilon \subset v^2$ denotes the set of ordered pair of nodes, called edges (each representing a data link). If the edges are not oriented, the graph is called "undirected" (Figure A2).

Figure A2: Undirected and directed graphs
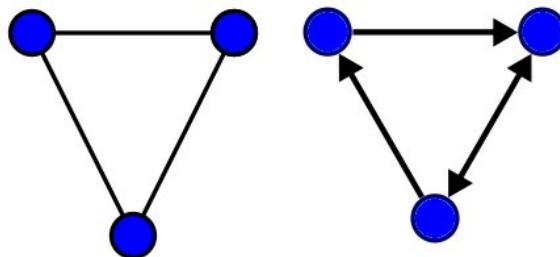
https://en.wikipedia.org/wiki/Graph_theory

---

[90] The reference refers to undirected graphs, used to model bi-directional communications networks.

Definition A2.2 (Set $\mathcal{N}_i$): The set of vehicles that vehicle i communicates is denominated $\mathcal{N}_i$, defined as:

$$\mathcal{N}_i = \{v_j \in v : e_{ij} \in \varepsilon\} \tag{A2.1}$$

For undirected graphs, $i \in \mathcal{N}_j \leftrightarrow j \in \mathcal{N}_i$ (bi-directional communication).

Definition A2.3 (Connected): $\mathcal{G}(v, \varepsilon)$ is connected if there exists a path connecting every two nodes.

Definition A2.4 (Complete Graph): $\mathcal{G}(v, \varepsilon)$ is completed if there exists a path connecting each pair of nodes.

Definition A2.5 (Adjacent Matrix): The adjacent matrix $A(\mathcal{G})$ of an undirected graph is a square matrix with rows and columns indexed by the nodes such that $A_{ij} = 1$ if $j \in \mathcal{N}_i$ and $A_{ij} = 0$, otherwise.

Definition A2.6 (Degree Matrix): The degree matrix $D(\mathcal{G})$ of an undirected graph is a diagonal square matrix such that $D_{ii} = |N_i|$ (the cardinality of N_i).

Definition A2.7 (Laplacian): The Laplacian L of a graph is defined as:

$$L = D - A \tag{A2.2}$$

The Laplacian L presents the following properties:

P1: L is positive semi-definite by construction.

P2: If $\mathcal{G}$ is undirected, L is symmetric.

P3: If $\mathcal{G}$ is undirected, L has an eigenvalue at zero with an associated right eigenvector 1 ($L[\mathbf{1}]_{nx1} = [\mathbf{0}]_{nx1}$).

P4: If $\mathcal{G}$ is connected, L has a simple eigenvalue at zero with an associated right eigenvector 1 and the remaining eigenvalues are all positive.

Definition A2.8 (Normalized Laplacian): The normalized Laplacian L_D of a graph is defined as:

$$L_D = D^{-1}(D - A) \tag{A2.3}$$

APPENDIX B – NUMERICAL DATA

Table B1: Controller / estimator gains

PFC	Outer-Loop	L-MPC	$K_k = \begin{bmatrix} 1 & 0 \\ 0 & 0.6 \end{bmatrix}$ $\quad Q = \begin{bmatrix} 2 & 0 & 0 \\ 0 & 2 & 0 \\ 0 & 0 & 0.1 \end{bmatrix}$ $\quad R = \begin{bmatrix} 1 & 0 \\ 0 & 0.5 \end{bmatrix}$
	Inner-Loop	FLC	$K_d = \begin{bmatrix} -50 & 0 \\ 0 & -50 \end{bmatrix}$
	-	MHE	$Q_* = \begin{bmatrix} 100 & 0 & 0 \\ 0 & 100 & 0 \\ 0 & 0 & 1000 \end{bmatrix}$ $\quad R_* = \begin{bmatrix} 0 & 0 \\ 0 & 0 \end{bmatrix}$
	-	OCSO	$K_{p_{obs}} = \begin{bmatrix} 1 & 0 \\ 0 & 1 \end{bmatrix}$ $\quad K_{c\_obs} = \begin{bmatrix} 1 & 0 \\ 0 & 1 \end{bmatrix}$
CC	-	-	$K_\xi = 0.5$ (for all vehicles)

Table B2: Medusa ASC inertia and hydrodynamic properties at the surface

Inertia	Added Mass	Linear damping	Nonlinear damping
$m = 17\ kg$	$X_{\dot{u}} = -20\ kg$	$X_u = -0.2\ kg/s$	$X_{|u|u} = -25\ kg/m$
$I_z = 1\ kg.m^2$	$Y_{\dot{v}} = -30\ kg$	$Y_v = -50\ kg/s$	$Y_{|v|v} = -0.01\ kg/m$
	$N_{\dot{r}} = -8.69\ kg.m^2$	$N_r = -4.14\ kg.m^2/s$	$N_{|r|r} = -6.23\ kg.m$
	$N_{\dot{v}} = 0\ kg.m$	-	$N_{v|v|} = 0\ kg$
	$Y_{\dot{r}} = 0\ kg.m$	-	$Y_{r|r|} = 0\ kg.m$

Table B3: Mares AUV inertia and hydrodynamic properties

Inertia	Added Mass	Linear damping	Nonlinear damping
$m = 32\ kg$	$X_{\dot{u}} = -1.74\ kg$	$X_u = 0\ kg/s$	$X_{|u|u} = -4.05\ kg/m$
$I_z = 4.73\ kg.m^2$	$Y_{\dot{v}} = -42.8\ kg$	$Y_v = 0\ kg/s$	$Y_{|v|v} = -113\ kg/m$
	$N_{\dot{r}} = -6.32\ kg.m^2$	$N_r = 0\ kg.m^2/s$	$N_{|r|r} = -1.57\ kg.m2$
	$N_{\dot{v}} = 0.0289\ kg.m$	-	$N_{v|v|} = 2.38\ kg$
	$Y_{\dot{r}} = 0.0289\ kg.m$	-	$Y_{r|r|} = 1.88\ kg.m$